TESIS DOCTORAL

SÍNTESIS Y CARACTERIZACIÓN DE MATERIALES HÍBRIDOS MESOPOROSOS ORGÁNICO-INORGÁNICOS PARA SU APLICACIÓN EN PROCESOS CATALÍTICOS

SYNTHESIS AND CHARACTERIZATION OF MESOPOROUS ORGANIC-INORGANIC HYBRID MATERIALS FOR THEIR APPLICATION IN CATALYTIC PROCESSES

Mª Ángeles Navarro Núñez

Directores:

Prof. Dr. Francisco José Romero Salguero

Prof. Drª Mª Dolores Esquivel Merino

Química Fina

Universidad de Córdoba. Facultad de Ciencias

Departamento de Química Orgánica

Junio, 2023

TITULO: *Síntesis y caracterización de materiales híbridos mesoporosos orgánico-inorgánicos para su aplicación en procesos catalíticos*

AUTOR: *María Ángeles Navarro Núñez*

Campus de Rabanales
Ctra. Nacional IV, Km. 396 A
14071 Córdoba

https://www.uco.es/ucopress/index.php/es/
ucopress@uco.es

TÍTULO DE LA TESIS:

SÍNTESIS Y CARACTERIZACIÓN DE MATERIALES HÍBRIDOS MESOPOROSOS ORGÁNICO-INORGÁNICOS PARA SU APLICACIÓN EN PROCESOS CATALÍTICOS

"SYNTHESIS AND CHARACTERIZATION OF ORGANIC-INORGANIC MESOPOROUS HYBRID MATERIALS FOR THEIR APPLICATION IN CATALYTIC PROCESSES"

DOCTORANDA: Mª Ángeles Navarro Núñez

INFORME RAZONADO DE LOS DIRECTORES DE LA TESIS

La presente memoria de Tesis Doctoral es el resultado del trabajo realizado por Dña. María de los Ángeles Navarro Núñez en el grupo de investigación "Catálisis Orgánica y Materiales Nanoestructurados" (FQM-346), perteneciente al Departamento de Química Orgánica de la Universidad de Córdoba.

La doctoranda ha desarrollado un gran número de competencias relacionadas con la investigación científica, que abarcan desde la aplicación del método científico hasta la difusión de los resultados de su investigación, tanto al público general como al especializado. La evolución de la doctoranda ha sido excelente, habiendo demostrado grandes progresos en los objetivos que se plantearon al inicio de su Tesis. El campo de los materiales híbridos es muy amplio y poseen un gran número de aplicaciones en diferentes ámbitos. En esta Tesis, diversos tipos de materiales híbridos, más específicamente organosílices, han sido empleados como catalizadores en dos tipos de procesos diferentes, uno de ellos relacionado con la química orgánica fina y el otro con la conversión de energía.

Los materiales sintetizados en esta Tesis han consistido concretamente en organosílices mesoporosas periódicas. Además de familiarizarse con la síntesis de este tipo de materiales, asistida por diferentes tipos de surfactantes, la doctoranda ha adquirido experiencia en la síntesis de precursores organosilícicos así como en la reactividad de grupos funcionales superficiales, lo que le ha permitido incorporar complejos metálicos superficiales de distinta naturaleza, en función del proceso catalítico perseguido.

Sin duda, una parte importante de la formación alcanzada por la doctoranda está referida a la caracterización de los materiales obtenidos. Ha aprendido el manejo y/o interpretación de técnicas muy variadas para conseguir información estructural, superficial y fisicoquímica, tales

como difracción de rayos X, microscopía de transmisión, adsorción de N_2, espectroscopia fotoelectrónica de rayos X, espectroscopias Raman, IR y UV-vis, y resonancia magnética nuclear, entre otras. Además, la doctoranda ha llevado a cabo los ensayos catalíticos de los materiales, para lo que ha necesitado el uso de reactores, incluyendo reactores fotoquímicos, y el análisis de los productos de reacción mediante cromatografía de gases.

La heterogeneización de complejos organometálicos es particularmente interesante para el desarrollo de nuevos catalizadores para reacciones de oxidación. En esta Tesis, se ha abordado el estudio de la reacción de epoxidación de estireno sobre una organosílice mesoporosa periódica con complejos de cobre superficiales. La doctoranda ha realizado numerosos experimentos encaminados a dilucidar la influencia de diferentes variables (oxidante, disolvente, temperatura, relación de reactivos) en el rendimiento y selectividad de la reacción.

Diversos complejos de cobalto que imitan la estructura de la cobalamina (vitamina B12) están siendo aplicados como catalizadores en procesos de fotosíntesis artificial. Entre ellos destacan dos familias, las cobaloximas y las ftalocianinas de cobalto. Siguiendo diferentes estrategias sintéticas, ambos tipos de complejos se han incorporado a la estructura de organosílices mesoporosas periódicas, cumpliendo así los correspondientes objetivos propuestos para esta Tesis.

La doctoranda ha estudiado dos tipos de materiales con ligandos superficiales de tipo piridina e imidazol, a los que se ha anclado un complejo de cobalto que ha dado lugar a la formación de unidades de cobaloxima. Estos han sido usados como catalizadores en sistemas fotocatalíticos para la producción de hidrógeno bajo irradiación visible. También se ha comparado el efecto ejercido por el ordenamiento de la organosílice, demostrando el mejor comportamiento catalítico de las organosílices mesoporosas periódicas en comparación con materiales análogos desordenados.

Entre los procesos químicos más desafiantes en la actualidad se encuentran, por razones evidentes, todos los relacionados con la transformación de CO_2. Uno de los objetivos de esta Tesis consistía en la aplicación de organosílices mesoporosas periódicas como catalizadores de fotorreducción de CO_2 a combustibles solares bajo irradiación visible. Para la consecución de este objetivo, se estableció una colaboración con el Dr. Souvik Roy de la Universidad de Lincoln en el Reino Unido, donde la doctoranda realizó una estancia de 3 meses. Tras la síntesis de un precursor silánico que contenía una fltalocianina de cobalto, se logró introducirla en la estructura de una organosílice mesoporosa periódica, habiéndose comprobado su buena actividad como catalizador para la conversión de CO_2 a CO.

En todos los procesos anteriores se ha evidenciado que la heterogeneización de los complejos metálicos en organosílices mesoporosas periódicas incrementa su actividad y estabilidad frente a los catalizadores homogéneos análogos.

Los extraordinarios avances sobre el estado del arte en los resultados obtenidos a lo largo de esta Tesis Doctoral han permitido su publicación como artículos en revistas científicas de prestigio en sus respectivos campos, amén de otras publicaciones como capítulos de libro y actas de congresos. Aunque algunos de los resultados no han sido publicados aún, próximamente serán enviados para su consideración.

La doctoranda ha realizado una intensa labor experimental que le ha permitido culminar con éxito los objetivos planteados en su plan de investigación. Junto a su extraordinaria formación, cabe destacar su alto grado de motivación y autonomía, lo que nos faculta para concluir que ha adquirido plena capacidad investigadora y, por tanto, suficiencia para abordar investigaciones futuras en el ámbito de la Química y ciencias afines.

La extraordinaria formación de la doctoranda en sus estudios de Grado y Máster se ha completado durante su etapa doctoral. Las actividades formativas han sido fundamentales en este sentido y cabe destacar su participación en numerosas jornadas, cursos y congresos nacionales e internacionales, así como en actividades de divulgación científica, destacando las presentaciones orales realizadas en diversas ocasiones.

En definitiva, la calidad de la Tesis Doctoral presentada y la formación adquirida a lo largo de sus estudios de Doctorado en el programa de Química Fina por Dña. María de los Ángeles Navarro Núñez son excelentes.

Por todo ello, autorizamos la presentación de la Tesis Doctoral.

Córdoba, 8 de Junio de 2023

Firma de los directores

ROMERO SALGUERO FRANCISCO JOSE - 30522472T

Firmado digitalmente por ROMERO SALGUERO FRANCISCO JOSE - 30522472T
Nombre de reconocimiento (DN): c=ES, serialNumber=IDCES-30522472T, givenName=FRANCISCO JOSE, sn=ROMERO SALGUERO, cn=ROMERO SALGUERO FRANCISCO JOSE - 30522472T
Fecha: 2023.06.19 12:17:58 +02'00'

ESQUIVEL MERINO MARIA DOLORES - 08879012T

Firmado digitalmente por ESQUIVEL MERINO MARIA DOLORES - 08879012T
Nombre de reconocimiento (DN): c=ES, serialNumber=IDCES-08879012T, givenName=MARIA DOLORES, sn=ESQUIVEL MERINO, cn=ESQUIVEL MERINO MARIA DOLORES - 08879012T
Fecha: 2023.06.19 13:01:40 +02'00'

Fdo.: Francisco José Romero Salguero

Fdo.: María Dolores Esquivel Merino

D. **Antonio Ángel Romero Reyes**, Director del Departamento de Química Orgánica de la Universidad de Córdoba.

CERTIFICA:

Que el presente Trabajo de Investigación, titulado **"SÍNTESIS Y CARACTERIZACIÓN DE MATERIALES HÍBRIDOS MESOPOROSOS ORGÁNICO-INORGÁNICOS PARA SU APLICACIÓN EN PROCESOS CATALÍTICOS"**, que constituye la Memoria presentada por Mª Ángeles Navarro Núñez para optar al titulo de Doctor en Química Orgánica de la Universidad de Córdoba, bajo la dirección de los profesores D. Francisco José Romero Salguero y Dña. Mª Dolores Esquivel Merino, así como en el departamento de Química de la Universidad de Lincoln (Reino Unido), durante la estancia de tres meses que realizó bajo la supervisión del Prof. Souvik Roy.

Y para que conste, firmo el presente certificado en Córdoba, a 8 de junio de 2023.

Fdo. D. Antonio Ángel Romero Reyes

Las investigaciones realizadas en la presente Memoria de Tesis Doctoral forman parte de un Plan de Investigación desarrollado por el grupo de investigación FQM-346. Este Plan de Investigación ha sido subvencionado con cargo a los Proyectos de Investigación de la Fundación Ramón Areces y del Ministerio de Ciencia e Innovación (RTI2018-101611-B-I00). Asimismo, estas investigaciones han recibido subvenciones de los Fondos Feder.

Por otra parte, la doctoranda ha disfrutado de una beca de movilidad Erasmus + del Campus de Excelencia Internacional Agroalimentario (ceiA3), de la Universidad de Córdoba, para la realización de una estancia de tres meses en el Departamento de Química de la Universidad de Lincoln (Reino Unido).

Mediante la defensa de esta Memoria de Tesis Doctoral se pretende optar a la obtención del **título de Doctor con Mención Internacional**, habida cuenta de que el doctorando reúne los requisitos para tal mención, según el artículo 35 de la Normativa Reguladora de los Estudios de Doctorado de la Universidad de Córdoba:

- La doctorando ha realizado una estancia de tres meses de duración en el grupo de investigación Molecular catalysis bajo la supervisión del profesor Souvik Roy, en la Universidad de Lincoln.

- Parte de la Memoria de la Tesis Doctoral se ha redactado en una lengua distinta a las lenguas oficiales de España

- Parte de los informes favorables de dos doctores expertos con experiencia acreditada, pertenecientes a una institución no española de Educación Superior:

  - Dra. Anna M. Kaczmarek (Ghent University, Belgium)
  - Dra. Ying-Ya Liu (Dalian University of Technology, Dalian)

- Un miembro del Tribunal que ha de evaluar la Tesis es un doctor experto con experiencia acreditada, perteneciente a una institución no española de Educación Superior, y es distinto del responsable de la estancia mencionada en el primer apartado:

  - Dr. Carlos Baleizão (Universidad de Lisboa, Portugal)

- La presentación de esta Tesis Doctoral se realizará en una lengua distinta de las lenguas oficiales de España.

ÍNDICE GENERAL

INDICE GENERAL

RESUMEN/SUMMARY

RESUMEN DE LA TESIS DOCTORAL "SÍNTESIS Y CARACTERIZACIÓN DE MATERIALES HÍBRIDOS MESOPOROSOS ORGÁNICO-INORGÁNICOS PARA SU APLICACIÓN EN PROCESOS CATALÍTICOS"

1. Introducción o motivación de la Tesis Doctoral

Desde su descubrimiento en el año 1999 [1–3], los materiales híbridos orgánico-inorgánicos mesoporosos ordenados (PMOs) han tenido una gran repercusión en el ámbito científico, ya que un mismo material combina las ventajas de la química orgánica, en cuanto a la introducción de diferentes grupos funcionales, con la estabilidad térmica que presentan los sustratos inorgánicos.

La síntesis de este tipo de materiales se realiza vía hidrólisis y condensación de diferentes precursores disilánicos en presencia de un agente director de la estructura (SDA), en un medio ácido o básico. De forma general, los precursores disilánicos con puentes orgánicos del tipo $(R'O)_3SiRSi(OR')_3$ son [4] mezclados con trialcoxiorganosilanos del tipo $(R'O)_3SiR$.

Una de las características más destacadas de los PMOs reside en que los grupos orgánicos (R) están ubicados en las paredes de los poros, es decir, los grupos funcionales forman parte de la estructura del material y están distribuidos homogéneamente por toda la red silícica. Además, estos materiales poseen elevadas áreas superficiales (hasta 1200 m^2/g), gruesas paredes porosas y elevados volúmenes de poro. Sus propiedades físico-químicas, como la flexibilidad o la hidrofobia, puede ser moduladas y, además, poseen una mayor estabilidad hidrotermal y mecánica que las sílices convencionales [5].

Por otro lado, nuevos grupos orgánicos pueden ser introducidos a través de un proceso de grafting [6] o mediante la post-funcionalización de los grupos

funcionales ya presentes en el material. Estos grupos funcionales pueden ser modificados mediante diferentes reacciones químicas (bromación, sulfonación, aminación, epoxidación, o reacciones de Diels-Alder) obteniéndose así una gran variedad de PMOs [7].

De este modo, según los grupos funcionales presentes, estos materiales tienen una gran aplicabilidad en diferentes campos tales como catálisis [8], cromatografía [9], adsorbentes de contaminantes [10], aplicaciones biomédicas [11] y fotocatálisis [12], entre otras.

2. Contenido de la investigación

La presente Tesis Doctoral engloba la síntesis, caracterización y aplicación de varios organosílices periódicas mesoporosas (PMOs) y su uso como catalizadores en diferentes reacciones químicas.

- En el artículo **"Copper-complexed dipyridyl-pyridazine functionalized periodic mesoporous organosilica as a heterogeneous catalyst for styrene epoxidation"** se ha sintetizado un PMO que posee fragmentos de tipo etileno y vinilo mediante un método de co-condensación entre el precursor disilánico 1,2-bis(trimetoxisilil)etano (BTME) y el precursor monosilánico viniltrietoxisilano (VTES), en una proporción molar del 80 % y 20 %, respectivamente. Los grupos vinilo presentes en el material fueron post-funcionalizados mediante una reacción de Diels-Alder con el compuesto 3-di-2-piridil-1,2,4,5-tetrazina, el cual actúa como dieno. A continuación, los aductos de nitrógeno formados durante la reacción se han utilizado para anclar iones cobre, dando lugar al catalizador denominado Cu@dppz-vPMO. Este nuevo catalizador ha sido utilizado en la reacción de epoxidación de estireno utilizando

terc-butilhidroperóxido (TBHP) como agente oxidante. También, se han optimizado algunas variables que influyen en la reacción, como la relación molar entre estireno y TBHP, el disolvente utilizado, el oxidante, y la temperatura de reacción.

- En el artículo **"Cobaloxime tethered pyridine-functionalized ethylene-bridged periodic mesoporous organosilica as an efficient HER catalyst"** se ha sintetizado un PMO que posee fragmentos de tipo etileno y unidades de piridina colgantes mediante el método de co-condensación entre los precursores silánicos 1,2-bis(trietoxisilil)etano y 2-(4-piridiletil)trietoxisilano, en una proporción molar del 80 % y 20 %, respectivamente. Sobre las unidades de piridina colgantes se ha formado un complejo tipo cobaloxima, disponiendo así de un nuevo catalizador heterogéneo. Dicho catalizador ha sido utilizado en la reacción fotocatalítica de producción de hidrógeno a partir de la ruptura de la molécula de agua ("*water splitting*") usando trietanolamina (TEOA) y eosin Y como agente donador de electrones y fotosensibilizador, respectivamente.

- En el capítulo "**Catalytic activity of cobaloxime complexes anchored to organosilicas in artificial photosynthesis: ordered vs. non-ordered materials**" se ha realizado la síntesis de una serie de materiales organosílicos usando 1,2-bis(trietoxisilil)etano y 2-(4-piridiletil)trietoxisilano como precursores silánicos. Se han modificado algunas variables experimentales que influyen en el proceso de síntesis como la relación molar entre los precursores silánicos, el tipo de surfactante (OTAB o CTAB), y la naturaleza del medio básico de reacción (NaOH o NH_3). De la modificación de todos estos parámetros que influyen en el ordenamiento del material, se han podido sintetizar tres organosílices mesoporosas con estructura ordenada y tres organosílices con estructura no

ordenada. A todos los materiales sintetizados se les ha incorporado el complejo de tipo cobaloxima para poder ser utilizados como catalizadores en la obtención de hidrógeno a partir de la ruptura fotocatalítica de la molécula de agua ("*water splitting*"). Durante todo este trabajo se ha puesto especial énfasis en destacar la importancia de las condiciones de síntesis de los materiales organosilícicos, ya que influyen de manera decisiva en el ordenamiento estructural y, por lo tanto, en sus posteriores propiedades catalíticas.

- En el artículo **"Improved photocatalytic H_2 evolution by cobaloxime-tehered imidazole-functionalized periodic mesoporous organosilica"** se ha realizado la síntesis de un catalizador de tipo PMO al que se le han incorporado unidades de cobaloxima sobre los grupos imidazol presentes en la estructura del material. Dicho catalizador ha sido usado en la reducción fotocatalítica del agua a hidrógeno. Los resultados catalíticos obtenidos han sido comparados con el mismo catalizador en fase homogénea. Se ha evidenciado que la inmovilización del complejo sobre una organosílice porosa aumenta la actividad catalítica del mismo.

- En el artículo **"Solar driven CO_2 reduction with a molecularly engineered periodic mesoporous organosilica containing cobalt phthalocyanine"** se ha realizado por primera vez y de manera eficaz la síntesis de un PMO a través de la co-condensación de un nuevo precursor silánico con puentes de ftalocianina de cobalto, CoPc(NCO), con 1,2-bis(trietoxisilil)etano. El PMO resultante se ha caracterizado con varias técnicas en cada etapa de síntesis. Finalmente, el catalizador CoPc-PMO ha sido utilizado en la reacción fotocatalítica de reducción de CO_2 a CO, usando rutenio tris-bipiridina $[Ru(bpy)_3]^{2+}$ como fotosensibilizador, y 1,3-dimetil-2-fenil-2,3-dihidro-1H-

benzo[d]imidazol (BIH) y trietanolamina (TEOA) como sustancias donadoras de electrones.

3. Conclusiones

Las investigaciones realizadas durante esta tesis permiten concluir que la incorporación de diversos complejos metálicos heterocíclicos en la estructura porosa de organosílices periódicas mesoporosas da lugar a la formación de catalizadores heterogéneos activos en diversos procesos, tanto orgánicos como relacionados con la fotosíntesis artificial.

Específicamente, el catalizador Cu@dppz-vPMO sintetizado a través de la modificación superficial de los grupos etileno presentes (reacción de Diels-Alder) y posterior complejación de iones cobre (0.13 mmol/g) es activo en la reacción de oxidación de estireno hacia óxido de estireno. Además del producto deseado, se obtienen productos como acetofenona, benzaldehído y alcohol bencílico. En las condiciones de reacción usadas, esto es, relación molar 1:2 entre el estireno y el TBHP, tolueno como disolvente, y temperatura de 90 ºC, se obtiene una conversión total de estireno del 59.1 % y una selectividad hacia óxido de estireno del 18.8 %. Cuando se optimizan algunas variables que influyen en la reacción como la temperatura, el disolvente utilizado, o la relación entre oxidante y sustrato, aumenta considerablemente la actividad catalítica. De este modo, con una relación 1:4 de estireno y TBHP, tolueno como disolvente y una temperatura de 100 ºC, el catalizador muestra un 86 % de conversión y un 41.9 % de selectividad hacia óxido de estireno. La estabilidad del catalizador es prácticamente constante tras cinco ciclos catalíticos, además de mantenerse una selectividad similar hacia los diferentes productos.

Diferentes catalizadores basados en unidades de cobaloxima inmovilizadas en organosílices mesoporosas ordenadas sintetizados con distintos precursores silánicos han sido utilizados en la reacción fotocatalítica de producción de hidrógeno a partir de la ruptura de la molécula de agua.

La actividad catalítica de los materiales con complejos de tipo cobaloxima unidos a unidades de piridina en la estructura de la organosílice reveló que los catalizadores con estructuras mesoporosas ordenadas (py_xPMO-Co) dan lugar a unos resultados catalíticos muy superiores a los catalizadores no ordenados (py_xOS-Co), obteniéndose una actividad máxima tras las primeras 4 h de reacción (TON= 244). La estabilidad de este catalizador permanece constante al menos durante dos ciclos catalíticos (TON= 222), aunque es necesaria una etapa previa de activación del catalizador.

La actividad catalítica no sólo depende del ordenamiento de la estructura y de la cantidad de centros activos presentes, sino también del tipo de ligando unido al complejo de cobalto. El catalizador homogéneo basado en ligandos de imidazol muestra una actividad catalítica superior al complejo con ligandos piridina (TON de 40 vs 26, respectivamente, tras 2.5 h de reacción). El PMO con ligandos imidazol posee mayor número de unidades de cobaloxima ancladas y da lugar a una mayor producción de hidrógeno. Su mayor actividad es debida al mayor pKa del ligando imidazol con respecto al ligando piridina.

Bajo condiciones óptimas, el PMO con unidades de ftalocianinas integradas en la estructura, el catalizador CoPc-PMO, aplicado en la reacción de fotorreducción de CO_2 muestra un TON de 1972 usando BIH como donador de electrones, siendo una actividad catalítica muy superior a otros sistemas similares. La selectividad hacía el CO se mantiene prácticamente constante alrededor del 65 % después de cuatro ciclos catalíticos.

4. Referencias

[1] S. Inagaki, S. Guan, Y. Fukushima, T. Ohsuna, O. Terasaki, Novel mesoporous materials with a uniform distribution of organic groups and inorganic oxide in their frameworks, J. Am. Chem. Soc. 121 (1999) 9611–9614. https://doi.org/10.1021/ja9916658.

[2] B.J. Melde, B.T. Holland, C.F. Blanford, A. Stein, Mesoporous sieves with unified hybrid inorganic/organic frameworks, Chem. Mater. 11 (1999) 3302–3308. https://doi.org/10.1021/cm9903935.

[3] T. Asefa, M.J. MacLachlan, N. Coombs, G.A. Ozin, Periodic mesoporous organosilicas with organic groups inside the channel walls, Nature. 402 (1999) 867–871. https://doi.org/10.1038/47229.

[4] A. Stein, Advances in microporous and mesoporous solids - Highlights of recent progress, Adv. Mater. 15 (2003) 763–775. https://doi.org/10.1002/adma.200300007.

[5] F. Hoffmann, M. Cornelius, J. Morell, M. Fröba, Periodic Mesoporous Organosilicas (PMOs): Past, Present, and Future, J. Nanosci. Nanotechnol. 6 (2006) 265–288. https://doi.org/10.1166/jnn.2006.902.

[6] T. Asefa, Z. Tao, Mesoporous silica and organosilica materials — Review of their synthesis and organic functionalization, Can. J. Chem. 90 (2012) 1015–1031. https://doi.org/10.1139/v2012-094.

[7] P. Van Der Voort, D. Esquivel, E. De Canck, F. Goethals, I. Van Driessche, F.J. Romero-Salguero, Periodic Mesoporous Organosilicas: from simple to complex bridges; a comprehensive overview of functions, morphologies and applications, Chem. Soc. Rev. 42 (2013) 3913–3955. https://doi.org/10.1039/C2CS35222B.

[8] D. Esquivel, E. Canck, C. Jimenez-Sanchidrian, P. Voort, F. Romero-Salguero, Periodic Mesoporous Organosilicas as Catalysts for Organic Reactions, Curr. Org. Chem. 18 (2014) 1280–1295. https://doi.org/10.2174/13852728196661404242043 23.

[9] T. Chen, X. Yang, S. Wang, G. Song, H. Zhou, W. Shen, L. Gao, A new ionic liquid bridged periodic mesoporous organosilicas stationary phase for per aqueous liquid chromatography and its application in the detection of biogenic amines, Talanta. 235 (2021) 122795. https://doi.org/10.1016/j.talanta.2021.122795.

[10] A. Modak, P. Bhanja, M. Selvaraj, A. Bhaumik, Functionalized porous organic materials as efficient media for the adsorptive removal of Hg(ii) ions, Environ. Sci. Nano. 7 (2020) 2887–2923. https://doi.org/10.1039/D0EN00714E.

[11] M.A. Wahab, J.N. Beltramini, Recent advances in hybrid periodic mesostructured organosilica materials: opportunities from fundamental to biomedical applications, RSC Adv. 5 (2015) 79129–79151. https://doi.org/10.1039/C5RA10062C.

[12] Y. Wang, N. Homs, P. Ramírez de la Piscina, Ti-containing hybrid mesoporous organosilicas as photocatalysts for H_2 production from ethanol, J. Mater. Res. Technol. 14 (2021) 2115–2123. https://doi.org/10.1016/j.jmrt.2021.07.104.

SUMMARY OF THE DOCTORAL THESIS "SYNTHESIS AND CHARACTERIZATION OF ORGANIC-INORGANIC MESOPOROUS HYBIRD MATERIALS FOR THEIR APPLICATION IN CATALYTIC PROCESSES"

1. Introduction or motivation of the Doctoral Thesis

Since their discovery in 1999 [1–3], ordered mesoporous organic-inorganic hybrid materials (PMOs) have had a major impact on the scientific community, because the same material has the advantages that provide organic chemistry, regarding the introduction of different functional groups, with the thermal stability of inorganic substrates.

The synthesis of these types of materials are carried out through hydrolysis and condensation processes of different silane precursors in the presence of a structure directing agent (SDA) in acid or basic media. In general way, the disilane precursors with bridged organic groups of the type $(R'O)_3SiRSi(OR')_3$ are mixed with trialkoxyorganosilanes of the type $(R'O)_3SiR$ [4].

One of the most remarkable characteristics of PMOs is that the organic groups (R) are located on the pore walls, that is, functional groups are part of the material structure, and they are homogeneously distributed in all the silica framework. Furthermore, these materials have high surface areas (up to 1200 m^2/g), thick pore walls and large pore volumes. Their physicochemical properties, such as flexibility or hydrophobicity, can be modulated and, in addition, they have a higher hydrothermal and mechanical stability than conventional silicas [5].

On the other hand, new organic groups can be introduced via grafting processes [6] or via post-functionalization of functional groups already present in the material. These functional groups can be modified through different chemical

reactions (bromination, sulfonation, amination, epoxidation, Diels-Alder reactions…), resulting in a huge variety of PMOs.

In this way, depending on the functional groups present in these materials, they will be applied in different fields such as, catalysis [8], chromatography [9], pollutant adsorption [10], biomedical applications [11], and photocatalysis [12], among others.

2. Research content

The present Doctoral Thesis encloses synthesis, characterization and applications of several periodic mesoporous organosilicas (PMOs) and their use as catalysts in different reactions.

- In the article **"Copper-complexed dipyridyl-pyridazine functionalized periodic mesoporous organosilica as a heterogeneous catalyst for styrene epoxidation",** a PMO with ethane and vinyl groups has been synthesized through a co-condensation method between the disilane 1,2-bis(trimethoxysilyl)ethane (BTME) and the monosilane vinyltriethoxysilane (VTES) in a molar ratio of 80 % and 20 %, respectively. The vinyl groups present in the material have been post-functionalized through a Diels-Alder reaction with 3,6-di-2-pyridyl-1,2,4,5-tetrazine, which acts as diene. Then, the surface adducts formed during reaction have been used to complex copper ions, resulting the catalyst Cu@dppz-vPMO. This new catalyst has been used in the styrene epoxidation reaction with tert-butyl hydroperoxide (TBHP) as oxidant agent. Also, some reaction variables have been optimized, such as the molar ratio of styrene to TBHP, the solvent, the oxidant and the reaction temperature.

- In the article **"Cobaloxime tethered pyridine-functionalized ethylene-bridged periodic mesoporous organosilica as an efficient HER catalyst",** an ethylene-bridged PMO containing pyridine moieties has been synthesized through a co-condensation method between the silane precursors 1,2-bis(triethoxysilyl)ethane and 2-(4-pyridylethyl)triethoxysilane in a molar ratio of 80 % and 20 %, respectively. A cobaloxime complex has been anchored on the pyridine groups to form the corresponding heterogeneous catalyst. The aforementioned catalyst has been used in photocatalytic water splitting for hydrogen production using triethanolamine (TEOA) and eosin Y as electron donor and photosensitizer, respectively.

- In the chapter **"Catalytic activity of cobaloxime complexes anchored to organosilicas in artificial photosynthesis: ordered vs. non-ordered materials",** several organosilane materials have been synthesized using 1,2-bis(triethoxysilyl)ethane and 2-(4-pyridylethyl)triethoxysilane as silane precursors. Different experimental variables such as the molar ratio between the silane precursors, the type of surfactant (OTAB or CTAB) and the nature of the basic media (NaOH or NH_3) have been modified. As a result, three ordered organosilicas and three non-ordered organosilicas could be synthesized. A cobaloxime complex has been anchored to all synthesized materials in order to be used as catalysts in photocatalytic hydrogen production from water. Throughout this research, special emphasis has been placed on highlighting the importance of the synthesis conditions, since they play an important role in their ordering and, therefore, in their subsequent catalytic properties.

- In the article **"Improved photocatalytic H_2 evolution by cobaloxime-tethered imidazole-functionalized periodic mesoporous organosilica",** a catalyst based on a PMO has been synthesized incorporating cobaloxime units on the imidazole groups present in the material. The aforementioned catalyst has been used in photocatalytic hydrogen production from water. The catalytic results obtained have been compared with the homogeneous complex. It has been observed that the immobilization of the complex on a porous organosilica increases the catalytic activity.

- In the article **"Solar driven CO_2 reduction with a molecularly engineered periodic mesoporous organosilica containing cobalt phthalocyanine",** the synthesis of a PMO incorporating a cobalt phthalocyanine silane derivative CoPc(NCO) and 1,2-bis(triethoxysilyl)ethane has been carried out for the first time and in an effective way. The resulting PMO has been characterized with different techniques at each stage of synthesis. Finally, the CoPc-PMO catalyst has been used in the photocatalytic CO_2 reduction using ruthenium tris(bipyridine) $[Ru(bpy)_3]^{2+}$ as photosensitizer, and 1,3-dimethyl-2-phenyl-2,3-dihydro-1H-benzo[d]imidazole (BIH) and triethanolamine (TEOA) as electron donors.

3. Conclusions

The investigations carried out during this Thesis lead to the conclusion that the incorporation of various heterocyclic metal complexes into the porous structure of periodic mesoporous organosilicas allows obtaining a variety of heterogeneous catalysts active in a various process, both organic and related to artificial photosynthesis.

Specifically, Cu@dppz-vPMO catalyst has been synthesized through surface modification of its vinyl groups through a Diels-Alder reaction and subsequent complexation of copper ions (0.13 mmol/g). This material has been active in the styrene oxidation reaction to form styrene oxide. Besides the desired product, the reaction also produces acetophenone, benzaldehyde and benzyl alcohol. Under the reaction conditions used, i.e., a molar ratio of 1:2 between styrene and TBHP, toluene as solvent and 90 ºC of temperature, a total conversion of 59.1 % and selectivity towards styrene oxide of 18.8 % have been obtained. When some reaction variables are optimized, such as temperature, solvent or molar ratio between oxidant and reactant, the catalytic activity substantially increases. In such a way, with a 1:4 molar ratio of styrene:TBHP, toluene as solvent and 100 ºC of temperature, the catalyst shows an 86 % of conversion and 41.9 % of selectivity. The activity of the catalyst remains almost constant after five catalytic cycles, including the selectivity towards to different products.

Different catalysts based on cobaloxime units immobilized in ordered mesoporous organosilicas have been synthesized and used in the photocatalytic hydrogen production from water.

The catalytic activity of molecular cobaloxime catalysts attached on pyridine units in the organosilica structure has revealed that the performance of catalysts with ordered structures (py_xPMO-Co) is higher than that of non-ordered catalysts (py_xOSCo), obtaining a maximum activity after 4 h of reaction (TON= 244). Additionally, the catalysts maintained their stability at least during two catalytic cycles (TON= 222), after a previous activation process.

The catalytic activity of cobaloximes not only depends on structure ordering and the number of active sites present but also on the type of ligand bound to the cobalt complex. A homogeneous catalyst based on imidazole ligands shows a higher catalytic activity than that with pyridine ligands (TON of 40 vs

26, respectively, at 2.5 h). Thus, a PMO with imidazole units has presented a higher concentration of complexed cobaloximes and, consequently, it exhibits a larger hydrogen production. Its increased activity is due to the higher pKa of imidazole than that of pyridine.

Under optimal conditions, a PMO with phthalocyanine units integrated in its framework, CoPc-PMO, was active as catalyst in the photoreduction of CO_2 with a TON of 1972, using BIH as electron donor. It has a much better performance than similar systems previously reported. CO selectivity is maintained at ca. 65 % throughout all four catalytic cycles.

4. References

[1] S. Inagaki, S. Guan, Y. Fukushima, T. Ohsuna, O. Terasaki, Novel mesoporous materials with a uniform distribution of organic groups and inorganic oxide in their frameworks, J. Am. Chem. Soc. 121 (1999) 9611–9614. https://doi.org/10.1021/ja9916658.

[2] B.J. Melde, B.T. Holland, C.F. Blanford, A. Stein, Mesoporous sieves with unified hybrid inorganic/organic frameworks, Chem. Mater. 11 (1999) 3302–3308. https://doi.org/10.1021/cm9903935.

[3] T. Asefa, M.J. MacLachlan, N. Coombs, G.A. Ozin, Periodic mesoporous organosilicas with organic groups inside the channel walls, Nature. 402 (1999) 867–871. https://doi.org/10.1038/47229.

[4] A. Stein, Advances in microporous and mesoporous solids - Highlights of recent progress, Adv. Mater. 15 (2003) 763–775. https://doi.org/10.1002/adma.200300007.

[5] F. Hoffmann, M. Cornelius, J. Morell, M. Fröba, Periodic Mesoporous Organosilicas (PMOs): Past, Present, and Future, J. Nanosci. Nanotechnol. 6 (2006) 265–288. https://doi.org/10.1166/jnn.2006.902.

[6] T. Asefa, Z. Tao, Mesoporous silica and organosilica materials — Review of their synthesis and organic functionalization, Can. J. Chem. 90 (2012) 1015–1031. https://doi.org/10.1139/v2012-094.

[7] P. Van Der Voort, D. Esquivel, E. De Canck, F. Goethals, I. Van Driessche, F.J. Romero-Salguero, Periodic Mesoporous Organosilicas: from simple to complex bridges; a comprehensive overview of functions, morphologies and applications, Chem. Soc. Rev. 42 (2013) 3913–3955. https://doi.org/10.1039/C2CS35222B.

[8] D. Esquivel, E. Canck, C. Jimenez-Sanchidrian, P. Voort, F. Romero-Salguero, Periodic Mesoporous Organosilicas as Catalysts for Organic Reactions, Curr. Org. Chem. 18 (2014) 1280–1295. https://doi.org/10.2174/13852728196661404242043 23.

[9] T. Chen, X. Yang, S. Wang, G. Song, H. Zhou, W. Shen, L. Gao, A new ionic liquid bridged periodic mesoporous organosilicas stationary phase for per aqueous liquid chromatography and its application in the detection of biogenic amines, Talanta. 235 (2021) 122795. https://doi.org/10.1016/j.talanta.2021.122795.

[10] A. Modak, P. Bhanja, M. Selvaraj, A. Bhaumik, Functionalized porous organic materials as efficient media for the adsorptive removal of Hg(ii) ions, Environ. Sci. Nano. 7 (2020) 2887–2923. https://doi.org/10.1039/D0EN00714E.

[11] M.A. Wahab, J.N. Beltramini, Recent advances in hybrid periodic mesostructured organosilica materials: opportunities from fundamental to biomedical applications, RSC Adv. 5 (2015) 79129–79151. https://doi.org/10.1039/C5RA10062C.

[12] Y. Wang, N. Homs, P. Ramírez de la Piscina, Ti-containing hybrid mesoporous organosilicas as photocatalysts for H_2 production from ethanol, J. Mater. Res. Technol. 14 (2021) 2115–2123. https://doi.org/10.1016/j.jmrt.2021.07.104.

CAPÍTULO 1.

INTRODUCCIÓN

INDICE

CAPITULO 1. INTRODUCCIÓN

Durante las últimas décadas, el campo de la nanotecnología ha motivado a los investigadores a estudiar la aplicabilidad de los materiales nanoestructurados en una amplia variedad de aplicaciones. Dentro esta familia, los materiales porosos atraen un gran interés como adsorbentes y catalizadores. Según la IUPAC, los materiales porosos se pueden clasificar en función del tamaño de poro en: microporosos (< 2nm), mesoporosos (entre 2 - 50 nm) y macroporosos (> 50nm) [1].

1.1 SÓLIDOS MICROPOROSOS (ZEOLITAS)

Los materiales microporosos engloban sólidos desde la sílice amorfa hasta sólidos cristalinos como las zeolitas [2]. Las zeolitas son aluminosilicatos cristalinos donde la carga negativa de la red se compensa con contraiones alcalinotérreos (Na^+, K^+ o Ca^{2+}). Las propiedades más importantes que destacan en estos materiales son:

- Elevada superficie específica y alta capacidad de adsorción.

- Capacidad de incorporar en la estructura diferentes especies metálicas.

- Control de su capacidad de adsorción, a través del carácter hidrófobo o hidrófilo de los componentes.

- El tamaño específico de los poros permiten que estos materiales puedan reconocer moléculas y puedan ser utilizados para aumentar la selectividad hacía un determinado producto.

Debido a estas propiedades, estos materiales muestran una alta aplicabilidad como adsorbentes o tamices moleculares. De ahí las razones para que se utilizan a escala industrial en la separación de hidrocarburos no lineales [3], eliminación de metales pesados [4], procesos de reducción [5], adsorción [6] y separación de gases [7], entre otras. A pesar de la gran aplicabilidad de estos materiales microporosos, uno de los principales inconvenientes que presentan es su pequeño tamaño de poro, el cual impide la adsorción de moléculas voluminosas.

1.2 SÓLIDOS MESOPOROSOS ORDENADOS

1.2.1 MATERIALES M41s

En 1988, Kato y col. [8] publicaron la síntesis de un material mesoporoso con distribución de poros uniforme y gran superficie específica. Este material mesoporoso estaba sintetizado a partir de un polisilicato llamado kanemita [$NaHSi_2O_5$-$3H_2O$] en presencia de un surfactante de tipo alquiltrimetilamonio. Estos materiales fueron generalmente denominados FSM-16 (*Folded Sheet Mesoporous Materials*). A pesar de que estos materiales constituyeron los primeros sólidos mesoporosos, no es hasta Octubre de 1992 cuando investigadores de la corporación "*Mobil Oil Research & Development*" publicaron la síntesis de los considerados primeros materiales mesoporosos ordenados, los denominados generalmente M41s. Los materiales M41s según su estructura, pueden clasificarse en materiales con simetría hexagonal *p6mm* (MCM-41), cúbica *Ia3d* (MCM-48) [9] o laminar *p2* (MCM-50) (Figura 1).

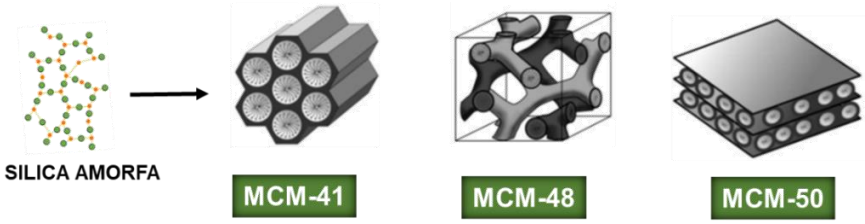

Figura 1. Estructuras de la familia de materiales mesoporosos ordenados M41s [2].

La fase hexagonal (MCM-41) es la fase más estable y común a concentraciones bajas de surfactante o agente director de la estructura. Esta estructura consiste en un empaquetamiento hexagonal de canales monodireccionales. La fase cúbica (MCM-48) es metaestable, por lo que es más complicada de formarse. Su estructura está formada por dos sistemas de canales tridimensionales independientes que se acoplan uno a otro formando una estructura cúbica. Por último, la fase laminar (MCM-50) se favorece cuando hay altas concentraciones de surfactante en la que se forma un apilamiento laminar de los mesoporos.

Entre las principales características de los materiales M41s destacan: su fácil síntesis, estructuras ordenadas con canales uniformes y distribución estrecha de tamaño de poro, y elevadas áreas superficiales (hasta 1200 m^2/g) con volúmenes de poro grandes [10].

Desde su descubrimiento, uno de los aspectos que mayor interés ha suscitado ha sido conocer el procedimiento por el cual las micelas del surfactante se van agregando para dar lugar a la estructura final. En este sentido, los investigadores de la Mobil Corporation [11] propusieron dos posibles mecanismos que explicaran su formación (Figura 2). Ambos presuponen la formación de la denominada estructura de cristal líquido (liquid-crystal

templating, LCT) de surfactante, bajo unas determinadas condiciones de temperatura y concentración.

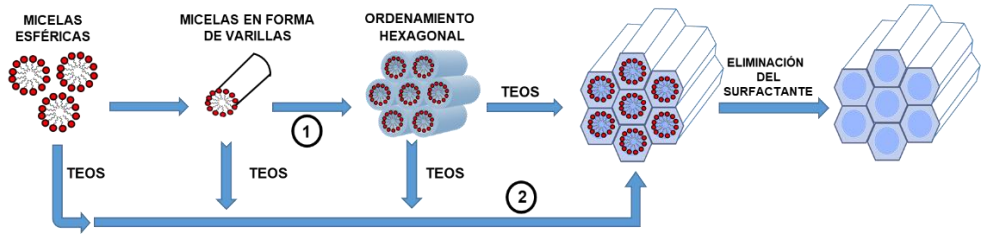

Figura 2. Representación esquemática de los dos posibles mecanismos de formación de los materiales M41s [11].

El primer mecanismo propuesto (1) sugiere que la formación del cristal líquido se forma antes de la adición de las especies inorgánicas. Para que el mecanismo 1 de formación se vea favorecido la concentración de moléculas de surfactante debe ser suficiente para que se forme la estructura de cristal líquido y, de esta forma, los aniones silicatos sirvan solamente para contrarrestar la carga de los agregados del surfactante. En cambio, en el mecanismo 2, las moléculas de silicato generadas en la mezcla de reacción influyen en el ordenamiento de las micelas de surfactante en la fase de cristal líquido. De este modo, la presencia del anión silicato no sirve solamente para contrarrestar la carga del surfactante sino que participa de forma activa en la formación y ordenamiento de la estructura de cristal líquido [12].

Surfactantes

Sin duda, en la síntesis de estos materiales, las moléculas de surfactante son una pieza clave en la formación de sus mesoestructuras ordenadas mediante sus interacciones con las especies inorgánicas.

Los surfactantes, o también llamados tensioactivos, son compuestos de naturaleza anfifílica cuyas moléculas están formadas por grupos hidrofílicos (cabezas polares) y por grupos hidrofóbicos (colas no polares). Los surfactantes se clasifican según la carga de sus grupos polares en: catiónicos, aniónicos, neutros y zwitteriónicos [13] (Figura 3). Una de las partes más importantes del surfactante es el contraión, el cual compensa la carga del grupo polar manteniendo la carga neutra de la molécula. De esta forma:

1) Los surfactantes aniónicos se disocian en un anión orgánico anfifílico y un catión que suele ser un metal alcalino o aminas protonadas.
2) Los surfactantes catiónicos se disocian en un catión orgánico anfifílico y un anión, siendo normalmente un haluro.
3) Los surfactantes neutros no se ionizan en disolución acuosa ya que poseen grupos hidrófilos tipo fenol, alcohol o amida. Dentro de este grupo se incluyen el polióxido de etileno (PEO) [14-15] o polióxido de propileno (PPO) [16].
4) Los surfactantes tipo zwitteriónicos poseen los grupos cabeza cargados de forma positiva o negativa, dependiendo del pH de la disolución, por lo que pueden actuar como surfactantes aniónicos, catiónicos o neutros [17].

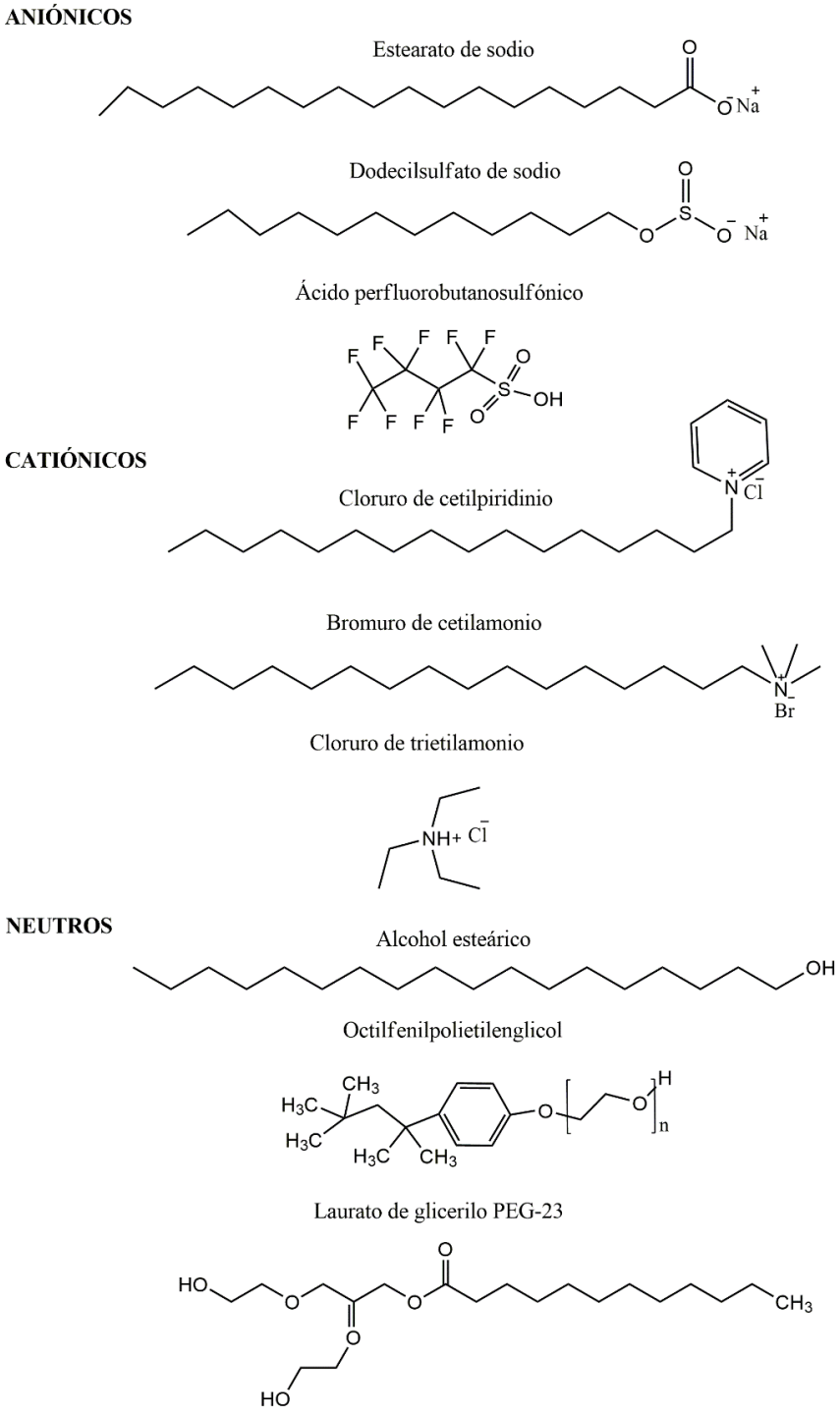

Figura 3. Tipos de surfactantes según la carga de los grupos polares.

Entre las características más relevantes de estos compuestos está su capacidad de autoorganizarse en forma de micelas, en las que los grupos polares y no polares se orientan según la naturaleza del medio en el que se encuentren. De este modo, en disolventes polares como el agua, los grupos hidrofóbicos (colas) están orientados hacia adentro mientras que los grupos hidrofílicos (cabezas) estarán orientados hacia afuera. Este tipo de micelas se llaman micelas normales [18]. Sin embargo, en disolventes apolares, los grupos hidrofóbicos están orientados hacia el exterior, denominándose así micelas inversas (Figura 4) [19].

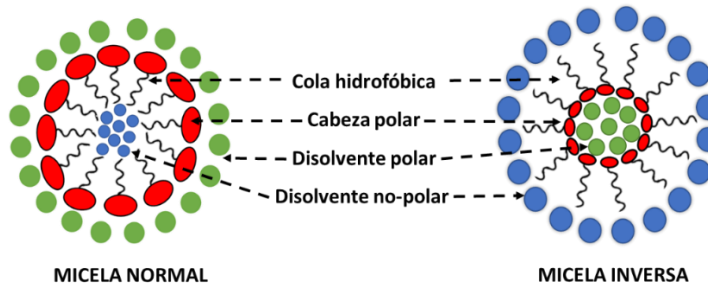

Figura 4. Esquema de una micela normal e inversa [20].

La formación de la mesoestructura de los materiales M41s depende de las interacciones entre las moléculas de surfactante y los silicatos, pudiéndose ser de tipo electrostática, típica de los surfactantes aniónicos y catiónicos, o por puentes de hidrógeno con surfactantes neutros [21].

A pesar de todas las ventajas que tienen los materiales M41s, exhiben baja estabilidad hidrotermal y mecánica debido al escaso grosor de las paredes (0.3 - 1 nm) y tamaño de poros pequeños (2 - 10 nm) [22]. En este sentido, y haciendo uso de surfactantes supramoleculares, surgen una nueva familia de materiales mesoestructurados ordenados con paredes más gruesas y mayores tamaños de poros, los denominados materiales SBA.

1.2.2 MATERIALES SBAs

En 1998, Stucky y col. [23] sintetizaron por primera vez una nueva familia de materiales de sílice mesoporosa altamente ordenados en medio fuertemente ácido mediante el uso de copolímeros de tres bloques no iónicos comercialmente disponibles. Este tipo de sólidos se designaron como materiales SBA (Santa Barbara Amorphous). Algunos materiales de esta familia que han mostrado un gran interés son: las SBA-1 [24], SBA-11 [25] y SBA-16 [21] con estructura cúbica, la SBA-14 [23] con estructura laminar o la SBA-15 [26] con estructura hexagonal, siendo este último el material más estudiado.

La síntesis de estos materiales hace uso principalmente de copolímeros de tres bloques no iónicos ($EO_nPO_mEO_n$), entre los que destacan el copolímero Pluronic P123 ($EO_{20}PO_{70}EO_{20}$) o el copolímero F127 ($EO_{106}PO_{70}EO_{106}$) [27]. En este caso, al ser surfactantes no iónicos, las interacciones entre el surfactante y el precursor silícico son mediante puentes de hidrógeno.

Estos materiales poseen una mayor estabilidad hidrotermal y mecánica que sus antecesores los materiales M41s al tener mayor grosor de pared (3 - 6 nm) y mayor tamaño de poro (5 - 30 nm) [28].

Además, otra ventaja que tiene este tipo de surfactantes es la posibilidad de modificar la mesoestructura final del material variando la longitud de las cadenas del copolímero [29].

1.3 MATERIALES HÍBRIDOS ORGÁNICOS-INORGÁNICOS MESOPOROSOS ORDENADOS

Poco después del descubrimiento de los materiales tipo SBA, numerosos grupos de investigación centraron sus esfuerzos en la incorporación de grupos orgánicos en la estructura de sílice con la idea de lograr una simbiosis de las propiedades de ambos componentes - orgánico e inorgánico - dentro de un mismo material. De ahí surgen, los denominados materiales híbridos orgánico-inorgánicos mesoporosos ordenados, nuevos materiales funcionales con propiedades muy diversas. La combinación de los componentes orgánicos e inorgánicos en un mismo material hace que estos materiales híbridos tengan unas características muy variables, ya que se pueden obtener diversos materiales sólo cambiando los fragmentos orgánicos. Estos, a la vez, tendrán una alta robustez y estabilidad térmica característica de los fragmentos inorgánicos presentes [30].

La síntesis de estos materiales híbridos se lleva a cabo por medio de tres rutas:

1) Modificación post-síntesis de materiales silícicos mediante "grafting"

La incorporación de los grupos orgánicos se realiza por condensación de organosilanos del tipo R-Si(OR')$_3$ con los grupos silanoles ya presentes en la superficie del material de sílice (Figura 5). Este tipo de estrategia trae consigo una serie de ventajas e inconvenientes que se detallan a continuación:

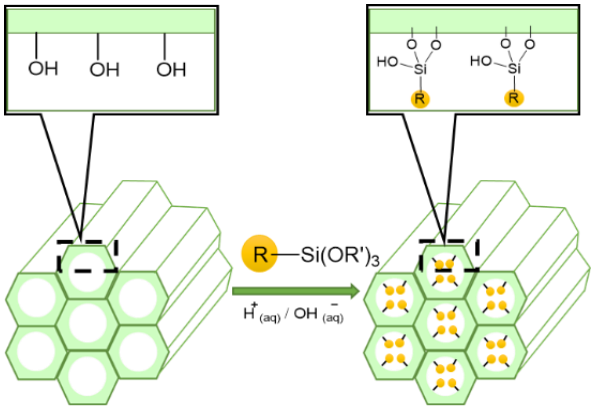

Figura 5. Modificación post-síntesis vía grafting

.

Ventajas

Al ser un proceso de post-funcionalización, la estructura silícica se mantiene después de añadir los grupos orgánicos, sin causar ningún daño. Además, este método puede ser usado como un método de funcionalización selectiva de la superficie externa e interna del material PMO mediante procedimientos secuenciales de grafting, dando así lugar a materiales con doble funcionalidad.

Por último, si se introducen grupos muy voluminosos, el aire del interior de los poros puede quedar confinado dentro, siendo éste un aspecto muy interesante para obtener materiales con baja constante eléctrica [31].

Inconvenientes

Uno de los grandes inconvenientes que tiene este proceso es la homogeneidad, ya que la inmovilización de los grupos orgánicos en la superficie del material depende de la accesibilidad del sistema poroso y de la diferente reactividad que pueda existir entre los grupos silanoles de la superficie y los

grupos organosilícicos añadidos. De este modo, si los silanoles reaccionan en la entrada del poro, la difusión de las moléculas posteriores se verá muy limitada y, por lo tanto, no habrá una disposición homogénea de los grupos orgánicos dentro de los poros.

Otro inconveniente para tener en cuenta es la diferencia de velocidad de condensación del organosilano, ya que podría reaccionar consigo mismo dando lugar a pequeñas cadenas que causarían el bloqueo de los poros.

En resumen, el método de síntesis vía grafting proporciona estructuras ordenadas funcionalizadas, pero con una escasa homogeneidad de los grupos orgánicos en la superficie del material silícico.

2) Método de síntesis directa (co-condensación)

El material híbrido orgánico-inorgánico es sintetizado mediante reacciones de co-condensación entre tetraalcoxisilanos (TEOS o TMOs) y trialcoxiorganosilanos del tipo R-Si(OR')$_3$ [32]. Este proceso, a diferencia del método de grafting, es un método de síntesis directa. Al adicionarse el organosilano durante el proceso de síntesis, el proceso de funcionalización tiene lugar en un único paso (Figura 6).

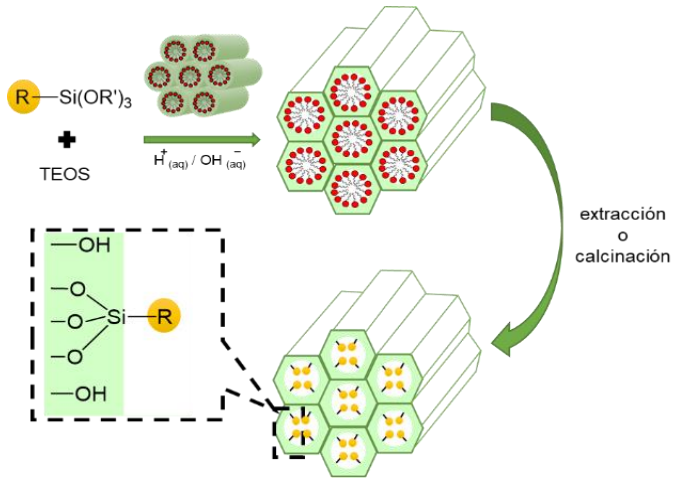

Figura 6. Proceso de co-condensación (síntesis directa).

Ventajas

Este tipo de estrategia da lugar a silicas funcionalizadas tanto en la superficie como en el interior de los poros. Por ello, para lograr estructuras ordenadas, el porcentaje del compuesto trialcoxiorganosilano en el medio de reacción no debe de exceder del 40 % [33].

Inconvenientes

El ordenamiento del material organosilícico disminuye con la concentración de trialcoxiorganosilanos. De este modo, si la concentración es muy alta se pueden llegar a formar materiales sin ordenamiento. Así, el aumento de grupos orgánicos que se incorporan puede influir en las propiedades texturales (área superficial, diámetro de poro y volumen de poro) de los materiales [34,35]. Por otro lado, la cantidad de grupos orgánicos que se introducen en el material es baja en comparación con la concentración de la que se parte al inicio.

3) Síntesis de materiales periódicos mesoporosos organosilícicos (PMOs)

En general, estos materiales se sintetizan vía hidrólisis y condensación de precursores organosilícicos puente en presencia de un agente director de la estructura en un medio básico, ácido o neutro [36,37]. Los precursores silánicos puente son del tipo $R'_3Si\text{-}R\text{-}SiR'_3$ donde R' es el grupo hidrolizable (grupos etoxi- o metoxi- en gran medida) y R es el grupo orgánico. En la Figura 7 se muestra un esquema general de síntesis de un material PMO. En el ejemplo mostrado, los precursores organosilícicos puente se hidrolizan y condensan alrededor de las micelas de surfactante, previamente formadas. A continuación, después de una etapa de envejecimiento, el surfactante es eliminado por métodos de extracción y no de calcinación, obteniéndose finalmente un material con ordenamiento hexagonal y estructura porosa.

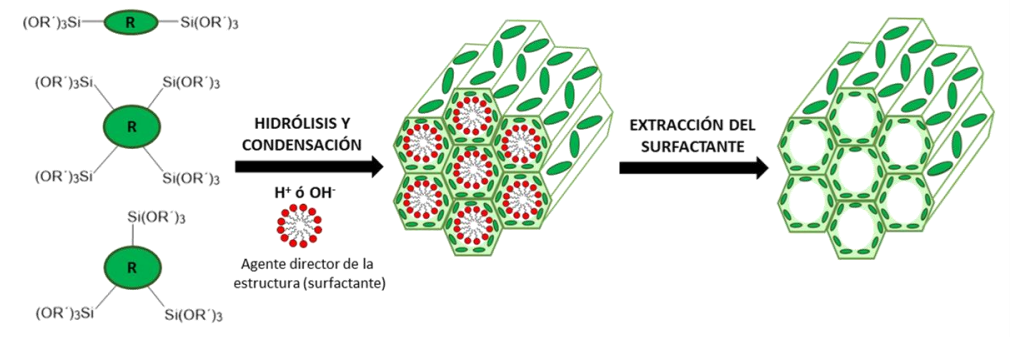

Figura 7. Síntesis de un material periódico mesoporoso organosilícico (PMO) a partir de alcoxisilanos puente con grupos orgánicos.

Una característica única que tienen los materiales PMO es que los grupos orgánicos (-R-) están localizados dentro de la pared del poro y están distribuidos

homogéneamente por la estructura silícica, lo que permite una mayor carga de grupos orgánicos y previene el bloqueo de los poros [38]. A través de su síntesis, se pueden introducir una gran variedad de puentes orgánicos, complejos metálicos o nanopartículas metálicas en los materiales PMO, los cuales modifican sus propiedades fisicoquímicas como flexibilidad, rigidez, hidrofobia, hidrofilia, estabilidad térmica o mecánica, entre otras.

A día de hoy, se ha logrado sintetizar una amplia variedad de PMOs con grupos orgánicos puente de diferente naturaleza: alifáticos, aromáticos, heterocíclicos o incluso quirales, entre otros [38,39].

1.4 PMOs (PERIODIC MESOPOROUS ORGANOSILICAS)

Los materiales periódicos mesoporososos organosilícicos, denominados de forma general por sus siglas, PMOs (*Periodic Mesoporous Organosilicas*), fueron sintetizados por primera vez en 1999 por tres grupos de investigación diferentes. El primer artículo, publicado por Inagaki y col. [40] describió la síntesis de PMOs a partir del precursor disilánico con puentes etano, 1,2-bis(trimetoxisilil)etano (BTME), usando cloruro de octadeciltrimetilamonio como surfactante bajo condiciones básicas. Los materiales PMOs resultantes mostraban estructuras de tipo bidimensional hexagonal (*p6mm*), tridimensional hexagonal (*P63/mmc*) o cúbica (*Pm-3n*). Poco después, Stein y col. [36] publicaron la síntesis de PMOs con puentes etano y eteno, haciendo uso de los precursores 1,2-bis(trietoxisilil)etano (BTEE) y 1,2-bis(trietoxisilil)eteno (BTEENE), respectivamente. En este caso, emplearon bromuro de hexadeciltrimetilamonio como agente director de la estructura bajo condiciones ácidas y básicas. Para el material con puentes etenos, estos autores confirmaron la accesibilidad a dichos compuestos orgánicos y la posibilidad de

funcionalizarlos mediante una reacción de bromación. Por último, Ozin y col. [41] desarrollaron la síntesis de PMOs con estructuras 2D hexagonales, a partir de mezclas de 1,2-bis(trietoxisilil)etano (BTEE) y TEOS, usando bromuro de hexadeciltrimetilamonio bajo condiciones básicas.

1.4.1 PMOs CON GRUPOS ORGÁNICOS SIMPLES

Numerosos factores influyen en la síntesis de los PMOs como son: tipo de surfactante, temperatura de reacción, proceso de extracción, naturaleza del puente silánico, relación entre los precursores silánicos, presencia de aditivos, etc. Entre ellos, la naturaleza del puente orgánico (-R-) influye decisivamente en la estructura del material, así como en las condiciones de síntesis. Aquellos PMOs con grupos orgánicos simples, de menor tamaño molecular, son los materiales conteniendo grupos etilenos (-CH_2-CH_2-), etilidenos (-CH=CH-), metilenos (-CH_2-) o fenilenos (-C_6H_4-). En la Figura 8 se muestran los precursores silícicos con grupos orgánicos puentes más sencillos empleados en la literatura.

1.4.1.1 PMOs con grupos etilenos (etano-PMOs)

Los precursores disilánicos con puentes etilenos son los más utilizados en la síntesis de PMOs, ya sean solos o mezclados con otros precursores organosilánicos. Entre ellos, destacan los precursores organosilícicos comerciales, 1,2-bis(trimetoxisilil)etano (BTME) y 1,2-bis(trietoxisilil)etano (BTEE).

La síntesis de este tipo de PMOs se puede llevar a cabo mediante el uso de una amplia variedad de surfactantes iónicos, no iónicos o mezclas binarias de ellos, entre otros. Los primeros PMOs con puentes etanos fueron sintetizados por Inagaki y col. [40], haciendo uso de un surfactante catiónico (OTAB, bromuro de octadeciltrimetilamonio) y variando la composición molar de la mezcla de

síntesis. Los materiales PMOs obtenidos mostraban simetría 2D-hexagonal (*P6mm*) o 3D-hexagonal ($P6_3/mmc$).

Desde entonces, han sido numerosos los procedimientos de síntesis para la preparación de materiales PMOs con puentes etanos. A partir del amplio estudio de estos materiales, actualmente se conoce que un pequeño cambio en las condiciones de síntesis puede provocar grandes cambios en la estructura final del material sintetizado [42].

Por ejemplo, el pH del medio de reacción influye de manera significativa en las propiedades del PMO. Normalmente, los PMOs son sintetizados en medios ácidos (pH < 1) en los que se usan ácidos fuertes, como, por ejemplo, ácido clorhídrico. Sin embargo, en 2015, Cool y col. [43] investigaron el uso de ácidos más débiles, como es el ácido fosfórico (H_3PO_4), y observaron que los PMOs sintetizados con ácido fosfórico poseían una estructura más ordenada, mayor tamaño de poro y mayor área superficial que los sintetizados con HCl.

El contraión de los surfactantes es otro de los factores que influye significativamente en la morfología y ordenamiento estructural de los PMOs. En medio ácido, se ha observado que, usando el mismo surfactante, pero con diferentes contraiones, se obtienen etano-PMOs con diferente simetría, 2D- o 3D-hexagonal o cúbica. También, Zhao y col. [44] estudiaron la influencia del contraión en medio básico mediante dos métodos, usando directamente surfactantes con diferentes contraiones (CTAX; X= Cl^-, Br^-...) o añadiendo diferentes sales sódicas a la mezcla de reacción.

Por otro lado, la adición de diferentes disolventes orgánicos también juega un papel muy importante en la formación de estructuras con diferentes tamaños de poros, ya que cambian las condiciones osmóticas del sistema. Por ejemplo, Zhao y col. [44] observaron que un aumento en la concentración de etanol en la

síntesis de un PMO usando surfactantes fluorocarbonados e hidrocarbonados conducía a un sistema multivesicular. Más recientemente, Teng y col. [45] describieron un nuevo método de síntesis para la preparación de películas delgadas de PMO con puentes etanos. Este método de síntesis consistía en sumergir el sustrato en una solución que contenía además de BTEE (precursor), CTAB (surfactante) y amoniaco (catalizador), etanol y decano como disolventes.

1.4.1.2 PMOs con grupos etilidenos (eteno-PMOs)

La síntesis de PMOs con grupos etilidenos es de gran interés debido a las múltiples posibilidades de funcionalización de los dobles enlaces de su estructura. Generalmente, el precursor disilánico con puentes etilidenos empleado en la síntesis de los materiales eteno-PMOS es el precursor comercial 1,2-bis(trietoxisilil)etileno (BTEENE) (80 % trans) o el sintetizado, con un 70 % trans, mediante el método descrito por Rzejak y col. [46]. En 2007, Van Der Voort y col. [47] sintetizaron por primera vez un PMO con grupos etilidenos a partir un nuevo precursor sintetizado 100 % E-bis(trietoxisilil)eteno.

Para la síntesis de este tipo de PMOs se ha utilizado una gran variabilidad de surfactantes, tanto de tipo iónicos (CTAB) y oligoméricos (Brij-56 o Brij-76) como poliméricos (P123), en diferentes medios de reacción, tanto ácidos como básicos.

1.4.1.3 PMOs con grupos metilenos (metano-PMOs)

Los precursores silánicos con grupos metilenos de tipo puente son los precursores más simples que pueden ser usados para la síntesis de PMOs. De entre los PMOs con puentes simples, estos PMOs han sido los menos estudiados. Los primeros PMOs sintetizados con 1,2-bis(trietoxisilil)metileno (BTEM) fueron llevados a cabo por el grupo de Ozin y col. [48] usando CTAB en medio básico.

1.4.1.4 PMOs con grupos fenilenos (benceno-PMOs)

El grupo aromático puente más utilizado es el benceno. Una característica resaltable en este tipo de materiales es que poseen un alto ordenamiento no sólo de los poros sino también de los grupos benceno que se encuentran en las paredes de la estructura [49,50]. El primer material PMO con puentes fenilenos fue sintetizado por Inagaki y col. [50] en 2004 a partir del precursor organosilánico 1,3-bis(trietoxisilil)benceno. Este material tenía una estructura no lineal, con un ordenamiento hexagonal y una estructura de tipo "*cristal-like*" de sus puentes orgánicos dentro de las paredes de los poros, mostrando periodicidad a lo largo de la estructura silícica. A partir de esta síntesis, una extensa variedad de benceno-PMOs se han sintetizado variando condiciones experimentales tales como la concentración de surfactante, el medio de reacción (ácido o básico) o la temperatura [51,52]. Así, en 2014, Funari y col. [53] estudiaron la influencia del tamaño del surfactante (polietilenglicol monodecil éter) en el grosor de pared de los benceno-PMOs obtenidos a partir del precursor 1,4-bis(trietoxisilil)benceno (BTEB) bajo condiciones ácidas. Los resultados mostraron que un aumento del grupo de cabeza del surfactante conducía a una disminución del grosor de pared así como del tiempo de formación del PMO.

Más adelante, y con el fin de proporcionar un método de síntesis más eficiente y menos contaminante, Patil y col. [54] emplearon CO_2 comprimido en la síntesis de benceno-PMOs como alternativa al medio ácido, básico o aditivos. El uso de CO_2 comprimido demostró su influencia en la morfología o estructura de los materiales sintetizados.

Otro factor que influye en la morfología y estructura de los PMOs es la interacción del precursor disilánico con el o los surfactantes utilizados. La presencia de poros de diferentes tamaños en un mismo material tiene un gran potencial de aplicación en diferentes campos, tales como la catálisis o la

cromatografía. En este contexto, Wong Chi Man y col. [55] publicaron un método de síntesis capaz de formar PMOs con diferentes tamaños de poro sólo ajustando la secuencia de adición del precursor disilánico (BTEB) y el surfactante (P123). De este modo, la adición del silano a la disolución de P123 dio lugar a la formación de PMOs con la misma porosidad (mesoestructura). Sin embargo, la adición de P123 sobre el organosilano en un intervalo de cinco minutos dio lugar a PMOs con varios tamaños de poro.

Etano-PMOs

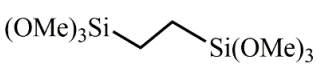

1,2-bis(trimetoxisilil)etano **(BTME)**

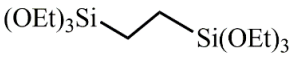

1,2-bis(trietoxisilil)etano **(BTEE)**

Eteno-PMOs

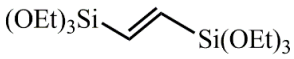

1,2-bis(trietoxisilil)etano **(BTEENE)**

Metano-PMOs

1,2-bis(trietoxisilil)metano **(BTEM)**

Benceno-PMOs

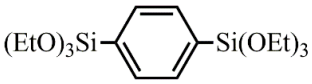

1,4-bis(trietoxisilil)benceno **(BTEM)**

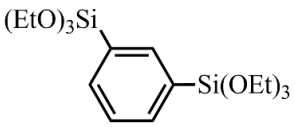

1,3-bis(trietoxisilil)benceno

Figura 8. Resumen de los precursores disilánicos más utilizados.

1.4.2 PMOs CON GRUPOS FUNCIONALES AVANZADOS

Aunque los PMOs con puentes sencillos, previamente descritos, han sido ampliamente estudiados, su superficie relativamente inerte ha limitado su aplicabilidad en otras áreas. Para su uso en otros campos de aplicación, se requiere la incorporación de grupos orgánicos funcionales avanzados. Dichos grupos se

han incorporado exitosamente en un material PMO a través de las estrategias de síntesis que se muestran en la Figura 9.

A) Modificación superficial post-síntesis (grafting)

Este tipo de estrategia requiere dos pasos; un primer paso en el que se realiza la síntesis del material periódico mesoporoso ordenado (PMO), y un segundo que implica una modificación superficial con un precursor organosilano del tipo (R'-Si(OEt)$_3$). A través de este método se obtienen materiales PMO funcionalizados con estructuras altamente ordenadas, pero con una escasa homogeneidad de los grupos orgánicos en la superficie del material.

B) Proceso de co-condensación con un precursor organosilano

Este método implica la adición del precursor organosilano R'-Si(OEt)$_3$ durante el proceso de síntesis del material PMO, por lo que dicho proceso de funcionalización se lleva a cabo en un solo paso. En este método de síntesis, el organosilano interviene de forma activa en el proceso sol-gel del material mesoporoso, por lo que hay que tenerlo en cuenta en el diseño del proceso de síntesis [56]. Ya que la adición del organosilano es antes de la formación del material, los grupos orgánicos están distribuidos homogéneamente por toda la estructura silícica, por lo que la cantidad de grupos orgánicos que se pueden incorporar es mucho mayor que con el método post-síntesis.

C) Proceso de co-condensación con un precursor disilánico

En general, en este tipo de síntesis se utilizan mezclas de precursores del tipo (R'O)$_3$Si-R-Si(OR')$_3$ que se hidrolizan y condensan alrededor de un agente director de la estructura (SDA) en un medio básico o ácido [37,57].

Una característica única que tienen los materiales PMO sintetizados a través de esta ruta es que todos los grupos orgánicos funcionales (R y R'') están localizados en la pared del poro y están distribuidos homogéneamente por la estructura silícica, lo que permite una mayor carga de materia orgánica y una prevención del bloqueo de los poros [38]. Otra ventaja de este tipo de materiales es que con el simple cambio del precursor orgánico utilizado, se pueden sintetizar una gran variedad de materiales con interesantes propiedades electrónicas, ópticas, magnéticas o de transferencia de carga [58,59].

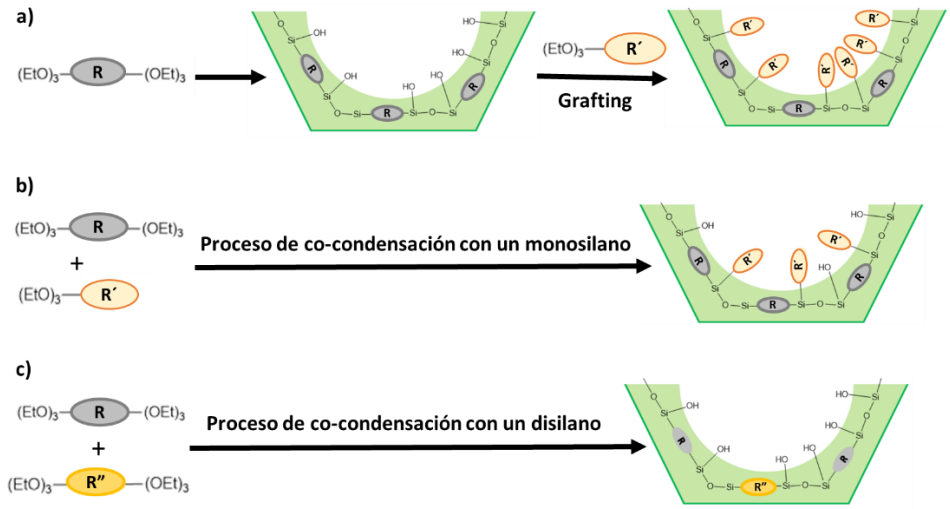

Figura 9. Introducción de nuevos grupos funcionales vía grafting (a), co-condensación con un monosilano (b), y con un disilano (c).

A continuación, se describen algunos de los PMOs con grupos funcionales avanzados sintetizados que han suscitado un mayor interés.

1.4.2.1 PMOs con grupos aromáticos

En 1999, Ozin y col. [60] sintetizaron y optimizaron las condiciones de reacción para la síntesis de PMOs usando los precursores disilánicos con grupos aromáticos, 1,4-bis(trietoxisilil)benceno, 2,5-bis(trietoxisilil)tiofeno, 1,1'-bis(trietoxisilil)ferroceno y 2,8-bis(trietoxisilil)bitiofeno usando CTAB como surfactante en condiciones básicas. Un poco más tarde, este mismo grupo de investigación, haciendo uso de una reacción de Grignard con clorotrietoxisilano, sintetizaron tres nuevos precursores disilánicos con grupos puentes de tolueno, p-xileno y p-dimetoxibenceno [61]. Todos los PMOs sintetizados mostraron ordenamiento hexagonal, con una organización "*cristal-like*" dentro de las paredes de los poros debido a las interacciones π-π, elevadas superficies, y altos volúmenes de poro.

También se han sintetizado PMOs con grupos bifenilos [62] usando 4,4´-bis(trietoxisilil)bifenilo como precursor; con grupos naftaleno [63] con precursores derivados del 2,6-naftaleno; con grupos antracenos [64] usando 2,6-bis(trifluorometanosulfoniloxi)antraceno, o con grupos piridinas [65], y bipiridinas [66] entre otros muchos.

1.4.2.2 PMOs con heteroátomos

El papel de los heteroátomos (N, S, P, O, etc…) en el campo de la química es bastante obvio, ya que pueden ser utilizados en una gran variedad de reacciones químicas [39]. En base a ello, los investigadores han tratado de incorporar este tipo de átomos en la estructura de los materiales PMOs. Las propiedades de los PMOs, tales como, su flexibilidad/rigidez, su hidrofobia/hidrofilia, su reactividad o estabilidad deben de ser tenidas en cuenta a la hora de introducir los nuevos heteroátomos en la estructura [67].

La síntesis de PMOs con precursores organosilánicos conteniendo heteroátomos normalmente hace uso de otros precursores silánicos como el tetraetilortosilicato (TEOS) o tetrametilortosilicato (TMOS) para formar mesofases más rígidas y ordenadas. Precursores organosilánicos con puentes de nitrógeno o azufre se han utilizado exitosamente en la síntesis de PMOs con puentes de azobencenos [68], de diimina/diacetilénicos [69] y de sulfuros [70], entre otros.

Así, en 2001, Gaber y col. [71] sintetizaron un PMO con grupos etano y amino usando como precursores silánicos el 1,2-bis(trietoxisililetano) (BTEE) y el N-(2-aminoetil)-3-aminopropiltrimetoxisilano (AAPTS) bajo condiciones básicas. Estos investigadores concluyeron que un aumento en la concentración de AAPTS en el gel de síntesis producía un descenso del área superficial y del volumen de poro del material PMO resultante. En 2014, Ngamcharussrivichai y col. [72] lograron sintetizar varios PMOs con diferentes cargas de grupos aminos mediante reacciones de co-condensación entre el precursor silánico BTEE y los precursores mono-, di- o tri- organosilánicos con átomos de nitrógeno. Se observó que la morfología del PMO se podía modificar variando la concentración de los precursores en el medio de reacción, obteniéndose esferas a mayores concentraciones del precursor con más grupos aminos. Más recientemente, Van Der Voort y col. [73] han sintetizado PMOs con puentes de dietilentriamina mediante co-condensación de un amino-precursor de cadena larga, (3-trimetoxisililpropil)dietilentriamina (5 % o 10 %), y 1,2-bis(trietoxisilil)etano. Los materiales obtenidos mostraron una elevada capacidad de adsorción de CO_2, así como una elevada actividad catalítica en la reacción de Knoevenagel.

Alternativamente, Kao y col. [74] han llevado a cabo la síntesis de un PMO con grupos puente benceno y grupos fosfato a través de los precursores silánicos 1,4-bis(trietoxisilil)benceno (BTEB) y 3-(trihidroxisilil)propil-metil-

fosfato de amonio (SPMP) usando Brij-S10 como surfactante bajo condiciones ácidas. El PMO resultante fue utilizado como adsorbente de colorantes en aguas residuales.

Por otro lado, la incorporación de grupos sulfuros en las paredes de los PMOs es muy atractiva ya que mejora la selectividad de estos materiales para la absorción de contaminantes. Así, Pérez-Quintanilla y col. [70] sintetizaron un PMO a partir de la co-condensación de bis(trietoxisililpropil)disulfuro (BTSPDS) y 5-mercapto-1-metiltetrazol en medio ácido. Estos autores encontraron que dicho material podía ser empleado como absorbente para la eliminación de Hg^{2+} de aguas potables. Además, estos grupos sulfuros pueden ser oxidados dando lugar a grupos sulfónicos utilizados en catálisis ácida [75]. Romero-Salguero y col. [76] han sintetizado satisfactoriamente un PMO con grupos -SH y $-SO_3$ como catalizador selectivo en la reacción de condensación entre fenol y acetona para dar bisfenol A.

1.4.2.3 PMOs con grupos quirales

Los compuestos quirales son muy importantes para la síntesis de fármacos, compuestos de química fina, vitaminas o la síntesis de materiales con unas propiedades óptimas específicas. Hay diferentes enfoques para obtener compuestos quirales entre los que se incluyen la derivatización química y la catálisis asimétrica. Esta última tiene gran interés debido a la gran variedad de sustratos que pueden ser convertidos con el uso de una pequeña cantidad de catalizadores quirales. La catálisis asimétrica heterogénea tiene ventajas sobre la homogénea debido a su fácil de purificación y separación de los productos sintetizados, además del reciclaje del catalizador [77]. En base a ello, un novedoso enfoque para la síntesis de estos catalizadores, aprovechando la estructura

mesoporosa de los materiales PMOs, es la de introducir estos grupos quirales directamente en los precursores disilánicos durante la propia síntesis del material.

El primer ejemplo de un material PMO quiral fue publicado en 2006 por Polarz y Kuschel [78]. Estos autores partieron del precursor 1,2-bis(trimetoxisilil)eteno y, tras la hidroboración enantioselectiva de los dobles enlaces con un catalizador de Rh con ligando quiral, (R)-(+)-2,2′-bis(difenilfosfino)-1,1′-binaftaleno (Rh-BINAP), obtuvieron el correspondiente precursor organosilánico quiral (Figura 10 a).

Por otro lado, normalmente, la síntesis de otros PMOs quirales requiere reacciones de co-condensación con otros precursores con el fin de obtener estructuras mesoporosas ordenadas. En este sentido, Corma y col. [79] describieron por primera vez la síntesis de un PMO quiral denominado ChiMO (*chiral mesostructured organosilica*) usando precursores bisilánicos de complejos de vanadio (Figura 10 b) con tetraetilortosilicato (TEOS) para la cianosililación asimétrica de benzaldehído.

En 2006, Li y col. [80] describieron la síntesis de varios PMOs conteniendo derivados de trans-(1R,2R)-diaminociclohexano por co-condensación con TMOS usando CTAB como surfactante en medio básico (Figura 10 c y d). Estos catalizadores enantioselectivos fueron utilizados en la hidrogenación asimétrica de diferentes cetonas. Algo más tarde, Gordillo y col. [81] sintetizaron un PMO quiral (ChiMO) usando un precursor disilánico de un derivado del ácido tartárico (Figura 10 e) con TEOS en medio básico y en presencia de CTAB como surfactante.

Más recientemente, y con el objetivo de aumentar el contenido de precursor quiral en los materiales mesoporosos y minimizar a la vez los pasos para su síntesis, ya que anteriormente todos los materiales mesoporosos

sintetizados tenían una carga máxima de 15 % de precursor quiral y su síntesis requería múltiples pasos, Villajos y col. [82] proponen un nuevo método de síntesis en un solo paso de un PMO usando monómeros puramente orgánicos como el 1,2-bis(trietoxisilil)etano y un precursor quiral con grupos tartrato (Figura 10 f). A través de este procedimiento, fue posible la incorporación del 50 % del precursor quiral manteniéndose la estructura ordenada del PMO.

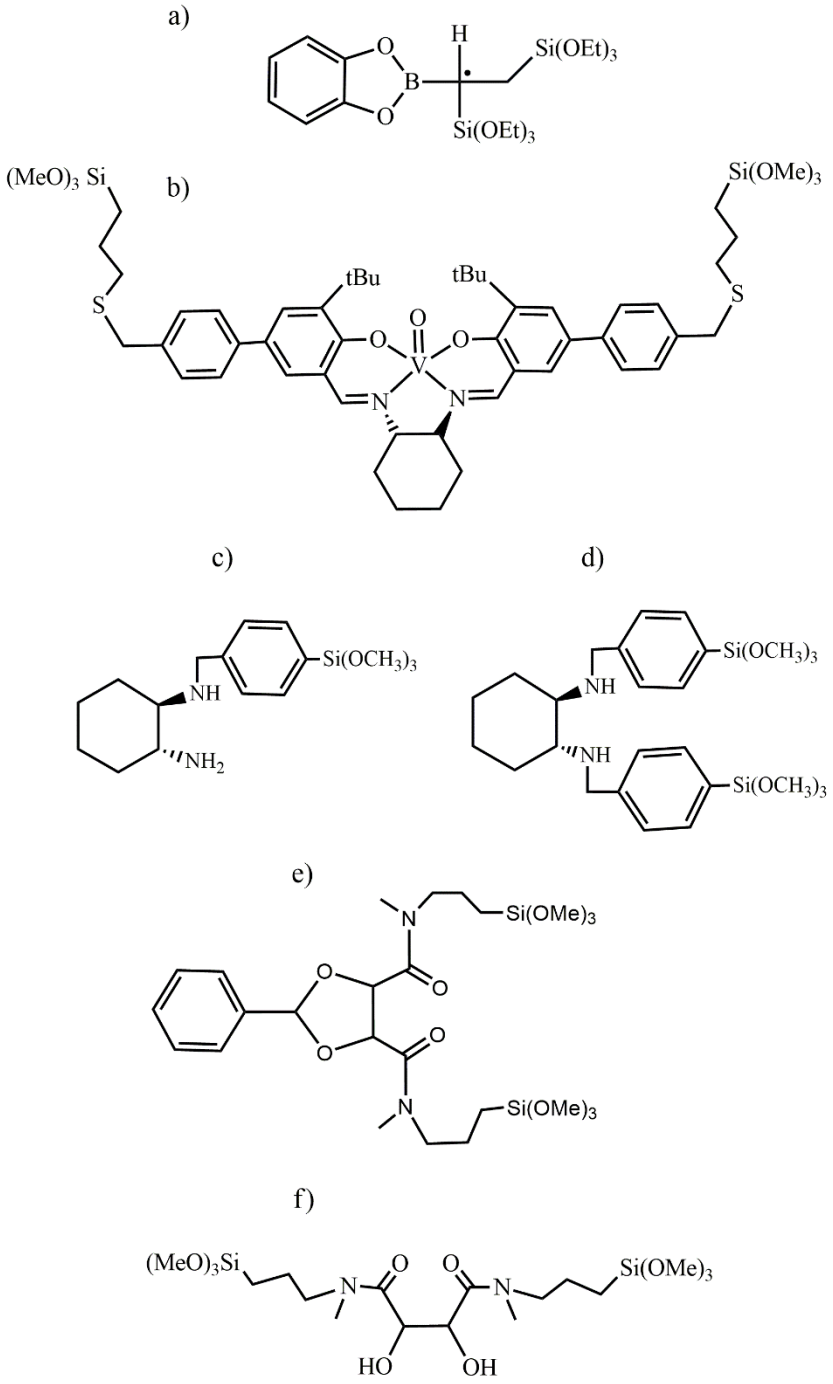

Figura 10. Ejemplos de precursores quirales incorporados en PMOs.

1.4.2.4 PMOs con complejos metálicos

La incorporación de complejos metálicos dentro de la estructura de los materiales PMOs ha atraído un gran interés para su aplicación en el campo de la catálisis. Una gran variedad de metales puede ser incorporados en la estructura del PMO para su posterior uso como catalizadores heterogéneos en reacciones catalíticas. Los centros metálicos se pueden introducir en la estructura del PMO mediante dos métodos: una primera estrategia en la que el metal está ya presente en el precursor silánico empleado en la síntesis del PMO o, una segunda, en el que el anclaje del centro metálico ocurre una vez obtenido el material PMO mediante un proceso de post-síntesis.

Anderson y col. [83] sintetizaron un Cr-PMO para la oxidación de ciclohexano en presencia de H_2O_2 y terc-butilhidroperóxido (TBHP). La selectividad hacía ciclohexanona fue mucho mayor que la obtenida con otros tipos de catalizadores similares basados en cromo. Bhaumik y col. [84] prepararon un nuevo PMO con nanopartículas de Ti (Ti-LHMS) para la oxidación de olefinas. Este catalizador mostró conversiones del 80 % y mantuvo su actividad catalítica durante cinco ciclos de reacción.

Por otro lado, varios autores han sintetizado PMOs a partir de precursores con porfirinas conteniendo metales como Fe, Cu o Sn, para su empleo en reacciones de oxidación de Baeyer-Villiger, reacciones de transferencia de hidrógeno o reacciones de degradación de azul de metileno [85].

1.4.3 POST-FUNCIONALIZACIÓN DE LOS GRUPOS PUENTE PRESENTES EN EL PMO

Como previamente se ha comentado, una de las ventajas que presentan los PMOs es la posibilidad de funcionalizar los grupos orgánicos presentes en su estructura. Los dobles enlaces presentes en los eteno-PMOs son los grupos puentes más propensos a ser convertidos en otros grupos funcionales mediante el empleo de una amplia variedad de reacciones orgánicas. Algunas de estas reacciones también han sido empleadas para la funcionalización de los anillos aromáticos puente de un PMO. A continuación, se explican aquellas reacciones más importantes que se han llevado a cabo para la funcionalización de los grupos puentes presentes en los PMOs (Figura 11).

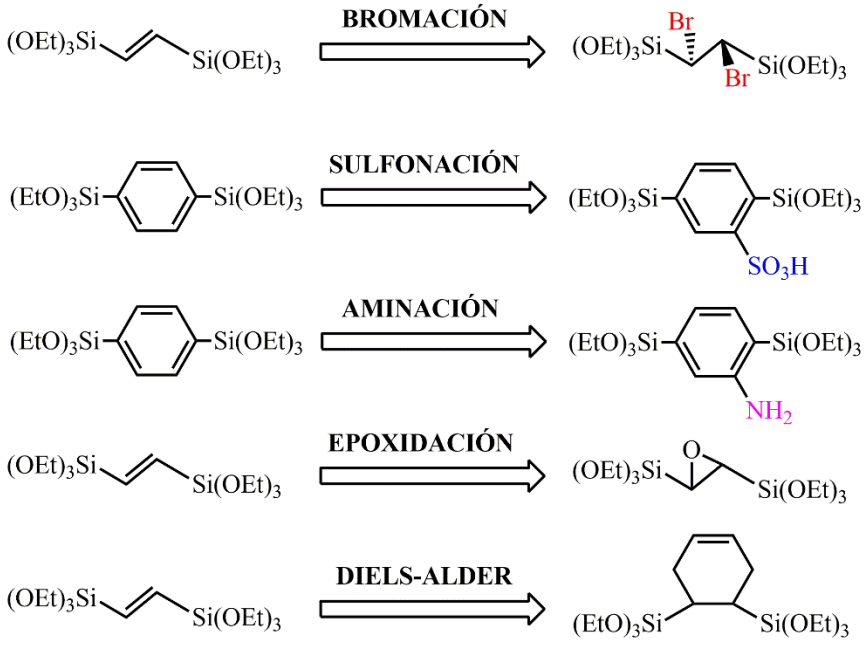

Figura 11. Reacciones de post-funcionalización más utilizadas en PMOs.

- **Bromación**

Es una de las reacciones más comunes para la funcionalización de dobles enlaces. Este tipo de reacción, basada en el ataque de la molécula de bromo sobre el doble enlace, emplea directamente bromo en fase gas o disuelto en algún disolvente clorado. Como ya se ha comentado previamente, la funcionalización de los dobles enlaces presentes en PMOs produce una disminución del área superficial, volumen y diámetro de poro. Este tipo de sustituyente, el bromo, tiene algunas ventajas frente a otros ya que al ser un buen grupo saliente puede ser fácilmente reemplazado a través de una sustitución nucleófila S_N2.

Desde que Stein y col. [36] hicieran uso de esta reacción en 1999 para conocer la accesibilidad de los dobles enlaces, numerosos investigadores se han basado en ella desde entonces. En 2007, Yoshitake y col. [86] usaron etilendiamina (EDA) como nucleófilo para obtener un material con átomos de nitrógeno a partir de un eteno-PMO sustituido por bromación. Otra posibilidad es el uso de reactivos de Grignard para la creación de enlaces C-C no hidrolizables. Siguiendo esta estrategia, Van Der Voort y col. [87] incorporaron grupos tioles sobre un eteno-PMO, previamente funcionalizado con átomos de bromo, usando 3-cloro-1-propanotiol como nucleófilo.

Además de la funcionalización de los dobles enlaces, este tipo de reacción también ha sido empleada en aquellos PMOs con grupos fenilenos. El primer ejemplo de bromación sobre un material benceno-PMO fue descrito por Cool y col. [88] en 2012. Estos investigadores emplearon tres procedimientos de funcionalización: *i)* bromo líquido con $AlCl_3$ como catalizador, *ii)* N-bromosuccinimida (NBS) con azobisisobutironitrilo (AIBN) como radical iniciador, y *iii)* bromato de sodio ($NaBrO_3$) disuelto en ácido sulfúrico, obteniendo para todos ellos una escasa funcionalización. En base a estos resultados, más recientemente, Cool y col. [89] proponen un procedimiento

alternativo a los ya empleados consistente en un primer paso de nitración con HNO_3, seguido de la reducción a anilina, y posterior bromación.

- **Sulfonación**

La incorporación de grupos sulfónicos en la estructura de los PMOs es un tema muy prometedor para su uso como catalizadores ácidos. Hay diferentes estrategias para la incorporación de estos grupos ácidos en los materiales. Estas estrategias incluyen: la sulfonación directa de los grupos fenilos del PMO usando H_2SO_4 como agente oxidante [90], o la oxidación de grupos tioles previamente introducidos mediante diferentes tipos de precursores silánicos. En 2002, Ohsuna y col. [49] realizaron la sulfonación directa sobre un PMO son grupos fenilenos con un gran ordenamiento tanto a escala meso- como a escala molecular. Estos autores, ese mismo año, sintetizaron un benceno-PMO [91] usando además el precursor 3-mercaptopropiltrimetoxisilano (MPTMS), donde los grupos tioles (-SH) introducidos eran oxidados a sulfónicos ($-SO_3H$) con el uso de HNO_3 concentrado a temperatura ambiente durante 24 horas. La caracterización antes y después de la oxidación reveló que las propiedades del PMO no se veían afectadas por el proceso de oxidación.

Por otro lado, en menor medida, los grupos etenos de los PMOs también han sido exitosamente funcionalizados con grupos sulfónicos ácidos. Más concretamente, Van Der Voort y col. [92] mostraron la exitosa sulfonación con ácido clorosulfónico de un PMO con puentes etenos en configuración *trans*-(E-ePMO).

- **Aminación**

En 2008, Inagaki y col. [93] proponen por primera vez la aminación en benceno-PMOs mediante dos pasos, un primer paso de nitración con una mezcla de H_2SO_4/HNO_3 seguida de una reducción con $SnCl_2$ y HCl. Este tipo de

materiales con grupos aminos se ha utilizado recientemente para la adsorción de dióxido de carbono (CO_2) y metano (CH_4) [94].

- **Epoxidación**

La reacción de epoxidación de dobles enlaces en PMOs fue optimizada por Inagaki y col. [95] en 2011 mediante espectroscopia FT-IR. Para ello, el epóxido fue formado por tratamiento del material eteno-PMO con TBHP.

La formación del epóxido y su posterior apertura permite la introducción de grupos alcoholes o aminos. Este tipo de estrategia permite crear materiales bifuncionales muy importantes para la catálisis ácido-básica. Así, Matsuoka y col. [96] siguiendo la estrategia comentada anteriormente, han logrado sintetizar un catalizador con grupos amino y alcoholes para su uso en reacciones tándem de oxidación de alcoholes y en la condensación de Knoevenagel.

- **Reacción de Diels-Alder**

Otra ruta para la modificación de dobles enlaces es la reacción de Diels-Alder. La reacción de Diels-Alder es una reacción de cicloadición [4+2] entre un dieno conjugado y una olefína que actúa como dienófilo, dando lugar a derivados del ciclohexeno. Para que la reacción se lleve a cabo, el dieno tiene que estar en conformación *cis*-, ya que si está en conformación *trans*- la reacción no tiene lugar, debido principalmente a la geometría de la molécula.

Dos rasgos característicos de esta reacción están conectados con el mecanismo; primero se forman dos enlaces de tipo sigma en el transcurso de la reacción, al mismo tiempo que se desvanecen dos enlaces tipo pi, de este modo, la reacción es altamente exotérmica. En segundo lugar, en la mayoría de los casos, la reacción de Diels-Alder sigue las reglas de Woodward-Hoffmann, es decir, transcurre en un solo paso permitido térmicamente [97].

La reacción de Diels-Alder sobre un material eteno-PMO fue llevada a cabo por primera vez por Kondo y col. [98,99] quiénes emplearon benzociclobuteno como dieno en la reacción de Diels-Alder con los puentes etilidénicos de un PMO. Una vez incorporados los anillos aromáticos colgantes en la superficie del PMO, el tratamiento con ácido sulfúrico concentrado permitió la introducción de grupos ácidos sulfónicos superficiales. En 2011, Romero-Salguero y col. [100] ampliaron el uso de la reacción de Diels-Alder para la modificación superficial de PMOs con dobles enlaces usando ciclopentadieno y antraceno como dienos. Se observó que el ordenamiento estructural y la estabilidad térmica de los materiales finales eran similares al material PMO de partida (e-PMO). Más tarde, en años posteriores, estos autores introdujeron compuestos N-heterocíclicos en PMOs con dobles enlaces a través de una reacción de Diels-Alder con derivados del pirrol (pirrol, N-metilpirrol, dimetilpirrol, trimetilpirrol y fenilpirrol) [101].

La incorporación de compuestos N-heterocíclicos sobre la superficie de los materiales PMOs abre una nueva posibilidad para el uso de estos materiales, además de en el campo de la catálisis y adsorción, como soportes para el anclaje de complejos lantánidos muy útiles por sus propiedades luminiscentes. Para ello, Van Der Voort y col. [102] publicaron la síntesis de un eteno-PMO funcionalizado con un derivado de tetrazina (dipiridilpiridazina, Dpdp) como soporte del ión Eu^{+3}. En este caso los dobles enlaces del PMO actúan como dienófilo y el derivado de tetrazina como dieno en la reacción de Diels-Alder. Un poco más tarde, Van Deun y col. [103] extendieron el uso de Dpdp-PMOs para el anclaje de otros lantánidos como el Nd^{+3} y Yd^{+3}.

1.5 APLICACIONES DE LOS PMOs

Los materiales de tipo PMOs, obtenidos a través de las diferentes estrategias sintéticas comentadas anteriormente, se han empleado en una gran variedad de campos, que incluyen catálisis [39], cromatografía [104], adsorción de residuos [105], aplicaciones ópticas [106] o biomédicas [107] y, muy recientemente, la fotocatálisis [108], entre otras muchas.

La introducción de esta Tesis Doctoral se va a centrar principalmente en una de las áreas de aplicación más recientes de estos materiales, la fotocatálisis artificial.

1.5.1 FOTOSÍNTESIS ARTIFICIAL

Satisfacer la creciente demanda de energía mundial, abordando a la misma vez el cambio climático, reduciendo las emisiones de gases que provocan el llamado efecto invernadero y mejorando la calidad del aire, es un desafío fundamental al que la sociedad se enfrenta. Según algunas investigaciones [109], se prevé que para el año 2050 la población mundial se duplique y, por lo tanto, así su demanda energética.

Ya que los problemas de la sociedad están vinculados con los avances científicos, la comunidad científica se enfrenta al desafío de encontrar rutas o métodos de producir energía suficiente, al mismo tiempo de minimizar los impactos negativos sobre el medio ambiente. En la actualidad, la generación de energía es la responsable de dos tercios de las emisiones mundiales de gases que provocan el efecto invernadero. Además, en la última asamblea de la Naciones Unidas sobre el cambio climático celebrada en Sharm El Sheikh (Egipto) (COP27), se puso de manifiesto la necesidad de promover la obtención de nuevas formas de energía respetuosas con el medioambiente.

Dentro de las energías renovables, la energía solar y eólica son las energías limpias con cero residuos y, dado que España es uno de los países con más horas de sol, la primera de ellas es la más idónea para apostar en un futuro próximo. De hecho, una sola hora de energía solar proporciona la misma energía que se consume en un año a nivel mundial [109,110].

Un paso fundamental en el uso de la energía solar es recolectar fotones de alta energía con un absorbente de luz para generar la separación de carga de electrones y huecos. En las celdas fotovoltaicas la energía solar es directamente convertida en electricidad. A pesar de que esta conversión a electricidad es de gran interés, ésta no puede ser almacenada en grandes cantidades y las baterías actuales no tienen la densidad energética suficiente para poder reemplazar completamente a los recursos naturales (carbón, gas natural, petróleo). En este caso, un nuevo enfoque que evitaría los inconvenientes anteriormente citados es la conversión directa de la energía solar en energía química, a través de un proceso similar a la **fotosíntesis natural**.

Durante el proceso de fotosíntesis natural, las plantas convierten la luz solar en energía química absorbiendo los fotones a través del fotosistema II en los cloroplastos, que da lugar a una separación de carga (electrón-hueco) necesario para las reacciones redox. En los huecos se produce el proceso de oxidación, donde el agua se oxida a oxígeno. Los electrones pasan al fotosistema I, a través de reacciones en cadena, para producir moléculas energéticas como el NADPH o el ATP, que serán usados a continuación en el ciclo de Calvin [111] (Figura 12).

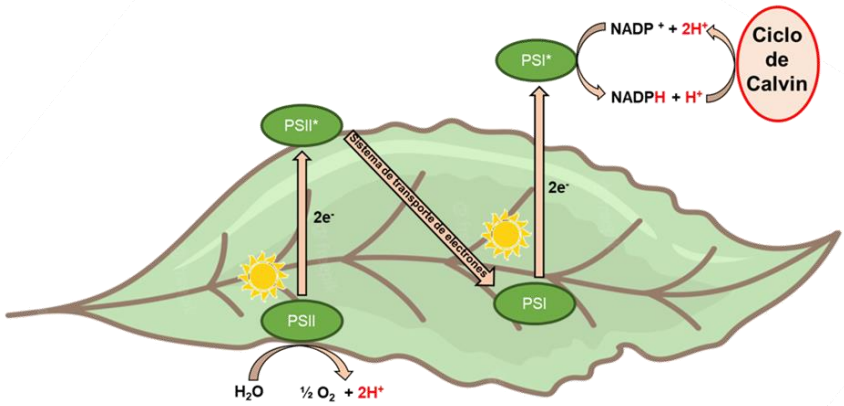

Figura 12. Fotosíntesis natural realizada por plantas.

El proceso de almacenamiento de energía solar en enlaces químicos llevado a cabo de forma natural por la plantas y algunos microorganismos, ha servido como fuente de inspiración a la comunidad científica en el desarrollo de sistemas catalíticos de fotosíntesis artificial [112] para la reducción de dióxido de carbono a metano, metanol, formaldehido y monóxido de carbono, o para la reducción de protones a hidrógeno [113].

Como ya se ha comentado anteriormente, para hacer uso de la energía solar es necesario el empleo de algún material (semiconductor o fotosensibilizador) que sea capaz de captar esa energía (Figura 13). En este caso, los semiconductores tienen las propiedades eléctricas idóneas para capturar los fotones mediante la separación de carga entre sus bandas de valencia y de conducción. Hay algunos semiconductores que después de ser iluminados pueden proporcionar el potencial electroquímico suficiente para dar lugar a la oxidación del agua/ reducción de los protones o la reducción de CO_2 a CO [114]. Así, desde el trabajo pionero de Fujishima y Honda [115], en el año 1972, donde utilizan un fotoánodo de TiO_2 para la rotura fotocatalítica de la molécula de agua ("*water splitting"*) para producir hidrógeno, una gran variedad de semiconductores

(Cu_2O, g-C_3O_4, Fe_2O_3, CdS, MoS_2…) han sido utilizados hasta la actualidad [116–118]. Alternativamente, de forma similar al uso de los semiconductores, los compuestos fotosensibilizadores se pueden utilizar en reacciones fotocatalíticas.

De forma general, un fotosensibilizador absorbe y convierte el fotón incidente en un estado excitado (fotosensibilizador*) que pueda transferir/aceptar un electrón a/desde un aceptor/donador para la creación de estados separados de carga, lo cual genera las fuerzas termodinámicas necesaria para la reducción de protones a hidrógeno o del CO_2 a CO.

Aunque el uso de semiconductores está muy extendido para aplicaciones fotocatalíticas, la introducción de esta tesis se va a centrar en la descripción de sistemas basados en elementos de transición abundantes en la Tierra como el hierro, el cobalto y el níquel, como catalizadores en reacciones fotocatalíticas promovidas por el uso de un fotosensibilizador.

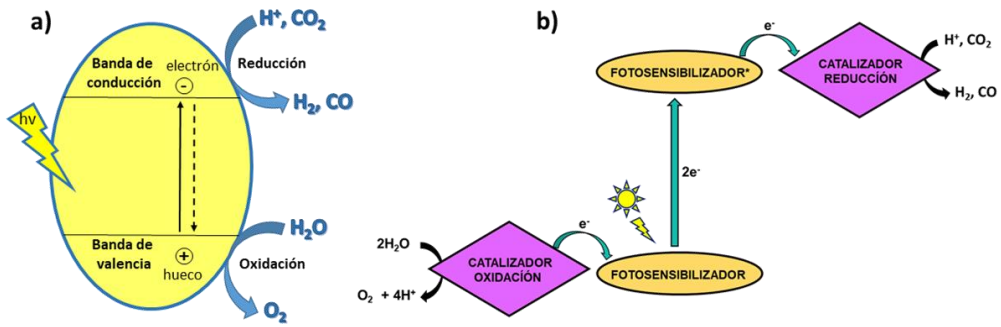

Figura 13. Esquema de un sistema fotocatalítico artificial, usando un semiconductor (**a**) o un fotosensibilizador (**b**).

1.5.1.1 Componentes de un sistema fotocatalítico artificial

Un sistema fotocatalítico artificial está formado principalmente por tres componentes, que deben de poseer unas características determinadas.

- **Sustancia donadora de electrones (*Sacrificial Electron Donor*, SED)**: Sustancia que provee electrones para la reducción de los protones. Se pueden usar compuestos inorgánicos como mezclas de Na_2S/Na_2SO_3 (sobre todo, con semiconductores), o compuestos orgánicos como alcoholes (metanol, etanol…), ácidos (fórmico, acético, dicloroacético, etilendiaminotetraacético EDTA…), aldehídos (formaldehído y acetaldehído) y aminas (trietanolamina TEOA o trietilamina TEA) [119].

- **Fotosensibilizador (*Photosensitizer*, PS)**: La elección del fotosensibilizador es fundamental para la captura de la luz solar y la generación y transferencia de los electrones excitados, el cual puede limitar la actividad catalítica del sistema. Las características fundamentales que debe de poseer un fotosensibilizador son:

    - Amplio rango de absorción, con un alto coeficiente de extinción molar en el rango del visible.

    - Adecuados potenciales redox para la transferencia de electrones del donador de electrones al fotosensibilizador.

    - Largos tiempos de vida en el estado excitado.

    - Alta fotoestabilidad que permita una producción de hidrógeno a largo tiempo.

    - Buena solubilidad en el medio de reacción.

Entre los fotosensibilizadores más utilizados, destacan el rosa de bengala y el eosin Y como compuestos orgánicos, y el $[Ru(bpy)_3]^{2+}$ o $[Ir(bpy)(ppy)_2]^{2+}$ como compuestos organometálicos [119].

- **Catalizador** [119]**:** Las funciones principales que debe de cumplir un catalizador son:

  - Evitar la rápida recombinación entre el electrón y el hueco.
  - Permitir la rápida difusión de los electrones y huecos en la superficie del semiconductor.
  - Poseer un potencial adecuado para la oxidación del agente de sacrificio o la reducción de los protones.
  - Ser fotoactivo bajo la luz solar (en el caso de los semiconductores), que está directamente relacionado con su banda prohibida (*bandgap*).
  - Poseer buena estabilidad química.
  - Ser lo más barato posible.

En la Figura 14 se muestran los fotosensibilizadores, las sustancias donadoras de electrones y catalizadores más utilizados en sistemas fotocatalíticos de producción de hidrógeno y reducción de CO_2.

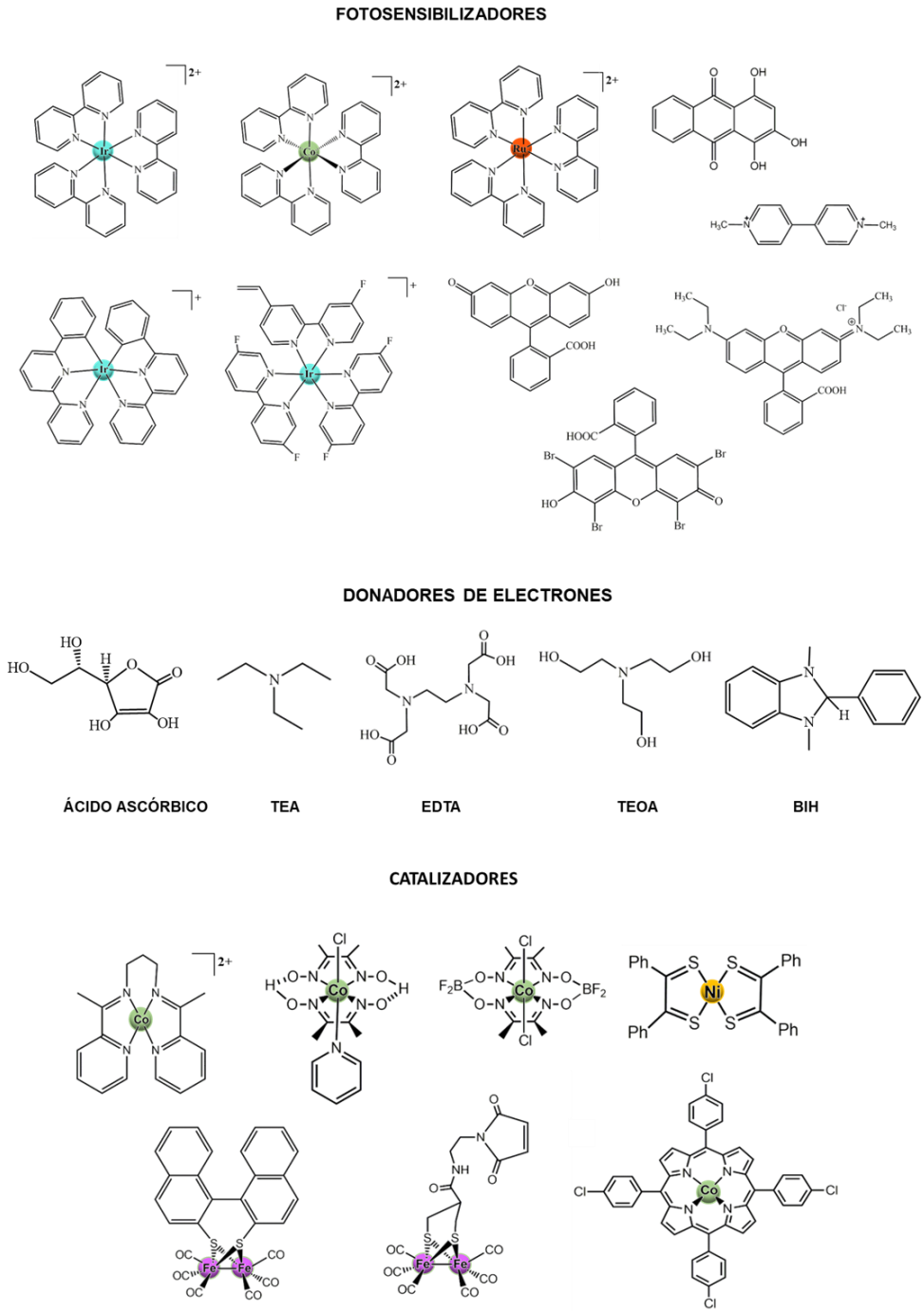

Figura 14. Fotosensibilizadores, donadores de electrones y catalizadores más utilizados en procesos fotocatalíticos de producción de hidrógeno y reducción de CO_2.

1.5.2 REDUCCIÓN DE PROTONES A HIDRÓGENO

Uno de los elementos que están tomando más interés en la actualidad es el **hidrógeno**. El hidrógeno es considerado uno de los mejores vectores energéticos debido a su alta densidad energética (142 kJ g^{-1}), tres veces mayor que la de otros combustibles fósiles. A partir de él se puede obtener energía eléctrica o térmica con altos rendimientos y sin nulas emisiones contaminantes de CO_2, ya que su combustión sólo produce como subproducto vapor de agua.

El gran problema del hidrógeno hasta ahora ha sido su modo de aplicación, que a diferencia de la energía solar o eólica que son fuentes de energía, es decir, se puede obtener energía directamente de ellas, el hidrógeno es un vector energético (cómo una batería) y necesita energía para producir posteriormente más energía. Esto se debe a que el hidrógeno, a pesar de ser el elemento más abundante del universo, menos del 1 % se encuentra presente como hidrógeno molecular. La mayor parte del hidrógeno terrestre se encuentra combinado con otros elementos formando compuestos, tales como agua o hidrocarburos (carbón, gas natural, petróleo…).

Según la fuente de partida de obtención del hidrógeno, se puede clasificar en:

-*Hidrógeno negro,* es el obtenido a partir de fuentes primarias de energía tales como combustibles fósiles (carbón, o petróleo) o de fuentes intermedias como productos de refinería, metanol o amoniaco. Dentro de este grupo está el *hidrógeno gris* procedente del gas natural y obtenido a partir de la técnica de reformado por vapor, y el *hidrógeno marrón* que se genera por la gasificación del carbón.

-*Hidrógeno azul*, es el obtenido a partir de hidrocarburos. Se produce sobre todo en yacimientos de gas natural, y es el más utilizado en la industria debido a sus bajas emisiones contaminantes.

-*Hidrógeno turquesa*, es un término acuñado recientemente por la Asociación Española del Hidrógeno. Es el hidrógeno obtenido a partir del gas natural, pero con la técnica de la pirólisis en la que el carbón que se obtiene está en estado sólido evitando de esta forma las emisiones contaminantes a la atmósfera.

-*Hidrógeno verde*, también conocido como hidrógeno renovable, se produce a partir de fuentes de energía renovables. El método más conocido de producción de hidrógeno verde es la electrólisis del agua, proceso que consiste en la separación de la molécula de agua en sus componentes (hidrógeno y oxígeno) mediante la aplicación de una corriente eléctrica obtenida de fuentes renovables. Este proceso, a pesar de que proporciona cierta esperanza de producir hidrógeno de una manera sostenible, al ser su materia prima, el agua, una fuente de hidrógeno abundante y renovable, requiere de ciertas mejoras tecnológicas y de nuevos electrocatalizadores metálicos sin metales nobles que puedan competir con los tradicionales basados en Pt.

1.5.2.1 Producción de hidrógeno mediante energía solar

Desde 1977 [120], la descomposición exclusivamente fotocatalítica del agua en hidrógeno y oxígeno empieza a ser uno de los métodos más prometedores para conversión y almacenamiento de luz solar, suponiendo una alternativa más barata a la electrólisis del agua con celdas fotoelectroquímicas para la producción de hidrógeno.

De forma artificial, la ruptura de la molécula de agua puede ser representada por dos semirreacciones (Figura 15), una reacción de oxidación para dar oxígeno (**ec.1**) y una reacción de reducción de protones a hidrógeno (**ec.2**). Desde el punto de vista termodinámico, las semirreacciones se dan con un potencial menor a -0.41 V (E H_2O/H_2 con un NHE a pH 7). Sin embargo, estas reacciones están cinéticamente desfavorecidas por lo que es necesario la presencia del correspondiente catalizador. Los complejos con metales de transición pueden albergar electrones a través de varias reacciones redox, lo que los hace unos candidatos idóneos para este tipo de reacciones [121].

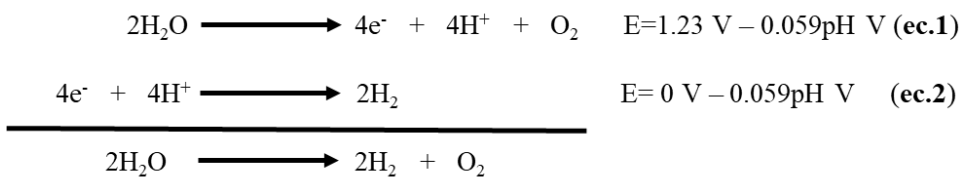

Figura 15. Ruptura de la molécula de agua; oxidación del agua y reducción de los protones. Los potenciales están referidos al electrodo normal de hidrógeno.

Estas reacciones requieren del uso de un fotosensibilizador que recoja la luz incidente y transfiera el equivalente de oxidación/reducción a un catalizador apropiado. Hasta el momento existen más sistemas artificiales que dirijan la reacción de reducción del agua, frente a la oxidación de esta.

El proceso de producción de hidrógeno de forma fotocatalítica se puede llevar a cabo a través de dos mecanismos (Figura 16). El proceso comienza por la absorción de la luz por parte del fotosensibilizador, que pasa a un estado excitado. Luego el fotosensibilizador excitado (PS*) se puede reducir por el electrón proporcionado por la molécula donadora de electrones; lo que se denomina ***reductive quenching***, o puede ser oxidado por el catalizador para la reducción de

los protones a agua, proceso denominado ***oxidative quenching***. Aunque ambos mecanismos se pueden llevar a cabo, en la mayoría de los casos, el mecanismo dominante es el *reductive quenching*, ya que normalmente las concentraciones de la sustancia donadora de electrones en el medio de reacción son muy elevadas respecto al resto de componentes de la reacción.

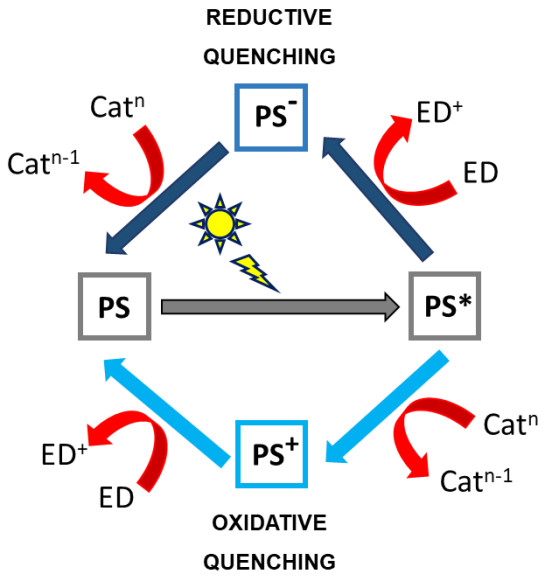

Figura 16. Posibles mecanismos de transferencia de electrones para la reducción de protones a hidrógeno por acción de un catalizador.

Los primeros sistemas fotocatalíticos artificiales para la producción de hidrógeno fueron publicados en 1977 por el grupo de Shilov [122] y Lehn y Sauvage [123]. Los primeros hicieron uso de un fotosensibilizador de tipo acridona y óxido de platino como catalizador, mientras que los segundos emplearon una sal de platino (K_2PtCl_6) como catalizador y rutenio tris-bipiridina $[Ru(bpy)_3]^{2+}$ como fotosensibilizador. Ambos grupos concluyeron que las nanopartículas de platino que se formaban durante la reacción eran realmente las especies catalíticas de dicho proceso [120]. Más tarde, y a partir de estas

investigaciones iniciales, tiene lugar la búsqueda de alternativas a estos sistemas basados en Pt. Por ejemplo, complejos macrocíclicos de diferentes metales [124,125] han sido ampliamente estudiados en la producción fotocatalítica de hidrógeno debido a la posibilidad de modular su actividad a través de la sustitución del tipo de ligando.

Por otro lado, durante las últimas décadas, el diseño molecular de catalizadores en producción fotocatalítica de hidrógeno se ha inspirado en la estructura de las metaloenzimas, que generalmente poseen metales de transición de la primera fila (Fe, Co y Ni) como centros activos [121,126].

1.5.2.2 Sistemas biológicos de reducción de protones

Existen algunos microorganismos con capacidad fotosintética que extraen los electrones de la molécula de hidrógeno para su metabolismo o eliminan el exceso de electrones mediante la reducción de protones para producir hidrógeno, a través de metaloenzimas llamadas hidrogenasas [127]. En función de los átomos metálicos presentes en el centro activo, estas metaloproteínas se dividen en: [FeNi]-, [FeFe]-, y [Fe]-hidrogenasas [109,128] (Figura 17).

En las [FeFe]-hidrogenasas, el centro metálico está coordinado a una subunidad Fe_2S_2 coordinada por un clúster Fe_4S_4 unido a una cisteína, junto con ligandos de cianuro (CN^-), monóxido de carbono (CO) y un puente de ditiolato (S-S). De esta forma, un centro de hierro tiene una coordinación hexagonal con configuración octogonal y el otro centro metálico esta pentacoordinado dejando un sitio activo libre para producción de hidrógeno [129].

En cambio, las [NiFe]-hidrogenasas están formadas por un átomo de níquel y otro de hierro, donde el níquel tiene una geometría plano-cuadrada distorsionada y está coordinado con cuatro ligandos de cisteína, de los cuales, dos de ellos están formando puente con el Fe. También existen una subclase de

[NiFe]-hidrogenasas con un ligando de selenocisteína coordinado con el centro de níquel en lugar de cisteína. Esta diferencia estructural es la razón de la alta tolerancia al oxígeno, y la alta producción de hidrógeno comparadas con otro tipo de hidrogenasas.

Comparado con las [NiFe]- y las [FeFe]-hidrogenasas, las [Fe]-hidrogenasas son únicas. Fueron identificadas y aisladas en 1990. Son las únicas hidrogenasas que necesitan solo un centro metálico de hierro, el cual está coordinado por un átomo de azufre de la molécula de cisteína, además de dos ligandos CO en posición cis y por un nitrógeno del ligando guanilpiridol [130].

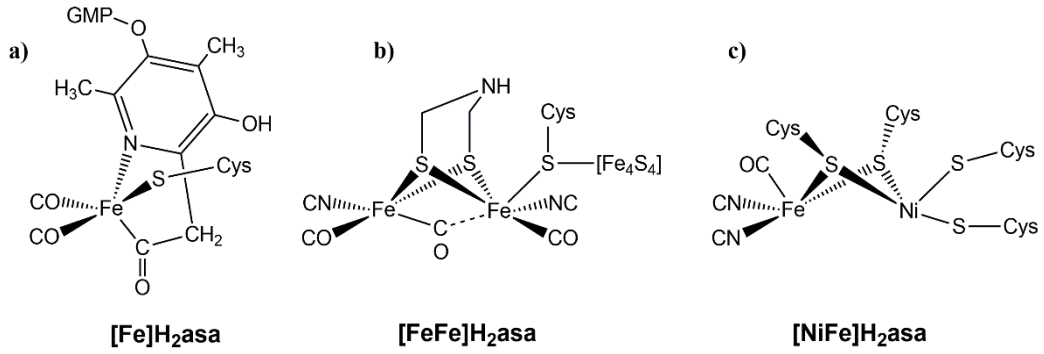

Figura 17. Estructura general de una [Fe]-hidrogenasa ([Fe]H_2asa) (a), [FeFe]-hidrogenasa ([FeFe]H_2asa) (b) y [FeNi]-hidrogenasa ([NiFe]H_2asa) (c).

Sistemas fotocatalíticos basados en hidrogenasas artificiales

Desde el descubrimiento de la estructura de las hidrogenasas y la elucidación del mecanismo por el que se forma hidrógeno, se han realizado grandes esfuerzos en la síntesis de compuestos químicos que imitan los sitios activos de las [FeFe]- y [FeNi]-hidrogenasas naturales [131].

El primer sistema fotocatalítico basado en las [FeFe]-hidrogenasas naturales fue publicado en 2008 por Weigand y col. [132]. Estos autores sintetizaron hidrogenasas con un puente tiolato al que se unía directamente una unidad de silafluoreno, la cual participaba como fotosensibilizador de la reacción. Desde ese momento, diferentes enfoques se han llevado a cabo para la formación de sistemas fotocatalíticos basados en hidrogenasas. Schröder y col. [133] estudiaron las diferencias en cuanto a estabilidad y producción de hidrógeno de dos sistemas basados en hidrogenasas en los que el fotosensibilizador de Re usado estaba o no anclado en el catalizador. Paralelamente, Weigand y col. [134] diseñaron sistemas moleculares basados en [FeFe]-hidrogenasas en las que se une un fluoreno o un silafluoreno como fotosensibilizador. Más recientemente, en 2018, Reek y col. [135] usaron una porfirina de zinc como segunda esfera de coordinación en la síntesis de una [FeFe]-hidrogenasa. Este nuevo compuesto sintetizado podía ser utilizado tanto como catalizador como fotosensibilizador en el proceso de producción de hidrógeno. En la actualidad, una gran variedad de sistemas fotocatalíticos basados en las [FeFe]- y [NiFe]-hidrogenasas son usados con diferentes fotosensibilizadores de Ir o Ru, entre otros [136–138].

A pesar de los numerosos estudios basados en el uso de [FeFe]-hidrogenasas como catalizadores homogéneos en reacciones de producción de hidrógeno, los resultados catalíticos en relación con el TON son muy bajos, debido principalmente a la inestabilidad del catalizador bajo las condiciones de la reacción.

1.5.2.3 Sistemas fotocatalíticos basados en complejos de cobalto (cobaloximas)

Debido a su abundancia, disponibilidad y bajo coste, los complejos de cobalto han surgido como una nueva alternativa a los complejos que se asemejan

a las hidrogenasas para su uso como catalizadores en la reacción fotocatalítica de reducción de protones a hidrógeno.

Complejos de cobalto de tipo cobaloximas, poliporfirinas, polipiridinas o macrociclos, se han usado en el proceso de reducción de protones a hidrógeno [139,140].

En 1966, las primeras "cobaloximas" (complejos de bis-glioximato de cobalto) fueron sintetizadas por Schrauzer y Windgassen [141], como modelos similares a la vitamina B_{12} [143,144]. Así, las moléculas pertenecientes a este tipo de familia se les acuñaron el término "*cobalamina*". A partir de entonces, el uso de este tipo de complejos y derivados se ha extendido debido a su fácil y rápida preparación, alta tolerancia al oxígeno, bajo coste, facilidad para intercambiar el ligando en posición axial, y considerable actividad catalítica [144,145].

De forma general, estos complejos se forman por la reacción de dimetilglioxima ($dmgH_2$) con cloruro o acetato de cobalto, dando lugar a la formación de un compuesto macrocíclico, $Co(dmgH)_2(L)_2$, donde el grupo L es cinéticamente lábil y puede ser ocupado por moléculas de disolvente o los contraiones de la sal usada. Por otro lado, los protones presentes en el macrociclo pueden ser sustituidos por BF_2 usando $(BF_3)*Et_2O$, que da lugar a complejos más estables sobre todo en solución ácida [146]. Compuestos similares se han sintetizado sustituyendo un ligando axial por diferentes alquilpiridinas [147]. De este modo, Rajeshwar y col. [148] estudiaron la descomposición del complejo molecular $Co(dmgH)_2(py)Cl$ y descubrieron que primero ocurría la rotura del ligando piridina, después la del ligando cloruro y, por último, la de los ligandos ecuatoriales.

El primer sistema fotocatalítico homogéneo, sin el uso de una sustancia mediadora (*electron relay*), fue desarrollado por Ziessel y col. [149]. Estaba compuesto por el complejo molecular $Co(dmgH)_2$ como catalizador, $[Ru(bpy)_3]^{2+}$ y TEOA como fotosensibilizador y donador de electrones, respectivamente. Desde ese momento, una amplia variedad de complejos con diferentes ligandos axiales se han estudiado [150,151].

En un inicio, este tipo de complejos, aunque no solubles en agua, fueron estudiados en procesos electroquímicos debido a sus bajos potenciales de oxidación/reducción, lo que los hace idóneos para producción de H_2. Conolly y Espenson [152] publicaron por primera vez el uso del catalizador $Co(dmgBF_2)(L)_2$ ($dmgBF_2$: difluoroboril-dimetilglioxima) y afirmaron que el paso limitante en el proceso era la transferencia de electrones en los puentes flúor. Sin embargo, trabajos posteriores llevados a cabo por diferentes grupos de investigación [153–155] proponen que el paso limitante en el proceso de reducción de los protones a hidrógeno viene de la labilidad del enlace axial Co-N entre el centro metálico y la piridina.

El grupo de Eisenberg [156] usó por primera vez complejos de $Co(dmgH)_2(py)Cl$ y derivados para producción de hidrógeno. Estos complejos fueron usados como catalizadores en una disolución de acetonitrilo/agua en presencia de TEOA como agente donador de electrones. Inicialmente, con este tipo de complejos se utilizaban fotosensibilizadores de Pt (II) [157]. Sin embargo, con el paso de los años se ha optimizado el uso de sistemas sin este metal. Durante la pasada década, una gran variedad de fotosensibilizadores ha sido utilizados con el catalizador $Co(dmgH)_2(py)Cl$). Entre ellos se incluyen, complejos metálicos de Ir [158,159], de Ru [160,161], o de Re [162]; o moléculas orgánicas como el eosin Y o el rosa de bengala [163].

Más recientemente, Coutsolelos y col. [164] estudiaron la influencia de diferentes ligandos con nitrógeno. Estos autores concluyeron que cobaloximas con ligandos electrodonadores como el N-metil imidazol daba lugar a elevados TONs; mientras que ligandos con grupos electroatractores eran menos estables. Los autores sugieren que cuanto más fuerte sea el enlace con los ligandos más tiempo de vida tiene el catalizador con TONs iniciales bajos, mientras que enlaces débiles dan lugar a TON altos al inicio y tiempos de vida del catalizador mucho más cortos.

En base a la estabilidad del sistema fotocatalítico, estudios posteriores sugieren que el cese de producción de H_2 es debido a la descomposición del catalizador, más específicamente, a intercambio de ligandos dmgH durante el proceso fotocatalítico y no por la degradación del fotosensibilizador. Estos autores mostraron como la adición de un exceso de dmgH daba lugar a un aumento en la longevidad del sistema [165].

Sistemas con fotosensibilizador y catalizador unidos covalentemente

Al igual que con los catalizadores basados en hidrogenasas, numerosas investigaciones están dirigidas al diseño de sistemas moleculares con la unión del fotosensibilizador al centro metálico de cobalto (Figura 18).

Los primeros sistemas de este tipo fueron desarrollados por Fontecave [166,167] y Sun [168] (**L1-L4**). Estos sistemas se basan en complejos moleculares de tipo cobaloxima y complejos de rutenio (o iridio) trisbipiridina o porfirinas de zinc modificadas que contengan un grupo piridil, el cual se coordine axialmente con el centro de cobalto.

También, Eisenberg y col. [169] (**L5**) desarrollaron un sistema con cobaloxima como catalizador al que le habían coordinado fluoresceína a través de un enlace amida. La adición de piridina al medio de reacción aumentaba la

eficiencia catalítica lo que sugería el lábil enlace del grupo piridina con el centro metálico. En base a estos resultados, estos autores dedujeron que el procedimiento de anclaje llevado a cabo no era el más idóneo.

Recientemente, Sakai y col. [170] (**L6**) sintetizaron un complejo molecular a través del ensamblaje in situ de dos sistemas supramoleculares de $[Ir(ppy)_2(bpy)]^+$ y $[Co(bpy)_3]^{2+}$.

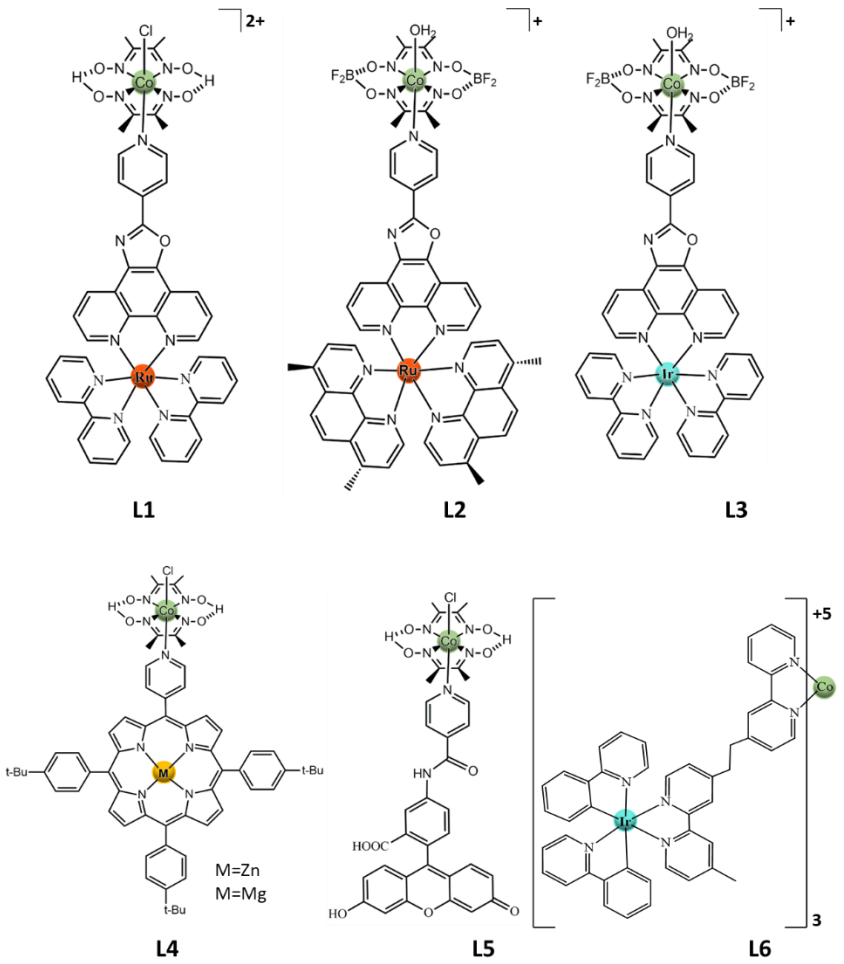

Figura 18. Ejemplos más destacados sobre sistemas fotocatalíticos con fotosensibilizador y catalizador unidos covalentemente [121].

Heterogeneización de complejos de cobaloxima

El desarrollo de diferentes estrategias para la inmovilización de complejos moleculares sobre diferentes soportes representa una eficaz alternativa para aumentar la tolerancia de este tipo de complejos en disoluciones acuosas y permitir el reciclaje de estos. Para su inmovilización, en la mayoría de los casos, es necesario una modificación química del soporte con algún ligando apropiado. La elección del ligando depende de la superficie del material y de la aplicación del catalizador, ya que para aplicaciones electrocatalíticas o fotocatalíticas, las propiedades del soportes, como la conductividad, morfología y estabilidad bajo condiciones experimentales, pueden cambiar considerablemente [119].

Desde el descubrimiento de las cobaloximas por Ziessel y col. [149], numerosos avances se han llevado a cabo para optimizar este tipo de sistemas como electro- o fotocatalizadores en la reacción de reducción de protones a hidrógeno. En el campo de la eletrocatálisis, Reisner [171] y Artero [172] han sido capaces de obtener excelentes resultados en la inmovilización de complejos de tipo cobaloxima sobre nanotubos de carbono con grupos piridina en la superficie.

Una nueva tendencia que se está atrayendo un gran interés, es la introducción de cobaloximas en materiales no conductores, para ser utilizados con luz visible. Hasta ahora, sólo algunos MOF (Metal Organic Frameworks) y COF (Covalent Organic Frameworks) han sido utilizados para tal fin. En el caso de los MOF, Ott y col. [173] publicaron por primera vez el anclaje de cobaloximas sobre un MIL-101 (Cr) clorometilado (Figura 19) para la formación de un catalizador híbrido de tipo MOF. La longevidad del catalizador molecular de cobaloxima se incrementó tras la incorporación en el MOF, sin embargo, su estabilidad estuvo limitada debido a la labilidad del enlace cobalto-piridina durante el proceso catalítico.

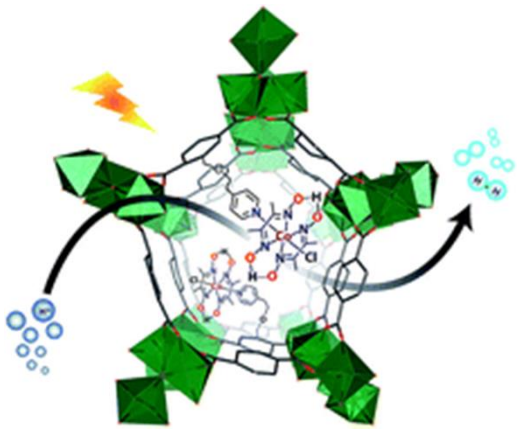

Figura 19. Estructura del catalizador MIL-101 con unidades de cobaloxima ancladas a su superficie para la producción de hidrógeno [174].

En el caso de los COF, Lotsch y col. [174] desarrollaron un catalizador basado en un COF-42 donde se ancló satisfactoriamente el complejo de cobaloxima. Estos autores observaron que la estructura del propio COF facilita la re-coordinación de la cobaloxima durante la reacción, mejorándose de este modo la reactividad y evitando la degradación del catalizador.

1.5.3 FOTORREDUCCIÓN DE CO_2

El dióxido de carbono (CO_2), es el principal producto que se obtiene de la combustión aerobia de compuestos que contienen carbón. De este modo, una gran cantidad de CO_2 es emitido a la atmósfera a través de la actividad humana, principalmente, de la quema de combustibles fósiles para obtener energía para el transporte y la producción industrial. Este CO_2 emitido a la atmósfera genera el llamado "*efecto invernadero"*, haciendo que la temperatura de la Tierra aumente y agravando así el cambio climático. En recientes conferencias internacionales de

las Naciones Unidas para el cambio climático (Madrid-Chile-2019, Glasgow-2021 y Egipto-2022) se ha puesto de manifiesto la necesidad de reducir un 45 % las emisiones de CO_2 en 2030 y estar en un 0 % de emisión para el 2050 [175].

El proceso de fotosíntesis de las plantas (Figura 12) donde a través de luz solar y moléculas sencillas se logra sintetizar moléculas más complejas, nos proporciona una estrategia factible para la captura de CO_2 y conversión de éste en un vector energético aprovechable, cerrando de ese modo, el ciclo del carbón y disminuyendo el antes mencionado efecto invernadero. El proceso de fotorreducción de CO_2 de forma artificial intenta simular tal proceso siendo necesario, como se ha comentado anteriormente, una sustancia donadora de electrones, un fotosensibilizador y un catalizador adecuado.

Recientemente, investigaciones relacionadas con la captura y uso de este CO_2 atmosférico están en auge. Uno de los grandes problemas que posee el CO_2 es que es una molécula muy estable (ΔG= -394.228 kJ/mol), por lo que su conversión necesita unas condiciones de presión y temperatura bastante drásticas.

La fotosíntesis artificial [176] abre una alternativa viable y sin condiciones peligrosas para la conversión de CO_2 en otros productos de interés como el monóxido de carbono, metano, etano, formaldehído o metanol usando luz visible y bajo unas condiciones de presión y temperatura normales.

En la Figura 20 (**ec.1**) se muestra el potencial necesario para reducir este CO_2. Este potencial es demasiado alto para ser conseguido de manera directa, por lo que una alternativa más favorable para activación de la molécula de CO_2 es a través de una serie de reacciones asistidas por protones y electrones que hacen posible que el CO_2 sea transformado en compuestos de interés (**ec.2-6**).

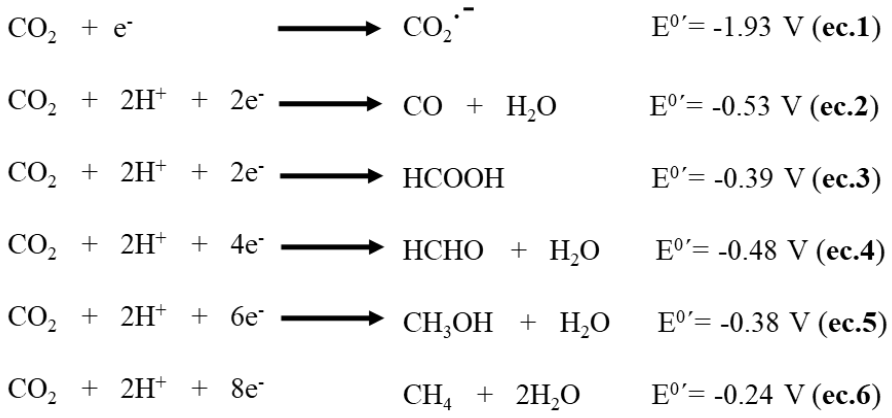

Figura 20. Reacciones de reducción de CO_2. Los valores de potencial están referidos al electrodo normal de hidrógeno (NHE) a pH 7.

En los siguientes apartados se describirán los primeros sistemas naturales usados para la fotorreducción del CO_2, así como el uso de catalizadores homogéneos basados en metales abundantes en la corteza terrestre (Fe, Co y Ni), y su posterior inmovilización en diferentes soportes.

1.5.3.1 Sistemas biológicos de reducción de CO_2

Las deshidrogenasas de monóxido de carbono (CODHs) son metaloenzimas que convierten el CO en CO_2. Existen dos tipos, las [CuMo]-CODHs y las [NiFe]-CODHs, pero sólo éstas últimas son capaces de reducir el CO_2 a CO [177] (Figura 21).

Considerando tanto a las hidrogenasas como a las deshidrogenasas de monóxido de carbono, en ambas enzimas biológicas están presentes metales de transición de la primera fila (Fe, Co y Ni) como centros activos, debido a la gran abundancia de éstos en la Tierra [178].

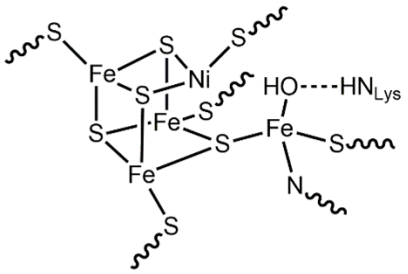

Figura 21. Estructura de una [NiFe]-CODHs natural.

Sistemas artificiales de reducción de CO_2

En la mayoría de los casos, la reducción de CO_2 se realiza de forma electrocatalítica, es decir, a través de una corriente eléctrica. Para ello, se utilizan complejos con diferentes centros metálicos como: Mn [179], Fe [180], Co [181], Ni [182], Cu [183] o Zn [184].

El primer sistema fotocatalítico para la reducción de CO_2 fue desarrollado por Ziessel y col. [149] en 1983. Éste se componía de $Ru(bpy)_3^{2+}$, como fotosensibilizador y TEOA como donador de electrones, y un nuevo complejo de Renio (I) (**C0**) como catalizador (Figura 22). Aunque el sistema mostró ser más selectivo a la reducción de CO_2 que al H_2O, la escasez y alto coste del centro metálico, hace poco viable este proceso. Como alternativa, durante las pasadas décadas, se han sintetizado una amplia variedad de catalizadores con metales

abundantes (Ni, Fe y Co) que sustituyen a los catalizados basados en renio (Figura 22).

1.5.3.2 Sistemas fotocatalíticos basados en Fe, Ni o Co

Las porfirinas (**C1**) y ftalocianinas de hierro, además de mostrar una gran actividad electroelectrocatalítica, son eficientes como catalizadores en el campo de la fotorreducción. Este tipo de complejos se caracteriza por tener una intensa banda de absorción en UV-vis, por lo que pueden actuar tanto como fotosensibilizadores como catalizadores. La degradación de este tipo de catalizadores ocurre a tiempos largos de radiación, a medida que va disminuyendo la selectividad. Por ello, para mejorar su estabilidad en este tipo de reacciones es necesario el uso de fotosensibilizadores que provean al sistemas fotones con menos energía [185].

En el caso de complejos basados en cobalto para la fotorreducción de CO_2 se utilizan principalmente complejos en los que este centro metálico está coordinado por 4 átomos de nitrógeno, que participan y estabilizan el estado de oxidación +1 del cobalto durante el proceso de catálisis.

En las primeras investigaciones desarrolladas en la reducción fotocatalítica de CO_2 a CO con radiación visible (> 400 nm) se usó $CoCl_2$ como catalizador en presencia de $Ru(bpy)_3^{2+}$ y TEOA o TEA como fotosensibilizador y donador de electrones, respectivamente. Aunque estos sistemas fueron activos, mostraron valores de TON muy bajos [186]. Más tarde, el uso de complejos de cobalto con ligandos N-heterocíclicos tales como bipiridinas (**C2**), fenantrolinas (**C3**) y derivados, lograron alcanzar mayores valores de conversión que las sales de cobalto, aunque no fueron extremadamente altos. Valores bajos de TON fueron también obtenidos con el uso de complejos de cobalto-ciclam (**C4**) [187]. Sin embargo, el empleo de complejos de tipo porfirina (**C5**), ftalocianina (**C6**), y

tetraporfirinas (**C7**) lograron superar los TON obtenidos con otros complejos hasta el momento [187].

El uso de complejos con centros metálicos de níquel se ha desarrollado a la par que los complejos de cobalto. Así, del mismo modo, para fotorreducción de CO_2 se han utilizado complejos macrocícicos con 4 átomos de nitrógeno como ligandos donadores. Los ligandos más utilizados son el ciclam (**C8**) y derivados, aunque todos ellos muestran valores de conversión muy bajos [188]. Un poco más tarde, y con el fin de mejorar los resultados catalíticos, se desarrollan sistemas moleculares donde el catalizador está unido de forma covalente con el fotosensibilizador, siendo este último, en la mayoría de los casos, $Ru(bpy)_3^{2+}$ (**C9**).

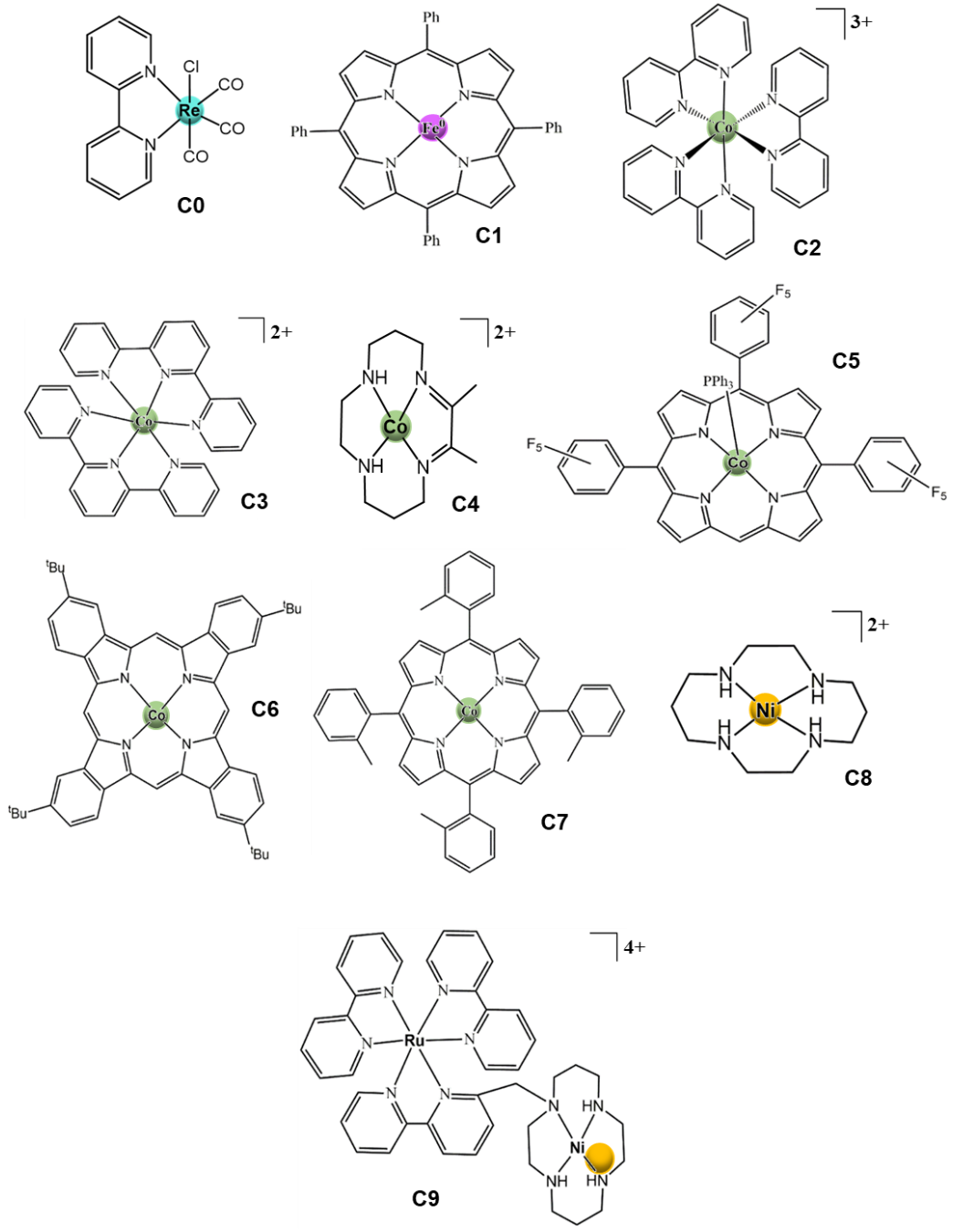

Figura 22. Catalizadores más utilizados en fotorreducción de CO_2.

1.5.3.3 Sistemas artificiales heterogéneos de reducción de CO_2

Aunque los sistemas con catalizadores homogéneos son eficaces en el proceso de reducción del CO_2, tienen desventajas asociadas al aislamiento y recuperación del catalizador, además de poseer baja estabilidad en disolución. La inmovilización de los complejos metálicos hace que las especies activas estén confinadas, resolviendo así los problemas relacionados con la desactivación del catalizador.

En la actualidad, los semiconductores son utilizados como soporte de complejos metálicos para su uso como catalizadores en fotorreducción de CO_2. De entre los semiconductores más utilizados destacan TiO_2, C_3N_4, Ta_2O_5, SnO_2 y CdSe, entre otros [189]. Estos semiconductores pueden ser modificados con diferentes ligandos de manera que la actividad catalítica del catalizador se vea aumentada. Sin embargo, es muy difícil de controlar las reacciones que ocurren en la superficie debido a la gran cantidad de sitios activos presentes.

El uso de materiales porosos como las silicas, las zeolitas, los COF o los MOFs tiene muchas ventajas, ya que, debido a su estructura porosa, en estos materiales se puede incorporar diferentes moléculas como el fotosensibilizador o el catalizador de la reacción. La proximidad de los componentes en la reacción facilita la transferencia electrónica entre ellos favoreciendo de este modo la cinética de la reacción.

En el caso de los MOFs, varios grupos de investigación han realizado grandes avances en el campo de la fotorreducción de CO_2 incorporando a la estructura del MOF diferentes complejos metálicos. El grupo de Li y Wang y col. [190,191] sintetizaron una serie de MOFs con diferentes centros metálicos que absorbían en la región del visible con conversiones elevadas de CO_2.

Uno de los inconvenientes que poseen este tipo de materiales es la estabilidad del MOF durante la reacción debido a la débil coordinación entre los ligandos y los centros metálicos que forman el MOF. De este modo, Lin y col. [192] incorporaron un complejo de Re en la estructura del MOF, [(Re(CO)$_3$(dcbpy)Cl] (dcbpy= ácido 2,2'-bipiridina-4,4'-dicarboxílico) y, aunque se alcanzó un TON de 10.9 a las 20 h, casi el 50 % de las especies de renio estaban presentes en disolución. Con la idea de mejorar la estabilidad de estos materiales, se sintetizaron MOFs basados en complejos metálicos con piridinas interconectadas [193] y porfirinas [194], obteniéndose resultados catalíticos prometedores.

Por otro lado, se ha podido comprobar que algunos materiales PMO además de las propiedades anteriormente citadas, exhiben unas propiedades únicas como antenas captadoras de luz [38]. Además, al ser materiales ordenados, con una distribución de poro uniforme, estos materiales son ideales para la construcción de sistemas fotocatalíticos heterogéneos [58] ya que; *i)* las especies fotocatalíticas se pueden colocar en el espacio poroso, *ii)* después de la adición de fotocatalizadores, hay suficientes espacios vacíos para una eficaz transferencia de masa debido al gran tamaño de poro (2 - 30 nm), comparados con otros materiales como materiales laminados o zeolitas, *iii)* por último, la gran área superficial y la estructura mesoporosa de estos materiales puede incrementar el número de sitios activos y, por lo tanto, mejorar la actividad fotocatalítica.

En 2010, Inagaki y col. [195] estudiaron por primera vez el uso de un PMO como catalizador en la fotorreducción de CO_2. Estos autores incorporaron complejos de Re sobre los grupos bifenilos presentes en las paredes del material PMO. En este caso, la luz absorbida por los grupos bifenilos es transferida al catalizador de renio. Aunque el sistema resultó ser de gran interés, la escasa

adsorción de luz en el visible por los grupos bifenilos no permitía un total aprovechamiento de la luz solar.

Hasta el momento, la única estrategia válida para el uso de PMOs como soportes en el campo de la fotocatálisis, es la síntesis de PMOs que contengan en su estructura ligandos bipiridinas, en los que se pueda anclar los diferentes complejos metálicos [66]. De este modo, diferentes PMO sintetizados por Ishida y col. [196] e Inagaki y col. [197] siguen la estrategia de complejar $Ru(bpy)(CO)_2Cl_2$ (como fotosensibilizador), $Re(bpy)(CO)_3Cl$ (catalizador) o ambos sobre PMO con grupos bipiridina en su estructura.

1.6 REFERENCIAS

[1] I. Union, O.F. Pure, A. Chemistry, Recommendations for the characterization of porous solids (Technical Report), Pure Appl. Chem. 66 (1994) 1739-1758. https://doi.org/10.1351/pac199466081739.

[2] A.J. Schwanke, R. Balzer, S. Pergher, Microporous and Mesoporous Materials from Natural and Inexpensive Sources, in: Handb. Ecomater., Springer International Publishing, Cham, 2017: pp. 1-22. https://doi.org/10.1007/978-3-319-48281-1_43-1.

[3] P. Bai, M.Y. Jeon, L. Ren, C. Knight, M.W. Deem, M. Tsapatsis, J.I. Siepmann, Discovery of optimal zeolites for challenging separations and chemical transformations using predictive materials modeling, Nat. Commun. 6 (2015) 1-9. https://doi.org/10.1038/ncomms6912.

[4] H.N. Tran, P. Van Viet, H.P. Chao, Surfactant modified zeolite as amphiphilic and dual-electronic adsorbent for removal of cationic and oxyanionic metal ions and organic compounds, Ecotoxicol. Environ. Saf. 147 (2018) 55-63. https://doi.org/10.1016/j.ecoenv.2017.08.027.

[5] H. Zhang, A. Li, W. Zhang, C. Shuang, Combination of Na-modified zeolite and anion exchange resin for advanced treatment of a high ammonia-nitrogen content municipal effluent, J. Colloid Interface Sci. 468 (2016) 128-135. https://doi.org/10.1016/j.jcis.2015.10.006.

[6] S. Boycheva, D. Zgureva, H. Lazarova, M. Popova, Comparative studies of carbon capture onto coal fly ash zeolites Na-X and Na-Ca-X, Chemosphere. 271 (2021) 129505. https://doi.org/10.1016/j.chemosphere.2020.129505.

[7] C. Algieri, E. Drioli, Zeolite membranes: Synthesis and applications, Sep. Purif. Technol. 278 (2022) 119295. https://doi.org/10.1016/j.seppur.2021.119295.

[8] T. Yanagisawa, T. Shimizu, K. Kuroda, C. Kato, The preparation of alkyltrimethylammonium-kanemite complexes and their conversion to microporous materials, Bull. Chem. Soc. Jpn. 63 (1990) 988–992. https://doi.org/10.1246/bcsj.63.988.

[9] A. Monnier, F. Schüth, Q. Huo, D. Kumar, D. Margolese, R.S. Maxwell, G.D. Stucky, M. Krishnamurty, P. Petroff, A. Firouzi, M. Janicke, B.F. Chmelka, Cooperative formation of inorganic-organic interfaces in the synthesis of silicate mesostructures, Science. 261 (1993) 1299-1303. https://doi.org/10.1126/science.261.5126.1299.

[10] V. Meynen, P. Cool, E.F. Vansant, Verified syntheses of mesoporous materials, Microporous Mesoporous Mater. 125 (2009) 170-223. https://doi.org/10.1016/j.micromeso.2009.03.046.

[11] S. Bhattacharyya, P. Ducheyne, Silica-based mesoporous nanospheres, Elsevier Ltd., 2011. https://doi.org/10.1016/b978-0-08-055294-1.00028-3.

[12] J.C. Vartuli, C.T. Kresge, M.E. Leonowicz, A.S. Chu, S.B. McCullen, I.D. Johnson, E.W. Sheppard, Synthesis of Mesoporous Materials: Liquid-Crystal Templating versus Intercalation of Layered Silicates, Chem. Mater. 6 (1994) 2070–2077. https://doi.org/10.1021/cm00047a029.

[13] V.M. Ortiz-Martínez, L. Gómez-Coma, A. Ortiz, I. Ortiz, Overview on the use of surfactants for the preparation of porous carbon materials by the sol-gel method: Applications in energy systems, Rev. Chem. Eng. 36 (2020) 771-787. https://doi.org/10.1515/revce-2018-0056.

[14] M. Omidi-Ghallemohamadi, A. Ahmadi-Khaneghah, H. Behniafar, Epoxy networks possessing polyoxyethylene unites and loaded by Jeffamine-modified graphene oxide nanoplatelets, Prog. Org. Coatings. 134 (2019) 264-271. https://doi.org/10.1016/j.porgcoat.2019.05.014.

[15] S.N. Afini M. Johari, N.A. Tajuddin, H. Hanibah, S.K. Deraman, A Review: Ionic Conductivity of Solid Polymer Electrolyte Based Polyethylene Oxide, Int. J. Electrochem. Sci. 16 (2021) 1-15. https://doi.org/10.20964/2021.10.53.

[16] J. Broda, M. Baczek, J. Fabia, R. Fryczkowski, Supramolecular structure of polypropylene fibers formed with addition of functionalized graphene oxide, Text. Res. J. 90 (2020) 2322-2335. https://doi.org/10.1177/0040517520919752.

[17] F.D. Souza, B.S. Souza, D.W. Tondo, E.C. Leopoldino, H.D. Fiedler, F. Nome, Imidazolium-based zwitterionic surfactants: Characterization of normal and reverse micelles and stabilization of nanoparticles, Langmuir. 31 (2015) 3587-3595. https://doi.org/10.1021/la504802k.

[18] I. Sharifi, H. Shokrollahi, M.M. Doroodmand, R. Safi, Magnetic and structural studies on $CoFe_2O_4$ nanoparticles synthesized by co-precipitation, normal micelles and reverse micelles methods, J. Magn. Magn. Mater. 324 (2012) 1854-1861. https://doi.org/10.1016/j.jmmm.2012.01.015.

[19] A. Khoshnood, A. Firoozabadi, Polar Solvents Trigger Formation of Reverse Micelles, Langmuir. 31 (2015) 5982-5991. https://doi.org/10.1021/la504658u.

[20] A.H. Kshash, A.S. Ismail, Minimizing evaporation of light hydrocarbons for Iraqi gasoline by using D-glucitol fatty acid esters as reduced pressure agents,synthesis and characterization, Pet. Coal. 61 (2019) 100-109.

[21] Y. Sakamoto, M. Kaneda, O. Terasaki, D.Y. Zhao, J.M. Kim, G. Stucky, H.J. Shin, R. Ryoo, Direct imaging of the pores and cages of three-dimensional mesoporous materials, Nature. 408 (2000) 449-453. https://doi.org/10.1038/35044040.

[22] K. Cassiers, T. Linssen, M. Mathieu, M. Benjelloun, K. Schrijnemakers, P. Van Der Voort, P. Cool, E.F. Vansant, A detailed study of thermal, hydrothermal, and mechanical stabilities of a wide range of surfactant assembled mesoporous silicas, Chem. Mater. 14 (2002) 2317-2324. https://doi.org/10.1021/cm0112892.

[23] D. Zhao, Q. Huo, J. Feng, B.F. Chmelka, G.D. Stucky, Nonionic Triblock and Star Diblock Copolymer and Oligomeric Surfactant Syntheses of Highly Ordered, Hydrothermally Stable, Mesoporous Silica Structures, J. Am. Chem. Soc. 120 (1998) 6024-6036. https://doi.org/10.1021/ja974025i.

[24] N. Parida, S.K. Badamali, Facile synthesis and catalytic activity of nanoporous SBA-1, J. Porous Mater. 29 (2022) 161-167. https://doi.org/10.1007/s10934-021-01154-5.

[25] J.M. Kim, G.D. Stucky, Synthesis of highly ordered mesoporous silica materials using sodium silicate and amphiphilic block copolymers, Chem. Commun. (2000) 1159–1160. https://doi.org/10.1039/b002362k.

[26] G.M. Ziarani, S. Roshankar, F. Mohajer, A. Badiei, The Synthesis and Application of Functionalized Mesoporous Silica SBA-15 as Heterogeneous Catalyst in Organic Synthesis, Curr. Org. Chem. 25 (2021) 361-387. https://doi.org/10.2174/1385272824999201210194444.

[27] Y. Cao, S. Yang, Y. Li, J. Shi, Cooperative organizations of small molecular surfactants and amphiphilic block copolymers: Roles of surfactants in the formation of binary co-assemblies, Aggregate. 2 (2021). https://doi.org/10.1002/agt2.49.

[28] D. Zhao, J. Feng, Q. Huo, N. Melosh, G.H. Fredrickson, B.F. Chmelka, G.D. Stucky, Triblock copolymer syntheses of mesoporous silica with periodic 50 to 300 angstrom pores, Science. 279 (1998) 548-552. https://doi.org/10.1126/science.279.5350.548.

[29] P. Kipkemboi, A. Fogden, V. Alfredsson, K. Flodström, Triblock copolymers as templates in mesoporous silica formation: Structural dependence on polymer chain length and synthesis temperature, Langmuir. 17 (2001) 5398-5402. https://doi.org/10.1021/la001715i.

[30] F. Hoffmann, M. Cornelius, J. Morell, M. Fröba, Silica-Based Mesoporous Organic-Inorganic Hybrid Materials, Angew. Chemie Int. Ed. 45 (2006) 3216-3251. https://doi.org/10.1002/anie.200503075.

[31] W. Wang, D. Grozea, S. Kohli, D.D. Perovic, G.A. Ozin, Water Repellent Periodic Mesoporous Organosilicas, ACS Nano. 5 (2011) 1267-1275. https://doi.org/10.1021/nn102929t.

[32] F. Hoffmann, M. Cornelius, J. Morell, M. Fröba, Silica-based mesoporous organic-inorganic hybrid materials, Angew. Chemie - Int. Ed. 45 (2006) 3216-3251. https://doi.org/10.1002/anie.200503075.

[33] M. Colilla, M. Vallet-Regí, Ordered mesoporous silica materials, 2017. https://doi.org/10.1016/B978-0-12-803581-8.10231-0.

[34] B.M. Estevão, I. Miletto, N. Hioka, L. Marchese, E. Gianotti, Mesoporous Silica Nanoparticles Functionalized with Amino Groups for Biomedical Applications, ChemistryOpen. 10 (2021) 1251-1259. https://doi.org/10.1002/open.202100227.

[35] C. Von Baeckmann, R. Guillet-Nicolas, D. Renfer, H. Kählig, F. Kleitz, A Toolbox for the Synthesis of Multifunctionalized Mesoporous Silica Nanoparticles for Biomedical Applications, ACS Omega. 3 (2018) 17496-17510. https://doi.org/10.1021/acsomega.8b02784.

[36] B.J. Melde, B.T. Holland, C.F. Blanford, A. Stein, Mesoporous sieves with unified hybrid inorganic/organic frameworks, Chem. Mater. 11 (1999) 3302-3308. https://doi.org/10.1021/cm9903935.

[37] A. Stein, Advances in microporous and mesoporous solids - Highlights of recent progress, Adv. Mater. 15 (2003) 763-75. https://doi.org/10.1002/adma.200300007.

[38] N. Mizoshita, T. Tani, S. Inagaki, Syntheses, properties and applications of periodic mesoporous organosilicas prepared from bridged organosilane precursors, Chem. Soc. Rev. 40 (2011) 789–800. https://doi.org/10.1039/c0cs00010h.

[39] B. Karimi, N. Ganji, O. Pourshiani, W.R. Thiel, Periodic mesoporous organosilicas (PMOs): From synthesis strategies to applications, Prog. Mater. Sci. 125 (2022) 100896. https://doi.org/10.1016/j.pmatsci.2021.100896.

[40] S. Inagaki, S. Guan, Y. Fukushima, T. Ohsuna, O. Terasaki, Novel mesoporous materials with a uniform distribution of organic groups and inorganic oxide in their frameworks, J. Am. Chem. Soc. 121 (1999) 9611-9614. https://doi.org/10.1021/ja9916658.

[41] T. Asefa, M.J. MacLachlan, N. Coombs, G.A. Ozin, Periodic mesoporous organosilicas with organic groups inside the channel walls, Nature. 402 (1999) 867-871. https://doi.org/10.1038/47229.

[42] F. Lin, X. Meng, E. Kukueva, M. Mertens, S. Van Doorslaer, S. Bals, P. Cool, New insights into the mesophase transformation of ethane-bridged PMOs by the influence of different counterions under basic conditions, RSC Adv. 5 (2015) 5553-5562. https://doi.org/10.1039/c4ra15849k.

[43] F. Lin, X. Meng, E. Kukueva, M. Kus, M. Mertens, S. Bals, S. Van Doorslaer, P. Cool, Novel method to synthesize highly ordered ethane-bridged PMOs under mild acidic conditions: Taking advantages of phosphoric acid, Microporous Mesoporous Mater. 207 (2015) 61-70. https://doi.org/10.1016/j.micromeso.2014.12.029.

[44] C.X.C. Lin, S. Jambhrunkar, P. Yuan, C.H.C. Zhou, G.X.S. Zhao, Design and synthesis of periodic mesoporous organosilica materials with a multi-compartment structure, RSC Adv. 5 (2015) 89397-89406. https://doi.org/10.1039/c5ra16497d.

[45] X. Ma, X. Su, J. Zhang, M. Dang, J. Tao, P. Xu, Y. Li, P. Lv, W. Wei, Z. Teng, Uniform and ordered periodic mesoporous organosilica thin films by a facile solution growth approach, J. Porous Mater. 25 (2018) 489-494. https://doi.org/10.1007/s10934-017-0460-8.

[46] B. Marciniec, H. Maciejewski, J. Guliński, L. Rzejak, Metathesis of silicon containing olefins: II. Synthesis of 1,2-bis(silyl)ethenes by metathesis of vinylsilanes, J. Organomet. Chem. 362 (1989) 273-279. https://doi.org/10.1016/0022-328X(89)87248-1.

[47] C. Vercaemst, M. Ide, B. Allaert, N. Ledoux, F. Verpoort, P. Van Der Voort, Ultra-fast hydrothermal synthesis of diastereoselective pure ethenylene-bridged periodic mesoporous organosilicas, Chem. Commun. (2007) 2261. https://doi.org/10.1039/b705412b.

[48] T. Asefa, M.J. MacLachlan, H. Grondey, N. Coombs, G.A. Ozin, Metamorphic channels in periodic mesoporous methylenesilica, Angew. Chemie - Int. Ed. 39 (2000) 1808-1811. https://doi.org/10.1002/(SICI)1521-3773(20000515)39:10<1808::AID-ANIE1808>3.0.CO;2-G.

[49] S. Inagaki, S. Guan, T. Ohsuna, O. Terasaki, An ordered mesoporous organosilica hybrid material with a crystal-like wall structure, Nature. 416 (2002) 304-307. https://doi.org/10.1038/416304a.

[50] M.P. Kapoor, Q. Yang, S. Inagaki, Organization of Phenylene-Bridged Hybrid Mesoporous Silisesquioxane with a Crystal-like Pore Wall from a Precursor with Nonlinear Symmetry, Chem. Mater. 16 (2004) 1209-1213. https://doi.org/10.1021/cm034898d.

[51] A. Birault, E. Molina, C. Carcel, J. Bartlett, N. Marcotte, G. Toquer, P. Lacroix-Desmazes, C. Gerardin, M. Wong Chi Man, Synthesis of lamellar mesostructured phenylene-bridged periodic mesoporous organosilicas (PMO) templated by polyion complex (PIC) micelles, J. Sol-Gel Sci. Technol. 89 (2019) 189-195. https://doi.org/10.1007/s10971-018-4667-1.

[52] M. Barczak, M. Gil, K. Terpiłowski, D. Kamiński, P. Borowski, Influence of bridged monomer on porosity and sorption properties of mesoporous silicas functionalized with diethylenetriamine groups, Adsorption. 25 (2019) 575-589. https://doi.org/10.1007/s10450-019-00047-z.

[53] V. Rebbin, A. Rothkirch, N. Ohta, T. Hikima, S.S. Funari, Size limit on the formation of periodic mesoporous organosilicas (PMOs), Langmuir. 30 (2014) 1900-1905. https://doi.org/10.1021/la404060a.

[54] W. Li, Y. Yang, X. Huang, Q. Wang, L. Liu, M. Wang, X. Tan, T. Luo, A.J. Patil, Compressed CO_2 mediated synthesis of bifunctional periodic mesoporous organosilicas with tunable porosity, Chem. Commun. 52 (2016) 9668-9671. https://doi.org/10.1039/c6cc04741f.

[55] M. Laird, C. Carcel, E. Oliviero, G. Toquer, P. Trens, J.R. Bartlett, M. Wong Chi Man, Single-template periodic mesoporous organosilica with organized bimodal mesoporosity, Microporous Mesoporous Mater. 297 (2020) 110042. https://doi.org/10.1016/j.micromeso.2020.110042.

[56] X. Li, J. Yuan, J. Du, H. Sui, L. He, Functionalized Ordered Mesoporous Silica by Vinyltriethoxysilane for the Removal of Volatile Organic Compounds through Adsorption/Desorption Process, Ind. Eng. Chem. Res. 59 (2020) 3511-3520. https://doi.org/10.1021/acs.iecr.9b06062.

[57] B.J. Melde, B.T. Holland, C.F. Blanford, A. Stein, Mesoporous sieves with unified hybrid inorganic/organic frameworks, Chem. Mater. 11 (1999) 3302-3308. https://doi.org/10.1021/cm9903935.

[58] P. Van Der Voort, D. Esquivel, E. De Canck, F. Goethals, I. Van Driessche, F.J. Romero-Salguero, Periodic Mesoporous Organosilicas: from simple to complex bridges; a comprehensive overview of functions, morphologies and applications, Chem. Soc. Rev. 42 (2013) 3913-3955. https://doi.org/10.1039/C2CS35222B.

[59] S.S. Park, M.S. Moorthy, C.S. Ha, Periodic mesoporous organosilicas for advanced applications, NPG Asia Mater. 6 (2014) 1-21. https://doi.org/10.1038/am.2014.13.

[60] C. Yoshina-Ishii, T. Asefa, N. Coombs, M.J. MacLachlan, G.A. Ozin, Periodic mesoporous organosilicas, PMOs: Fusion of organic and inorganic chemistry 'inside' the channel walls of hexagonal mesoporous silica, Chem. Commun. (1999) 2539-2540. https://doi.org/10.1039/a908252b.

[61] G. Temtsin, T. Asefa, S. Bittner, G.A. Ozin, Aromatic PMOs: Tolyl, xylyl and dimethoxyphenyl groups integrated within the channel walls of hexagonal mesoporous silicas, J. Mater. Chem. 11 (2001) 3202-3206. https://doi.org/10.1039/b103960c.

[62] Y. Li, A. Keilbach, M. Kienle, Y. Goto, S. Inagaki, P. Knochel, T. Bein, Hierarchically structured biphenylene-bridged periodic mesoporous organosilica, J. Mater. Chem. 21 (2011) 17338. https://doi.org/10.1039/c1jm12023a.

[63] N. Mizoshita, Y. Goto, M.P. Kapoor, T. Shimada, T. Tani, S. Inagaki, Fluorescence Emission from 2,6-Naphthylene-Bridged Mesoporous Organosilicas with an Amorphous or Crystal-Like Framework, Chem. - A Eur. J. 15 (2009) 219–226. https://doi.org/10.1002/chem.200801238.

[64] Y. Goto, K. Nakajima, N. Mizoshita, M. Suda, N. Tanaka, T. Hasegawa, T. Shimada, T. Tani, S. Inagaki, Synthesis and optical properties of 2,6-anthracene-bridged periodic mesostructured organosilicas, Microporous Mesoporous Mater. 117 (2009) 535-540. https://doi.org/10.1016/j.micromeso.2008.07.035.

[65] M. Waki, N. Mizoshita, T. Ohsuna, T. Tani, S. Inagaki, Crystal-like periodic mesoporous organosilica bearing pyridine units within the framework, Chem. Commun. 46 (2010) 8163. https://doi.org/10.1039/c0cc01944e.

[66] M. Waki, Y. Maegawa, K. Hara, Y. Goto, S. Shirai, Y. Yamada, N. Mizoshita, T. Tani, W.-J. Chun, S. Muratsugu, M. Tada, A. Fukuoka, S. Inagaki, A Solid Chelating Ligand: Periodic Mesoporous Organosilica Containing 2,2′-Bipyridine within the Pore Walls, J. Am. Chem. Soc. 136 (2014) 4003-4011. https://doi.org/10.1021/ja4131609.

[67] M.C. Burleigh, S. Jayasundera, C.W. Thomas, M.S. Spector, M.A. Markowitz, B.P. Gaber, A versatile synthetic approach to periodic mesoporous organosilicas, Colloid Polym. Sci. 282 (2004) 728-733.

[68] M. Abboud, A. Sayari, Microporous and Mesoporous Materials Novel family of periodic mesoporous organosilicas containing azobenzene within the pore walls, Microporous Mesoporous Mater. 249 (2017) 157-164. https://doi.org/10.1016/j.micromeso.2017.04.061.

[69] M. Haghighat, M. Golshekan, F. Shirini, Periodic Mesoporous Organosilica Containing Bridged N -Sulfonic Acid Groups: Promotion of the Synthesis of N,N'-Diarylformamidines, Benzoxazoles, Benzothiazoles and Benzimidazoles, ChemistrySelect. 4 (2019) 7968-7975. https://doi.org/10.1002/slct.201900885.

[70] M. Imamoglu, D. Perez-Quintanilla, I. Sierra, Bifunctional periodic mesoporous organosilicas with sulfide bridges as effective sorbents for Hg(II) extraction from environmental and drinking waters, Microporous Mesoporous Mater. 229 (2016) 90-97. https://doi.org/10.1016/j.micromeso.2016.04.023.

[71] M.C. Burleigh, M.A. Markowitz, M.S. Spector, B.P. Gaber, Amine-Functionalized Periodic Mesoporous Organosilicas, Chem. Mater. 13 (2001) 4760-4766. https://doi.org/10.1021/cm0105763.

[72] N. Suriyanon, P. Punyapalakul, C. Ngamcharussrivichai, Synthesis of periodic mesoporous organosilicas functionalized with different amine-organoalkoxysilanes via direct co-condensation, Mater. Chem. Phys. 149-150 (2015) 701–712. https://doi.org/10.1016/j.matchemphys.2014.11.030.

[73] A.M. Kaczmarek, S. Abednatanzi, D. Esquivel, C. Krishnaraj, H.S. Jena, G. Wang, K. Leus, R. Van Deun, F.J. Romero-Salguero, P. Van Der Voort, Amine-containing (nano-) Periodic Mesoporous Organosilica and its application in catalysis, sorption and luminescence, Microporous Mesoporous Mater. 291 (2020) 109687. https://doi.org/10.1016/j.micromeso.2019.109687.

[74] J.R. Deka, C.-L. Liu, T.-H. Wang, W.-C. Chang, H.-M. Kao, Synthesis of highly phosphonic acid functionalized benzene-bridged periodic mesoporous organosilicas for use as efficient dye adsorbents, J. Hazard. Mater. 278 (2014) 539-550. https://doi.org/10.1016/j.jhazmat.2014.06.016.

[75] J.E. Castanheiro, L. Guerreiro, I.M. Fonseca, A.M. Ramos, Mesoporous silica containing sulfonic acid groups as catalysts for the alpha-pinene methoxylation, Stud. Surf. Sci. Catal. 174 (2008) 1319-1322. https://doi.org/10.1016/S0167-2991(08)80132-2.

[76] D. Esquivel, J. Amaro-Gahete, N. Caballero-Casero, C. Jiménez-Sanchidrián, J.R. Ruiz, S. Rubio, P. Van Der Voort, F.J. Romero-Salguero, Tailoring Bifunctional Periodic Mesoporous Organosilicas for Cooperative Catalysis, ACS Appl. Nano Mater. 3 (2020) 2373-2382. https://doi.org/10.1021/acsanm.9b02493.

[77] C. Li, H. Zhang, D. Jiang, Q. Yang, Chiral catalysis in nanopores of mesoporous materials, Chem. Commun. (2007) 547-558. https://doi.org/10.1039/B609862b.

[78] S. Polarz, A. Kuschel, Preparation of a Periodically Ordered Mesoporous Organosilica Material Using Chiral Building Blocks, Adv. Mater. 18 (2006) 1206-1209. https://doi.org/10.1002/adma.200502647.

[79] C. Baleizão, B. Gigante, D. Das, M. Alvaro, H. Garcia, A. Corma, Synthesis and catalytic activity of a chiral periodic mesoporous organosilica (ChiMO), Chem. Commun. (2003) 1860-1861. https://doi.org/10.1039/B304814D.

[80] D. Jiang, Q. Yang, H. Wang, G. Zhu, J. Yang, C. Li, Periodic mesoporous organosilicas with trans-(1R,2R)-diaminocyclohexane in the framework: A potential catalytic material for asymmetric reactions, J. Catal. 239 (2006) 65-73. https://doi.org/10.1016/j.jcat.2006.01.018.

[81] R.A. García, R. Van Grieken, J. Iglesias, V. Morales, D. Gordillo, Synthesis of Chiral Periodic Mesoporous Silicas Incorporating Tartrate Derivatives in the Framework and Their Use in Asymmetric Sulfoxidation, Chem. Mater. 20 (2008) 2964-2971. https://doi.org/10.1021/cm703050u.

[82] R.A. Garcia, R. Van Grieken, J. Iglesias, V. Morales, N. Villajos, Facile one-pot approach to the synthesis of chiral periodic mesoporous organosilicas SBA-15-type materials, J. Catal. 274 (2010) 221-227. https://doi.org/10.1016/j.jcat.2010.07.003.

[83] S. Shylesh, C. Srilakshmi, A.P. Singh, B.G. Anderson, One step synthesis of chromium-containing periodic mesoporous organosilicas and their catalytic activity in the oxidation of cyclohexane, Microporous Mesoporous Mater. 99 (2007) 334-344. https://doi.org/10.1016/j.micromeso.2006.09.029.

[84] A. Modak, M. Nandi, A. Bhaumik, Titanium containing periodic mesoporous organosilica as an efficient catalyst for the epoxidation of alkenes, Catal. Today. 198 (2012) 45-51. https://doi.org/10.1016/j.cattod.2012.03.074.

[85] S.S. Park, M.S. Moorthy, C.-S. Ha, Periodic mesoporous organosilica (PMO) for catalytic applications, Korean J. Chem. Eng. 31 (2014) 1707-1719. https://doi.org/10.1007/s11814-014-0221-1.

[86] K. Nakai, Y. Oumi, H. Horie, T. Sano, H. Yoshitake, Bromine addition and successive amine substitution of mesoporous ethylenesilica: Reaction, characterizations and arsenate adsorption, Microporous Mesoporous Mater. 100 (2007) 328-339. https://doi.org/10.1016/j.micromeso.2006.11.023.

[87] E. De Canck, L. Lapeire, J. De Clercq, F. Verpoort, P. Van Der Voort, New Ultrastable Mesoporous Adsorbent for the Removal of Mercury Ions, Langmuir. 26 (2010) 10076-10083. https://doi.org/10.1021/la100204d.

[88] G. Smeulders, V. Meynen, K. Houthoofd, S. Mullens, J.A. Martens, B.U.W. Maes, P. Cool, Is their potential for post-synthetic brominating reactions on benzene bridged PMOs?, Microporous Mesoporous Mater. 164 (2012) 49-55. https://doi.org/10.1016/j.micromeso.2012.06.033.

[89] W. Huybrechts, G. Mali, P. Kuśtrowski, T. Willhammar, M. Mertens, S. Bals, P. Van Der Voort, P. Cool, Post-synthesis bromination of benzene bridged PMO as a way to create a high potential hybrid material, Microporous Mesoporous Mater. 236 (2016) 244-249. https://doi.org/10.1016/j.micromeso.2016.09.003.

[90] M.P. Kapoor, M. Yanagi, Y. Kasama, T. Yokoyama, S. Inagaki, T. Shimada, H. Nanbu, L.R. Juneja, Self-assembly of cubic phenylene bridged mesoporous hybrids from allylorganosilane precursors, J. Mater. Chem. 16 (2006) 3305. https://doi.org/10.1039/b607133c.

[91] Q. Yang, M.P. Kapoor, S. Inagaki, Sulfuric Acid-Functionalized Mesoporous Benzene−Silica with a Molecular-Scale Periodicity in the Walls, J. Am. Chem. Soc. 124 (2002) 9694-9695. https://doi.org/10.1021/ja026799r.

[92] E. De Canck, C. Vercaemst, F. Verpoort, P. Van Der Voort, A new sulphonic acid functionalized periodic mesoporous organosilica as a suitable catalyst, in: Stud. Surf. Sci. Catal., Elsevier B.V., 2010: pp. 365-368. https://doi.org/10.1016/S0167-2991(10)75061-8.

[93] M. Ohashi, P. Kapoor, S. Inagaki, Chemical modification of crystal-like mesoporous phenylene-silica with amino group, Chem. Commun. (2008) 841-843. https://doi.org/10.1039/B716141G.

[94] M.A.O. Lourenço, C. Siquet, M. Sardo, L. Mafra, J. Pires, M. Jorge, M.L. Pinto, P. Ferreira, J.R.B. Gomes, Interaction of CO_2 and CH_4 with Functionalized Periodic Mesoporous Phenylene–Silica: Periodic DFT Calculations and Gas Adsorption Measurements, J. Phys. Chem. C. 120 (2016) 3863-3875. https://doi.org/10.1021/acs.jpcc.5b11844.

[95] M. Sasidharan, S. Fujita, M. Ohashi, Y. Goto, K. Nakashima, S. Inagaki*, Novel synthesis of bifunctional catalysts with different microenvironments, Chem. Commun. 47 (2011) 10422-10424. https://doi.org/10.1039/c1cc13825a.

[96] Y. Horiuchi, D. Do Van, Y. Yonezawa, M. Saito, S. Dohshi, T. Kim, M. Matsuoka, Synthesis and bifunctional catalysis of metal nanoparticle-loaded periodic mesoporous organosilicas modified with amino groups, RSC Adv. 5 (2015) 72653-72658. https://doi.org/10.1039/C5RA13090E.

[97] P. Wessig, G. Müller, The Dehydro-Diels-Alder Reaction, Chem. Rev. 108 (2008) 2051–2063. https://doi.org/10.1021/cr0783986.

[98] K. Nakajima, I. Tomita, M. Hara, S. Hayashi, K. Domen, J.N. Kondo, A Stable and Highly Active Hybrid Mesoporous Solid Acid Catalyst, Adv. Mater. 17 (2005) 1839-1842. https://doi.org/10.1002/adma.200500426.

[99] K. Nakajima, I. Tomita, M. Hara, S. Hayashi, K. Domen, J.N. Kondo, Development of highly active SO_3H-modified hybrid mesoporous catalyst, Catal. Today. 116 (2006) 151-156. https://doi.org/10.1016/j.cattod.2006.01.022.

[100] D. Esquivel, E. De Canck, C. Jimenez-Sanchidrian, P. Van Der Voort, F.J. Romero-Salguero, Formation and functionalization of surface Diels-Alder adducts on ethenylene-bridged periodic mesoporous organosilica, J. Mater. Chem. 21 (2011) 10990-10998. https://doi.org/10.1039/C1JM11315A.

[101] D. Esquivel, E. De Canck, C. Jiménez-Sanchidrián, F.J. Romero-Salguero, P. Van Der Voort, Pyrrole PMOs, incorporating new N-heterocyclic compounds on an ethene-PMO through Diels-Alder reactions, Mater. Chem. Phys. (2014). https://doi.org/10.1016/j.matchemphys.2014.08.004.

[102] D. Esquivel, A.M. Kaczmarek, R. Van Deun, F.J. Romero-salguero, P. Van Der Voort, Eu^{3+}@PMO: synthesis, characterization and luminescence properties, J. Mater. Chem. C. 3 (2015) 2909-2917. https://doi.org/10.1039/C4TC02553A.

[103] A.M. Kaczmarek, D. Esquivel, J. Ouwehand, P. Van Der Voort, F.J. Romero-Salguero, R. Van Deun, Temperature dependent NIR emitting lanthanide-PMO/silica hybrid materials, Dalt. Trans. 46 (2017) 7878-7887. https://doi.org/10.1039/C7DT01620D.

[104] B. Liu, H. Li, K. Quan, J. Chen, H. Qiu, Periodic mesoporous organosilica for chromatographic stationary phases: From synthesis strategies to applications, TrAC Trends Anal. Chem. 158 (2023) 116895. https://doi.org/10.1016/j.trac.2022.116895.

[105] S. Andrade, B. Castanheira, S. Brochsztain, Periodic mesoporous organosilicas containing naphthalenediimides within the pore walls for asphaltene adsorption, Microporous Mesoporous Mater. 294 (2020) 109909. https://doi.org/10.1016/j.micromeso.2019.109909.

[106] A.M. Kaczmarek, P. Van Der Voort, Light-Emitting Lanthanide Periodic Mesoporous Organosilica (PMO) Hybrid Materials, Materials (Basel). 13 (2020) 566. https://doi.org/10.3390/ma13030566.

[107] M.A. Wahab, J.N. Beltramini, Recent advances in hybrid periodic mesostructured organosilica materials: opportunities from fundamental to biomedical applications, RSC Adv. 5 (2015) 79129-79151. https://doi.org/10.1039/C5RA10062C.

[108] S. Inagaki, Synthesis and Optical Applications of Periodic Mesoporous Organosilicas, in: 2018: pp. 11-34. https://doi.org/10.1016/bs.enz.2018.09.004.

[109] J. Barber, P.D. Tran, From natural to artificial photosynthesis, J. R. Soc. Interface. 10 (2013) 20120984. https://doi.org/10.1098/rsif.2012.0984.

[110] M.B. Tahir, A.M. Asiri, T. Nawaz, A perspective on the fabrication of heterogeneous photocatalysts for enhanced hydrogen production, Int. J. Hydrogen Energy. 45 (2020) 24544-24557. https://doi.org/10.1016/j.ijhydene.2020.06.301.

[111] M. Gibbs, Photosynthesis, Annu. Rev. Biochem. 36 (1967) 757-784. https://doi.org/10.1146/annurev.bi.36.070167.003545.

[112] B. Zhang, L. Sun, Artificial photosynthesis: opportunities and challenges of molecular catalysts, Chem. Soc. Rev. 48 (2019) 2216-2264. https://doi.org/10.1039/C8CS00897C.

[113] D.R. Whang, D.H. Apaydin, Artificial Photosynthesis: Learning from Nature, ChemPhotoChem. 2 (2018) 148-160. https://doi.org/10.1002/cptc.201700163.

[114] C. Bie, L. Wang, J. Yu, Challenges for photocatalytic overall water splitting, Chem. 8 (2022) 1567-1574. https://doi.org/10.1016/j.chempr.2022.04.013.

[115] A. FUJISHIMA, K. HONDA, Electrochemical Photolysis of Water at a Semiconductor Electrode, Nature. 238 (1972) 37-38. https://doi.org/10.1038/238037a0.

[116] S.A. Shah, I. Khan, A. Yuan, MoS_2 as a Co-Catalyst for Photocatalytic Hydrogen Production: A Mini Review, Molecules. 27 (2022) 3289. https://doi.org/10.3390/molecules27103289.

[117] K. Su, S. Deng, L. Li, Q. Qin, J. Yang, Y. Chen, S. Zhang, J. Chen, g-C_3N_4 Derived Materials for Photocatalytic Hydrogen Production: A Mini Review on Design Strategies, J. Renew. Mater. 10 (2022) 653-663. https://doi.org/10.32604/jrm.2022.018556.

[118] Y. Wei, H. Qin, J. Deng, X. Cheng, M. Cai, Q. Cheng, S. Sun, Semiconductor Photocatalysts for Solar-to-Hydrogen Energy Conversion: Recent Advances of CdS, Curr. Anal. Chem. 17 (2021) 573-589. https://doi.org/10.2174/1573411016666200106103712.

[119] J. Corredor, M.J. Rivero, C.M. Rangel, F. Gloaguen, I. Ortiz, Comprehensive review and future perspectives on the photocatalytic hydrogen production, J. Chem. Technol. Biotechnol. 94 (2019) 3049-3063. https://doi.org/10.1002/jctb.6123.

[120] E. Amouyal, Photochemical production of hydrogen and oxygen from water: A review and state of the art, Sol. Energy Mater. Sol. Cells. 38 (1995) 249-276. https://doi.org/10.1016/0927-0248(95)00003-8.

[121] W.T. Eckenhoff, R. Eisenberg, Molecular systems for light driven hydrogen production, Dalt. Trans. 41 (2012) 13004. https://doi.org/10.1039/c2dt30823a.

[122] D.A.Iv. A. E. Shilov, B. V. Koryakin and T. S. Dzhabier, No Title, S.S.S.R. 233 (1977).

[123] J. M. Lehn and J. P. Sauvage, No Title, Nouv. J. Chim. 1 (1977).

[124] G.M. Brown, B.S. Brunschwig, C. Creutz, J.F. Endicott, N. Sutin, Homogeneous catalysis of the photoreduction of water by visible light. Mediation by a tris(2,2'-bipyridine)ruthenium(II)-cobalt(II) macrocycle system, J. Am. Chem. Soc. 101 (1979) 1298-1300. https://doi.org/10.1021/ja00499a051.

[125] C. V. Krishnan, N. Sutin, Homogeneous catalysis of the photoreduction of water by visible light. 2. Mediation by a tris(2,2'-bipyridine)ruthenium(II)-cobalt(II) bipyridine system, J. Am. Chem. Soc. 103 (1981) 2141-2142. https://doi.org/10.1021/ja00398a066.

[126] L. Tong, L. Duan, A. Zhou, R.P. Thummel, First-row transition metal polypyridine complexes that catalyze proton to hydrogen reduction, Coord. Chem. Rev. 402 (2020) 213079. https://doi.org/10.1016/j.ccr.2019.213079.

[127] S. Li, F. Li, X. Zhu, Q. Liao, J.-S. Chang, S.-H. Ho, Biohydrogen production from microalgae for environmental sustainability, Chemosphere. 291 (2022) 132717. https://doi.org/10.1016/j.chemosphere.2021.132717.

[128] J.W. Peters, G.J. Schut, E.S. Boyd, D.W. Mulder, E.M. Shepard, J.B. Broderick, P.W. King, M.W.W. Adams, [FeFe]- and [NiFe]-hydrogenase diversity, mechanism, and maturation, Biochim. Biophys. Acta-Mol. Cell Res. 1853 (2015) 1350-1369. https://doi.org/10.1016/j.bbamcr.2014.11.021.

[129] R. Cammack, Hydrogenase sophistication, Nature. 397 (1999) 214-215. https://doi.org/10.1038/16601.

[130] T. Xu, C.-J.M. Yin, M.D. Wodrich, S. Mazza, K.M. Schultz, R. Scopelliti, X. Hu, A Functional Model of [Fe]-Hydrogenase, J. Am. Chem. Soc. 138 (2016) 3270-3273. https://doi.org/10.1021/jacs.5b12095.

[131] T. Xu, D. Chen, X. Hu, Hydrogen-activating models of hydrogenases, Coord. Chem. Rev. 303 (2015) 32-41. https://doi.org/10.1016/j.ccr.2015.05.007.

[132] R. Goy, U. Apfel, C. Elleouet, D. Escudero, M. Elstner, H. Görls, J. Talarmin, P. Schollhammer, L. González, W. Weigand, A Silicon-Heteroaromatic System as Photosensitizer for Light-Driven Hydrogen Production by Hydrogenase Mimics, Eur. J. Inorg. Chem. 2013 (2013) 4466-4472. https://doi.org/10.1002/ejic.201300537.

[133] P.A. Summers, J.A. Calladine, F. Ghiotto, J. Dawson, X.-Z. Sun, M.L. Hamilton, M. Towrie, E.S. Davies, J. McMaster, M.W. George, M. Schröder, Synthesis and Photophysical Study of a [NiFe] Hydrogenase Biomimetic Compound Covalently Linked to a Re-diimine Photosensitizer, Inorg. Chem. 55 (2016) 527–536. https://doi.org/10.1021/acs.inorgchem.5b01744.

[134] R. Goy, L. Bertini, H. Görls, L. De Gioia, J. Talarmin, G. Zampella, P. Schollhammer, W. Weigand, Silicon-Heteroaromatic [FeFe] Hydrogenase Model Complexes: Insight into Protonation, Electrochemical Properties, and Molecular Structures, Chem. - A Eur. J. 21 (2015) 5061-5073. https://doi.org/10.1002/chem.201406087.

[135] R. Becker, S. Amirjalayer, P. Li, S. Woutersen, J.N.H. Reek, An iron-iron hydrogenase mimic with appended electron reservoir for efficient proton reduction in aqueous media, Sci. Adv. 2 (2016). https://doi.org/10.1126/sciadv.1501014.

[136] J. Chen, W.R. Browne, Photochemistry of iron complexes, Coord. Chem. Rev. 374 (2018) 15-35. https://doi.org/10.1016/j.ccr.2018.06.008.

[137] H. Tang, M.B. Hall, Biomimetics of [NiFe]-Hydrogenase: Nickel- or Iron-Centered Proton Reduction Catalysis?, J. Am. Chem. Soc. 139 (2017) 18065-18070. https://doi.org/10.1021/jacs.7b10425.

[138] G. Caserta, S. Roy, M. Atta, V. Artero, M. Fontecave, Artificial hydrogenases: biohybrid and supramolecular systems for catalytic hydrogen production or uptake, Curr. Opin. Chem. Biol. 25 (2015) 36-47. https://doi.org/10.1016/j.cbpa.2014.12.018.

[139] S. Losse, J.G. Vos, S. Rau, Catalytic hydrogen production at cobalt centres, Coord. Chem. Rev. 254 (2010) 2492-2504. https://doi.org/10.1016/j.ccr.2010.06.004.

[140] X. Zhao, P. Wang, M. Long, Electro- and Photocatalytic Hydrogen Production by Molecular Cobalt Complexes With Pentadentate Ligands, Comments Inorg. Chem. 37 (2017) 238-270. https://doi.org/10.1080/02603594.2016.1266618.

[141] G.N. Schrauzer, R.J. Windgassen, Über Cobaloxime(II) und deren Beziehung zum Vitamin B_{12r}, Chem. Ber. 99 (1966) 602-610. https://doi.org/10.1002/cber.19660990234.

[142] G.N. Schrauzer, R.J. Holland, Hydridocobaloximes, J. Am. Chem. Soc. 93 (1971) 1505-1506. https://doi.org/10.1021/ja00735a040.

[143] Gerhard N. Schrauzer, Organocobalt chemistry of vitamin B_{12} model compounds (cobaloximes), Acc. Chem. Res. 1 (1968) 97-103. https://doi.org/10.1021/ar50004a001.

[144] S. Roy, M. Bacchi, G. Berggren, V. Artero, A Systematic Comparative Study of Hydrogen-Evolving Molecular Catalysts in Aqueous Solutions, ChemSusChem. 8 (2015) 3632-3638. https://doi.org/10.1002/cssc.201501002.

[145] N. Bresciani-Pahor, M. Forcolin, L.G. Marzilli, L. Randaccio, M.F. Summers, P.J. Toscano, Organocobalt B_{12} models: axial ligand effects on the structural and coordination chemistry of cobaloximes, Coord. Chem. Rev. 63 (1985) 1-125. https://doi.org/10.1016/0010-8545(85)80021-7.

[146] G.N. Schrauzer, R.J. Windgassen, Alkylcobaloximes and Their Relation to Alkylcobalamins, J. Am. Chem. Soc. 88 (1966) 3738-3743. https://doi.org/10.1021/ja00968a012.

[147] M. Razavet, V. Artero, M. Fontecave, J. Fourier, D. Cb, K. Bat, G. Cedex, Proton Electroreduction Catalyzed by Cobaloximes : Functional Models for Hydrogenases, 44 (2005) 4786-4795.

[148] K.L. Brown, G. Jang, R. Segal, K. Rajeshwar, Thermolysis of alkyl(aquo)- and alkyl(pyridine)cobaloximes in the solid state. Influence of the alkyl group on axial cobalt-ligand bond stability and correlation with solution properties, Inorganica Chim. Acta. 128 (1987) 197-205. https://doi.org/10.1016/S0020-1693(00)86546-9.

[149] J. Hawecker, J.-M. Lehn, R. Ziessel, Efficient photochemical reduction of CO_2 to CO by visible light irradiation of systems containing $Re(bipy)(CO)_3X$ or $Ru(bipy)_3^{2+}$-Co^{2+} combinations as homogeneous catalysts, J. Chem. Soc., Chem. Commun. (1983) 536-538. https://doi.org/10.1039/C39830000536.

[150] V. Artero, M. Chavarot-Kerlidou, M. Fontecave, Splitting water with cobalt, Angew. Chemie - Int. Ed. 50 (2011) 7238-7266. https://doi.org/10.1002/anie.201007987.

[151] J. Willkomm, E. Reisner, Photo- and electrocatalytic H_2 evolution with cobalt oxime complexes, Bull. Japan Soc. Coord. Chem. 71 (2018) 18-29. https://doi.org/10.4019/bjscc.71.18.

[152] P. Connolly, J.H. Espenson, Cobalt-catalyzed evolution of molecular hydrogen, Inorg. Chem. 25 (1986) 2684-2688. https://doi.org/10.1021/ic00236a006.

[153] T.M. Mccormick, Z. Han, D.J. Weinberg, W.W. Brennessel, P.L. Holland, R. Eisenberg, Impact of Ligand Exchange in Hydrogen Production from Cobaloxime-Containing Photocatalytic Systems, Inorg. Chem. 50 (2011) 10660–10666. https://doi.org/10.1021/ic2010166.

[154] M.A.W. Lawrence, M.J. Celestine, E.T. Artis, L.S. Joseph, D.L. Esquivel, A.J. Ledbetter, D.M. Cropek, W.L. Jarrett, C.A. Bayse, M.I. Brewer, A.A. Holder, Computational, electrochemical, and spectroscopic studies of two mononuclear cobaloximes: The influence of an axial pyridine and solvent on the redox behaviour and evidence for pyridine coordination to cobalt(i) and cobalt(II) metal centres, Dalt. Trans. 45 (2016) 10326-10342. https://doi.org/10.1039/C6DT01583B.

[155] G. Li, D.P. Estes, J.R. Norton, S. Ruccolo, A. Sattler, W. Sattler, Dihydrogen Activation by Cobaloximes with Various Axial Ligands, Inorg. Chem. 53 (2014) 10743-10747. https://doi.org/10.1021/ic501975r.

[156] T.M. McCormick, B.D. Calitree, A. Orchard, N.D. Kraut, F. V. Bright, M.R. Detty, R. Eisenberg, Reductive side of water splitting in artificial photosynthesis: New homogeneous photosystems of great activity and mechanistic insight, J. Am. Chem. Soc. 132 (2010) 15480-15483. https://doi.org/10.1021/ja1057357.

[157] P. Du, K. Knowles, R. Eisenberg, A homogeneous system for the photogeneration of hydrogen from water based on a platinum(II) terpyridyl acetylide chromophore and a molecular cobalt catalyst, J. Am. Chem. Soc. 130 (2008) 12576-12577. https://doi.org/10.1021/ja804650g.

[158] M. Yang, J.E. Yarnell, K. El Roz, F.N. Castellano, A Robust Visible-Light-Harvesting Cyclometalated Ir(III) Diimine Sensitizer for Homogeneous Photocatalytic Hydrogen Production, ACS Appl. Energy Mater. 3 (2020) 1842-1853. https://doi.org/10.1021/acsaem.9b02269.

[159] S. Takizawa, R. Kano, N. Ikuta, S. Murata, An anionic iridium(III) complex as a visible-light absorbing photosensitizer, Dalt. Trans. 47 (2018) 11041-11046. https://doi.org/10.1039/C8DT02477D.

[160] E. Rousset, I. Ciofini, V. Marvaud, G.S. Hanan, Facile One-Pot Synthesis of Ruthenium(II) Quaterpyridine-Based Photosensitizers for Photocatalyzed Hydrogen Production, Inorg. Chem. 56 (2017) 9515-9524. https://doi.org/10.1021/acs.inorgchem.7b00771.

[161] S. Guo, K.-K. Chen, R. Dong, Z.-M. Zhang, J. Zhao, T.-B. Lu, Robust and Long-Lived Excited State Ru(II) Polyimine Photosensitizers Boost Hydrogen Production, ACS Catal. 8 (2018) 8659-8670. https://doi.org/10.1021/acscatal.8b02226.

[162] B. Probst, M. Guttentag, A. Rodenberg, P. Hamm, R. Alberto, Photocatalytic H_2 Production from Water with Rhenium and Cobalt Complexes, Inorg. Chem. 50 (2011) 3404–3412. https://doi.org/10.1021/ic102317u.

[163] T. Lazarides, T. Mccormick, P. Du, G. Luo, B. Lindley, R. Eisenberg, Making Hydrogen from Water Using a Homogeneous System Without Noble Metals, J. Am. Chem. Soc. 131 (2009) 9192-9194. https://doi.org/10.1021/ja903044n.

[164] A. Panagiotopoulos, K. Ladomenou, D. Sun, V. Artero, A.G. Coutsolelos, Photochemical hydrogen production and cobaloximes: The influence of the cobalt axial N-ligand on the system stability, Dalt. Trans. 45 (2016) 6732–6738. https://doi.org/10.1039/c5dt04502a.

[165] T. Lazarides, T. McCormick, P. Du, G. Luo, B. Lindley, R. Eisenberg, Making hydrogen from water using a homogeneous system without noble metals, J. Am. Chem. Soc. 131 (2009) 9192-9194. https://doi.org/10.1021/ja903044n.

[166] A. Fihri, V. Artero, A. Pereira, M. Fontecave, Efficient H_2-producing photocatalytic systems based on cyclometalated iridium- and tricarbonylrhenium-diimine photosensitizers and cobaloxime catalysts, Dalt. Trans. (2008) 5567. https://doi.org/10.1039/b812605b.

[167] A. Fihri, V. Artero, M. Razavet, C. Baffert, W. Leibl, M. Fontecave, Cobaloxime-based photocatalytic devices for hydrogen production, Angew. Chemie - Int. Ed. 47 (2008) 564-547. https://doi.org/10.1002/anie.200702953.

[168] P. Zhang, M. Wang, C. Li, X. Li, J. Dong, L. Sun, Photochemical H_2 production with noble-metal-free molecular devices comprising a porphyrin photosensitizer and a cobaloxime catalyst, Chem. Commun. 46 (2010) 8806-8808. https://doi.org/10.1039/c0cc03154b.

[169] T.M. McCormick, Z. Han, D.J. Weinberg, W.W. Brennessel, P.L. Holland, R. Eisenberg, Impact of Ligand Exchange in Hydrogen Production from Cobaloxime-Containing Photocatalytic Systems, Inorg. Chem. 50 (2011) 10660-10666. https://doi.org/10.1021/ic2010166.

[170] S. Jasimuddin, T. Yamada, K. Fukuju, J. Otsuki, K. Sakai, Photocatalytic hydrogen production from water in self-assembled supramolecular iridium-cobalt systems, Chem. Commun. 46 (2010) 8466. https://doi.org/10.1039/c0cc02486d.

[171] B. Reuillard, J. Warnan, J.J. Leung, D.W. Wakerley, E. Reisner, A Poly(cobaloxime)/Carbon Nanotube Electrode: Freestanding Buckypaper with Polymer-Enhanced H_2-Evolution Performance, Angew. Chemie - Int. Ed. 55 (2016) 3952–3957. https://doi.org/10.1002/anie.201511378.

[172] S. Donck, J. Fize, E. Gravel, E. Doris, V. Artero, Supramolecular assembly of cobaloxime on nanoring-coated carbon nanotubes: Addressing the stability of the pyridine-cobalt linkage under hydrogen evolution turnover conditions, Chem. Commun. 52 (2016) 11783-11786. https://doi.org/10.1039/c6cc06059e.

[173] S. Roy, A. Bhunia, N. Schuth, M. Haumann, S. Ott, Light-driven hydrogen evolution catalyzed by a cobaloxime catalyst incorporated in a MIL-101(Cr) metal-organic framework, Sustain. Energy Fuels. 2 (2018) 1148-1152. https://doi.org/10.1039/c8se00072g.

[174] K. Gottschling, G. Savasci, H. Vignolo-González, S. Schmidt, P. Mauker, T. Banerjee, P. Rovó, C. Ochsenfeld, B. V. Lotsch, Rational Design of Covalent Cobaloxime-Covalent Organic Framework Hybrids for Enhanced Photocatalytic Hydrogen Evolution, J. Am. Chem. Soc. 142 (2020) 12146-12156. https://doi.org/10.1021/jacs.0c02155.

[175] UN. Secretary-General, Report of the Secretary-General on the 2019 Climate Action Summit and the way forward in 2020, in: 2019. https://digitallibrary.un.org/record/3850027.

[176] X. Fang, S. Kalathil, E. Reisner, Semi-biological approaches to solar-to-chemical conversion, Chem. Soc. Rev. 49 (2020) 4926-4952. https://doi.org/10.1039/C9CS00496C.

[177] A. Majumdar, Bioinorganic modeling chemistry of carbon monoxide dehydrogenases: description of model complexes, current status and possible future scopes, Dalt. Trans. 43 (2014) 12135. https://doi.org/10.1039/C4DT00729H.

[178] A. Bachmeier, F. Armstrong, Solar-driven proton and carbon dioxide reduction to fuels - lessons from metalloenzymes, Curr. Opin. Chem. Biol. 25 (2015) 141–151. https://doi.org/10.1016/j.cbpa.2015.01.001.

[179] A. Sinopoli, N.T. La Porte, J.F. Martinez, M.R. Wasielewski, M. Sohail, Manganese carbonyl complexes for CO_2 reduction, Coord. Chem. Rev. 365 (2018) 60-74. https://doi.org/10.1016/j.ccr.2018.03.011.

[180] R. Bonetto, F. Crisanti, A. Sartorel, Carbon Dioxide Reduction Mediated by Iron Catalysts: Mechanism and Intermediates That Guide Selectivity, ACS Omega. 5 (2020) 21309–21319. https://doi.org/10.1021/acsomega.0c02786.

[181] M. Usman, M. Humayun, M.D. Garba, L. Ullah, Z. Zeb, A. Helal, M.H. Suliman, B.Y. Alfaifi, N. Iqbal, M. Abdinejad, A.A. Tahir, H. Ullah, Electrochemical Reduction of CO_2: A Review of Cobalt Based Catalysts for Carbon Dioxide Conversion to Fuels, Nanomaterials. 11 (2021) 2029. https://doi.org/10.3390/nano11082029.

[182] J.-W. Wang, W.-J. Liu, D.-C. Zhong, T.-B. Lu, Nickel complexes as molecular catalysts for water splitting and CO_2 reduction, Coord. Chem. Rev. 378 (2019) 237–261. https://doi.org/10.1016/j.ccr.2017.12.009.

[183] W. Ye, X. Guo, T. Ma, A review on electrochemical synthesized copper-based catalysts for electrochemical reduction of CO_2 to C^{2+} products, Chem. Eng. J. 414 (2021) 128825. https://doi.org/10.1016/j.cej.2021.128825.

[184] H. Louis, O.U. Akakuru, P. Monday, O.O. Funmilayo, A review on the state-of-the-art advances for CO_2 electro-chemical reduction using metal complex molecular catalysts, Eclética Química J. 44 (2019) 11. https://doi.org/10.26850/1678-4618eqj.v44.1.2019.p11-39.

[185] J. Bonin, M. Chaussemier, M. Robert, M. Routier, Homogeneous Photocatalytic Reduction of CO_2 to CO Using Iron(0) Porphyrin Catalysts: Mechanism and Intrinsic Limitations, ChemCatChem. 6 (2014) 3200-3207. https://doi.org/10.1002/cctc.201402515.

[186] R. Ziessel, J. Hawecker, J.-M. Lehn, Photogeneration of Carbon Monoxide and of Hydrogen via Simultaneous Photochemical Reduction of Carbon Dioxide and Water by Visible-Light Irradiation of Organic Solutions Containing Tris(2,2-bipyridine)ruthenium(II) and Cobalt(II) Species as Homogeneous Ca, Helv. Chim. Acta. 69 (1986) 1065–1084. https://doi.org/10.1002/hlca.19860690514.

[187] F. Wang, Artificial Photosynthetic Systems for CO_2 Reduction: Progress on Higher Efficiency with Cobalt Complexes as Catalysts, ChemSusChem. 10 (2017) 4393-4402. https://doi.org/10.1002/cssc.201701385.

[188] T.D. Cook, S.F. Tyler, C.M. McGuire, M. Zeller, P.E. Fanwick, D.H. Evans, D.G. Peters, T. Ren, Nickel Complexes of C-Substituted Cyclams and Their Activity for CO_2 and H+ Reduction, ACS Omega. 2 (2017) 3966–3976. https://doi.org/10.1021/acsomega.7b00714.

[189] S. Wang, X. Han, Y. Zhang, N. Tian, T. Ma, H. Huang, Inside-and-Out Semiconductor Engineering for CO_2 Photoreduction: From Recent Advances to New Trends, Small Struct. 2 (2021) 2000061. https://doi.org/10.1002/sstr.202000061.

[190] D. Wang, R. Huang, W. Liu, D. Sun, Z. Li, Fe-Based MOFs for Photocatalytic CO_2 Reduction: Role of Coordination Unsaturated Sites and Dual Excitation Pathways, ACS Catal. 4 (2014) 4254-4260. https://doi.org/10.1021/cs501169t.

[191] S. Wang, W. Yao, J. Lin, Z. Ding, X. Wang, Cobalt Imidazolate Metal-Organic Frameworks Photosplit CO_2 under Mild Reaction Conditions, Angew. Chemie Int. Ed. 53 (2014) 1034-1038. https://doi.org/10.1002/anie.201309426.

[192] C. Wang, Z. Xie, K.E. DeKrafft, W. Lin, Doping Metal-Organic Frameworks for Water Oxidation, Carbon Dioxide Reduction, and Organic Photocatalysis, J. Am. Chem. Soc. 133 (2011) 13445-13454. https://doi.org/10.1021/ja203564w.

[193] S. Zhang, L. Li, S. Zhao, Z. Sun, J. Luo, Construction of Interpenetrated Ruthenium Metal-Organic Frameworks as Stable Photocatalysts for CO_2 Reduction, Inorg. Chem. 54 (2015) 8375-8379. https://doi.org/10.1021/acs.inorgchem.5b01045.

[194] Z. Liang, H.-Y. Wang, H. Zheng, W. Zhang, R. Cao, Porphyrin-based frameworks for oxygen electrocatalysis and catalytic reduction of carbon dioxide, Chem. Soc. Rev. 50 (2021) 2540-2581. https://doi.org/10.1039/D0CS01482F.

[195] H. Takeda, M. Ohashi, T. Tani, O. Ishitani, S. Inagaki, Enhanced Photocatalysis of Rhenium(I) Complex by Light-Harvesting Periodic Mesoporous Organosilica, Inorg. Chem. 49 (2010) 4554–4559. https://doi.org/10.1021/ic1000914.

[196] Y. Kuramochi, M. Sekine, K. Kitamura, Y. Maegawa, Y. Goto, S. Shirai, S. Inagaki, H. Ishida, Photocatalytic CO_2 Reduction by Periodic Mesoporous Organosilica (PMO) Containing Two Different Ruthenium Complexes as Photosensitizing and Catalytic Sites, Chem. - A Eur. J. 23 (2017) 10301-10309. https://doi.org/10.1002/chem.201701466.

[197] M. Waki, K.I. Yamanaka, S. Shirai, Y. Maegawa, Y. Goto, Y. Yamada, S. Inagaki, Re(bpy)$(CO)_3$Cl Immobilized on Bipyridine-Periodic Mesoporous Organosilica for Photocatalytic CO_2 Reduction, Chem. - A Eur. J. 24 (2018) 3846-3853. https://doi.org/10.1002/chem.201705792.

CAPÍTULO 2.

HIPÓTESIS Y OBJETIVOS

HIPÓTESIS Y OBJETIVOS

A continuación, se plantean las hipótesis y los objetivos propuestos para la realización de la presente Tesis Doctoral.

Hipótesis 1

La epoxidación de olefinas es una de las reacciones con mayor interés en química orgánica, ya que los epóxidos son importantes intermedios en gran variedad de reacciones útiles para la síntesis de productos farmacéuticos, agroquímicos o perfumes. Tradicionalmente, la síntesis de epóxidos se ha llevado a cabo utilizando oxidantes peligrosos, tales como perácidos, y generando una gran cantidad de residuos peligrosos para el medioambiente. En la actualidad, se usan oxidantes más seguros, tales como el oxígeno molecular, peróxido de hidrógeno o terc-butilhidroperóxido (TBHP), entre otros. Recientes estudios para la epoxidación de olefinas utilizando complejos basados en metales de transición están teniendo gran importancia en el campo de la catálisis. Aunque se han logrado altos porcentajes de conversión utilizando complejos de metales de transición en fase homogénea, la inmovilización de estos complejos sobre diversos soportes ha ganado interés en los últimos años para su uso como catalizadores heterogéneos. Materiales porosos tales como zeolitas, carbones activados, redes metal-orgánicas (MOFs) u organosílices mesoporosas pueden ser utilizados para tal fin.

Concretamente, la funcionalización de materiales silícicos porosos se puede realizar mediante dos procesos, esto es, el método de síntesis directa (proceso de *co-condensación*) y un proceso de modificación postsíntesis (*grafting*). El método de co-condensación da lugar a una distribución homogénea de los grupos funcionales por toda la estructura silícica, en deterioro de la

estructura porosa ordenada, es decir, a mayor cantidad de grupos funcionales introducidos peor será el ordenamiento. En cambio, en el proceso de *grafting* se obtienen materiales con un gran ordenamiento, pero la distribución de los grupos funcionales introducidos postsíntesis no es homogénea en toda la estructura, concentrándose sobre todo en la entrada de los poros y en la superficie externa. Tanto los métodos de co-condensación como de *grafting* pueden ir seguidos de procesos de funcionalización de los grupos o fragmentos orgánicos introducidos.

Para la oxidación de alquenos, se han anclado complejos de cobre con ligandos bipiridina en la superficie de materiales porosos tales como las organosílices mesoporosas de tipo SBA-15 o MCM-41.

Nuestro grupo de investigación ha publicado varios trabajos en los que se describe la síntesis de organosílices periódicas mesoporosas con ligandos superficiales de tipo dipiridil-piridazina, que han sido utilizados para formar diversos complejos con metales lantánidos y poseían propiedades luminiscentes.

En base a los antecedentes expuestos conjeturamos que la formación de complejos superficiales de cobre con ligandos de tipo dipiridil-piridazina puede dar lugar a la obtención de catalizadores heterogéneos activos en epoxidación de alquenos.

Objetivo 1

El primer objetivo propuesto para esta Tesis Doctoral es sintetizar un novedoso catalizador formado por un material periódico mesoporoso organosilícico (PMO) obtenido a través del proceso de co-condensación entre dos precursores silánicos, 1,2-bis(trietoxisilil)etano (BTEE) y viniltrietoxisilano (VTES), posterior reacción de Diels-Alder con el compuesto 3,6-di-2-piridil-1,2,4,5-tetrazina y formación de un complejo de cobre, y ensayar

su actividad en la oxidación selectiva de estireno a óxido de estireno usando como oxidante terc-butilhidroperóxido (TBHP).

Los resultados obtenidos se recogen en el capítulo 3, en el artículo: **"Copper-complexed dipyridyl-pyridazine functionalized periodic mesoporous organosilica as a heterogeneous catalyst for styrene epoxidation"**.

Hipótesis 2

El aumento de la población unido a la escasez o agotamiento de recursos energéticos no renovables (petróleo, carbón o gas natural) han incentivado a la comunidad científica a la búsqueda de nuevas formas de energía respetuosas con el medio ambiente. El hidrógeno se considera como uno de los vectores energéticos más atractivos para un futuro próximo ya que su combustión con el oxígeno sólo produce vapor de agua, nada nocivo para el medio ambiente.

Un nuevo proceso de obtención de hidrógeno es a partir de la ruptura de la molécula de agua con la acción de la luz solar (proceso fotoquímico), el cual está ganando cada vez más interés. Concretamente, el uso de catalizadores basados en elementos abundantes en la Tierra, como pueden ser el hierro, el cobalto o el níquel, es cada vez más frecuente. Los complejos de tipo cobaloxima, esto es, complejos de bis(dimetilglioximato)cobalto (III), son ideales para este fin, ya que son fáciles de sintetizar, poseen moderada fotoestabilidad y tienen alta eficiencia a bajos potenciales de reducción.

Principalmente, las cobaloximas han sido utilizadas en forma homogénea e inmovilizadas en electrodos de diferente naturaleza para aplicaciones electrocatalíticas. No sólo materiales conductores han sido utilizados para la

inmovilización de cobaloximas, en los últimos años materiales porosos no conductores como los MOFs o los COFs están siendo utilizados para tal fin.

Por todo ello, se puede hipotetizar que la inmovilización de complejos de tipo cobaloxima en diferentes organosílices periódicas mesoporosas debido a sus excelentes propiedades estructurales puede conducir a la obtención de catalizadores heterogéneos activos y estables para la producción de hidrógeno por acción de la luz visible.

Objetivo 2

El segundo objetivo de esta Tesis doctoral consiste en sintetizar un material periódico organosilícico con estructura porosa ordenada mediante el método de co-condensación entre los precursores silánicos 1,2-bis(trietoxisilil)etano y 2-(4-piridiletil)trietoxisilano, a continuación anclar un complejo de tipo cobaloxima sobre los grupos piridina colgantes y, posteriormente, estudiar su actividad como catalizador heterogéneo en la reacción de disociación fotocatalítica del agua, utilizando eosin Y como fotosensibilizador, TEOA como agente de sacrificio, y luz visible como fuente de radiación.

Los resultados obtenidos se recogen en el capítulo 4, en el artículo: **"Cobaloxime tethered pyridine-functionalized ethylene-bridged periodic mesoporous organosilica as an efficient HER catalyst"**.

Objetivo 3

El tercer objetivo planteado en esta Tesis es comparar la actividad catalítica en la producción de hidrógeno de un complejo de tipo cobaloxima unido

a varios soportes silícicos con sistemas porosos ordenados y no ordenados obtenidos en diferentes condiciones de síntesis.

Los resultados obtenidos de esta investigación quedan recogidos en el capítulo 5, **"Catalytic activity of cobaloxime complexes anchored to organosilicas in artificial photosynthesis: Ordered vs. non-ordered materials".**

Objetivo 4

El cuarto objetivo de esta Tesis Doctoral es comparar la actividad catalítica de un complejo de tipo cobaloxima anclado en dos organosílices mesoporosas ordenadas con diferentes grupos funcionales en su estructura (piridina e imidazol) en la reacción fotocatalítica de producción de hidrógeno.

Los resultados obtenidos durante esta investigación están recogidos en el capítulo 6, en el artículo: **"Improved Photocatalytic H_2 Evolution by Cobaloxime-Tethered Imidazole-Functionalized Periodic Mesoporous Organosilica".**

Hipótesis 3

El cambio climático, generado principalmente por la alta concentración de CO_2 presente en la atmosfera, ha producido un gran interés en el desarrollo de procesos para sustraer este CO_2 de la atmosfera y transformarlo en productos de interés. Uno de los grandes desafíos actuales es la fotorreducción de CO_2, es decir, la descomposición de CO_2 a través de luz solar en otros productos de interés como monóxido de carbono, ácido fórmico o metanol.

Los catalizadores basados en ftalocianinas de cobalto han sido estudiados en el campo de la eletrocatálisis para tal fin. Debido a sus excelentes propiedades catalíticas se han inmovilizado en electrodos, en materiales reticulares o en semiconductores.

Por otro lado, el diseño de un catalizador poroso ayuda a la difusión del resto de componentes necesarios para la reacción catalítica. De ahí que la integración de estos complejos de cobalto en materiales micro o mesoporosos como los MOFs o COFs está despertando gran interés en el campo de la fotocatálisis. En este contexto, los materiales periódicos mesoporosos ordenados (PMO) son una familia de materiales idóneos para ser utilizados para este fin ya que poseen elevadas superficies específicas y se puede modelar su hidrofobia y su tamaño de poro.

Objetivo 5

El quinto objetivo fijado para esta Tesis se centra en sintetizar un nuevo catalizador heterogéneo con centros metálicos de cobalto para su utilización en la reducción fotocatalítica de CO_2, integrando mediante co-condensación las unidades de ftalocianinas de cobalto (CoPc) en la estructura silícica de un material periódico mesoporoso ordenado (PMO).

Los resultados obtenidos se recogen en el capítulo 7, en el artículo: **“Solar driven CO_2 reduction with a molecularly engineered periodic mesoporous organosilica containing cobalt phthalocyanine”.**

CHAPTER 3.

RESULTS AND DISCUSSION

(PAPER 1)

Chapter 3. **Copper-complexed dipyridyl-pyridazine functionalized periodic mesoporous organosilica as heterogeneous catalyst for styrene epoxidation**

PAPER 1

Copper-complexed dipyridyl-pyridazine functionalized periodic mesoporous organosilica as heterogeneous catalyst for styrene epoxidation

Mª Ángeles Navarro,[a] Juan Amaro-Gahete,[a] José R. Ruiz,[a] César Jiménez-Sanchidrián,[a] Francisco J. Romero-Salguero[a*] and Dolores Esquivel[a*]

[a]*Departamento de Química Orgánica, Instituto Universitario de Nanoquímica (IUNAN), Facultad de Ciencias, Universidad de Córdoba, 14071 Córdoba, España*

Corresponding authors: Email address; qo2rosaf@uco.es (F.J.R.-S.); q12esmem@uco.es (D.E.)

Paper

Copper-complexed dipyridyl-pyridazine functionalized periodic mesoporous organosilica as a heterogeneous catalyst for styrene epoxidation

M. Ángeles Navarro, Juan Amaro-Gahete, José R. Ruiz, César Jiménez-Sanchidrián, Francisco J. Romero-Salguero and Dolores Esquivel

A novel copper organometallic complex anchored on periodic mesoporous organosilica was synthesized and used as a catalyst in styrene epoxidation.

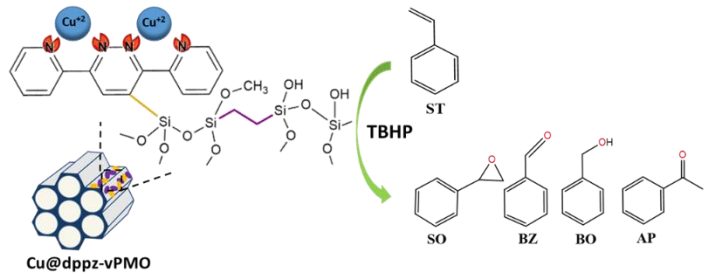

The article was first published on 23 Feb 2022
Dalton Trans., 2022, **51**, 4884-4897
https://doi.org/10.1039/D2DT00018K

ABSTRACT

A new heterogenous catalyst has been synthesized by immobilization of a copper complex on dipyridyl-pyridazine functionalized periodic mesoporous organosilica (dppz-vPMO). This ordered support was firstly prepared by a co-condensation reaction between vinyltriethoxysilane and 1,2-bis(trimethoxysilyl)ethane and further post-functionalized through a hetero Diels-Alder reaction with 3,6-di-2-pyridyl-1,2,4,5-tetrazine. Techniques such as XRD, N_2 isotherms, TEM, ^{13}C NMR, XPS and DRIFT, among others, were employed to characterize the surface functionalized materials. These results have proven the ordered mesostructure of the materials as well as the presence of novel nitrogen-chelating heterocyclic compounds in the pore surface after the post-modification process.

Additionally, it has been confirmed the successful anchoring of a copper complex on the dipyridyl-pyridazine (dppz) ligands. The resulting material was evaluated as heterogenous catalyst in the epoxidation of styrene using tert-butylhydroperoxide (TBHP) as oxidant. Under optimized reaction conditions, Cu@dppz-vPMO showed a high styrene conversion (86.0 %) and a remarkable selectivity to styrene oxide (41.9 %). Indeed, this catalyst provided excellent catalytic results in terms of stability, reaction rate, conversion and selectivity compared to other bipyridine-like copper catalysts.

Keywords: periodic mesoporous organosilicas; Diels-Alder reaction; dipyridyl-pyridazine; copper complex; epoxidation reactions.

3.1 INTRODUCTION

Epoxidation of olefins is one of the most relevant reactions in organic synthesis since the resultant epoxide products are important and versatile intermediates for the synthesis of a wide variety of fine chemicals, pharmaceuticals, agrochemicals, and perfumes, among others [1–4]. While traditional methods for the synthesis of epoxides are characterized by using stoichiometric amounts of harmful oxidants (peracids) and generate enormous waste [5–7], the recent synthetic methodologies in this field are focused to overcome them. Thus, the use of safer oxidizing agents, such as tert-butyl hydroperoxide (TBHP), molecular oxygen or hydrogen peroxide in the styrene epoxidation opens an economic and environmental alternative. However, their characteristic low reactivity and selectivity in this type of reaction when they are used alone has led to the use of such oxidants in combination with transition-metal catalysts [3,8]. Over the last decades, a wide variety of ions, oxides and complexes of transition metals have been explored through homogeneous catalytic processes. Despite these systems lead to high yields in the epoxidation reactions, their immobilization on solid supports have gained much more attention from an environmental and economical perspective due to their potential applications in industry [9–14]. Nowadays, the development of efficient heterogenized catalytic systems for the epoxidation of olefins remains a challenge [4,15–17]. Different types of porous materials, such as zeolites [18], polymers [19], mesoporous silicas [14], activated carbons [20] or MOFs [21] have been employed as supports of transition metal complexes for liquid phase epoxidation of olefins.

Studies on epoxidation reactions catalysed by heterogenized Schiff-bases and other Cu(II)-complexes catalysts have received a great deal of attention during recent years. Depending on the support, different synthetic

approaches have been adopted to integrate them on their framework for the oxidation of olefins. Thus, Spodine et al. [22] were the first who reported the synthesis of a MOF with Cu(II) centers coordinated to bipy (2,2'-bipyridine) and H_4btec (1,2,4,5-benzenetetracarboxylic acid) ligands as a heterogeneous catalyst for oxidation reactions. More recently, Cu species have been incorporated within the framework of a Ga- [23] and Zr-based metal organic framework [24] with bipyridine linkers by a post-synthetic modification method with $CuCl_2$ and $CuBr_2$, respectively. Furthermore, another family of ordered porous materials that have attracted a great interest due to their unique features are mesoporous organosilicas. The first attempts were based on the confinement of copper (II) complexes with bipyridine ligands in the mesoporous channels of MCM-41 for oxidation de alkenes [25,26]. Later, a more developed strategy involved the covalent attachment or grafting of organic compounds within the mesochannels of silica materials and subsequent complexation with copper. Most of the studies reported the functionalization of highly ordered 2D-hexagonal mesoporous silicas, such as MCM-41 and SBA-15 materials, with 3-aminopropyltriethoxysilane followed by its condensation with a suitable aldehyde to produce a coordinating Schiff-base ligand [27–29]. Although these heterogenous systems have shown to be effective for liquid phase oxidation of olefins, the drawbacks associated to grafting procedures are well known. As an alternative to mesoporous organosilicas, the synthesis of periodic mesoporous organosilicas (PMOs) is able to produce well-ordered mesoporous structures with a uniform distribution of the organic functionality into the pore walls [30–32]. Since their discovery, a wide variety of metal and metal complexes have been directly integrated during the PMO synthesis or alternatively, through post-modification processes for catalytic applications [33]. Copper complexes have been

successfully supported on ionic liquid based PMO materials for the synthesis of propargylamines or polyhydroquinolines through the three-component coupling reaction of amines, aldehydes and alkynes [34] or Hantzsch reaction [35], respectively. More recently, Inagaki et al. [36] reported the immobilization of a Cu complex on a periodic mesoporous organosilica containing 2,2'-bipyridine ligands as bridging organic groups. The resulting catalysts were evaluated in the Mukaiyama epoxidation of cyclohexene as a model radical reaction. To the best our knowledge, no more examples of copper supported PMO materials have been described.

As above-mentioned, the presence of organic moieties in the PMO framework allows these materials to be modified through organic reactions. One of the reactions that have been extensively investigated by our research group is the Diels-Alder reaction. The double bonds on the walls of an ethenylene-bridged PMO have acted as dienophiles for the Diels-Alder reaction with common dienes, such as cyclopentadiene and anthracene [37], pyrrole derivatives [38] and tetrazine [39,40]. This latter diene gave rise to dipyridyl-pyridazine moieties on the PMO surface, which can form interesting chelates with metal ions. Following this approach, we have recently investigated the synthesis of mesoporous silica materials decorated with dipyridyl-pyridazine (dppz) ligands, which were further attached to lanthanide (Ln^{3+}) complexes (Ln^{3+} = Er^{3+}, Yb^{3+}, Nd^{3+} or Eu^{3+}/Tb^{3+} mixture) and used as potential ratiometric thermometer materials [40,41].

Herein, we report the preparation of a novel periodic mesoporous organosilica (PMO) with ethane bridges in the silica framework and pendant vinyl groups in the pore channels, which was post-functionalized with dipyridyl-pyridazine moieties through a hetero Diels-Alder reaction with 3,6-di-2-pyridyl-1,2,4,5-tetrazine. Subsequently, this material was

grafted with a Cu^{2+} complex for producing a suitable heterogenous catalyst for epoxidation reactions.

3.2 EXPERIMENTAL SECTION

3.2.1. Synthesis of vinyl-functionalized ethylene-bridged PMO (vPMO)

Periodic mesoporous organosilica was synthesized according to the procedure described in literature for the synthesis of thiol-functionalized mesoporous ethane-silicas with some modifications [42]. Typically, Pluronic P123 ($EO_{20}PO_{70}EO_{20}$, MW = 5800, Sigma–Aldrich) (0.5 g) and KCl (3.49 g) were dissolved in HCl solution (16.5 mL, 2M) and H_2O (3.75 mL) under vigorous stirring at 45 ºC. Next, a mixture with a molar composition ratio of 80 % of 1,2-bis(trimethoxysilyl)ethane (BTME, 2.84 mmol) and 20 % of vinyltriethoxysilane (VTES, 0.71 mmol) was added dropwise to the above solution. The reaction mixture was stirred at 45 ºC for 24 h and following aged at 100 ºC under static conditions for 24 h. The white solid product was recovered by filtration and thoroughly washed with distilled water. To remove the surfactant, 1 g of as-synthetized material was refluxed in a solution containing 50 mL ethanol and 1 mL HCl solution (37%) for 24 h. This process is repeated twice, the white solid was recovered by filtration, washed with acetone and dried under vacuum at 100 ºC. The material synthesized was named *vPMO*.

3.2.2 Post-functionalization of vPMO by Diels-Alder reaction with 3,6-di-2-pyridyl-1,2,4,5-tetrazine.

The organic ligand 3,6-di-2-pyridyl-1,2,4,5-tetrazine (dppz) was synthetized according to a previously reported procedure [40]. This compound was used as diene in the surface Diels-Alder reaction of vinyl-functionalized ethylene-bridged PMO. Thus, 0.6 g of vPMO was added to a mixture containing 0.5 g of 3,6-di-2-pyridyl-1,2,4,5-tetrazine and 40 mL of dodecane. The reaction

mixture was stirred at 150 ºC for 13 days under inert atmosphere. The resulting material was collected by vacuum filtration and washed with chloroform. In order to remove possible unreacted diene physically adsorbed into the pores, the material was refluxed in chloroform during 24 h. This procedure was repeated twice. Then, the solid was collected by vacuum filtration and dried at 100 ºC. Finally, the solid product was aromatized using $NaNO_2$ as oxidant to dehydrogenate de dihydropyridazine ring of the surface adduct. Thus, 0.15 g of material were dissolved in 7 mL of acetic acid and in small portions 0.21 g of $NaNO_2$ were added. The mixture was kept under stirring at 65 ºC for 2 h. Then, the solid was recovered by vacuum filtration, washed with ethanol twice and dried at 100 ºC overnight. The final material was named *dppz-vPMO*.

3.2.3 Immobilization of Cu complexes on the surface Diels-Alder adducts.

To immobilize Cu complexes on the surface of Diels-Alder adducts [24], 0.063 g of $CuCl_2 \cdot 2H_2O$ was dissolved in acetonitrile (15 mL) and then 0.1 g of dppz-vPMO was added to the solution. The mixture was stirred at room temperature for 24 h. Afterwards, it was filtered and washed several times with chloroform to guarantee the complete removal of any physisorbed copper salt. The material was dried under vacuum at 100 ºC and named as *Cu@dppz-vPMO.*

3.2.4 Characterization techniques

X-ray powder diffraction (XRD) patterns were collected on a Bruker D8 Discover A25 diffractometer using Cu Kα radiation (λ = 1.5406 Å) with an applied voltage and current of 40 kV and 300 mA, respectively. Nitrogen adsorption experiments were carried out at -196 ºC using an Autosorb-iQ MP/MP-XR instrument. Prior to the measurements, all the samples were degassed at 120 °C for 24 h. Specific surface areas were calculated from the linear regions of Brunauer-Emmett-Teller (BET) plots (P/P_0 = 0.1 - 0.20). Pore size distributions

were obtained using the density functional theory method (DFT) (DFT kernel: silica, cylindrical pores, nonlinear DFT (NLDFT) equilibrium model). Raman spectra were acquired with a Renishaw Raman instrument by excitation with green laser light (532 nm). High-resolution Transmission Electron Microscopy images were recorded on a JEOL JEM 1400 microscope at an accelerating voltage of 300 kV. The diffuse reflectance infrared Fourier transform spectra were recorded on a Perkin-Elmer 2000 FTIR spectrometer equipped with a diffuse reflectance environmental chamber (Harrick) connected to a temperature controller. The sample was heated in situ from room temperature to 150 °C under nitrogen. Spectra were collected between 1000 and 4000 cm^{-1}. The ^{13}C CP/MAS NMR spectra were recorded on a Bruker Avance III HD 400 WB spectrometer at 100.61 MHz. Chemical shifts were referenced to tetramethylsilane (TMS). X-ray photoelectron spectroscopy (XPS) were recorded on a SPECS Phoibos HAS 3500 150 MCD X-ray photoelectron spectrometer with a monochromatic Al anode (1486.7 eV). Accurate binding energies have been determined with respect to the position of Si 2p at 103.4 eV. XPS survey spectrum was collected at a pass energy of 60eV, while high-resolution XPS spectra were obtained at a pass energy of 40 eV and a resolution of 0.1 eV. UV-vis spectra were recorded on an UV-visible diffuse reflectance spectrophotometer Varian Carey IE UV-vis equipped with a 110 nm integration sphere. ICP-MS analysis was performed on a Perkin Elmer NexIONTM 350X ICP Mass Spectrometer".

3.2.5 Epoxidation of styrene

Epoxidation reaction of styrene was carried out in a two necked round-bottom glass reactor equipped with a magnetic stirring bar and a reflux condenser. Toluene and nitrobenzene were used as solvent and internal standard, respectively [24]. Typically, 50 mg of catalyst was added to a solution containing styrene (0.058 mL, 0.5 mmol), tert-butyl hydroperoxide (TBHP, 0.2 mL, 0.5 mmol),

nitrobenzene (0.082 mL, 0.8 mmol) and toluene (2 mL). Afterwards, the reaction mixture was kept under stirring at 90 ºC for 1 h. Sample aliquots (0.2 mL) were taken out from the mixture and diluted with toluene. The products were analysed and quantified in a Varian gas chromatograph with a capillary column (VF-1MS, 15 m x 0.25 mm ID) and a flame ionization detector (FID) and using standard compounds. After the reaction, the catalyst was filtered off, washed with acetonitrile and dried under vacuum at 90 ºC, and then reused directly without further purification. The recyclability of the Cu@dppz-vPMO catalyst was investigated during five consecutive runs.

One blank reaction was carried out without adding any catalyst under the same experimental conditions.

3.3 RESULTS AND DISCUSSION

3.3.1 Synthesis and characterization of materials

The copper (II) complex was immobilized on dppz-vPMO support as illustrated on Scheme 1. Firstly, vinyl-functionalized ethylene-bridged PMO (vPMO) was prepared by co-condensation reaction between 1,2-bis(trimethoxysilyl)ethane (80 %) and vinyltriethoxysilane (20 %) using P123 as template under acidic conditions. Next, the pendant double bonds of vPMO acted as dienophiles in a hetero Diels-Alder reaction with a substituted tetrazine (3,6-di-2-pyridyl-1,2,4,5-tetrazine, dptz), giving rise to the formation of surface dipyridyl-pyridazine (dppz) units. Thus, the dppz-vPMO support was functionalized with nitrogen-based chelating heterocycles providing suitable ligands for anchoring Cu(II) complexes. The copper complex on dipyridyl-pyridazine functionalized PMO was finally synthesized by coordinating the copper salt ($CuCl_2 \cdot 2H_2O$) with dppz-vPMO support.

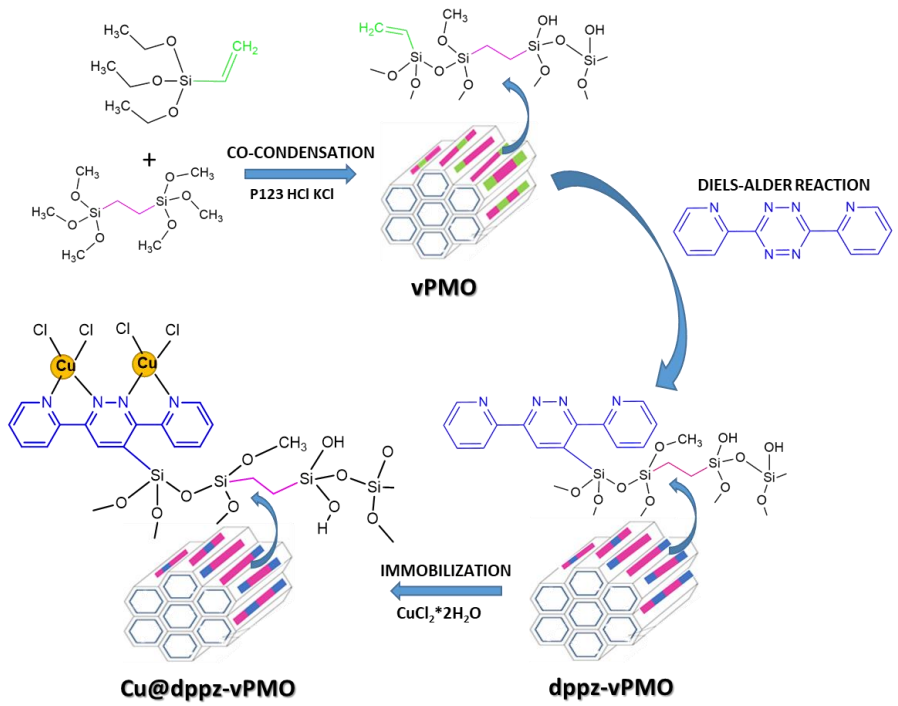

Scheme 1. Synthesis procedure of Cu@dppz-vPMO catalyst.

The XRD diffraction pattern of vinyl-functionalized ethylene-bridged PMO (vPMO) displayed a low peak (100) at $2\theta = 0.9$ and two small second-order (110) and (200) peaks at higher incidence angles, characteristic of materials with 2D-hexagonal pore mesostructure (*P6mm*) (Fig 1). After Diels-Alder reaction with 3,6-di-2-pyridyl-1,2,4,5-tetrazine, the resulting dppz-vPMO material showed a similar diffraction pattern, indicating that the mesoscopic ordering of the parent material remained intact after the surface modification reaction. Likewise, after immobilization of Cu-complexes on the dipyridyl-pyridazine units, the initial ordered mesoporous structure was preserved [41]. These results indicate the great stability of the pristine mesostructure after Diels-Alder and immobilization reactions. Recently, Inagaki et al. reported that the mesostructure ordering of bipyridine-bridged PMO during the immobilization of Cu-complexes

was damaged when the solid was dispersed in protic solvents, such as methanol and water [36].

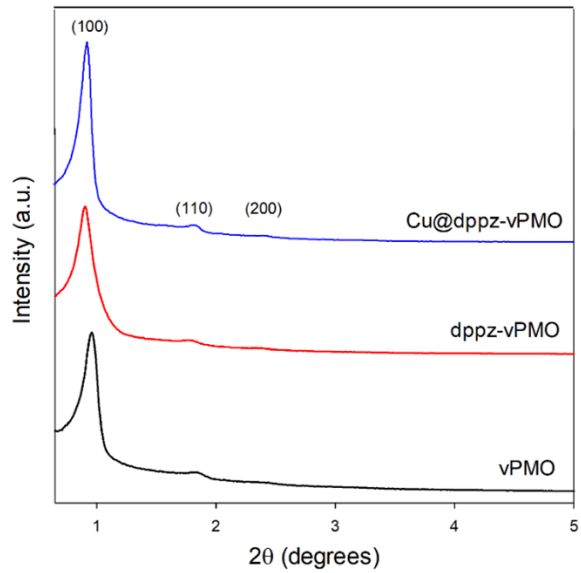

Fig 1. XRD patterns of vPMO, dppz-vPMO and Cu@dppz-vPMO.

The nitrogen adsorption-desorption isotherms of the different materials are shown in Fig 2. All materials exhibited type-IV isotherms with H1-type hysteresis loops at relative pressures of 0.5-0.7, confirming the presence of uniform cylindrical mesopores. The average pore diameter and narrow pore size distribution of the PMO materials confirmed the presence of pores in the mesopore range (Fig 2, right). Textural properties (S_{BET}, V_p and D_p) of the periodic mesoporous organosilica materials are listed in Table 1. vPMO has a high S_{BET} of 849 m^2 g^{-1} and pore volume of 0.86 cm^3 g^{-1}. After Diels-Alder reaction, a slight decrease of surface area and pore volume were appreciated. In addition, the immobilization of the copper complex on the surface Diels-Alder adducts gave rise to a higher decrease of S_{BET} (421 m^2 g^{-1}) and pore volume (0.50 cm^3 g^{-1}). The pore wall thickness increased after Diels-Alder reaction with the tetrazine derivative due to the volume occupied by the organic fragments. Similar results

were previously reported in this type of reaction with the same diene and other dienophiles [39,40].

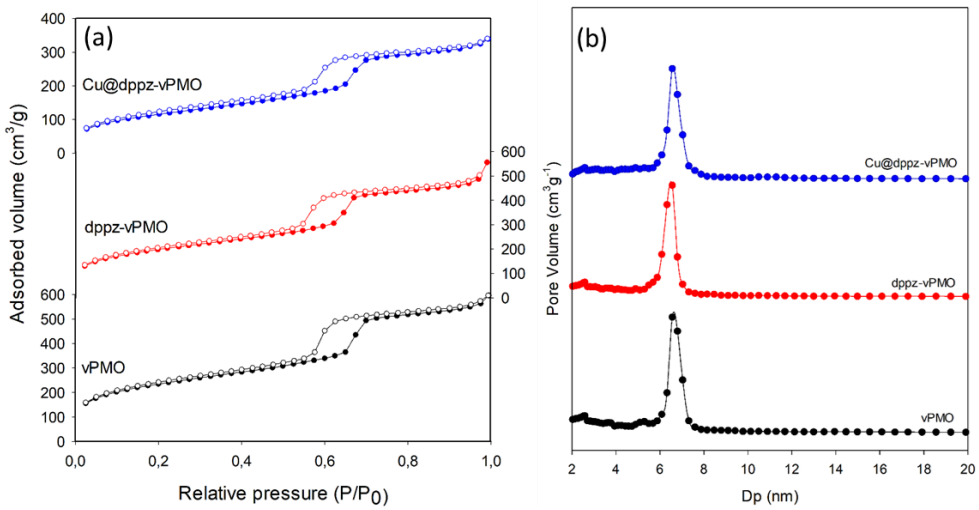

Fig 2. N_2 adsorption-desorption isotherms (a) and pore size distributions (b) of periodic mesoporous organosilica materials.

Table 1. Physicochemical properties of synthesized periodic mesoporous organosilicas[a]

Sample	d_{100} (nm)	a_0	S_{BET} ($m^2\ g^{-1}$)	V ($cm^3\ g^{-1}$)	D[b] (nm)	t[c] (nm)
vPMO	9.2	10.6	849	0.86	6.6	4.0
dppz-vPMO	9.6	11.1	715	0.78	6.6	4.5
Cu@dppz-vPMO	9.7	11.2	421	0.50	6.6	4.6

[a] d_{100}, (100) spacing; S_{BET}, BET surface area; V, pore volume; D, pore diameter; t, wall thickness.
[b] calculated by the DFT method
[c] calculated from (a_0 – D), where $a_0 = 2d_{100}/\sqrt{3}$

In addition to the PXRD and nitrogen sorption measurements, TEM images corroborated the structural ordering of the synthesized materials (Fig 3).

TEM images of vPMO revealed the highly ordered hexagonally array of straight mesoporous channels. These uniform pore channels were retained after functionalization and complexation processes.

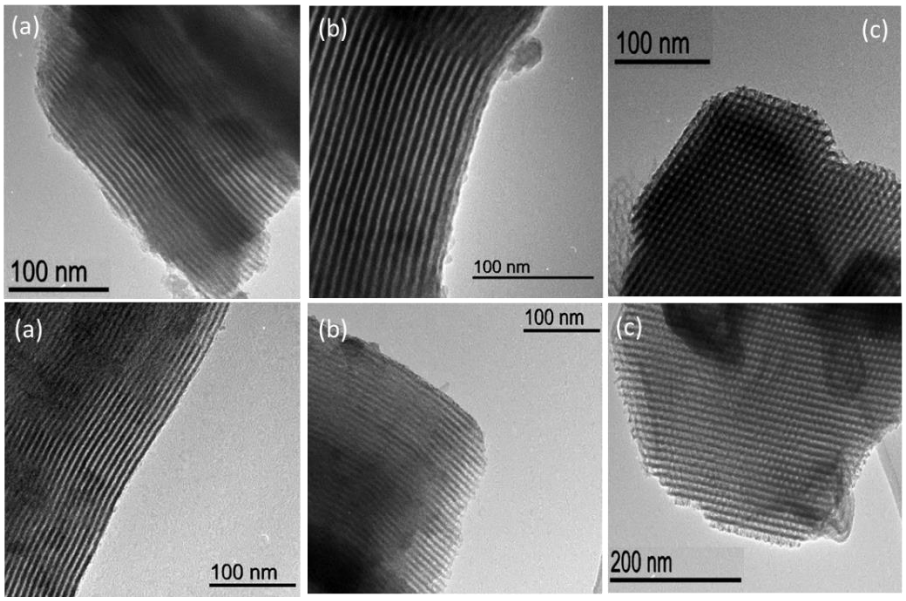

Fig 3. TEM images of vPMO (a), dppz-vPMO (b) and Cu@dppz-vPMO (c).

The presence of both organic moieties, i.e. bridging ethylene groups in the silica framework and vinyl groups in the channel pores, on the parent material as well as the resulting surface Diels-Alder adducts on dppz-vPMO have been confirmed by DRIFT and solid-state ^{13}C CP/MAS NMR measurements (Fig 4). DRIFT spectrum of vPMO (Fig 4a) showed bands at 3050 and 1591 cm^{-1} associated to =CH and C=C stretching vibrations of vinyl groups, respectively. Additionally, several signals in the C-H stretching region, below 3000 cm^{-1}, are characteristic of the ethylene bridges in the silica framework and the remaining surfactant into pores. After Diels-Alder reaction, dppz-vPMO showed additional vibrational signals associated to the C=N stretching (1560 cm^{-1}) and skeletal vibrational (1360 - 1600 cm^{-1}) of the dipyridyl-pyridazine units [43].

The solid-state ^{13}C CP/MAS NMR spectrum of vPMO (Fig 4b) showed an intense signal at 5 ppm and signals at 130 and 137 ppm corresponding to the Csp^3 and Csp^2 of the ethane and vinyl groups, respectively [44,45]. Additionally, signals at 21 and 58 ppm could be assigned to non-hydrolysed methoxy ($-OCH_3$) and ethoxy ($-OCH_2CH_3$) groups remaining after the synthesis procedure. Small signals at 71 and 76 ppm are characteristic of P123 surfactant residues, still present in the pores after three successive extractions. After Diels-Alder reaction, new signals appeared in the aromatic region (149 – 125 ppm) corresponding to the aromatic carbons present in the surface adducts [39].

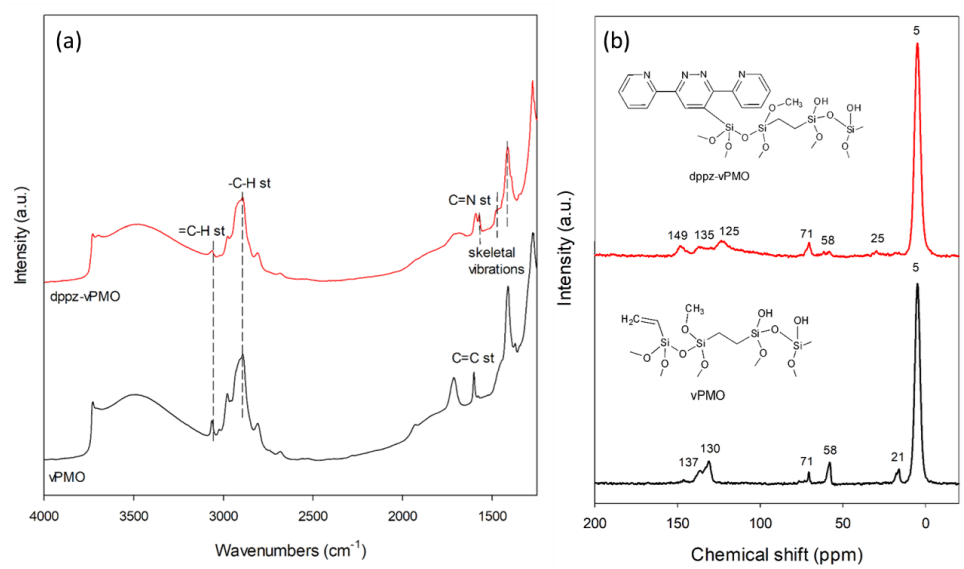

Fig 4. DRIFT spectra (a) and ^{13}C CP/MAS NMR spectra (b) of vPMO and dppz-vPMO.

XPS measurements were performed to obtain surface information of the samples and confirm the incorporation and oxidation state of copper. Survey spectrum of dppz-vPMO (Fig 5a) indicated the presence of Si, C, O and N in the surface analysis of the sample. After copper immobilization on the dipyridyl-pyridazine adducts, additional signals associated to Cu were present for the Cu@dppz-vPMO sample. The N1s XPS spectrum (Fig 5b) for dppz-vPMO

only exhibited a component centered at 400.6 eV attributed to the nitrogen atoms in the pyridine and pyridazine rings [46]. A slight shift (0.3 eV) of the binding energy toward a higher value was observed after copper complexation, in accordance with the electronic interaction between copper and nitrogen atoms in the sample. Furthermore, the Cu2p XPS spectrum (Fig 5c) for Cu@dppz-vPMO showed two characteristic peaks at 934.8 and 954.6 eV, which correspond to $Cu2p_{3/2}$ and $Cu2p_{1/2}$, respectively. The appearance of shake-up satellite bands at 940-950 eV confirmed the presence of Cu^{2+} [14,47].

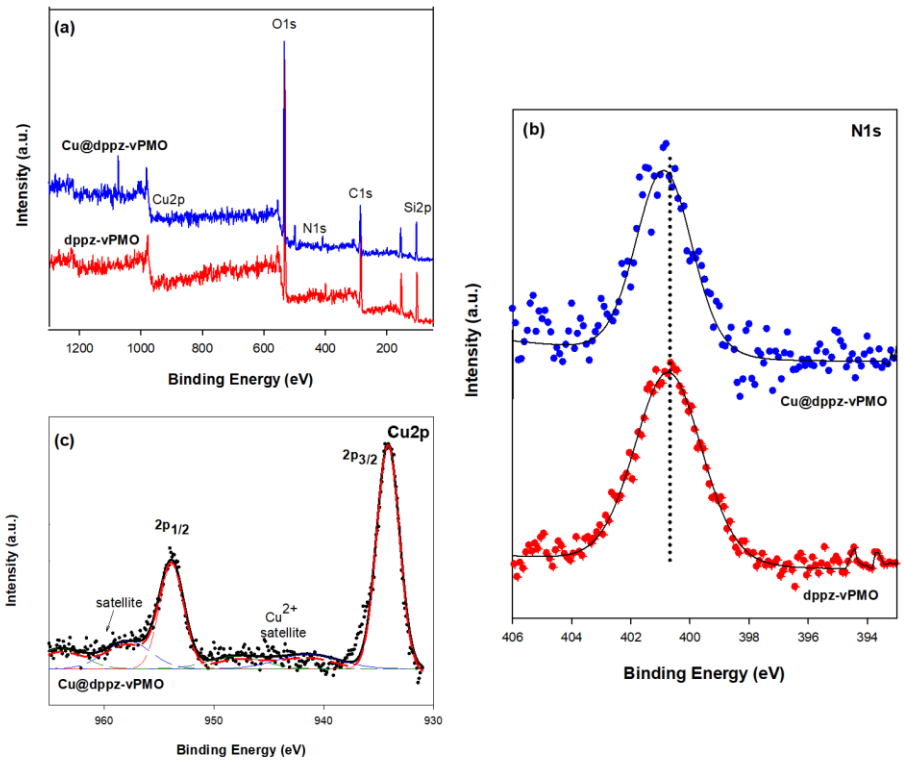

Fig 5. XPS spectra of dppz-vPMO and Cu@dppz-vPMO: (a) survey scan, (b) N1s and (c) Cu2p.

The presence and coordination of the copper complex was further corroborated using UV-vis diffuse reflectance spectroscopy. Fig 6 shows UV-vis

diffuse reflectance spectra of dppz-vPMO and Cu@dppz-vPMO. The material dppz-vPMO exhibited two adsorption bands in the region of 260-320 nm and 500-600 nm which are attributed to the π-π* and n-π electronic transitions of dipyridyl-pyridazine units [48]. After copper immobilization, the UV-vis diffuse reflectance spectrum of Cu@dppz-vPMO exhibited a wide adsorption ranging from 300-500 nm, with maxima centered at 320 and 380 nm. These bands could be assigned to ligand to metal charge transfer (LMCT). Furthermore, it showed a relatively broad band in the range of 600-800 nm, which may be attributed to the d-d transition at the metal centre. Similar adsorption patterns were observed for Cu^{2+} complexes with N- and O-donor Schiff base ligands anchored on mesoporous silica [29].

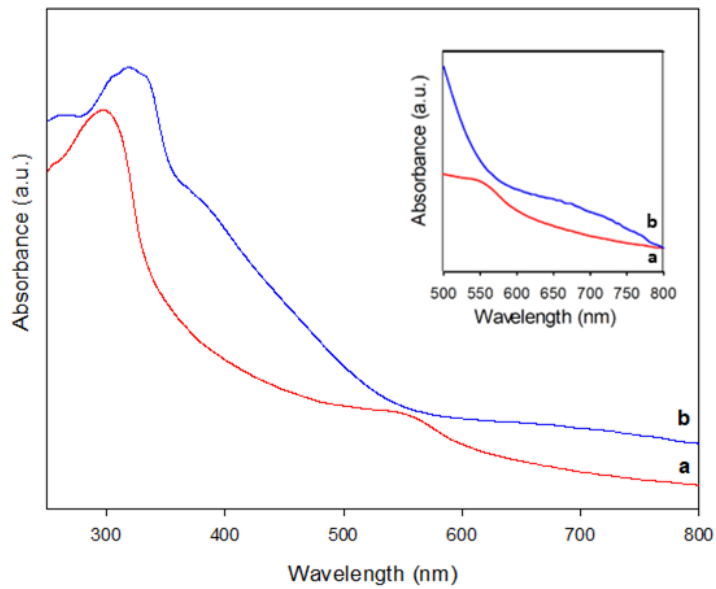

Fig 6. UV-Vis diffuse reflectance spectra of dppz-vPMO (a) and Cu@dppz-vPMO (b) materials.

The nitrogen content in dppz-vPMO determined by elemental analysis was 0.18 mmol g^{-1}. Furthermore, the copper loading for Cu@dppz-vPMO calculated

by ICP-MS was 0.13 mmol g^{-1}. Accordingly, the Cu/N ratio on the catalyst was 0.72, slightly higher to the theorical one (Cu/N = 0.5). This would confirm the coordination of some cupper species on the free silanol groups at the pore surfaces of dppz-vPMO [49].

3.3.2 Catalytic activity in styrene epoxidation

As above-mentioned, the olefins epoxidation is an interesting organic reaction to produce value-added chemicals. In this work, Cu@dppz-vPMO was employed as heterogenous catalyst in the styrene reaction with tert-butyl hydroperoxide (TBHP) as oxidant. The conversion of styrene and the selectivities to different products are displayed in Table 2. Obviously, the blank reaction gave a lower conversion (19.3 %) as resulted from the autoxidation of styrene by TBHP. Without any catalyst, non-formation of styrene oxide (SO) was appreciated. When $CuCl_2$ was essayed as homogeneous catalyst, the conversion of styrene was 50.5 % but SO was not obtained. Interestingly, our heterogenous catalytic system, Cu@dppz-vPMO, reached a higher conversion (59.1%) and a SO selectivity of 18.8 %. Other oxidants, such as hydrogen peroxide and oxone, were tested in the styrene oxidation. Under similar conditions, the oxidation reaction did not proceed with oxone as oxidant. Unlike, a styrene conversion of 67.0 % and a high selectivity to BZ (87.6 %) was obtained using H_2O_2 as oxidizing agent.

Table 2. Catalytic activities for selective oxidation of styrene

Entry	Catalyst	Oxidant	Conversion (%)	Selectivity[d] (%)			
				SO	BZ	AP	BO
1	Blank[a]	TBHP	19.3	-	63.9	24.6	11.6
2	$CuCl_2$*$2H_2O$[a]	TBHP	50.5	-	76.7	-	23.4
3	Cu@dppz-vPMO[a]	TBHP	59.1	18.8	58.3	4.3	18.6
5	Cu@dppz-vPMO[b]	H_2O_2	67.0	3.5	87.6	8.6	0.3
6	Cu@dppz-vPMO[c]	Oxone	--	---	---	---	---
7	Cu@dppz-vPMO[e]	TBHP	73.1	36.1	45.9	3.4	14.6

[a]Reaction conditions: 50 mg of catalyst, 0.5 mmol of styrene, 1 mmol of TBHP, 2 mL of solvent (toluene); reaction temperature, 90 ºC; reaction time, 1 h.

[b]Reaction conditions: 50 mg of catalyst, 0.5 mmol of styrene, 1 mmol of H_2O_2 (30%), 2 mL of solvent (acetonitrile); reaction temperature, 90 ºC; reaction time, 1 h.

[c]Reaction conditions: 50 mg of catalyst, 0.5 mmol of styrene, 1 mmol of Oxone (dissolved 0.8 ml of water), 2 mL of solvent (toluene); reaction temperature, 90 ºC; reaction time, 1 h.

[d]SO = styrene oxide, BZ = benzaldehyde, AP = acetophenone, BO = benzyl alcohol

[e]Optimized conditions: 50 mg catalyst, 0.5 mmol styrene, 2 mmol TBHP, 2 mL solvent (toluene), reaction temperature 100 ºC, reaction time 1h.

Based on the experimental findings of this work and previous literature [15,22,29,50], a plausible reaction mechanism for epoxidation of styrene with TBHP over Cu@dppz-vPMO catalyst has been proposed in Scheme 2. The mechanism begins with the formation of oxygenated intermediary species (*Cu(III)-peroxo*) (**I**) after the coordination of TBHP to the Cu(II) centre. Later, the reaction between the double bonds of styrene and species **I** can occur by two possible reaction pathways according to the observed products. The dominant reaction path (Path 1) consists of a concerted oxygen transfer, giving rise to the cyclic intermediate (**II**) and t-butanol. Subsequently, the cleavage of the Cu-O

bond yields styrene oxide (**SO**) together with the simultaneous regeneration of the Cu (II) centre. Additionally, the ring-opening of the epoxide by attack of TBHP can form the peroxide **III** and **IV**, resulting in the formation of benzyl alcohol (**BO**) and benzaldehyde (**BZ**), respectively. This latter could also be formed by direct oxidation of BO with TBHP [51,52]. Furthermore, the oxidation of styrene to acetophenone (**AP**), also detected as reaction product, proceeds via the formation of intermediate peroxo metallocycle species (**IV**) that are formed by the interaction of the peroxo group with the double bonds of styrene molecules (Path 2).

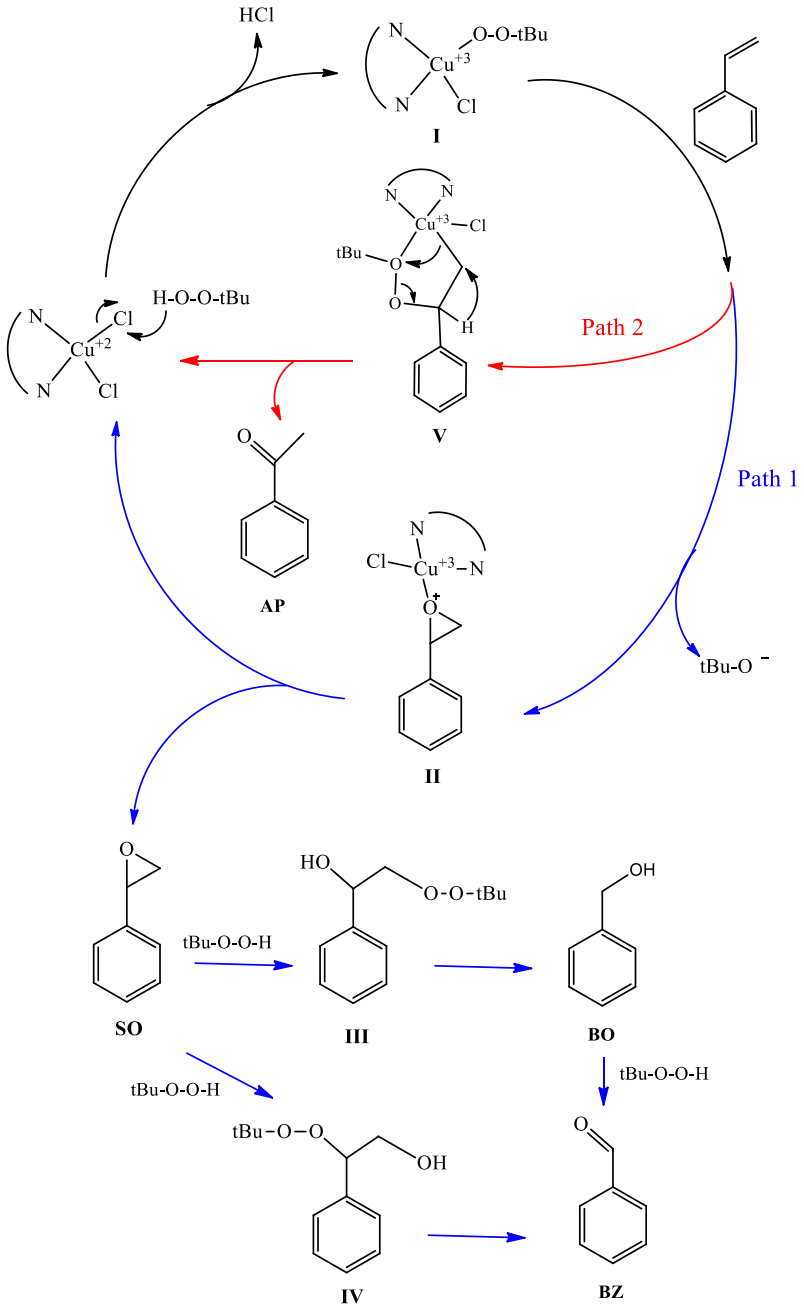

Scheme 2. Proposed mechanism for styrene epoxidation reaction over Cu@dppz-vPMO catalysts using TBHP as oxidant.

The recycling test of Cu@dppz-vPMO catalyst was conducted for five successive cycles under the foresaid reaction conditions. As shown in Fig 7a, the selectivity to all products was kept practically constant during the successive catalytic cycles. Although the styrene conversion remained stable (ca. 60%) during the catalytic cycles, a slight drop of conversion was appreciated in the third cycle. This could be ascribed to the blockage of the active sites by some products molecules that remained adsorbed on the catalyst surface after its filtration and washing. Indeed, the catalytic activity was recovered in the following runs. These results confirmed the high stability of the copper complex on dipyridyl-pyridazine functionalized PMO material in the styrene epoxidation reaction, similar to other copper-supported mesoporous materials reported in literature [36,50]. Furthermore, N_2 adsorption-desorption isotherms (Fig. 7b) and TEM image (Fig. 7c) of Cu@dppz-vPMO after the first and fifth catalytic cycle, corroborated the high mesostructural stability of the material under the oxidative conditions employed.

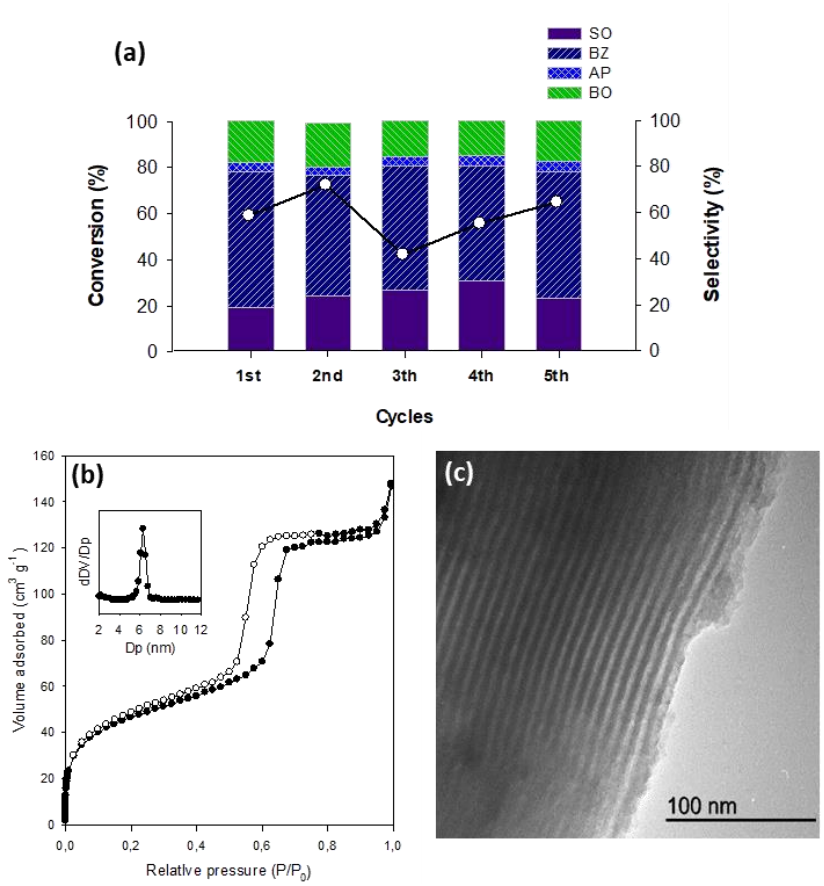

Fig 7. (a) Recycling test of Cu@dppz-vPMO in the styrene epoxidation reaction for five cycles. Reaction conditions: 50 mg of catalyst, 0.5 mmol of styrene, 1 mmol of TBHP, 2 mL of solvent (toluene); reaction temperature, 90 ºC; reaction time, 1 h. (b) N_2 adsorption-desorption isotherms of Cu@dppz-vPMO after one reaction cycle. (c) TEM image of Cu@dppz-vPMO after five reaction cycles.

To optimize the reaction conditions, the effect of various reaction parameters - *solvent, temperature and substrate/oxidant molar ratio* - that may affect the conversion and selectivity of the styrene epoxidation was examined (Fig 8). Initially, in order to evaluate the influence of the solvent, the epoxidation reaction was performed with a molar ratio of 1:2 (styrene:TBHP) and different solvents (acetonitrile, benzonitrile, dichloromethane, dimethylformamide and

toluene) (Fig 8a). Using acetonitrile and benzonitrile at 80 and 90 ºC, respectively, a higher styrene conversion was obtained. Previous studies have reported that nitriles, with a high dielectric constant, are excellent solvents in styrene epoxidation with TBHP due to an increased solubility of the reactants and therefore a better accessibility to the active sites of the catalyst [53,54]. No SO was obtained in acetonitrile, being BZ the major reaction product. The selectivity to SO increased up to 15 % in benzonitrile. Unlike, using dichloromethane and dimethylformamide as solvents at 40 and 120 ºC, respectively, the conversion was found to be zero. The highest SO selectivity (18 %) was reached in toluene.

To evaluate the influence of the temperature on styrene epoxidation, it was performed at 60, 80, 90 and 100 ºC in toluene (Fig 8b). The higher the temperature, the higher the conversion and selectivity to SO. This positive trend in conversion and selectivity with temperature is consistent with previous reports that also found that vinyl C-H bonds of styrene molecules were more active at higher temperatures [28]. Additionally, another reaction parameter widely studied in the epoxidation reaction is the styrene/TBHP molar ratio [50] (Fig 8c). A remarkably improvement on the styrene conversion from 73 % to 86 % was obtained when increasing the styrene/TBHP molar ratio from 1:2 to 1:4. Also, the selectivity towards the epoxide increased to a great extend from 30 to 41.9 %.

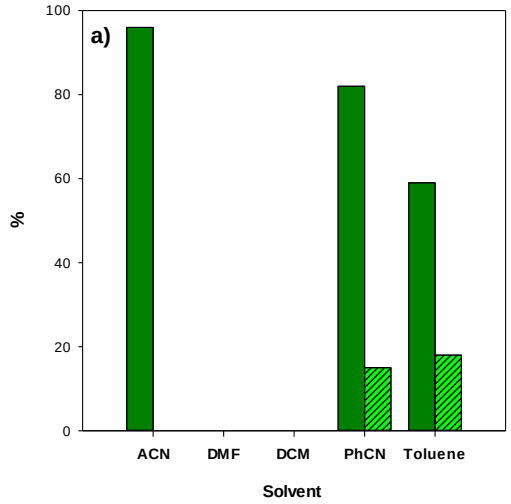
a)
100
80
60
40
20
0
%
ACN
DMF
DCM
PhCN
Toluene
Solvent

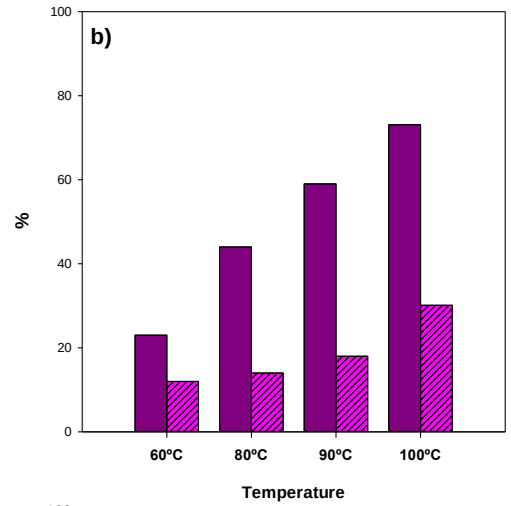
b)
100
80
60
40
20
0
%
60°C
80°C
90°C
100°C
Temperature

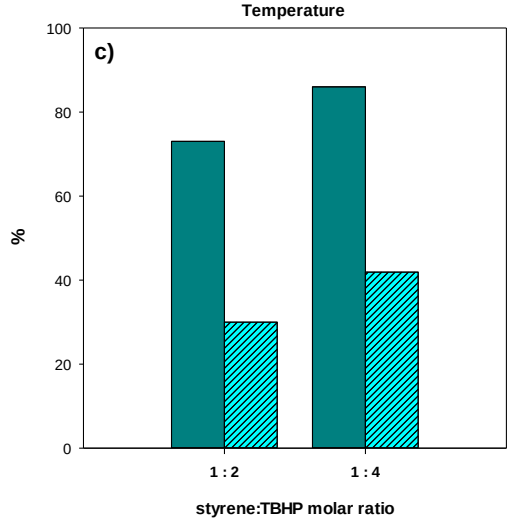
c)
100
80
60
40
20
0
%
1 : 2
1 : 4
styrene:TBHP molar ratio

Fig 8. Effect of reaction parameters on the epoxidation of styrene with TBHP (conversion and SO selectivity are indicated in filled and dashed bars, respectively) (a) Effect of solvent (ACN=acetonitrile; DMF=dimethylformamide; DCM=dichloromethane PhCN=benzonitrile;), (b) Effect of reaction temperature and (c) Effect of styrene/TBHP molar ratio. Reaction conditions: (a) styrene, 0.5 mmol; TBHP, 1 mmol; solvent, 2 mL; catalyst, 50 mg; T = 90 ºC; t = 1h; (b) styrene, 0.5 mmol; TBHP, 1 mmol; toluene, 2 mL; catalyst, 50 mg; t = 1h (c) styrene, 0.5 mmol; toluene, 2 mL; catalyst, 50 mg; T = 100 ºC; t = 1h.

Once the optimal reaction conditions have been established (solvent, toluene; temperature, 100 ºC; styrene:TBHP molar ratio, 1:4) for Cu@dppz-vPMO catalyst, it is worth mentioning the excellent yield achieved (86.0 %) and the remarkable epoxide selectivity (41.9 %). Furthermore, copper loading for the recycled catalyst was 0.125 mmol g^{-1}, which indicates that barely exists any leaching of copper species to the solution during epoxidation reaction. We have compared the catalytic performance of our catalyst with previously reported heterogeneous copper-based catalysts in the epoxidation of styrene with TBHP (Table 3). As can be seen, the performance of such catalytic systems depends directly on the active species of Cu (II) present on the support. Compared with those systems where copper is coordinated to nitrogen-chelating heterocyclic compounds comparable to the dppz ligands of our catalyst (i.e. bipyridine groups) (entries 2 and 3), Cu@dppz-vPMO (entry 1) possesses the highest styrene conversion and epoxide selectivity at shorter reaction times (1 h). By contrast, those systems based on Cu(II) Schiff base complexes anchored onto two-dimensional (entry 5) or three-dimensional (entry 6) mesoporous silicas as well as graphene oxide (entry 7) showed slightly larger styrene conversions and much higher selectivity to epoxide than those over Cu@dppz-vPMO. It is interesting to note that all of them required around 6-7 h or even longer reaction times to achieve these results for the epoxidation of styrene.

Table 3. Comparison of the catalytic activity of Cu@dppz-vPMO with previously reported heterogeneous copper-based catalysts in the epoxidation of styrene with TBHP.

Entry	Catalyst	Time (h)	T (ºC)	Conversion (%)	SO Selectivity (%)	Ref.
1	Cu@dppz-vPMO[a]	1	100	86.0	41.9	This work
2	$[Cu(H_2btec)(bipy)]_\infty$[b]	24	75	23.7	71.0	[22]
3	$[Cu_2(\mu_2\text{-}O)(4,4´\text{-}bpy)_3(SiW_{12}O_{40})(H_2O)]$[c]	10	70	74.4	44.0	[55]
4	CuY[d]	1	60	20.9	29.5	[56]
5	Cu-AMM[e]	24	60	86.3	95	[29]
6	Cu-NH_2-KIT-6[f]	6	80	98.6	97.8	[50]
7	Cu-NH_2-GO[g]	7	80	94.3	99.0	[57]

[a]Optimized conditions

[b]$[Cu(H_2btec)(bipy)]_\infty$: metal-organic framework $[Cu(H_2btec)(bipy)]$ (H_4btec=1,2,4,5-benzenetetracarboxylic acid; bipy= 2,2´-bipyridine)

[c]$[Cu_2(\mu_2\text{-}O)(4,4´\text{-}bpy)_3(SiW_{12}O_{40})(H_2O)]$: 3D Keggin-based coordination polymer

[d]CuY: copper (II) phthalocyanine encapsulated in zeolite Y.

[e]Cu-AMM: copper (II) Schiff complex anchored mesoporous material with 2D-hexagonal structure.

[f]Cu-NH_2-KIT-6: copper (II) Schiff complex onto amine-functionalized KIT-6.

[g]Cu-NH_2-GO: copper (II) Schiff complex supported onto graphene oxide.

3.4 CONCLUSIONS

In summary, a novel heterogeneous copper-based catalyst was successfully synthesized through the immobilization of a copper complex onto periodic mesoporous organosilica containing surface dipyridyl-pyridazine ligands. XRD, TEM and N_2 adsorption-desorption results revealed that the ordered mesostructure of the parent material remained intact after post-functionalization and complexation. In addition, a detailed study of the surface functionalized materials by different characterization techniques confirmed the presence of N-chelating heterocyclic units in the surface pores resulting from the Diels-Alder reaction as well as the subsequent anchoring of the copper complex. The resulting catalyst showed to be highly active in the epoxidation of styrene with remarkable selectivity to styrene oxide. Furthermore, it has been shown that Cu@dppz-vPMO catalyst exhibits a high stability under the reaction conditions and could be reused at least during five cycles without significant loss of its activity and selectivity.

3.5 REFERENCES

[1] G. Centi, F. Cavani, F. Trifirò, Trends and Outlook in Selective Oxidation, in: Sel. Oxid. by Heterog. Catal., 2001: pp. 1–24. https://doi.org/10.1007/978-1-4615-4175-2_1.

[2] H. Adolfsson, Transition Metal-Catalyzed Epoxidation of Alkenes, in: Mod. Oxid. Methods, 2005: pp. 21–49. https://doi.org/10.1002/9783527632039.ch2.

[3] B.S. Lane, K. Burgess, Metal-catalyzed epoxidations of alkenes with hydrogen peroxide, Chem. Rev. 103 (2003) 2457–2473. https://doi.org/10.1021/cr020471z.

[4] A.S. Sharma, V.S. Sharma, H. Kaur, R.S. Varma, Supported heterogeneous nanocatalysts in sustainable, selective and eco-friendly epoxidation of olefins, Green Chem. 22 (2020) 5902–5936. https://doi.org/10.1039/d0gc01927e.

[5] J.M. Judge, Organic peroxides, J. Polym. Sci. Part B Polym. Lett. 10 (1972) 230–231. https://doi.org/10.1002/pol.1972.110100316.

[6] G.A. Barf, R.A. Sheldon, Ruthenium catalyzed epoxidations: mechanistic and synthetic aspects, J. Mol. Catal. A. Chem. 102 (1995) 23–39. https://doi.org/10.1016/1381-1169(95)00089-5.

[7] H. Kwart, D.M. Hoffman, Observations regarding the Mechanism of Olefin Epoxidation with per Acids, J. Org. Chem. 31 (1966) 419–425. https://doi.org/10.1021/jo01340a017.

[8] S. Shit, U. Yadava, D. Saha, Roland Fröhlich, 2,2′-Bipyridyl-acetylphenolato mixed ligand copper(II) complexes: Syntheses, characterizations and catalytic activity in styrene epoxidation, J. Coord. Chem. 66 (2013) 66–76. https://doi.org/10.1080/00958972.2012.747088.

[9] H.J. Zhan, Q.H. Xia, X.H. Lu, Q. Zhang, H.X. Yuan, K.X. Su, X.T. Ma, Selective epoxidation of styrene with air catalyzed by CoO_x and CoO_x/SiO_2 without any reductant, Catal. Commun. 8 (2007) 1472–1478. https://doi.org/10.1016/j.catcom.2006.12.026.

[10] Y. Li, Y. He, J. Feng, D. Li, D. Trans, D.O.I. Cdtf, Synthesis of a highly dispersed CuO catalyst on CoAl-HT for the epoxidation of styrene, Dalt. Trans. 46 (2017) 13463–13471. https://doi.org/10.1039/C7DT02247F.

[11] Y. Zhang, F. Yang, R. Gao, W. Dai, Manganese-Doped CeO_2 Nanocubes as Highly Efficient Catalysts for Styrene Epoxidation with TBHP, Appl. Surf. Sci. 471 (2019) 767–775. https://doi.org/10.1016/j.apsusc.2018.11.246.

[12] M. Niakan, Z. Asadi, M. Masteri-farahani, Immobilization of salen molybdenum complex on dendrimer functionalized magnetic nanoparticles and its catalytic activity for the epoxidation of olefins, Appl. Surf. Sci. 481 (2019) 394–403. https://doi.org/10.1016/j.apsusc.2019.03.088.

[13] G.R. Lucía Rossi-Fernández, Viviana Dorn, A new and efficient methodology for olefin epoxidation catalyzed by supported cobalt nanoparticles, J. Org. Chem. 17 (2021) 519–526. https://doi.org/10.3762/bjoc.17.46.

[14] R. Wang, X. Liu, F. Yang, S. Gao, S. Zhou, Y. Kong, Neighboring Cu toward Mn site in confined mesopore to trigger strong interplay for boosting catalytic epoxidation of styrene, Appl. Surf. Sci. 537 (2021) 148100. https://doi.org/10.1016/j.apsusc.2020.148100.

[15] M.S. Batra, R. Dwivedi, R. Prasad, Recent Developments in Heterogeneous Catalyzed Epoxidation of Styrene to Styrene Oxide, ChemistrySelect. 4 (2019) 11636–11673. https://doi.org/10.1002/slct.201902396.

[16] S. Impeng, T. Roongcharoen, P. Maitarad, H. Wu, C. Chitpakdee, V. Promarak, L. Shi, S. Namuangruk, High Selective Catalyst for Ethylene Epoxidation to Ethylene Oxide : A DFT Investigation, Appl. Surf. Sci. 513 (2020) 145799. https://doi.org/10.1016/j.apsusc.2020.145799.

[17] M.A. Andrade, M.D.R.S. Martins, Selective Styrene Oxidation to Benzaldehyde over Recently Developed Heterogeneous Catalysts, Molecules. 26 (2021) 1680. https://doi.org/10.3390/molecules26061680.

[18] R. Bera, C. Adhikary, Catalytic potency of zeolite Y immobilized copper-2,2′-bipyridine hybrid complex in oxidation of olefins, J. Porous Mater. 28 (2021) 695–702. https://doi.org/10.1007/s10934-020-01023-7.

[19] B. Shi, H. Yu, S. Gao, L. Zhang, Y. Liu, K. Huang, Microporous and Mesoporous Materials Copper complex supported on hollow porous nanosphere frameworks with improved catalytic activity for epoxidation of olefins, Microporous Mesoporous Mater. 294 (2019) 109890. https://doi.org/10.1016/j.micromeso.2019.109890.

[20] S. Madadi, S. Kaliaguine, Activated Carbon-Supported Ruthenium as a Catalyst for the Solvent- and Initiator-Free Aerobic Epoxidation of Limonene, ACS Sustain. Chem. Eng. 9 (2021) 10557–10568. https://doi.org/10.1021/acssuschemeng.1c02597.

[21] C. Chen, P. Shen, M. Wan, N. Ding, X. Shi, X. Wang, N. Zhang, Size-selective epoxidation of ole fi ns in two new metal-organic framework constructed from six-coordinated tetranuclear Cu (II) SBUs, Microporous Mesoporous Mater. 232 (2016) 167–173. https://doi.org/10.1016/j.micromeso.2016.06.013.

[22] K. Brown, S. Zolezzi, P. Aguirre, D. Venegas-Yazigi, V. Paredes-García, R. Baggio, M.A. Novak, E. Spodine, $[Cu(H_2btec)(bipy)]_\infty$: A novel metal organic framework (MOF) as heterogeneous catalyst for the oxidation of olefins, J. Chem. Soc. Dalt. Trans. (2009) 1422–1427. https://doi.org/10.1039/b810414j.

[23] Y.Y. Liu, K. Leus, T. Bogaerts, K. Hemelsoet, E. Bruneel, V. Van Speybroeck, P. Van Der Voort, Bimetallic-organic framework as a zero-leaching catalyst in the aerobic oxidation of cyclohexene, ChemCatChem. 5 (2013) 3657–3664. https://doi.org/10.1002/cctc.201300529.

[24] T. Toyao, K. Miyahara, M. Fujiwaki, T.H. Kim, S. Dohshi, Y. Horiuchi, M. Matsuoka, Immobilization of Cu complex into Zr-based MOF with bipyridine units for heterogeneous selective oxidation, J. Phys. Chem. C. 119 (2015) 8131–8137. https://doi.org/10.1021/jp512749y.

[25] P. Karandikar, M. Agashe, K. Vijayamohanan, A.J. Chandwadkar, $Cu2^+$-perchlorophthalocyanine immobilized MCM-41: Catalyst for oxidation of alkenes, Appl. Catal. A Gen. 257 (2004) 133–143. https://doi.org/10.1016/j.apcata.2003.07.007.

[26] M. Ghadiri, F. Farzaneh, M. Ghandi, M. Alizadeh, Immobilized copper(II) complexes on montmorillonite and MCM-41 as selective catalysts for epoxidation of alkenes, J. Mol. Catal. A Chem. 233 (2005) 127–131. https://doi.org/10.1016/j.molcata.2005.01.046.

[27] S. Jana, B. Dutta, R. Bera, S. Koner, Anchoring of copper complex in MCM-41 matrix: A highly efficient catalyst for epoxidation of olefins by tert-BuOOH, Langmuir. 23 (2007) 2492–2496. https://doi.org/10.1021/la062409t.

[28] J. Hu, K. Li, W. Li, F. Ma, Y. Guo, Selective oxidation of styrene to benzaldehyde catalyzed by Schiff base-modified ordered mesoporous silica materials impregnated with the transition metal-monosubstituted Keggin-type polyoxometalates, Appl. Catal. A Gen. 364 (2009) 211–220. https://doi.org/10.1016/j.apcata.2009.05.058.

[29] M. Nandi, P. Roy, H. Uyama, A. Bhaumik, Functionalized mesoporous silica supported copper(ii) and nickel(ii) catalysts for liquid phase oxidation of olefins, Dalt. Trans. 40 (2011) 12510–12518. https://doi.org/10.1039/c1dt10157a.

[30] T. Asefa, M.J. MacLachlan, N. Coombs, G.A. Ozin, Periodic mesoporous organosilicas with organic groups inside the channel walls, Nature. 402 (1999) 867–871. https://doi.org/10.1038/47229.

[31] S. Inagaki, S. Guan, Y. Fukushima, T. Ohsuna, O. Terasaki, Novel mesoporous materials with a uniform distribution of organic groups and inorganic oxide in their frameworks, J. Am. Chem. Soc. 121 (1999) 9611–9614. https://doi.org/10.1021/ja9916658.

[32] B.J. Melde, B.T. Holland, C.F. Blanford, A. Stein, Mesoporous sieves with unified hybrid inorganic/organic frameworks, Chem. Mater. 11 (1999) 3302–3308. https://doi.org/10.1021/cm9903935.

[33] P. Van Der Voort, D. Esquivel, E. De Canck, F. Goethals, I. Van Driessche, F.J. Romero-Salguero, Periodic Mesoporous Organosilicas: from simple to complex bridges; a comprehensive overview of functions, morphologies and applications, Chem. Soc. Rev. 42 (2013) 3913–3955. https://doi.org/10.1039/C2CS35222B.

[34] M. Gholinejad, B. Karimi, A. Aminianfar, M. Khorasani, One-Pot Preparation of Propargylamines Catalyzed by Heterogeneous Copper Catalyst Supported on Periodic Mesoporous Organosilica with Ionic Liquid Framework, Chempluschem. 80 (2015) 1573–1579. https://doi.org/10.1002/cplu.201500167.

[35] D. Elhamifar, H. Ardeshirfard, Phenyl and ionic liquid based bifunctional periodic mesoporous organosilica supported copper: An efficient nanocatalyst for clean production of polyhydroquinolines, J. Colloid Interface Sci. 505 (2017) 1177–1184. https://doi.org/10.1016/j.jcis.2017.07.010.

[36] S. Ishikawa, Y. Maegawa, M. Waki, S. Inagaki, Well-controlled radical-based epoxidation catalyzed by copper complex immobilized on bipyridine-periodic mesoporous organosilica, Appl. Catal. A Gen. 575 (2019) 87–92. https://doi.org/10.1016/j.apcata.2019.02.007.

[37] D. Esquivel, E. De Canck, C. Jimenez-Sanchidrian, P. Van Der Voort, F.J. Romero-Salguero, Formation and functionalization of surface Diels-Alder adducts on ethenylene-bridged periodic mesoporous organosilica, J. Mater. Chem. 21 (2011) 10990–10998. https://doi.org/10.1039/C1JM11315A.

[38] D. Esquivel, E. De Canck, C. Jiménez-Sanchidrián, F.J. Romero-Salguero, P. Van Der Voort, Pyrrole PMOs, incorporating new N-heterocyclic compounds on an ethene-PMO through Diels-Alder reactions, Mater. Chem. Phys. (2014). https://doi.org/10.1016/j.matchemphys.2014.08.004.

[39] D. Esquivel, A.M. Kaczmarek, C. Jiménez-Sanchidrián, R. Van Deun, F.J. Romero-Salguero, P. Van Der Voort, Eu^{3+}@PMO: synthesis, characterization and luminescence properties, J. Mater. Chem. C. **3** (2015) 2909–2917. https://doi.org/10.1039/C4TC02553A.

[40] A.M. Kaczmarek, D. Esquivel, J. Ouwehand, P. Van Der Voort, F.J. Romero-Salguero, R. Van Deun, Temperature dependent NIR emitting lanthanide-PMO/silica hybrid materials, Dalt. Trans. 46 (2017) 7878–7887. https://doi.org/10.1039/C7DT01620D.

[41] A.M. Kaczmarek, D. Esquivel, B. Laforce, L. Vincze, P. Van Der Voort, F.J. Romero-Salguero, R. Van Deun, Luminescent thermometer based on Eu^{3+}/Tb^{3+}-organic-functionalized mesoporous silica, Luminescence. 33 (2018) 567–573. https://doi.org/10.1002/bio.3447.

[42] Q. Yang, J. Liu, J. Yang, L. Zhang, Z. Feng, J. Zhang, C. Li, Acid catalyzed synthesis of ordered bifunctionalized mesoporous organosilicas with large pore, Microporous Mesoporous Mater. **77** (2005) 257–264. https://doi.org/10.1016/j.micromeso.2004.09.009.

[43] S. Samanta, S. Das, P. Biswas, Synthesis of 3,6-di(pyridin-2-yl)-1,2,4,5-tetrazine (pytz) capped silver nanoparticles using 3,6-di(pyridin-2-yl)-1,4-dihydro-1,2,4,5-tetrazine as reducing agent: Application in naked eye sensing of Cu^{2+}, Ni^{2+} and Ag^{+} ions in aqueous solution and paper p, Sensors Actuators, B Chem. 202 (2014) 23–30. https://doi.org/10.1016/j.snb.2014.05.036.

[44] T. Asefa, M. Kruk, M.J. Maclachlan, N. Coombs, H. Grondey, M. Jaroniec, G.A. Ozin, V. Uni, S.G. Street, K. State, V. Uni, R. V October, V. Re, M. Recei, V. June, Novel Bifunctional Periodic Mesoporous Organosilicas, BPMOs : Synthesis, Characterization, Properties and in-Situ Selective Hydroboration - Alcoholysis Reactions of Functional Groups, J. Am. Chem. Soc. 123 (2001) 8520–8530. https://doi.org/10.1021/ja0037320.

[45] T.T. Igarashi Naoko, Tanaka Yoshinori, Nakata Shin-ichi, Increased Stability of Organically Modified MCM-41 Synthesized by a One-step Procedure, Chem. Lett. 28 (1999). https://doi.org/10.1246/cl.1999.1.

[46] J. Amaro-Gahete, A.M. Kaczmarek, D. Esquivel, C. Jiménez-Sanchidrián, P. Van Der Voort, F.J. Romero-Salguero, Luminescent Graphene-Based Materials via Europium Complexation on Dipyridylpyridazine-Functionalized Graphene Sheets, Chem. - A Eur. J. 25 (2019) 6823–6830. https://doi.org/10.1002/chem.201900512.

[47] G. Avgouropoulos, T. Ioannides, Selective CO oxidation over CuO-CeO_2 catalysts prepared via the urea – nitrate combustion method, Appl. Catal. A Gen. 244 (2003) 155–167. https://doi.org/10.1016/S0926-860X(02)00558-6.

[48] R. Hoogenboom, G. Kickelbick, U.S. Schubert, Synthesis and Characterization of Novel Substituted 3,6-Di(2-pyridyl)pyridazine Metal-Coordinating Ligands, European J. Org. Chem. 2003 (2003) 4887–4896. https://doi.org/10.1002/ejoc.200300505.

[49] Y. Naganawa, Y. Maegawa, H. Guo, S.S. Gholap, S. Tanaka, K. Sato, S. Inagaki, Y. Nakajima, Heterogeneous hydrosilylation reaction catalysed by platinum complexes immobilized on bipyridine-periodic mesoporous organosilicas, Dalt. Trans. 48 (2019) 5534–5540. https://doi.org/10.1039/C9DT00078J.

[50] J. Sun, Q. Kan, Z. Li, G. Yu, H. Liu, X. Yang, Q. Huo, J. Guan, Different transition metal (Fe^{2+}, Co^{2+}, Ni^{2+}, Cu^{2+} or VO^{2+}) Schiff complexes immobilized onto three-dimensional mesoporous silica KIT-6 for the epoxidation of styrene, RSC Adv. 4 (2014) 2310–2317. https://doi.org/10.1039/c3ra45599h.

[51] N. Gogoi, T. Begum, S. Dutta, U. Bora, P.K. Gogoi, Rice husk derived nanosilica supported Cu (II) complex: An efficient heterogeneous catalyst for oxidation of alcohols using TBHP, RSC Adv. 5 (2015) 95344–95352. https://doi.org/10.1039/c5ra21148d.

[52] P.H.O. Santiago, C.M. Aiube, J.L. de Macedo, C.C. Gatto, Hydrazone-derived copper(II) coordination polymer as a selective liquid-phase catalyst: Synthesis, crystal structure and performance towards benzyl alcohol oxidation, Mol. Catal. 496 (2020) 111177. https://doi.org/10.1016/j.mcat.2020.111177.

[53] C. Saux, L.B. Pierella, Applied Catalysis A : General Studies on styrene selective oxidation to benzaldehyde catalyzed by Cr-ZSM-5: Reaction parameters effects and kinetics, "Applied Catal. A, Gen. 400 (2011) 117–121. https://doi.org/10.1016/j.apcata.2011.04.021.

[54] B. Li, X. Luo, Y. Zhu, X. Wang, Immobilization of Cu(II) in KIT-6 supported Co_3O_4 and catalytic performance for epoxidation of styrene, Appl. Surf. Sci. 359 (2015) 609–620. https://doi.org/10.1016/j.apsusc.2015.10.131.

[55] F. Yu, X.J. Kong, Y.Y. Zheng, Y.P. Ren, L.S. Long, R. Bin Huang, L.S. Zheng, pH-dependent assembly of 0D to 3D Keggin-based coordination polymers: Structures and catalytic properties, J. Chem. Soc. Dalt. Trans. (2009) 9503–9509. https://doi.org/10.1039/b911606k.

[56] S. Seelan, S. Sinha, D. Srinivas, S. Sivasanker, Spectroscopic investigation and catalytic activity of copper (II) phthalocyanine encapsulated in zeolite Y, J. Mol. Catal. A Chem. 157 (2000) 163–171. https://doi.org/10.1016/S1381-1169(99)00432-X.

[57] H. Su, Z. Li, Q. Huo, J. Guan, Q. Kan, Immobilization of transition metal (Fe^{2+}, Co^{2+}, VO^{2+} or Cu^{2+}) Schiff base complexes onto graphene oxide as efficient and recyclable catalysts for epoxidation of styrene, RSC Adv. 4 (2014) 9990–9996. https://doi.org/10.1039/c3ra47732k.

CHAPTER 4.

RESULTS AND DISCUSSION

(PAPER 2)

Chapter 4. **Cobaloxime tethered pyridine-functionalized ethylene-bridged periodic mesoporous organosilica as efficient HER catalyst**

PAPER 2

Cobaloxime tethered pyridine-functionalized ethylene-bridged periodic mesoporous organosilica as efficient HER catalyst

M[a] Ángeles Navarro,[a] Daniel Cosano,[a] Asamanjoy Bhunia,[b] Laura Simonelli,[c] Vlad Martin-Diaconescu,[c] Francisco J. Romero-Salguero[a]* and Dolores Esquivel[a]*

[a]*Department of Organic Chemistry, Nanochemistry and Fine Chemistry Research Institute (IUIQFN), Faculty of Sciences, University of Córdoba, Campus de Rabanales, Marie Curie Building, Ctra. Nnal. IV, km 396, 14071 Córdoba, Spain.*

[b]*Department of Chemistry, Inorganic Chemistry Section, Jadavpur University, Kolkata 700032, India*

[c]*ALBA Synchrotron Light Facility, Carrer de la Llum 2-26, 08290 Cerdanyola del Vallès, Spain*

Corresponding authors: Email address (qo2rosaf@uco.es (F.J.R.-S.); q12esmem@uco.es (D.E.)

Paper

Cobaloxime tethered pyridine-functionalized ethylene-bridged periodic mesoporous organosilica as an efficient HER catalyst

M. Ángeles Navarro, Daniel Cosano, Asamanjoy Bhunia, Laura Simonelli, Vlad Martin-Diaconescu, Francisco J. Romero-Salguero and Dolores Esquivel

A novel cobaloxime–PMO hybrid material as an efficient hydrogen evolution catalyst under photocatalytic conditions.

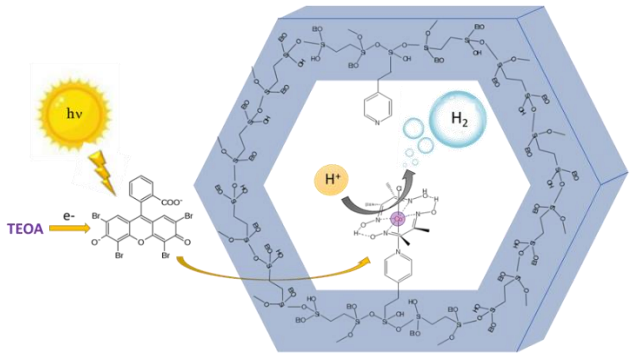

The article was first published on 26 Nov 2021
Sustainable Energy Fuels, 2022, **6**, 398-407
https://doi.org/10.1039/D1SE01437D

ABSTRACT

An efficient cobaloxime hydrogen production catalyst has been synthesized through coordination of a cobalt complex ($Co(dmgH_2)(dmgH)Cl_2$) on an ethylene-bridged periodic mesoporous organosilica (PMO) containing pyridine moieties. The effective assembly of cobaloxime units through cobalt-pyridine axial bond on the porous channels of the PMO was clearly evidenced by different techniques, including ^{13}C NMR, Raman, IR and XPS. The catalyst was investigated for the hydrogen evolution reaction in a visible-light activated system in the presence of a photosensitizer (eosin Y) and a sacrificial electron donor (TEOA). It showed a good photocatalytic performance on the HER with a TON of 119 at 6 h, largely exceeding the catalytic activity of the homogeneous

counterpart, $Co(dmgH)_2pyCl$, under the conditions studied. The process was proven to be photocatalytic and heterogeneous. The studied system has the cobaloxime catalyst with the highest turnover reported to date for a heterogeneous catalyst under photocatalytic conditions. After reactivation treatment with the $Co(dmgH_2)(dmgH)Cl_2$ complex, the catalytic system was able to maintain its activity after two recycling experiments.

Keywords: cobaloxime; axial pyridine ligand; periodic mesoporous organosilicas; hydrogen evolution reaction.

4.1 INTRODUCTION

In response to the dramatic increase of atmospheric levels of CO_2 due to the worldwide strong dependence on fossil fuels to obtain energy, scientists have been working on the development and implementation of sustainable carbon-free energy sources [1].

Among them, solar energy is by far the most feasible and promising alternative to carbon fuels. Theoretically, the incident solar energy on the earth every hour is more than enough to satisfy all energy demanded by humans for the entire year [2,3]. Although electricity generation from the sun using photovoltaic cells currently contributes more than 3.5 % of the world's electricity [4], there exists barriers to the complete implementation of solar energy. The daily and seasonal fluctuations of solar flux along with the absence of methods for storing and dispatching on demand have not allowed its development as a major primary energy source.

Alternatively, an interesting approach inspired by natural photosynthesis is solar driven water-splitting, able to store energy in chemical bonds (H_2 and O_2) [5,6]. As a result of the well-known complications in driving both half-reactions [7], most of the studies have been focused on the reductive side of water splitting to obtain hydrogen as an energy vector. However, a hydrogen economy requires the design of cost-effective and efficient catalysts for hydrogen production through an economically viable process. In this context, molecular catalysts based on earth-abundant element (Co, Ni and Fe) complexes play an important role in water splitting [8]. Particularly, cobalt based compounds have emerged as efficient molecular systems for both water oxidation [9,10] and hydrogen evolution reactions [11,12] in the last decade. Specifically, cobaloxime (cobalt bis-glyoximato complexes) compounds are among the most widely studied for electro- and photocatalytic hydrogen production due to their facile synthesis and

tunable catalytic properties. These systems show high activity for proton reduction in aqueous solution at low overpotential [13–17].

Since the pioneering studies by Ziessel and co-workers in this field [18], numerous breakthroughs have been made in the design of efficient cobaloxime-based molecular systems for the electro- and photocatalytic hydrogen evolution reaction (HER) [19,20]. One of the most versatile approaches to improve the electrocatalytic HER activity of cobaloximes is their immobilization on electroactive surfaces containing pyridine ligands. It is well documented by experimental [21–24] and computational [25–27] studies that the presence of aromatic N-donor group substituents in the axial position increases the catalytic efficiency of cobaloximes in hydrogen evolution. During the last decade, Reisner [28,29] and Artero [30,31] have led the research in this field, achieving good electrocatalytic HER activities with cobaloxime catalysts integrated into carbon-based nanomaterials. Recently, similar studies have been extended to other semiconductor substrates where H_2 production cobaloxime catalysts have been successfully assembled on electrode surfaces [32,33]. Another interesting approach involves immobilizing cobaloxime units on non-conducting surfaces for H_2 evolution under light-driven conditions. To the best of our knowledge, only MOFs (Metal Organic Frameworks) and, more recently, COFs (Covalent Organic Frameworks) have been employed as a support for this purpose. Ott et al. [34] reported the first example of anchoring a cobaloxime catalyst onto chloromethylated MIL-101(Cr) for photocatalytic H_2 production. Recently, this research group has successfully integrated cobaloxime as a metallo-linker for MOF synthesis and has demonstrated that this system can act as an electrocatalyst for extended periods of time [35]. In the field of COFs, Lotsch et al. [36] immobilized a cobaloxime catalyst on propargyl-functionalized COF-42 for the HER. This strategy improved the photocatalytic activity of cobaloxime compared with equivalent unbound cobaloxime. As an alternative to these previous porous

supports, periodic mesoporous organosilicas (PMOs) are a different family of hybrid materials with great potential to immobilize molecular catalysts. The framework of PMOs is more hydrophobic than that of silicas and endows PMOs with a higher hydrothermal stability [37]. In addition, the well-defined ordered mesostructure, characteristic of these materials, facilitates the diffusion and accessibility of reactants to active centers [38]. PMOs, prepared from organo-bridged alkoxysilane precursors in the presence of a surfactant, are characterized by highly ordered structures with organic groups homogeneously distributed in the silica framework. A wide variety of organic groups have been successfully integrated into the silica walls of PMOs for applications such as catalysis, adsorption, chromatography, drug release and luminescence, among others [39–42]. One of the advantages of this synthetic strategy is the possibility to incorporate different functional organic groups in the silica walls and the channel pores of PMOs to provide attachment points for assembling homogeneous catalysts. Recently, an example of it was reported by Inagaki et al. who incorporated an [FeFe]-hydrogenase model complex on the pore surface of a periodic mesoporous organosilica containing thiol groups to make an efficient heterogeneous HER catalyst. The material showed a greater TON than the homogeneous system due to the improvement of the stability of the [FeFe]-complex on the pore surface of the PMO [43]. Taking this into consideration, PMOs with appropriate functional groups in their framework could act as excellent scaffolds for assembling other HER catalysts. Immobilizing cobaloxime molecular complexes within PMO supports with high surface areas and porous structures with tailored hydrophobicity/hydrophilicity could increase the stability of the cobaloxime catalyst confined into the mesopores and allow easy catalyst recycling by filtration.

Herein, we report for the first time the incorporation of a cobaloxime catalyst [$Co(dmgH_2)(dmgH)Cl_2$] on the pore surface of an ethylene-bridged

periodic mesoporous organosilica containing pyridine groups. The pyridine groups located at the pore channels provide attachment points to assemble cobaloxime catalysts on the PMO surface. The resulting material, py-etPMO-Co, was fully characterized and investigated for the photocatalytic HER. It showed to be a very efficient catalyst for hydrogen production, largely exceeding the photocatalytic activity of the homogeneous catalyst under the same conditions.

4.2 EXPERIMENTAL SECTION

4.2.1 Chemicals

Dimethylglyoxime (99 %, Aldrich), cobalt (II) chloride hexahydrate (Acros Organics) and acetone (Aldrich) were used in the synthesis of cobaloxime complex. Octadecyltrimethylammonium bromide (ODTMA, Aldrich) and sodium hydroxide (NaOH, 99% Aldrich) were used as supplied. The organosilica precursors, 1,2-bis(triethoxysilyl)ethane (97 %) and 2-(4-pyridilethyl)triethoxysilane) (95 %), were obtained from abcr for the synthesis of pyridine-functionalized ethylene-bridged PMO. Both precursors were used as purchased without further purification. Acetonitrile (99.7 %, PanReac), eosin Y (>95 %, TCI) and triethanolamine (TEOA, >99 % Sigma-Aldrich) were used for the photocatalytic hydrogen evolution reaction.

4.2.2 Synthesis procedures

4.2.2.1 Synthesis of cobaloxime complexes [Co(dmgH$_2$)(dmgH)Cl$_2$ and Co(dmgH)$_2$pyCl]

Cobaloxime complex, Co(dmgH$_2$)(dmgH)Cl$_2$, was synthesized according to a procedure previously reported [42]. In a typical synthesis, $CoCl_2.6H_2O$ (0.5 g, 2.1 mmol) was dissolved in acetone (15 mL) and then, dimethylglyoxime (0.49 g, 4.2 mmol) was added. The resulting mixture was stirred for 10 min at room

temperature. Afterwards, the mixture was filtered to remove any undissolved reactive. The filtrate was allowed to stand overnight to form green crystals. They were collected by filtration and washed with acetone. $Co(dmgH_2)(dmgH)Cl_2$ was dried under vacuum at 80 ºC. For the synthesis of the cobaloxime with axial pyridine ligand, $Co(dmgH_2)(dmgH)Cl_2$ (0.33 g, 0.9 mmol) was suspended in chloroform (8.5 mL) and then, pyridine (0.18 g) was added dropwise (Scheme 1) [42]. Afterwards, water (3 mL) was added to the solution and stirring continued for 2 h. The aqueous phase was separated by decantation, while the organic phase was washed with three portions of water (15 mL each). The solution was concentrated by rotary evaporation and a precipitate was obtained by addition of ethanol. The final product was recovered by filtration, washed with ethanol, and dried under vacuum at 100 ºC.

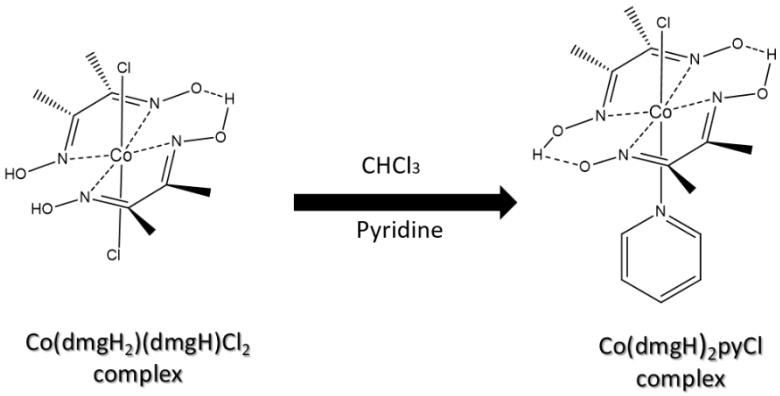

Scheme 1. Structures of cobaloxime complexes.

4.2.2.2 Synthesis of pyridine-functionalized ethylene-bridged PMO (py-etPMO)

In a typical synthesis,[43] ODTMA surfactant (0.85 g) was dissolved in a solution of NaOH (6 M, 0.89 mL) and distilled water (53 mL). After stirring the solution at room temperature for 24 h, a mixture of organosilane precursors with molar ratio 80 % of 1,2-bis(triethoxysilyl)ethane and 20 % of

2-(4-pyridylethyl)triethoxysilane was added dropwise under vigorous stirring. The resulting mixture was stirred at room temperature for 24 h, after which it was aged at 97 ºC for 48 h under static conditions. The white precipitate was recovered by filtration and washed with distilled water. To remove the surfactant, 1 g of as-synthesized material was refluxed in a solution containing 50 mL ethanol and 1 mL HCl solution (37% wt.) for 12 h. After repeating this extraction process twice, the final material was filtered out and dried at 120 ºC under vacuum. It was named *py-etPMO*.

4.2.2.3 Anchoring of cobaloxime catalyst $Co(dmgH_2)(dmgH)Cl_2$ on py-etPMO

The material py-etPMO (0.5 g) was dispersed in 10 mL of methanol and then, $Co(dmgH_2)(dmgH)Cl_2$ complex (0.546 mmol) was added [44]. The mixture was kept under stirring at 65 ºC for 24 h. Subsequently, the solid was recovered by filtration and washed thoroughly with CH_3OH. To remove unreacted complex, the resulting solid was refluxed with 50 mL of CH_3OH for 12 h. This procedure was repeated twice. Finally, the solid was washed with DMSO, collected by filtration and dried under vacuum at 80 ºC. The catalyst was named py-etPMO-Co. A schematic illustration of the synthetic procedure of the cobaloxime-PMO hybrid material (py-etPMO-Co) is depicted in Scheme 2.

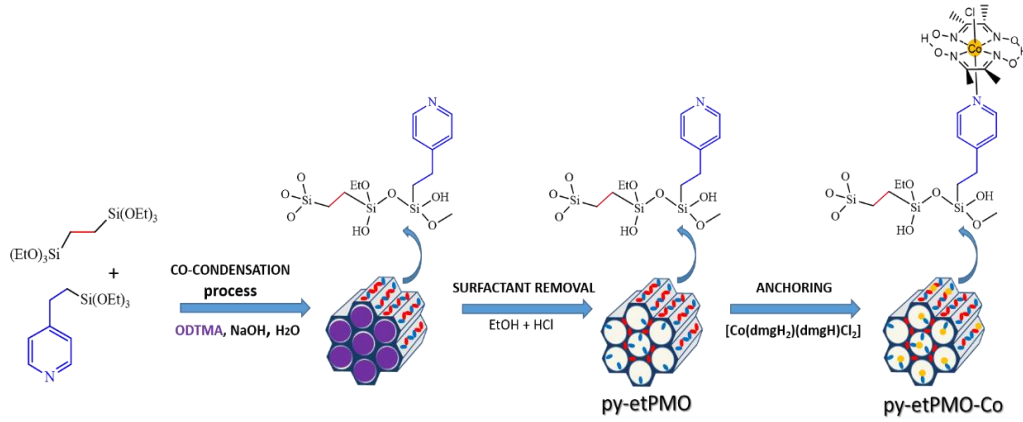

Scheme 2. Synthesis route of cobaloxime-PMO hybrid catalyst (py-etPMO-Co).

4.2.3 Photocatalytic studies

For the photocatalytic experiment, py-etPMO-Co (1 mg) was suspended in a CH_3CN:H_2O (1:1) solution (11.4 mL). The aqueous solution contains triethanolamine (TEOA, 10 %) adjusted to pH 7 with HCl (37 %) and the acetonitrile solution contains dissolved eosin Y (0.05 mM). The reaction tube was sealed, and the mixture was purged with N_2 for 30 min. Then, the reaction mixture was irradiated with a Xe lamp (ORIEL, 300 W) equipped with (Newport filter, FSQGC400) at a distance of 10 cm. Sample aliquots were taken using a gas-tight syringe and quantified by gas chromatography (Shimadzu GC-2010 Plus) equipped with a barrier discharge ionization detector (BID) and a ShinCarbon ST column (2 m × 2 mm i.d.). For the homogenous test, $[Co(dmgH)_2pyCl]$ was used as the catalyst under similar conditions.

4.2.4 Leaching test

A photocatalytic reaction with py-etPMO-Co was carried out as indicated previously, but after 1 h the reaction mixture was filtered off with a nylon membrane filter (0.45μm) to remove the catalyst particles. Then, the clear solution was transferred to a reaction tube under a N_2 atmosphere and irradiated for 2 h.

4.2.5 Catalyst re-activation process

After reaction, the catalyst was recovered by centrifugation and washed with methanol and acetonitrile in order to eliminate possible residues of eosin Y and TEOA in the pores. The re-activation process was similar to that used to anchor cobaloxime complex in py-etPMO material.

4.2.6 Characterization

X-ray powder diffraction (XRD) patterns were collected on a Bruker D8 Discover A25 diffractometer using Cu Kα radiation. N_2 adsorption-desorption isotherms were measured at -196 °C using an Autosorb-iQ MP/MP-XR instrument. Prior to measurement, all the samples were outgassed overnight at 120 °C. The surface area was calculated using the Brunauer-Emmett-Teller (BET) method and pore size distribution was determined using Density Functional Theory (DFT) method. Raman spectra of the samples were acquired with a Renishaw Raman instrument with green laser light (532 nm). FT-IR measurements were carried out on a Bruker Alpha II spectrometer. The solid-state ^{13}C CP/MAS NMR spectra were recorded on a Bruker Avance III HD 400 WB spectrometer at 13 kHz. An overall of 1500 free induction decays were accumulated for each measurement. The excitation pulse and recycle time for ^{13}C CP/MAS NMR were 3.6 ms and 2 s, respectively. Chemical shifts were referenced to tetramethylsilane (TMS) standard. X-ray photoelectron spectroscopy (XPS) were recorded on a SPECS Phoibos HAS 3500 150 MCD X-ray photoelectron spectrometer with a monochromatic Al anode (1486.7 eV). Accurate binding energies have been determined with respect to the position of Si 2p at 103.4 eV. High-resolution Transmission Electron Microscopy images were recorded on a JEOL JEM 1400 microscope. Scanning Electron Microscopy imaging and Energy-dispersive X-ray (EDX) spectroscopy measurements were performed on a JEOL JSM 7800F microscope. Inductively coupled plasma mass

spectrometry (ICP-MS) for isotope ^{59}Co was measured using a NexION 350X spectrometer. Prior to the measurement, the sample was digested in an UltraWave microwave system.

Co K-edge x-ray absorption spectra were collected at the CLÆSS beamline of the ALBA synchrotron [45]. The synchrotron radiation was monochromatized by means of a double crystal Si(111) monochromator, while the higher harmonics were rejected by choosing proper angles and coatings for the collimating and focusing mirrors. The absorption data were acquired in transmission mode. The powdered samples were mixed uniformly in a boron nitride matrix and pressed into pellets to ensure an absorption jump close to 1. Several scans were measured to ensure reproducibility and a good signal to noise ratio. The data treated by the Demeter package [46].

4.3 RESULTS AND DISCUSSION

4.3.1 Characterization of the cobaloxime-PMO hybrid catalyst

The powder X-ray diffraction (PXRD) pattern of pyridine-functionalized ethylene-bridged PMO revealed three reflection peaks in the low-angle region ($2\theta < 5$) with lattice d-spacings of 49, 28 and 25 Å, respectively. These peaks can be indexed to (100), (110) and (200) reflections of a highly ordered 2D-hexagonal (*p6mm*) structure (Fig. 1a, blue line) [47]. The unit cell parameter of the hexagonal lattice (a_0) was 57 Å. After the incorporation of $Co(dmgH)(dmgH_2)Cl_2$ complex, the resulting py-etPMO-Co material showed similar diffraction peaks to the parent material py-etPMO (Fig. 1a, blue line). Transmission electron microscopy (TEM) of py-etPMO (Fig. S1) corroborated a highly ordered arrangement of uniform pores. These uniform pore channels were retained after cobaloxime anchoring on the pyridine groups located on the pore surface of PMO (Fig. 1b). These results together with the well-resolved XRD patterns demonstrated the

formation of a highly ordered mesostructure, which was preserved after the coordination of the cobalt complex on the pyridine ligands.

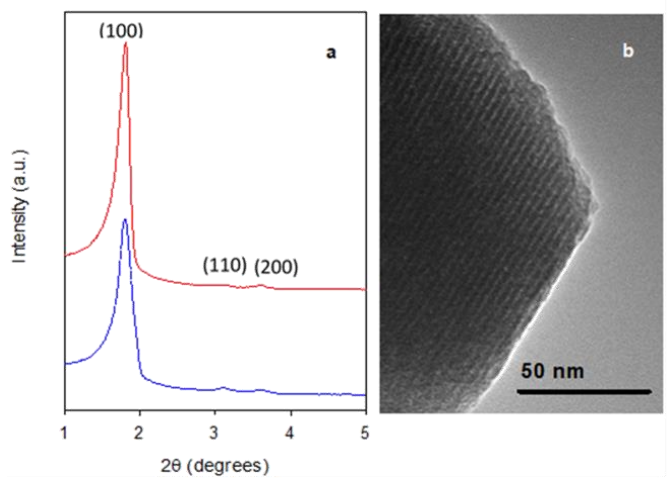

Fig 1. (a) PXRD of py-etPMO (blue) and py-etPMO-Co (red) and (b) TEM image of py-etPMO-Co.

Nitrogen adsorption-desorption isotherms of py-etPMO and py-etPMO-Co displayed a type-IV isotherm with a capillary condensation step at P/P0 = 0.3 – 0.6, characteristic of mesoporous materials. Non-distinctive hysteresis loop was appreciated for both materials (Fig. 2). The BET surface area, pore volume and pore diameter are summarized in Table 1. The incorporation of the cobaloxime catalyst on the pore surface of py-etPMO caused a slight decrease of the S_{BET}, the pore volume and pore size values and a slight increase of the wall-thickness.

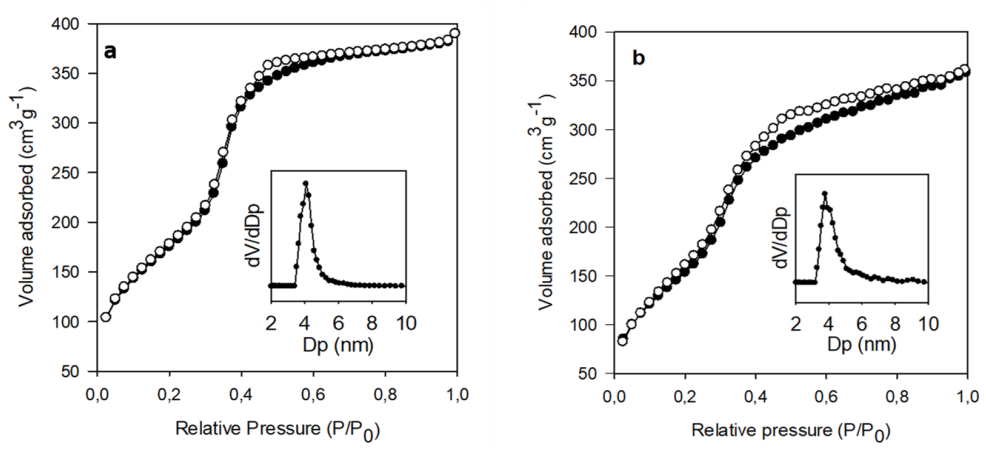

Fig 2. N_2 adsorption-desorption isotherms and pore size distributions (inset) of py-etPMO (a) and py-etPMO-Co materials (b).

Table 1. Physicochemical properties of periodic mesoporous organosilicas.

Sample	a_0[a] (nm)	S_{BET} (m^2/g)	V_p (cm^3/g)	D_p[b] (nm)	Wall thickness[c] (nm)
py-etPMO	5.7	683	0.55	4.1	1.6
py-etPMO-Co	5.6	651	0.51	3.8	1.8

[a] Unit cell parameter calculated $a_0 = \frac{2d_{100}}{\sqrt{3}}$,

[b] Calculated from DFT-analysis

[c] Calculated from the difference between a_0 and D_p

The presence of ethylene bridges as well as pyridylethyl moieties in the silica framework of PMO was confirmed by ^{13}C CP/MAS NMR measurements (Fig. 3 and Fig. S2). An intense signal centered at 5 ppm corresponded to the sp^3 carbon atoms of the ethylene bridges [48]. In addition, signals at 20, 30, 123 and

148 ppm were due to the pyridylethyl moieties incorporated on the channel pores [47]. A remaining signal at 58 ppm was associated to nonhydrolyzed ethoxy groups (-OCH_2CH_3) from the organosilane precursors. After incorporation of the cobaloxime complex on the pore surface of py-etPMO, new signals appeared at 158 and 13 ppm associated to the C=N and CH_3 groups, respectively, from the glyoximate ligand [49,50]. Additional signals at 40 and 50 ppm were attributed to residual DMSO and CH_3OH used to remove unreacted cobaloxime complex after the immobilization process [51].

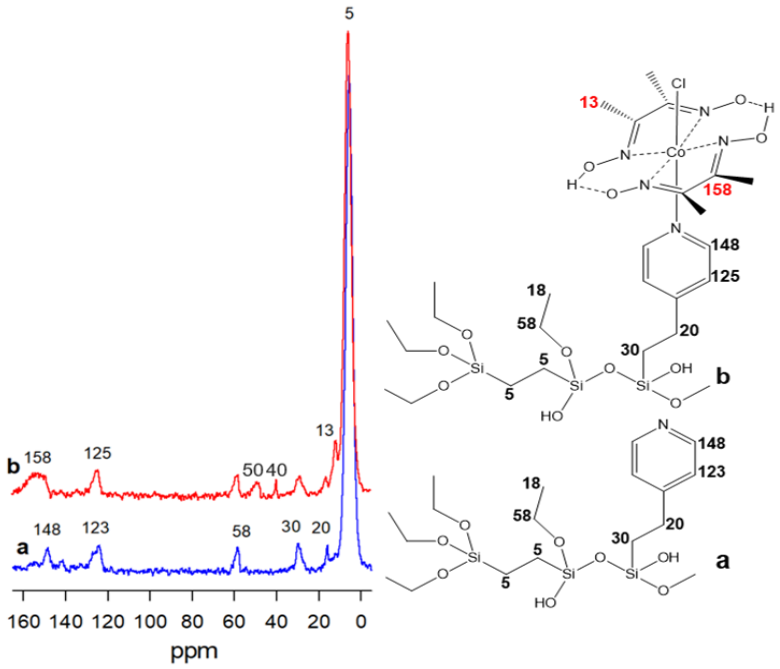

Fig 3. ^{13}C CP/MAS NMR spectra of py-etPMO (a) and py-etPMO-Co (b).

Raman and IR measurements further corroborated the presence of the cobaloxime at the pore surface of the py-etPMO. The Raman spectrum of py-etPMO showed a peak at 3100 cm^{-1} attributed to the =C-H stretching vibrations from the pyridine ring. Several signals in the region of 1500–1600 cm^{-1} were assigned to the C=C stretching of heteroaromatic rings. After cobaloxime

coordination, additional vibration modes at 1650 and 1220 cm^{-1} were related to C=N and N-O stretching, respectively, of the cobaloxime catalyst (Fig. 4) [50]. FT-IR results evidenced the coordination of cobalt on pyridine groups located on the PMO surface. Small vibration signals characteristic of the cobaloxime with axial pyridine ligands were observed at 1247 (νN-O) and 515 (νCo-N) cm^{-1} (Fig S3) [52–54].

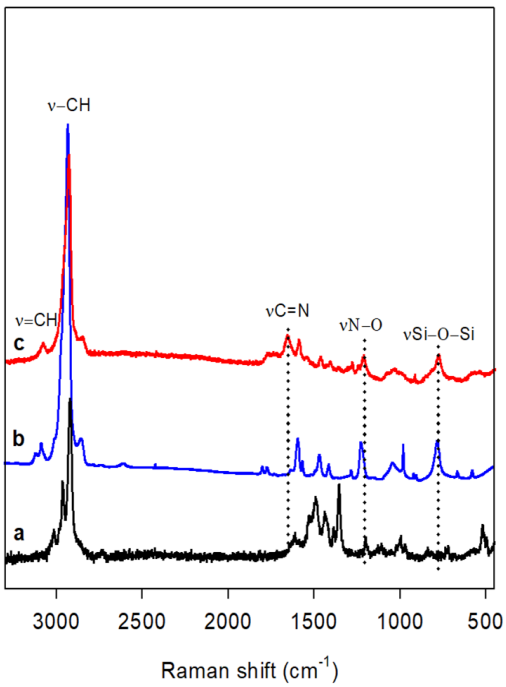

Fig 4. Raman spectra of $Co(dmgH_2)(dmgH)Cl_2$ complex (a), py-etPMO (b) and py-etPMO-Co (c).

The analysis of the samples by X-ray photoelectron spectroscopy (XPS) provided additional evidence of the successful immobilization of the cobaloxime complex on the PMO material. Survey spectrum of py-etPMO showed the presence of Si, C, N and O elements at the surface. Additional peaks associated with Co and Cl elements from cobaloxime units were present in the survey spectrum of py-etPMO-Co (Fig. S4). High-resolution N1s core of py-etPMO

showed two nitrogen contributions at 401.0 and 404.5 eV, which could be ascribed to pyridyl and protonated-pyridyl nitrogens of the pyridylethyl moieties in the silica framework of PMO, respectively (Fig. 5 (a)). Protonated-pyridyl nitrogens (+H-N-pyridinic) could be generated during the removal template under acidic conditions. For py-etPMO-Co, only a contribution centered at 401.2 eV was present. This peak would encompass contributions of the pyridyl nitrogen coordinated and non-coordinated to the Co centers as well as the glyoximate ligands of the cobaloxime [23]. Co 2p core region for py-etPMO-Co exhibited two signals centered at 781.5 eV ($2p_{3/2}$) and 796.5 ($2p_{1/2}$) eV in a 2:1 ratio (Fig. 5 (b)). The splitting of 15.0 eV and the lack of shake-up satellite bands clearly evidenced the presence of cobalt in +3 oxidation state [55]. These results are consistent with previous reports on cobaloxime grafted on semiconductors [23] or carbon nanotubes [54].

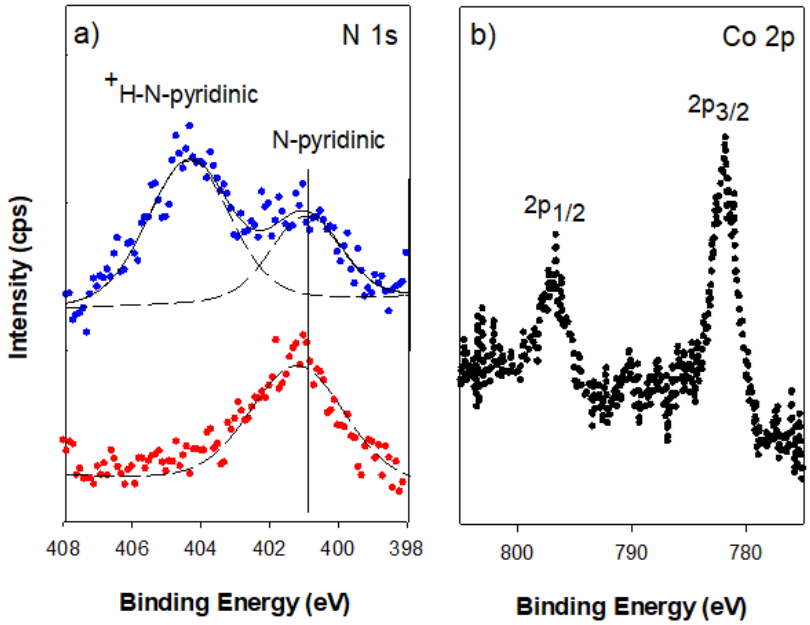

Fig 5. (a) N1s core level XPS spectra of py-etPMO (blue) and py-etPMO-Co (red). (b) Co2p core level XPS spectrum of py-etPMO-Co.

The pyridine content in the PMO support, py-etPMO, was analyzed by elemental analysis (Table S1). Based on the elemental analysis results, the nitrogen content was 0.41 mmol g^{-1}. Furthermore, the cobaloxime loading incorporated on the pore surface of py-etPMO-Co was 0.16 mmol Co per gram of catalyst. Accordingly, the cobaloxime/nitrogen ratio on py-etPMO-Co catalyst was 0.4. It means that approximately half of pyridine groups pendant on the PMO were coordinated to the cobaloxime complex, leaving uncoordinated pyridines available to recoordinate cobaloxime units during the photocatalytic experiments [56]. The incorporated cobaloximes were homogeneously distributed throughout the py-etPMO-Co particles according to SEM-EDX (Fig. S5).

In order to ensure that the coordination of the cobaloxime complexes occurs on the pendant pyridine units located on the PMO surface, an ethylene-bridged periodic mesoporous organosilica containing only ethane moieties in the silica walls [55] has been synthetized (see ESI for ethylene-bridged PMO synthesis). This material was dispersed in CH_3OH and stirred at 65 ºC overnight in the presence of $Co(dmgH_2)(dmgH)Cl_2$ complex. The negligible amount of cobalt in the resulting material by ICP-MS (0.792×10^{-3} mmol of Co per mg of material) clearly confirmed that only pyridine ligands on py-etPMO act as attachment points to assemble cobaloxime catalyst.

Co K-edge x-ray absorption spectroscopy (XAS) has been exploited to access the local electronic and structural properties around the cobalt centers. Figure 6 panel a depicts the x-ray absorption near edge structure (XANES), while panel b and c show the k^2 weighted extended x-ray absorption fine structure (EXAFS) oscillations and their relative Fourier. The XANES region is consistent with Co^{3+} oxidation state and its overall edge shape indicates an octahedral local structure, with the spectral differences corresponding to change in the ligands and distortions. Both the reported XANES and EXAFS signals are in good agreement

with the crystal structure of cobaloxime complex. More in particular, both the spectral features around 8 $Å^{-1}$ in the k and 1.9 Å in the R spaces are signature of a similar local environment [31].

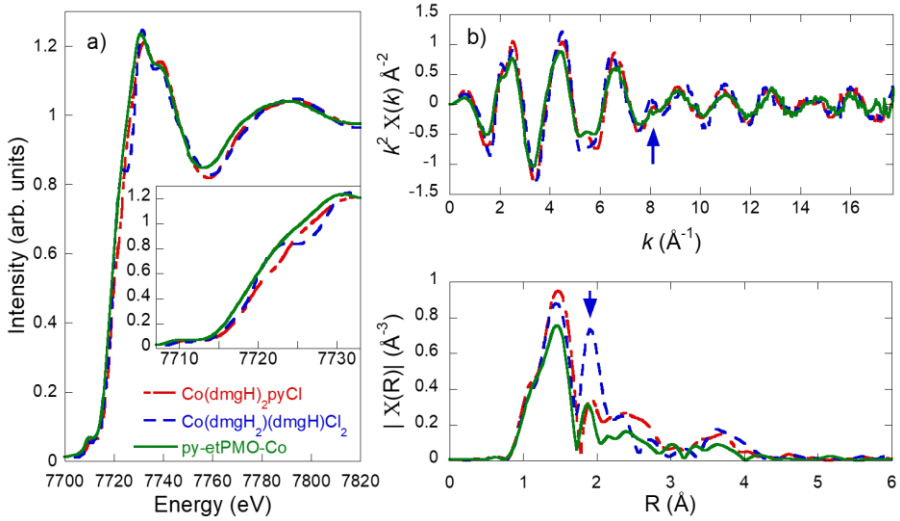

Fig 6. (a) Co K-edge XANES spectra collected over py-etPMO-Co, $Co(dmgH)_2pyCl$ and $Co(dmgH_2)(dmgH)Cl_2$ samples. The inset shows a zoom on the rising edges. (b) k^2 weighted EXAFS oscillations and (c) their relative Fourier transforms obtained from the 2.9-16.4 $Å^{-1}$ k range. The arrows highlight the spectral features characterizing the apical bonds (Co-Cl or Co-N (py)).

4.3.2 Catalytic activity

The potential of py-etPMO-Co as a catalyst for the hydrogen evolution reaction was investigated in a visible light-activated system in the presence of a photosensitizer and a sacrificial electron donor. In this work, eosin Y (EY) and triethanolamine (TEOA) were chosen since they are commonly used when cobaloximes are essayed for HER (Scheme 3) [25,47,50]. All components present in the water reduction – sacrificial electron donor, photosensitizer and catalyst – are necessary to drive hydrogen evolution reaction.

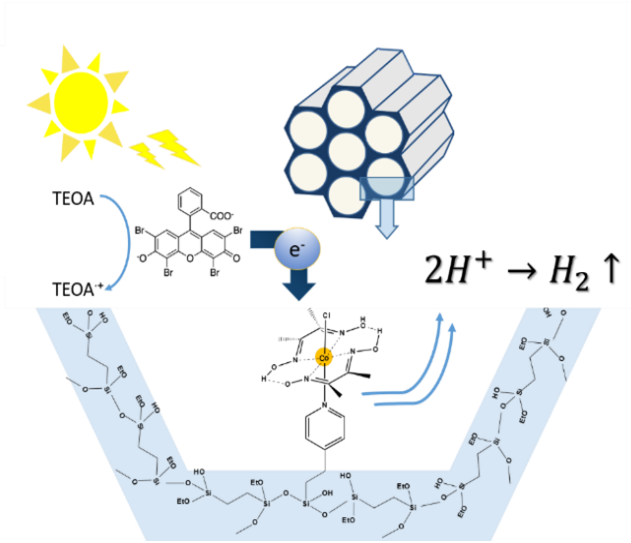

Scheme 3. Schematic representation of photocatalytic hydrogen production with py-etPMO-Co as catalyst.

In a typical photocatalytic experiment, py-etPMO-Co (1 mg) was suspended into the nitrogen purged CH_3CN:H_2O (1:1) solution containing EY (0.05 mM) and TEOA (4.29 mmol) ([EY]:[Co] = 3.75). Upon irradiation with visible light (>400 nm), the hydrogen evolving activity of the catalyst was examined by monitoring the headspace gas by GC at different time intervals.

Preliminary studies were performed to optimize the EY concentration in our light-driven catalytic system (Fig S6).

The photocatalytic activity of py-etPMO-Co under conditions previously mentioned is shown in Fig. 7a. As can be observed, the HER was levelled off after 4 h irradiation with an initial H_2 evolution rate of 3.54 mmol h^{-1} g^{-1}. This corresponds to a hydrogen production maximum of ~18 mmol with a TON of 113. This H_2 production value largely exceeded that reported by Ott et col. [32] for a cobaloxime catalyst immobilized on MIL-101(Cr) under similar light-driven conditions where a TON of 18 was obtained at similar irradiation times. Therefore, we can hypothesize that the studied ordered mesoporous system provides an improved accessibility of all components to the cobaloxime centers for the hydrogen production. Furthermore, compared to other heterogenized molecular HER catalysts reported in literature, our py-etPMO-Co catalyst is among the most active systems for light-driven hydrogen evolution. (Table S2).

Control tests were performed to confirm the key role of all components -*EY, catalyst, TEOA and light*- for photocatalytic HER. For all cases, the absence of one component in the light-driven system evolved a negligible amount of hydrogen (Fig. 7b). Similarly, no hydrogen was detected when py-etPMO-Co was substituted with py-etPMO.

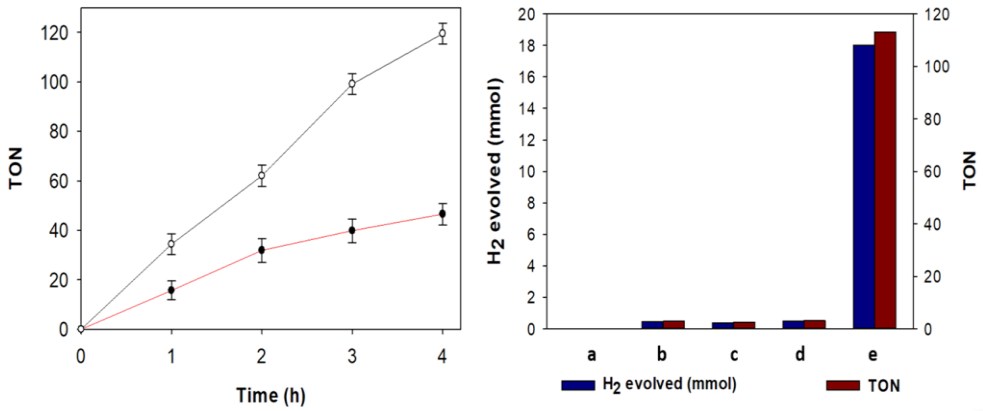

Fig 7. (a) Photocatalytic proton reduction with py-etPMO-Co (black) and $Co(dmgH)_2pyCl$ (red) as catalysts. (b) Control tests for py-etPMO-Co in HER without one component: light (a), TEOA (b), EY (c) and catalyst (d), compared to the HER system with all components (e).

Additionally, a leaching test was undertaken to assure that the hydrogen production reaction occurred heterogeneously with the cobaloxime catalyst anchored on the PMO mesochannels. After catalyst removal, the hydrogen evolution reaction did not proceed, thus confirming that hydrogen production was not catalyzed by active homogeneous cobaloxime species leached out from py-etPMO-Co (Fig. S7).

However, after photocatalytic experiments, ICP-MS (0.034 µmol Co per mg) and XPS measurements (Fig. S8) of py-etPMO-Co material reflected that the cobaloxime complex was released from the mesoporous support during the H_2 production process. These findings were consistent with previous studies reported on electro- and photocatalytic HER that have questioned the stability of the pyridine-cobalt axial bond in the Co(I) oxidation state during the photocatalytic experiment [26,29,32,57]. A weak linkage between the Co(I) and the pyridine grafted on the PMO surface could be responsible of the leaching of the

cobaloxime complex to the solution during the reaction. In order to prove that the cobalt center is detached to the axial pyridine ligands, py-etPMO-Co catalyst after photocatalytic reaction was collected and reactivated after treatment with $Co(dmgH_2)(dmgH)Cl_2$ complex. After that, the reactivated catalyst was collected and washed thoroughly with methanol and acetonitrile to remove any uncoordinated cobaloxime. ICP-MS analysis of the reactivated py-etPMO-Co catalyst gave 0.15 mmol Co per mg, similarly to the fresh catalyst, confirming the almost total restoration of the starting material. The reactivated catalyst was evaluated in HER under identical conditions to the fresh catalyst, and it showed a comparable photocatalytic activity with a TON value of 110 after 4 h irradiation (Fig. 8). After a second reactivation treatment, the py-etPMO-Co maintained the initial activity. These results revealed that the hydrogen production is catalyzed by the cobaloxime catalyst immobilized on the pore surface of the PMO hybrid material, which can be restored to its initial activity during two recycling cycles. This total restoration of the catalytic activity of the PMO material was remarkable since the cobaloxime anchored on MIL-101 reported by Ott et col. [58] achieved approximately 60 % of its initial activity. These results evidence the good accessibility of the pyridine ligands positioned in the mesochannels of PMO, therefore facilitating its total restoration during the recycling tests.

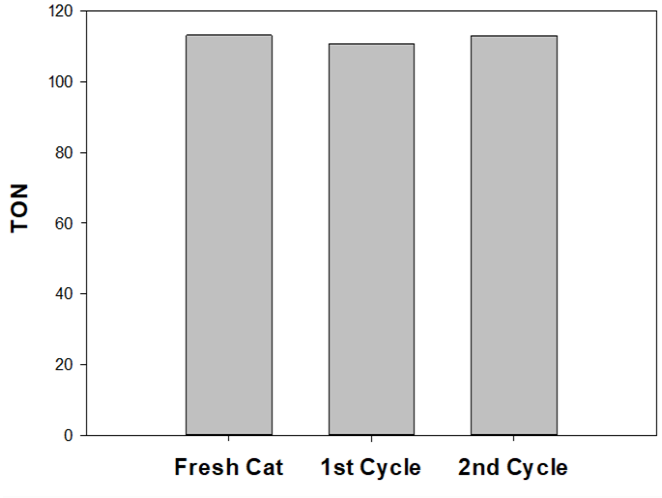

Fig 8. Recycling tests on py-etPMO-Co during 4 h.

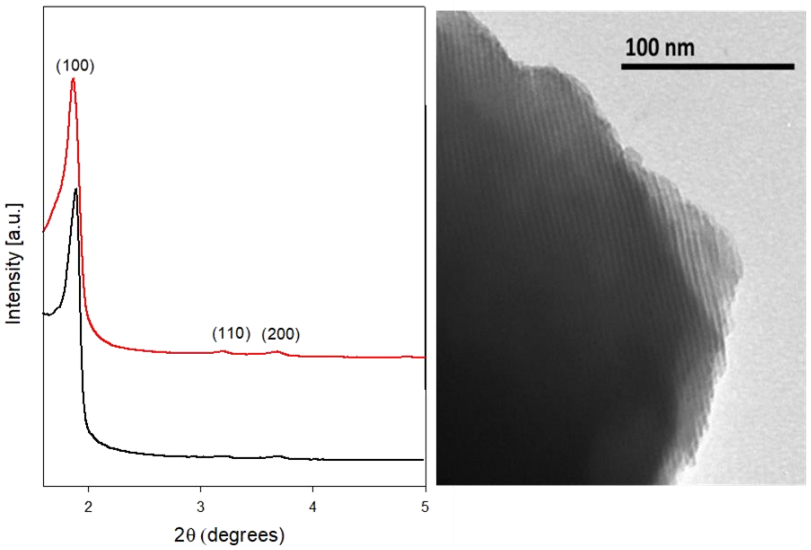

Fig 9. (a) PXRD of py-etPMO-Co before (red) and after (black) photocatalysis (b) TEM image of py-etPMO-Co after photocatalytic reaction.

Furthermore, structural and textural properties of the py-etPMO-Co after photocatalysis were preserved, which confirmed the high mesostructural stability of the material under the photocatalytic conditions employed (Fig. 9). Clearly, the high hydrophobicity of the PMO framework determines its good stability in aqueous media [37,59].

4.4 CONCLUSIONS

A novel cobaloxime-PMO hybrid material was prepared via complexation of cobaloxime units on the pyridine moieties present on the surface of an ethylene-bridged PMO material. This strategy allows obtaining an efficient hydrogen evolving catalyst in presence of EY as photosensitizer and TEOA as sacrificial electron donor, achieving a TON of 113. This system shows an enhanced photocatalytic performance under the studied conditions in comparison to its homogeneous counterpart, which suggests an increased stability of the cobaloxime catalyst confined into the mesopores. Although this system was able to restore its initial catalytic activity during two recycling experiments, a previous reactivation process was needed to coordinate cobaloxime centers on the PMO material. These results confirm that its applicability during continuous photocatalytic processes is still limited due to the inherent instability of the cobalt-pyridine axial bond during the photocatalytic reaction. Future studies are being addressed to enhance the photocatalytic stability of Co-py linkages on PMO mesochannels.

4.7 REFERENCES

[1] T. Lauvaux, K.R. Gurney, N.L. Miles, K.J. Davis, S.J. Richardson, A. Deng, B.J. Nathan, T. Oda, J.A. Wang, L. Hutyra, J. Turnbull, Policy-Relevant Assessment of Urban CO_2 Emissions, Environ. Sci. Technol. 54 (2020) 10237–10245. https://doi.org/10.1021/acs.est.0c00343.

[2] N.S. Lewis, D.G. Nocera, Powering the planet : Chemical challenges in solar energy utilization, Proc Natl Acad Sci U S A. 103 (2006) 15729–15736.

[3] K.L. Bren, Multidisciplinary approaches to solar hydrogen, Interface Focus. 5 (2015) 1–12. https://doi.org/10.1098/rsfs.2014.0091.

[4] I.E.A. Pvps, A. Report, P. Power, S. Programme, ANNUAL REPORT 2020 PHOTOVOLTAIC POWER SYSTEMS PROGRAMME, Int. Energy Agency Photovolt. Power Syst. Program. (2020).

[5] N. Abas, E. Kalair, A. Kalair, Q. ul Hasan, N. Khan, Nature inspired artificial photosynthesis technologies for hydrogen production: Barriers and challenges, Int. J. Hydrogen Energy. 45 (2020) 20787–20799. https://doi.org/10.1016/j.ijhydene.2019.12.010.

[6] T. Keijer, T. Bouwens, J. Hessels, J.N.H. Reek, Supramolecular strategies in artificial photosynthesis, Chem. Sci. 12 (2021) 50–70. https://doi.org/10.1039/d0sc03715j.

[7] R. Eisenberg, H.B. Gray, Preface on making oxygen, Inorg. Chem. 47 (2008) 1697–1699. https://doi.org/10.1021/ic800155g.

[8] P. Du, R. Eisenberg, Catalysts made of earth-abundant elements (Co, Ni, Fe) for water splitting: Recent progress and future challenges, Energy Environ. Sci. 5 (2012) 6012–6021. https://doi.org/10.1039/c2ee03250c.

[9] M.W. Kanan, J. Yano, Y. Surendranath, M. Dinca, V.K. Yachandra, D.G. Nocera, Structure and Valency of a Cobalt-Phosphate Water Oxidation Catalyst Determined by in Situ X-ray Spectroscopy, J. Am. Chem. Soc. 132 (2010) 13692–13701. https://doi.org/10.1021/ja1023767.

[10] Q. Yin, J.M. Tan, C. Besson, Y. V Geletii, D.G. Musaev, A.E. Kuznetsov, Z. Luo, K.I. Hardcastle, C.L. Hill, A Fast Soluble Carbon-Free Molecular Water Oxidation Catalyst Based on Abundant Metals, Science. 328 (2010) 342–346.

[11] W.R. Mcnamara, Z. Han, P.J. Alperin, W.W. Brennessel, P.L. Holland, R. Eisenberg, A Cobalt–Dithiolene Complex for the Photocatalytic and Electrocatalytic Reduction of Protons, J. Am. Chem. Soc. 133 (2011) 15368–15371. https://doi.org/10.1021/ja207842r.

[12] B.D. Stubbert, J.C. Peters, H.B. Gray, Rapid Water Reduction to H_2 Catalyzed by a Cobalt Bis(iminopyridine) Complex, J. Am. Chem. Soc. 133 (2011) 18070–18073. https://doi.org/10.1021/ja2078015.

[13] J.L. Dempsey, B.S. Brunschwig, J.R. Winkler, H.B. Gray, Hydrogen evolution catalyzed by cobaloximes, Acc. Chem. Res. 42 (2009) 1195–2004.

[14] V. Artero, M. Chavarot-Kerlidou, M. Fontecave, Splitting water with cobalt, Angew. Chemie - Int. Ed. 50 (2011) 7238–7266. https://doi.org/10.1002/anie.201007987.

[15] M. Natali, A. Luisa, E. Iengo, F. Scandola, Efficient photocatalytic hydrogen generation from water by a cationic cobalt (II) porphyrin, Chem. Commun. 50 (2014) 1842–1844. https://doi.org/10.1039/c3cc48882a.

[16] N. Kaeffer, M. Chavarot-Kerlidou, V. Artero, Hydrogen evolution catalyzed by cobalt diimine-dioxime complexes, Acc. Chem. Res. 48 (2015) 1286–1295. https://doi.org/10.1021/acs.accounts.5b00058.

[17] D. Dolui, S. Khandelwal, P. Majumder, A. Dutta, The odyssey of cobaloximes for catalytic H_2 production and their recent revival with enzyme-inspired design, Chem. Commun. 56 (2020) 8166–8181. https://doi.org/10.1039/d0cc03103h.

[18] J. Hawecker, J. Lehn, R. Ziessel, Efficient Photochemical Reduction of CO, to CO by Visible Light Irradiation of Systems containing $Re(bipy)(CO)_X$ or $Ru(bipy)_3^{2+}$-Co^{2+} Combinations as Homogeneous Catalysts, J. Chem. Soc., Chem. Commun. (1983) 536–538. https://doi.org/10.1039/C39830000536.

[19] S.R. Soltau, J. Niklas, P.D. Dahlberg, O.G. Poluektov, D.M. Tiede, K.L. Mulfort, L.M. Utschig, Aqueous light driven hydrogen production by a Ru-ferredoxin-Co biohybrid, Chem. Commun. 51 (2015) 10628–10631. https://doi.org/10.1039/c5cc03006d.

[20] F. Lakadamyali, E. Reisner, Photocatalytic H_2 evolution from neutral water with a molecular cobalt catalyst on a dye-sensitised TiO_2 nanoparticle, Chem. Commun. 47 (2011) 1695–1697. https://doi.org/10.1039/c0cc04658b.

[21] M. Razavet, V. Artero, M. Fontecave, Proton electroreduction catalyzed by cobaloximes: Functional models for hydrogenases, Inorg. Chem. 44 (2005) 4786–4795. https://doi.org/10.1021/ic050167z.

[22] D.W. Wakerley, E. Reisner, Development and understanding of cobaloxime activity through electrochemical molecular catalyst screening, Phys. Chem. Chem. Phys. 16 (2014) 5739–5746. https://doi.org/10.1039/c4cp00453a.

[23] A. Panagiotopoulos, K. Ladomenou, D. Sun, V. Artero, A.G. Coutsolelos, Photochemical hydrogen production and cobaloximes: The influence of the cobalt axial N-ligand on the system stability, Dalt. Trans. 45 (2016) 6732–6738. https://doi.org/10.1039/c5dt04502a.

[24] D. Dolui, S. Khandelwal, A. Shaik, D. Gaat, V. Thiruvenkatam, A. Dutta, Enzyme-Inspired Synthetic Proton Relays Generate Fast and Acid- Stable Cobalt-Based H_2 Production Electrocatalysts, ACS Catal. 9 (2019) 10115–10125. https://doi.org/10.1021/acscatal.9b02953.

[25] Y.K. Jiang, J.H. Liu, DFT studies of cobalt hydride intermediate on cobaloxime-catalyzed H_2 evolution pathways, Int. J. Quantum Chem. 112 (2012) 2541–2546. https://doi.org/10.1002/qua.23246.

[26] A. Kahnt, K. Peuntinger, C. Dammann, T. Drewello, R. Hermann, S. Naumov, B. Abel, D.M. Guldi, Kinetic studies of the reduction of $[Co(dmgH)_2(py)(Cl)]$ revisited: Mechanisms, products, and implications, J. Phys. Chem. A. 118 (2014) 4382–4391. https://doi.org/10.1021/jp501947y.

[27] J. Chen, P.H.L. Sit, Thermodynamic Properties of Hydrogen-Producing Cobaloxime Catalysts: A Density Functional Theory Analysis, ACS Omega. 4 (2019) 582–592. https://doi.org/10.1021/acsomega.8b02107.

[28] N.M. Muresan, J. Willkomm, D. Mersch, Y. Vaynzof, E. Reisner, Immobilization of a molecular cobaloxime catalyst for hydrogen evolution on a mesoporous metal oxide electrode, Angew. Chemie - Int. Ed. 51 (2012) 12749–12753. https://doi.org/10.1002/anie.201207448.

[29] B. Reuillard, J. Warnan, J.J. Leung, D.W. Wakerley, E. Reisner, A Poly(cobaloxime)/Carbon Nanotube Electrode: Freestanding Buckypaper with Polymer-Enhanced H_2-Evolution Performance, Angew. Chemie - Int. Ed. 55 (2016) 3952–3957. https://doi.org/10.1002/anie.201511378.

[30] E.S. Andreiadis, P.A. Jacques, P.D. Tran, A. Leyris, M. Chavarot-Kerlidou, B. Jousselme, M. Matheron, J. Pécaut, S. Palacin, M. Fontecave, V. Artero, Molecular engineering of a cobalt-based electrocatalytic nanomaterial for H_2 evolution under fully aqueous conditions, Nat. Chem. 5 (2013) 48–53. https://doi.org/10.1038/nchem.1481.

[31] S. Donck, J. Fize, E. Gravel, E. Doris, V. Artero, Supramolecular assembly of cobaloxime on nanoring-coated carbon nanotubes: addressing the stability of the pyridine–cobalt linkage under hydrogen evolution turnover conditions, Chem. Commun. 52 (2016) 11783–11786. https://doi.org/10.1039/C6CC06059E.

[32] B.L. Wadsworth, A.M. Beiler, D. Khusnutdinova, S.I. Jacob, G.F. Moore, Electrocatalytic and Optical Properties of Cobaloxime Catalysts Immobilized at a Surface-Grafted Polymer Interface, ACS Catal. 6 (2016) 8048–8057. https://doi.org/10.1021/acscatal.6b02194.

[33] C. Tapia, E. Bellet-Amalric, D. Aldakov, F. Boudoire, K. Sivula, L. Cagnon, V. Artero, Achieving visible light-driven hydrogen evolution at positive bias with a hybrid copper-iron oxide|TiO_2-cobaloxime photocathode, Green Chem. 22 (2020) 3141–3149. https://doi.org/10.1039/d0gc00979b.

[34] S. Roy, A. Bhunia, N. Schuth, M. Haumann, S. Ott, Light-driven hydrogen evolution catalyzed by a cobaloxime catalyst incorporated in a MIL-101(Cr) metal-organic framework, Sustain. Energy Fuels. 2 (2018) 1148–1152. https://doi.org/10.1039/c8se00072g.

[35] S. Roy, Z. Huang, A. Bhunia, A. Castner, A.K. Gupta, X. Zou, S. Ott, Electrocatalytic Hydrogen Evolution from a Cobaloxime-Based Metal-Organic Framework Thin Film, J. Am. Chem. Soc. 141 (2019) 15942–15950. https://doi.org/10.1021/jacs.9b07084.

[36] K. Gottschling, G. Savasci, H. Vignolo-González, S. Schmidt, P. Mauker, T. Banerjee, P. Rovó, C. Ochsenfeld, B. V. Lotsch, Rational Design of Covalent Cobaloxime-Covalent Organic Framework Hybrids for Enhanced Photocatalytic Hydrogen Evolution, J. Am. Chem. Soc. 142 (2020) 12146–12156. https://doi.org/10.1021/jacs.0c02155.

[37] P. Van Der Voort, D. Esquivel, E. De Canck, F. Goethals, I. Van Driessche, F.J. Romero-Salguero, Periodic Mesoporous Organosilicas: from simple to complex bridges; a comprehensive overview of functions, morphologies and applications, Chem. Soc. Rev. 42 (2013) 3913–3955. https://doi.org/10.1039/C2CS35222B.

[38] D. Esquivel, E. Canck, C. Jimenez-Sanchidrian, P. Voort, F. Romero-Salguero, Periodic Mesoporous Organosilicas as Catalysts for Organic Reactions, Curr. Org. Chem. 18 (2014) 1280–1295. https://doi.org/10.2174/13852728196661404242043 23.

[39] D. Esquivel, E. De Canck, C. Jimenez-Sanchidrian, P. Van Der Voort, F.J. Romero-Salguero, Formation and functionalization of surface Diels–Alder adducts on ethenylene-bridged periodic mesoporous organosilica, J. Mater. Chem. 21 (2011) 10990–10998. https://doi.org/10.1039/C1JM11315A.

[40] W.J. Hunks, G.A. Ozin, Periodic mesoporous phenylenesilicas with ether or sulfide hinge groups a new class of PMOs with ligand channels, Chem. Commun. (2004) 2426–2427. https://doi.org/10.1039/B410397A.

[41] N. Mizoshita, T. Tani, S. Inagaki, Syntheses, properties and applications of periodic mesoporous organosilicas prepared from bridged organosilane precursors, Chem. Soc. Rev. 40 (2011) 789–800. https://doi.org/10.1039/c0cs00010h.

[42] A.M. Kaczmarek, S. Abednatanzi, D. Esquivel, C. Krishnaraj, H.S. Jena, G. Wang, K. Leus, R. Van Deun, F.J. Romero-Salguero, P. Van Der Voort, Amine-containing (nano-) Periodic Mesoporous Organosilica and its application in catalysis, sorption and luminescence, Microporous Mesoporous Mater. 291 (2020) 109687. https://doi.org/10.1016/j.micromeso.2019.109687.

[43] T. Himiyama, M. Waki, D. Esquivel, A. Onoda, T. Hayashi, A Heterogeneous Hydrogen-Evolution Catalyst Based on a Mesoporous Organosilica with a Diiron Catalytic Center Modelling [FeFe]-Hydrogenase, ChemCatChem. 10 (2018) 4894–4899. https://doi.org/10.1002/cctc.201801257.

[44] W.C. Trogler, R.C. Stewart, Cis and Trans Effects on the Proton Magnetic Resonance Spectra of Cobaloximes, Inorg. Chem. **13** (1974) 1564–1570. https://doi.org/10.1021/ic50137a005.

[45] M. Waki, N. Mizoshita, T. Tani, S. Inagaki, Periodic mesoporous organosilica derivatives bearing a high density of metal complexes on pore surfaces, Angew. Chemie-International Ed. 50 (2011) 11667–11671. https://doi.org/10.1002/anie.201104063.

[46] A.M. Kaczmarek, D. Esquivel, B. Laforce, L. Vincze, P. Van Der Voort, F.J. Romero-Salguero, R. Van Deun, Luminescent thermometer based on Eu^{3+}/Tb^{3+}-organic-functionalized mesoporous silica, Luminescence. 33 (2018) 567–573. https://doi.org/10.1002/bio.3447.

[47] L. Simonelli, C. Marini, W. Olszewski, M.Á. Pérez, N. Ramanan, G. Guilera, V. Cuartero, MATERIALS SCIENCE | RESEARCH ARTICLE CLÆSS : The hard X-ray absorption beamline of the ALBA CELLS synchrotron MATERIALS SCIENCE | RESEARCH ARTICLE CLÆSS : The hard X-ray absorption beamline of the ALBA CELLS synchrotron, Cogent Phys. 3 (2016) 1–10. https://doi.org/10.1080/23311940.2016.1231987.

[48] B. Ravel, M. Newville, ATHENA , ARTEMIS , HEPHAESTUS : data analysis for X-ray absorption spectroscopy using IFEFFIT, J. Synchrotron Radiat. 12 (2005) 537–541. https://doi.org/10.1107/S0909049505012719.

[49] M. Waki, N. Mizoshita, T. Ohsuna, T. Tani, S. Inagaki, Crystal-like periodic mesoporous organosilica bearing pyridine units within the framework, Chem. Commun. 46 (2010) 8163. https://doi.org/10.1039/c0cc01944e.

[50] M.I. López, D. Esquivel, C. Jiménez-Sanchidrián, F.J. Romero-Salguero, P. Van Der Voort, A "one-step" sulfonic acid PMO as a recyclable acid catalyst, J. Catal. 326 (2015) 139–148. https://doi.org/10.1016/j.jcat.2015.04.008.

[51] T. Banerjee, F. Haase, G. Savasci, K. Gottschling, C. Ochsenfeld, B. V. Lotsch, Single-Site Photocatalytic H_2 Evolution from Covalent Organic Frameworks with Molecular Cobaloxime Co-Catalysts, J. Am. Chem. Soc. 139 (2017) 16228–16234. https://doi.org/10.1021/jacs.7b07489.

[52] D.A. Thornton, Metal complexes of pyridine: infrared and raman spectra with particular reference to isotopic labelling studies, Coord. Chem. Rev. 104 (1990) 251–295. https://doi.org/10.1016/0010-8545(90)80044-T.

[53] G.R. Fulmer, A.J.M. Miller, N.H. Sherden, H.E. Gottlieb, A. Nudelman, B.M. Stoltz, J.E. Bercaw, K.I. Goldberg, NMR Chemical Shifts of Trace Impurities: Common Laboratory Solvents, Organics, and Gases in Deuterated Solvents Relevant to the Organometallic Chemist, Organometallics. 29 (2010) 2176–2179. https://doi.org/10.1021/om100106e.

[54] A. Krawicz, J. Yang, E. Anzenberg, J. Yano, I.D. Sharp, G.F. Moore, Photofunctional construct that interfaces molecular cobalt-based catalysts for H_2 production to a visible-light-absorbing semiconductor, J. Am. Chem. Soc. 135 (2013) 11861–11868. https://doi.org/10.1021/ja404158r.

[55] F. Hoffmann, M. Güngerich, P.J. Klar, M. Fröba, Vibrational spectroscopy of periodic mesoporous organosilicas (PMOs) and their precursors: a closer look, J. Phys. Chem. C. 111 (2007) 5648–5660. https://doi.org/10.1021/jp0668596.

[56] T.J. Chuang, C.R. Brundle, D.W. Rice, Interpretation of the X-Ray photoemission spectra of cobalt oxides and cobalt oxide surfaces, Surf. Sci. 59 (1976) 413–429. https://doi.org/10.1016/0039-6028(76)90026-1.

[57] J. Willkomm, N.M. Muresan, E. Reisner, Enhancing H_2 evolution performance of an immobilised cobalt catalyst by rational ligand design, Chem. Sci. 6 (2015) 2727–2736. https://doi.org/10.1039/c4sc03946g.

[58] T. Lazarides, T. Mccormick, P. Du, G. Luo, B. Lindley, R. Eisenberg, Making Hydrogen from Water Using a Homogeneous System Without Noble Metals, J. Am. Chem. Soc. 131 (2009) 9192–9194. https://doi.org/10.1021/ja903044n.

[59] D. Esquivel, C. Jiménez-Sanchidrián, F.J. Romero-Salguero, Comparison of the thermal and hydrothermal stabilities of ethylene, ethylidene, phenylene and biphenylene bridged periodic mesoporous organosilicas, Mater. Lett. 65 (2011) 1460–1462. https://doi.org/10.1016/j.matlet.2011.02.037.

Supplementary Information

Synthesis of ethylene-bridged PMO

Ethylene-bridged PMO material was synthesized following a procedure described by Burleigh and col. [1]. Typically, 6 gr of Brij 76 was added in a solution containing 19.6 ml of HCl and 279 ml of H_2O. The mixture was stirred at 50 ºC for 24 h. Afterwards, 15.9 ml of bis-silane precursor, 1,2-bis(triethoxysilyl)ethane, was added dropwise to the clear solution and it was stirred at 50 ºC for 24 h. Then, the mixture was aged at 90 ºC overnight under static conditions. The final solid was filtered under vacuum and washed with plenty of water.

To remove the surfactant, 1g of synthetized material was refluxed in acid ethanolic solution (1ml conc. HCl: 50 ml ethanol) for 12h. This process was repeated twice. Finally, the white solid was collected and dried under vacuum at 120 ºC overnight (Scheme S1).

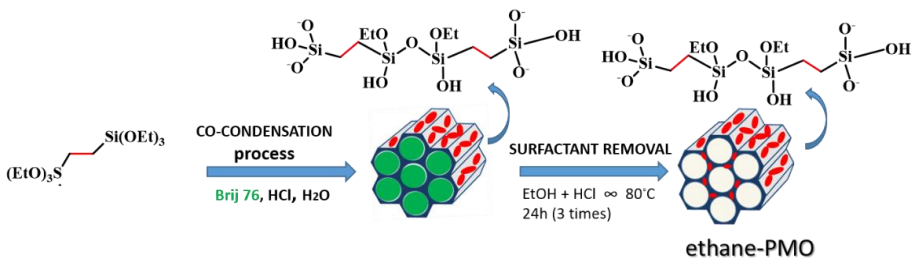

Scheme S1. Synthesis route of ethylene-bridged PMO material.

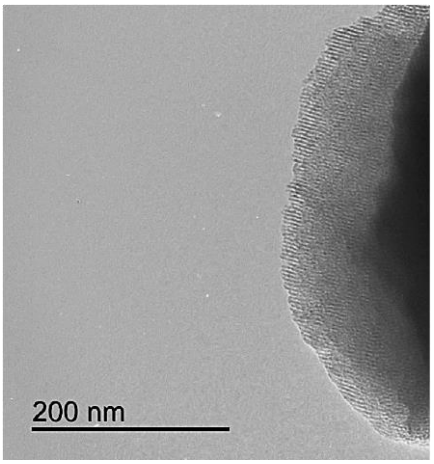

Fig S1. TEM image of py-etPMO.

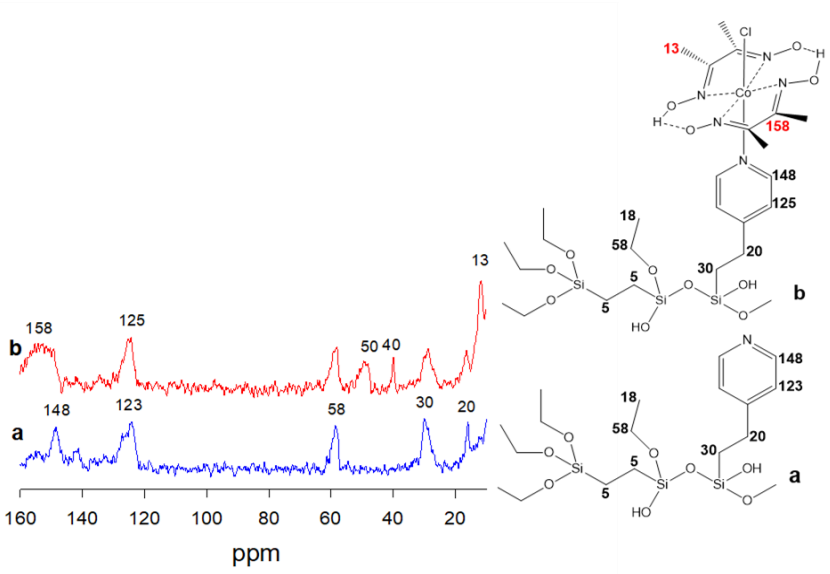

Fig S2. ^{13}C CP/MAS NMR spectra of py-etPMO (a) and py-etPMO-Co (b) excluding signal associated to Csp^3 of the ethylene bridges.

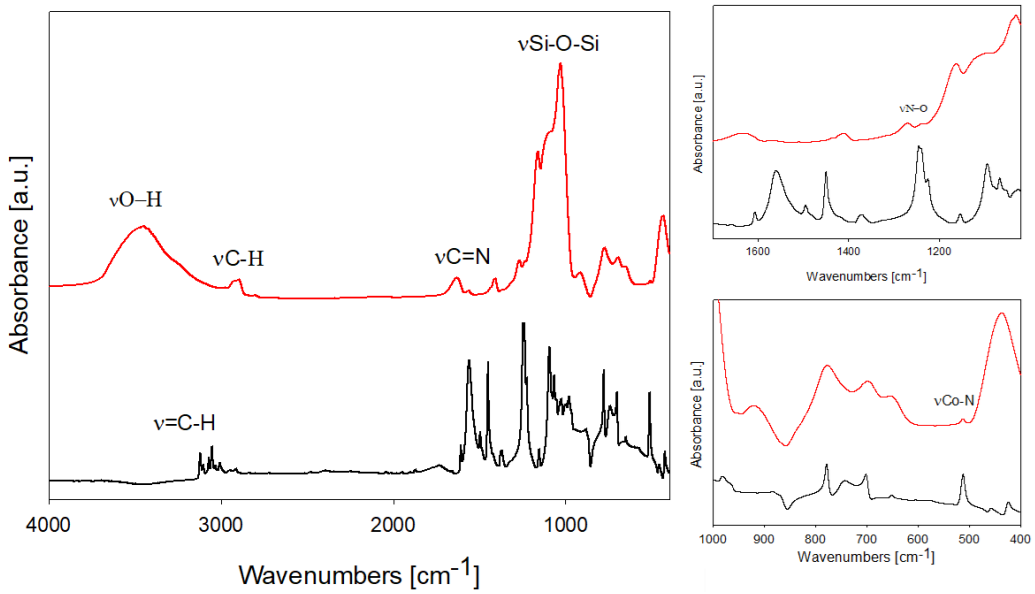

Fig S3. FT-IR spectra of $Co(dmgH)_2pyCl$ complex (black) and py-etPMO-Co catalyst (red).

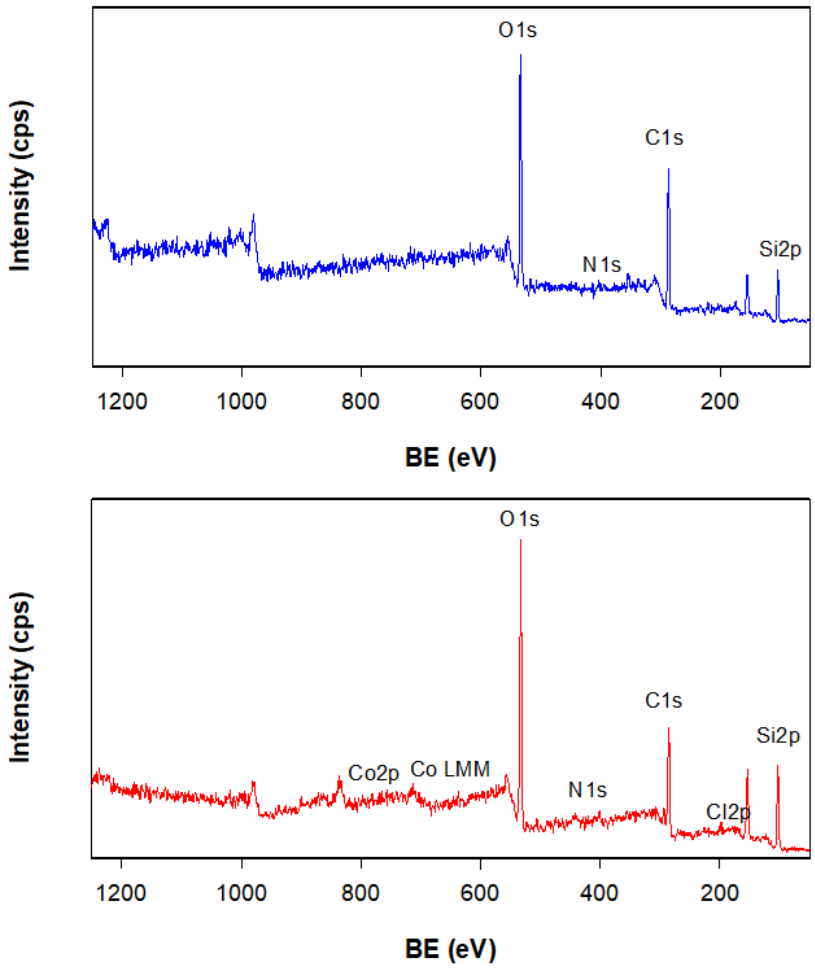

Fig S4. Survey spectra of py-etPMO (blue) and py-etPMO-Co (red).

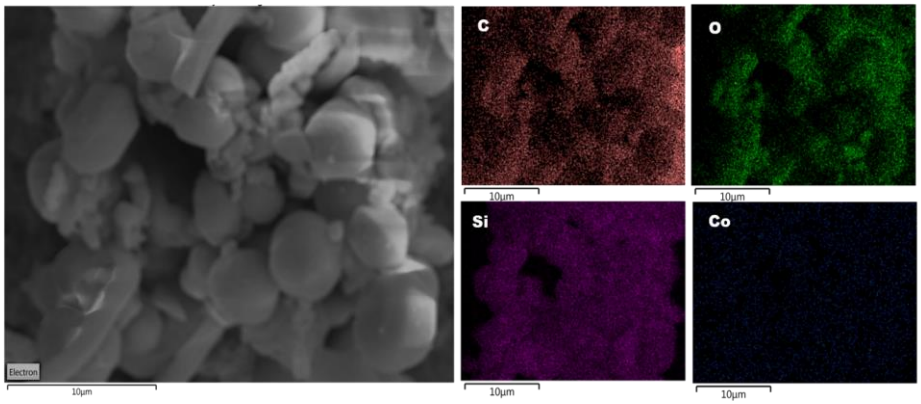

Fig S5. SEM image of py-etPMO-Co and corresponding EDX elemental analysis maps.

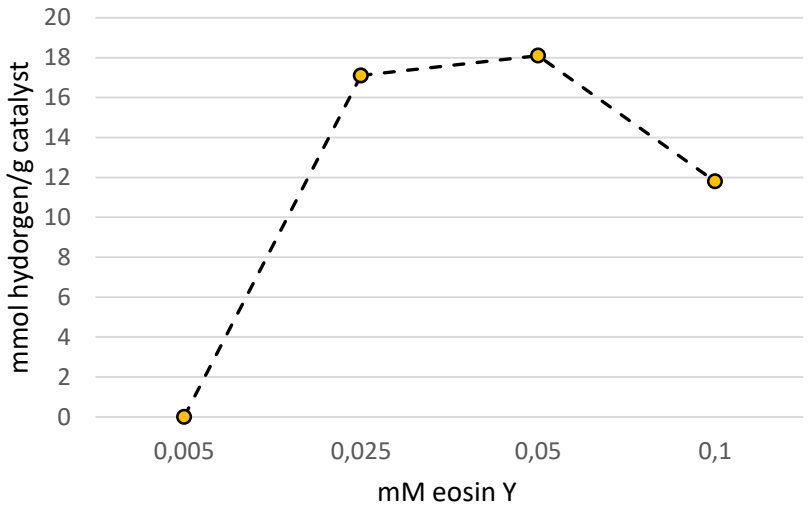

Fig S6. Effect of EY concentration on hydrogen production activity of pyetPMO-Co (catalyst, 1 mg; TEOA, 0.75 mM; reaction time, 4 h).

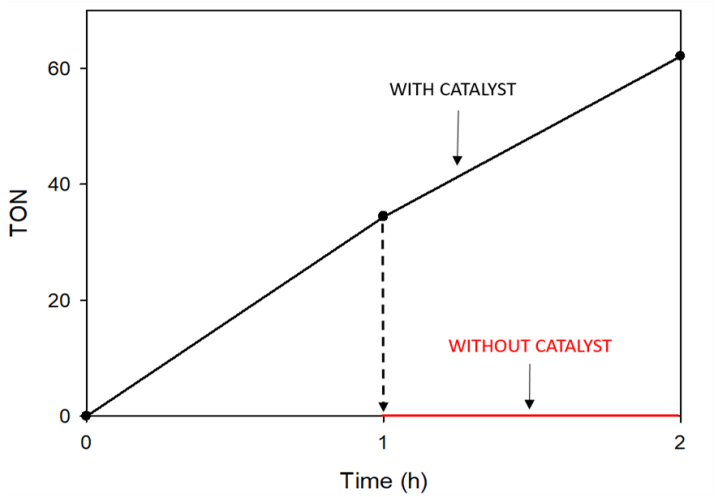

Fig S7. Catalytic test after removing catalyst.

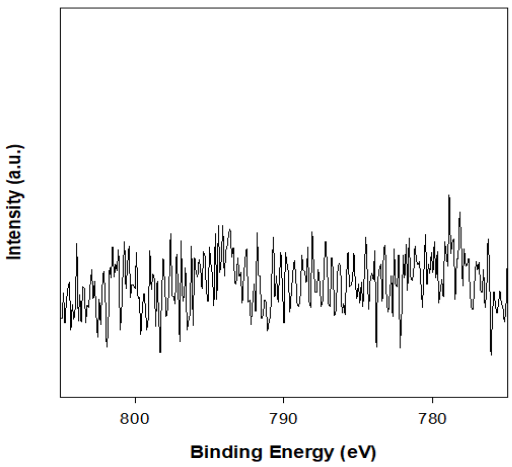

Fig S8. Co2p XPS spectrum of py-etPMO-Co after photocatalysis.

Table S1. Compositional analysis of py-etPMO and py-etPMO-Co

Sample	% Nitrogen[a]	mmol of Nitrogen per mg	mmol of Co per mg[b]
py-etPMO	0.57	0.41	n.d
py-etPMO-Co	n.d	n.d	0.16
ethane-PMO	-	-	0.792×10^{-3}

[a] Calculated by elemental analysis

[b] Obtained by ICP-MS

Table S2. Comparison of the photocatalytic performance of py-etPMO-Co for HER with previously reported heterogenized molecular hydrogen evolution reaction catalysts

Catalyst	**Support**	**External Sensitizer**	**Time (h)**	**H_2 evolution rate (mmol · g^{-1})**	**TON**	**Ref**
$Co(dmgH_2)(dmgH)Cl_2$	py-etPMO	eosin	4 h	18.1	113	This work
$Co(dmgH)_2$(4-HEP)Cl[a]	MIL-101(Cr)	eosin	5h	8	20	[2]
$Co(dmgH_2)(dmgH)$pyCl	COF	-	13 h	11.8	170	[3]
Cobaloxime – complex	Polymer	$Ru(bpy)_3Cl_2$	5h	0.9	2.8	[4]
[FeFe]-(dcbdt)$(CO)_6$[b]	Zr(IV)-MOF	$Ru(bpy)_3Cl_2$	2.5h	3.5	5.9	[5]
Fe_2(cbdt)$(CO)_6$][c]	MIL-101(Cr)	$Ru(bpy)_3Cl_2$	2.3h	3	18.5	[6]
$Fe_2S_2(CO)_6$-complex	UiO-MOF	polypyridyl ruthenium	50h	0.032	16	[7]
[FeFe]-hydrogenase	SH-PMO	$[Ru(bpy)_3]Cl_2$	2h	0.0009	12	[8]

[a]4-HEP: 4-(2-hydroxyethyl)pyridine

[b]dcbdt: 1,4-dicarboxylbenzene-2,3-dithiolate

[c]cbdt: 3-carboxybenzene-1,2-dithiolate

REFERENCES

[1] M.C. Burleigh, S. Jayasundera, C.W. Thomas, M.S. Spector, M.A. Markowitz, B.P. Gaber, A versatile synthetic approach to periodic mesoporous organosilicas, Colloid Polym. Sci. 282 (2004) 728–733.

[2] S. Roy, A. Bhunia, N. Schuth, M. Haumann, S. Ott, Light-driven hydrogen evolution catalyzed by a cobaloxime catalyst incorporated in a MIL-101(Cr) metal-organic framework, Sustain. Energy Fuels. 2 (2018) 1148–1152. https://doi.org/10.1039/c8se00072g.

[3] K. Gottschling, G. Savasci, H. Vignolo-González, S. Schmidt, P. Mauker, T. Banerjee, P. Rovó, C. Ochsenfeld, B. V. Lotsch, Rational Design of Covalent Cobaloxime-Covalent Organic Framework Hybrids for Enhanced Photocatalytic Hydrogen Evolution, J. Am. Chem. Soc. 142 (2020) 12146–12156. https://doi.org/10.1021/jacs.0c02155.

[4] R.R. Haikal, X. Wang, Y.S. Hassan, M.R. Parida, B. Murali, O.F. Mohammed, P.J. Pellechia, M. Fontecave, M.H. Alkordi, Porous-Hybrid Polymers as Platforms for Heterogeneous Photochemical Catalysis, ACS Appl. Mater. Interfaces. 8 (2016) 19994–20002. https://doi.org/10.1021/acsami.6b05031

[5] S. Pullen, H. Fei, A. Orthaber, S.M. Cohen, S. Ott, Enhanced photochemical hydrogen production by a molecular diiron catalyst incorporated into a metal-organic framework, J. Am. Chem. Soc. 135 (2013) 16997–17003. https://doi.org/10.1021/ja407176p.

[6] S. Roy, V. Pascanu, S. Pullen, G. González Miera, S. Ott, Catalyst accessibility to chemical reductants in metal–organic frameworks, Chem. Commun. 53 (2017) 3257–3260. https://doi.org/10.1039/C7CC00022G.

[7] A.W. of iron hydrogenase active sites into a stable photosensitizing metal-organic framework for enhanced hydrogen production Wang, X. Song, Z. Hong, Incorporation of iron hydrogenase active sites into a stable photosensitizing metal-organic framework for enhanced hydrogen production, Appl. Catal. B, Environ. 258 (2019) 117979. https://doi.org/10.1016/j.apcatb.2019.117979.

[8] T. Himiyama, M. Waki, D. Esquivel, A. Onoda, T. Hayashi, A Heterogeneous Hydrogen-Evolution Catalyst Based on a Mesoporous Organosilica with a Diiron Catalytic Center Modelling [FeFe]-Hydrogenase, ChemCatChem. 10 (2018) 4894–4899. https://doi.org/10.1002/cctc.201801257

CHAPTER 5.

RESULTS AND DISCUSSION

Chapter 5 **"Catalytic activity of cobaloxime complexes anchored to organosilicas in artificial photosynthesis: Ordered vs. non-ordered materials".**

ABSTRACT

Cobaloxime-based hydrogen production catalysts are known for their easy synthesis and tuneable catalytic properties. Considering the benefits of their heterogenization on solid supports, different attempts have been led to immobilize them on surface solids of both conductive and isolating character for electro- and photochemical H_2 evolution, respectively. Periodic mesoporous organosilicas (PMOs) with well-ordered structures, high surface areas and pore volumes and easy surface functionality open a unique opportunity as potential scaffolds for mounting molecular cobaloxime catalysts. In the present study, two series of ordered and non-ordered organosilica materials containing ethylene bridges in the pore walls and pendant pyridine groups on the pore channels were compared as supports to axially coordinate a molecular cobaloxime catalyst, $Co(dmgH_2)(dmgH)Cl_2$. All solids were characterized by X-ray diffraction, N_2 adsorption-desorption isotherms, IR-TF, Raman, ^{13}C solid state NMR, EXAFS and ICP-MS. Photocatalytic hydrogen evolution activity of the cobaloxime-hybrid catalysts was evaluated using eosin Y as photosensitizer and TEOA as sacrificial electron donor under UV-vis light irradiation. The results showed that cobaloximes anchored on ordered organosilicas displayed the highest H_2 production yields (8 - 42.4 mmol H g^{-1}_{cat}) compared to their analogues supported on non-ordered organosilicas (1.40 - 14.6 mmol H_2 g^{-1}_{cat}). These findings evidence that ordered nanostructures stabilize the cobaloxime catalysts on their mesopore, improving the photocatalytic activity of the homogenous counterpart.

Keywords: cobaloxime; PMOs; organosilicas; hydrogen production.

5.1 INTRODUCTION

Nowadays, the generation and storage of energy are issues of vital importance to maintain our current way of life. Due to the precipitous population growth, the global energy demand shows an increasing trend, which it is expected that rises around 10 billion in 2050s [1]. Although fossil fuels are the dominating energy source to meet energy requirements for much of the world, they are exhaustible, and their use contributes to greater environmental pollution and global warming besides being sources of conflict and tools of geopolitical blackmail [2]. In this context, it is a priority for the scientific community to find renewable, clean and zero-carbon emissions alternatives to produce and store energy [3,4]. The use and development of clean energies, such as wind, hydroelectric or solar energy provides a good solution to the energy crisis [5], but they generate electricity, which is difficult to store and transport. For instance, the energy provided by the sun is the endless energy source available on our planet which is able to satisfy the global energy consumption by humans in an entire year, however the lack of an efficient storing procedure and its intermittent nature have not led to this total implementation as energy source [6]. Alternatively, in recent years, artificial photosynthesis-based technologies are positioned as an interesting approach for the conversion of the solar energy into chemical bonds - H_2 and O_2 -.

Currently, hydrogen is increasingly recognised as future fuel due to its properties [7]. This molecule only produces water as a by-product and the energy content per mass unit in hydrogen is three times higher than that of hydrocarbons which converts it to a clean and energy rich solar fuel [8].

Among the different approaches to produce H_2, water electrolysis has been a subject of wide study during last decades. On this process, electricity provides the energy needed for water splitting, which results in hydrogen and oxygen, thus

transforming electrical energy into chemical energy. For this purpose, Pt-based materials are positioned as the most effective electrocatalyst for hydrogen evolution reaction (HER). Unfortunately, Pt is a noble metal, scarce and expensive, thus limiting its commercial application [9,10].

As alternative, bioinspired molecular systems synthesized with earth abundant elements (Fe, Co or Ni) have recently shown a great potential for artificial photosynthesis, i.e. the conversion of sunlight into chemical fuels by water splitting [11–16]. Particularly, cobaloximes (cobalt complexes with diglyoxime ligands) have received a huge interest due to their easy synthesis, moderate photostability and high efficiency at low reduction potentials. Since the first example of a cobaloxime catalyst in light-driven hydrogen evolution reported in 1983 by Ziessel and co-workers [17], extensive advances have been achieved on this field in terms of activity and stability. A wide variety of cobaloxime-based molecular systems have been explored for electro- and photocatalytic hydrogen production [18,19]. While early attempts employed molecular cobaloxime catalysts in solution, most recent studies have focused on the assembly of such cobaloxime-based molecular systems on different solid surfaces to be used in heterogeneous systems. Electroactive surfaces of common semiconductors, such as carbon nanotubes or GaP [20–22], functionalized with pyridine groups have allowed the immobilization of cobaloxime catalysts, showing improved and prolonged electrocatalytic HER activity with respect to homogeneous systems. Not only conductive materials have been employed as supports of cobaloxime catalysts, recently this approach has been extended to non-conductive materials for light-driven hydrogen evolution. In 2018, Ott et al. [23] were the first who anchored a cobaloxime catalyst inside the pores of a chromium terephthalate metal-organic framework, MIL-101(Cr), for photocatalytic hydrogen production. More recently, Lotsch et al. [24] applied a similar strategy to obtain cobaloxime-covalent organic framework hybrids for HER. They showed that the confinement

of cobaloxime catalyst into the porous channels of the COF is responsible for the prolonged activity as well as the improved photocatalytic activity with respect to the homogeneous counterpart. Furthermore, the presence of larger pore channels would facilitate the accessibility of all components to the cobaloxime centers thereby increasing the hydrogen production. In this respect, the properties of the periodic mesoporous organosilicas, called PMOs, make them particularly attractive candidates for this purpose. This family of hybrid materials, synthesized from bridged-organosilanes of the type $(R'O)_3Si\text{-}R\text{-}Si(OR')_3$, are characterized to possess highly ordered mesostructures with a homogenous distribution of organic groups into the silica framework, and larger pore sizes [25]. Taking advantages of these unique properties, recently, we have successfully prepared a cobaloxime-PMO hybrid material through the coordination of a cobalt complex on a PMO containing a certain amount of pendant pyridine moieties. As previous studies, the cobaloxime-PMO assembly showed an improved photocatalytic performance compared to the homogenous counterpart, as well as resulted to be one of the most active heterogenized molecular cobaloxime catalysts reported in literature due to its ordered arrangement of mesoporous channels. Based on these findings, we decided to extent these investigations on the design of ordered and non-ordered PMO materials containing different loadings of surface pyridine groups as attachment points to assembly molecular cobaloxime catalysts and compare their activity for light-driven photocatalytic hydrogen production.

Herein, we first describe the synthesis and characterization of series of ordered and non-ordered organosilicas supports containing ethylene bridges and pendant pyridylethyl moieties on the pore channels at different ratios, and then employ these latter pyridine groups as ligands to axially coordinate a cobaloxime core. All cobaloxime-hybrid materials (ordered and non-ordered) were evaluated as catalysts for the photocatalytic hydrogen production under visible irradiation.

5.2 EXPERIMENTAL SECTION

5.2.1 Materials and reagents

All required reagents for the synthesis of the different PMO materials including octadecyltrimethylammonium bromide (OTAB), cetyltrimethylammonium bromide (CTAB), sodium hydroxide (99 %) and 1,2-bis(triethoxysilyl)ethane (96 %, BTEE, **precursor 1**) were acquired from Sigma-Aldrich. 2-(4-pyridylethyl)triethoxysilane) (95 %, **precursor 2**) and ammonia solution (25 wt% in water) were supplied by abcr and PanReac, respectively. Cobaloxime complex was synthesized using: dimethylglyoxime (99 %, Sigma-Aldrich), acetone (>99.5 %, Sigma- Aldrich), cobalt (II) chloride hexahydrate (Acros Organics), methanol (>99.9 % PanReac), pyridine (>99.9 %, Sigma-Aldrich), and chloroform (99.9 %, Sigma-Aldrich). All hydrogen production photocatalytic experiments were performed using acetonitrile (99.7 %, PanReac) and Milli-Q-water as solvents, eosin Y (>95 %, TCI) and triethanolamine (>99 %, Sigma-Aldrich) as photosensitizer and sacrificial electron donor, respectively. All chemicals were used as received without further purification.

5.2.2 Synthesis of materials

5.2.2.1. Synthesis of periodic mesoporous organosilicas (PMO)

In a general synthesis [26], a mixture of OTAB (0.85 g), aqueous NaOH solution (6 M, 0.89 mL) and milli-Q water (53 mL) was stirred at room temperature overnight. Then, a mixture of precursors (**1** and **2,** 2.04 mmol) with different molar composition was added dropwise with rapid stirring at room temperature. After 24 h, the white suspension was aged at 100 ºC for 4 days. The white precipitate was recovered by filtration and washed with distilled water and

ethanol. Later, the white solid was dried under vacuum at 100 ºC overnight. For the surfactant removal, the as-synthesized material (1 g) was stirred in acidic ethanol (1mL of 37 % HCl in 50 mL of EtOH) at 70 ºC for 12h. After repeating this extraction process twice, the final material was filtered out, washed with ethanol and dried at 100 ºC under vacuum. These PMO materials were named as *py$_x$PMO*, where x is the percentage of **precursor 2** (2-(4-pyridylethyl)triethoxysilane)) added in the reaction mixture (see Table 1).

5.2.2.2. Synthesis of organosilica materials (OS)

In a typical synthesis [27], CTAB (0.54 g) was dissolved in a solution containing 25 mL of distilled water and 1.78 mL of ammonia solution. Afterwards, the mixture of silane precursors (8.8 mmol in total) was added dropwise, and the solution was kept under stirring at room temperature overnight. Subsequently, it was aged at 90 ºC for 4 days under static conditions. The white precipitate was recovered by filtration and washed thoroughly with distilled water and ethanol. The surfactant was removed following a similar extraction process to that used to remove OTAC molecules. Finally, the white solid was dried under vacuum at 100 ºC overnight. These organosilica materials were named as *py$_x$OS*, where x is the percentage of **precursor 2** added in the reaction mixture (see Table 1).

Table 1. Nomenclature of the different materials synthesized by co-condensation reaction of 1,2-bis(triethoxysilyl)ethane (**precursor 1**) and 2-(4-pyridylethyl)triethoxysilane) (**precursor 2**) under basic conditions.

Material	Precursor 1 (%)	Precursor 2 (%)	Surfactant	Reaction medium
py_{10}PMO	90	10	OTAB	NaOH
py_{20}PMO	80	20	OTAB	NaOH
py_{30}PMO	70	30	OTAB	NaOH
py_{10}OS	90	10	CTAB	NH_3
py_{20}OS	80	20	CTAB	NH_3
py_{30}OS	70	30	CTAB	NH_3

5.2.2.3. Immobilization of the dichlorocobaloxime complex, $Co(dmgH_2)(dmgH)Cl_2$

Dichlorocobaloxime complex, $Co(dmgH_2)(dmgH)Cl_2$, was synthesized following the procedure previously reported by Costa et al. [28]. For the anchoring of the cobaloxime complex on the supports, $Co(dmgH_2)(dmgH)Cl_2$ complex (0.35 g) was added to a suspension of the hybrid material (0.5 g) in 10 mL of methanol. The mixture was kept under stirring at 65 ºC for 24 h. Subsequently, the solid was filtered and washed with methanol. To assure the complete removal of unreacted complex, the resulting solid was refluxed with 50 mL of CH_3OH for 12 h. This procedure was repeated twice. Finally, the material was recovered by filtration and dried under vacuum at 80 ºC. The series of obtained catalysts were named as *py_xPMO-Co* or *py_xOS-Co*, depending on the support employed.

5.2.3 Materials characterization

X-ray powder diffraction (XRD) patters were collected in a Bruker D8 Discover A25 diffractometer using Cu Kα radiation. N_2 adsorption-desorption isotherms were obtained at -196 ºC in an Autosorb-iQ MP/MP-XR instrument. Before the measurement, all samples were outgassed at 120 ºC overnight. The Brunauer-Emmett-Teller (BET) method was used for determining the surface area and the Density Functional Theory (DFT) method to obtain the pore size distribution. Raman spectra of the samples were acquired with a Renishaw Raman instrument with green laser light (532 nm). FT-IR measurements were carried out on a Bruker Alpha II spectrometer. High-resolution transmission electron microscopy images were recorded on a JEOL JEM 1400 microscope. Solid-state CP/MAS ^{13}C NMR spectra were obtained in a Bruker Avance III HD 400 WB spectrometer at 13 kHz. An overall 1500 free induction decays were accumulated for each measurement. The excitation pulse and recycle time for CP/MAS ^{13}C NMR were 3.6 ms and 2 s, respectively. Chemical shifts were referenced to tetramethylsilane (TMS) standard. Inductively coupled plasma mass spectrometry (ICP-MS) for ^{59}Co isotope was measured using a NexION 350X spectrometer. Before to the measurement, the sample was digested in an UltraWave microwave system.

Co K-edge x-ray absorption spectra were collected at the CLÆSS beamline [29] of the ALBA synchrotron. The synchrotron radiation was monochromatized by means of a double crystal Si(111) monochromator, with higher harmonics rejected by choosing the proper angles and coatings for the collimating and focusing mirrors. The absorption data were acquired in transmission mode. The powdered samples were mixed uniformly in a boron nitride matrix and pressed into pellets to ensure an absorption jump close to 1. Several scans were measured to ensure reproducibility and a good signal to noise

ratio. The data was treated with the Demeter [30] package and the energy was calibrated to the first inflection point of Co foil taken as 7709 eV.

5.2.4 Photocatalytic hydrogen evolution

The photocatalytic hydrogen production tests were carried out in a flash vial with constant stirring under visible light irradiation ($\lambda \geq 400$ nm). Typically, 1 mg of catalyst was dispersed in an acetonitrile - water mixture (1:1) adjusted a pH 7 with HCl (37 %), containing dissolved eosin Y (EY, 0.05 mM) and triethanolamine (TEOA, 10 %). The reaction mixture was degassed by N_2 bubbling for 30 min. Subsequently, it was irradiated with a 300W Xenon lamp equipped with a Newport filter, FSQGC400, at 10 cm distance. Aliquots of 50 µL were taken periodically to monitor the hydrogen evolution and analyzed on a Shimadzu GC-2010 Plus equipped with a barrier discharge ionization detector (BID) and a ShinCarbon ST column (2 m × 2 mm i.d.).

5.2.4.1 Catalyst re-activation after photocatalytic reaction

After evaluation of the photocatalytic activity of all catalysts, the most active catalyst (py_{30}PMO-Co) was selected to carry out the recyclability tests. After reaction, the solid was recovered by centrifugation and then washed with methanol and acetonitrile in order to remove eosin Y and TEOA remaining into the pores. The re-activation process was similar to that used for the immobilization of the cobaloxime complex. Later, the resulting solid was washed with methanol to remove the excess of non-complexed cobaloxime. Finally, this material was dried under vacuum at 80 ºC overnight.

5.3 RESULTS AND DISCUSSION

5.3.1 Characterization of the PMOs and organosilica materials

5.3.1.1. Structural and textural properties

Powder X-ray diffraction (PXRD) patterns of py_xPMO and py_xOS materials are shown in **Fig S1**. All py_xPMO materials displayed an intense diffraction peak around $2\theta \approx 1.8^{o}$ accompanied by two weak peaks at higher incidence angles. These peaks correspond to (100), (110) and (200) reflections, typical of materials with 2D hexagonal (*p6mm*) mesostructures [26]. For this series of materials, an increase in the content of the monosilane precursor, from 10 to 30 %, in the synthesis gel gave rise to a decrease in the mesostructure ordering [31–33]. However, the absence of these peaks for those materials synthesized with CTAB (py_xOS) confirmed non-ordered structures, thus revealing the decisive role of the synthesis conditions to obtain highly ordered mesostructures [34]. After anchoring of the cobaloxime complex, ($Co(dmgH)(dmgH_2)Cl_2$), on the pendant pyridine groups of py_xPMO and py_xOS materials, PXRD patterns remained unchanged compared to the parent materials (**Fig 1**). These findings were further confirmed by transmission electron microscopy (TEM). TEM images of the py_xPMO-Co catalysts (**Fig 2** (a,b,c)) revealed highly ordered structures with parallel channel pores of uniform diameter, while py_xOS-Co catalysts (**Fig 2** (d,e,f)) consisted of agglomerated nanoparticles with some observable pores in the meso range.

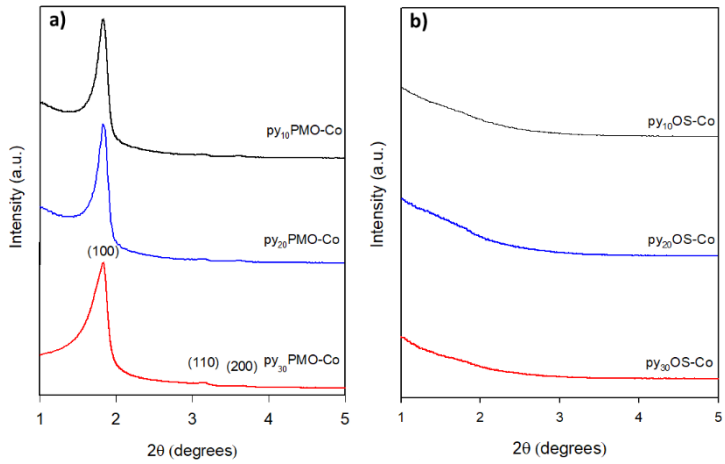

Fig 1. XRD patterns of py_xPMO-Co (**a**) and py_xOS-Co (**b**) catalysts.

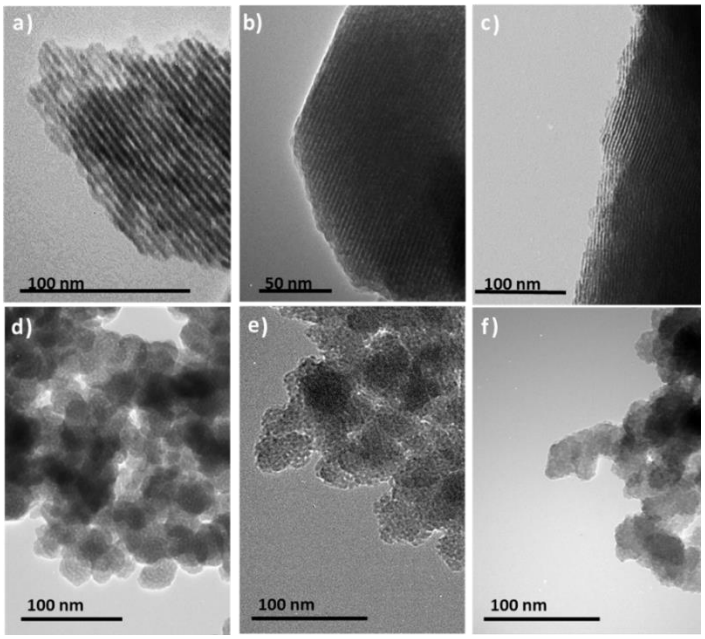

Fig 2. TEM images of py_{10}PMO-Co (a), py_{20}PMO-Co (b), py_{30}PMO-Co (c), py_{10}OS-Co (d), py_{20}OS-Co (e) and py_{30}OS-Co (f).

Nitrogen adsorption-desorption isotherms as well as DFT pore size distributions of all synthesized materials are displayed in **Fig S2.** As it can be observed, py_xPMO materials exhibited type-IV isotherms according to IUPAC classification with the step at relative pressures of 0.4, characteristic of ordered mesoporous structures [35]. All these materials exhibited a non-distinctive hysteresis loop, typical of materials with small mesopores. The narrow pore size distribution and the average pore diameter confirmed the presence of uniform pores in the mesopore range (4.0 – 4.5 nm) for all materials synthesized with OTAB as surfactant. Conversely, those organosilica supports synthesized with CTAB as template in ammonia solution, presented a type-II isotherm with high N_2 uptake at higher relative pressures, stating macroporosity in the structures. As observed from DTF pore size distributions, this spanned the entire range, from micro to macropores. According to the textural properties listed in Table S1, PMO materials showed S_{BET} values ranged from 683 – 852 $m^2\ g^{-1}$ and pore volumes from 0.57 – 0.84 $cm^3\ g^{-1}$. However, lower surface areas (< 260 $m^2\ g^{-1}$) were obtained for all non-ordered organosilica materials. On the basis of obtained results, a decrease on the surface area and pore volume when the loading of 2-(4-pyridylethyl)triethoxysilane) (**precursor 2**) increased from 10 % to 30 % in the gel synthesis was appreciated on py_xOS materials. Nevertheless, this tendency was not appreciated from 20 % to 30 % for py_xPMO materials, where surface area and pore size values were higher. After immobilization of the cobaloxime complex on the pore surface of the supports, non-differences were appreciated in the isotherm-type (**Fig 3**), but nevertheless, a slight decrease of the surface area and the pore volume was observed compared to the parent materials [36]. Additionally, a slight increase of the wall-thickness was indicative of the decoration of the pores with cobaloxime units (**Table 2**).

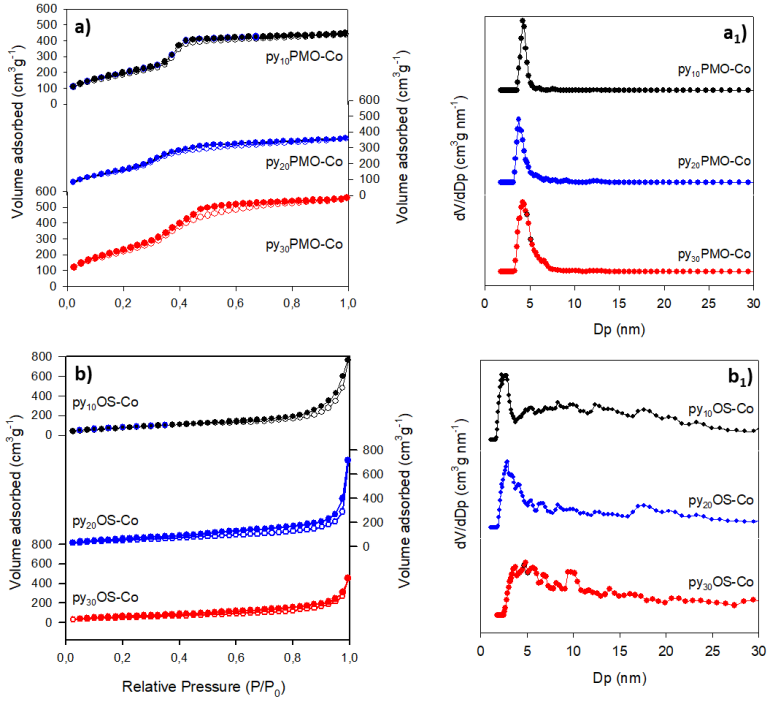

Fig 3. Nitrogen adsorption-desorption isotherms (left) and DFT pore size distributions (right) for py_xPMO-Co (a, a_1) and py_xOS-Co (b, b_1) catalysts.

Table 2. Textural properties of py_xPMO-Co and py_xPMO-Co catalysts.

MATERIAL	S_{BET} (m^2/g)	V_p[a] (cm^3/g)	D_p[a] (nm)	a_0[b] (nm)	Wall thickness[c] (nm)	Co-loading[d] (mmol/g)	Co/N ratio
py_{10}PMO-Co	715	0.65	4.3	5.8	1.5	0.06	0.55
py_{20}PMO-Co	651	0.53	3.8	5.6	1.8	0.16	0.40
py_{30}PMO-Co	901	0.82	4.3	5.5	1.3	0.17	0.25
py_{10}OS-Co	323	0.94	n.d.	n.d.	n.d.	0.02	0.03
py_{20}OS-Co	198	0.75	n.d.	n.d.	n.d.	0.10	0.07
py_{30}OS-Co	198	0.55	n.d.	n.d.	n.d.	0.13	0.09

[a] Calculated from DFT analysis

[b] Unit cell parameter calculated from formula, $a_0=2d_{100}/\sqrt{3}$

[c] Calculated from the difference between a_0 and D_p

[d] Determined by ICP-MS

Raman spectra of the supports, py_xPMO and py_xOS, are shown in **Fig S3.** All samples showed the characteristics vibration bands of both organosilane precursors, thus corroborating their successful incorporation on the silica framework. Vibration modes at 3080 (C=H stretching), 1600 (C=N stretching) and 1500-1400 cm^{-1} (C=C stretching) characteristics of pyridine groups were present on all supports. The stretching bands at 2840 and 2890 cm^{-1} are attributed to asymmetric and symmetric C-H stretching in the organosilane precursors. Furthermore, the typical Si-O-Si stretching vibration band at 1025 cm^{-1} present in all samples is attributed to the condensed Si-O-Si network. Raman spectra of the catalysts, given in **Fig 4**, showed a similar pattern to the supports. The presence of a N-O stretching band at 1220 cm^{-1} and a slight increase in the intensity of the C=N band, associated to the dimethylglioximato ligands belongs to the cobaloxime complex, confirmed the coordination of cobalt complex on pyridine groups located on the surface of the materials [37].

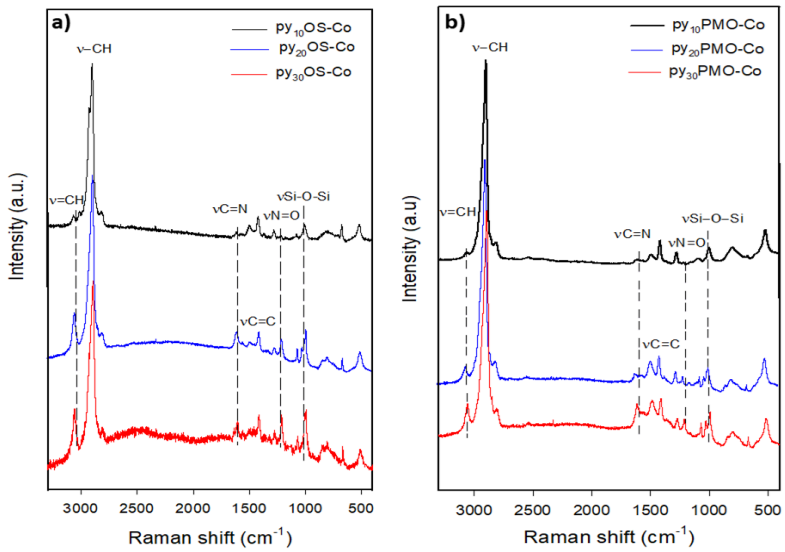

Fig 4. Raman spectra of py_xPMO-Co (**a**) and py_xOS-Co (**b**) catalysts.

FT-IR measurements confirmed the results obtained by Raman spectroscopy. Besides those stretching modes previously identified for the catalysts, the presence of the cobaloxime complex was evidenced by weak stretching vibration peaks of N-O and Co-$N_{(DH)}$ at 1230 and 513 cm^{-1}, respectively, characteristics of these metal complex (**Fig 5** and **Fig S4**) [38,39]. However, these characteristic peaks of the complex are non-existent on the py_xPMO and py_xOS supports (**Fig S5**).

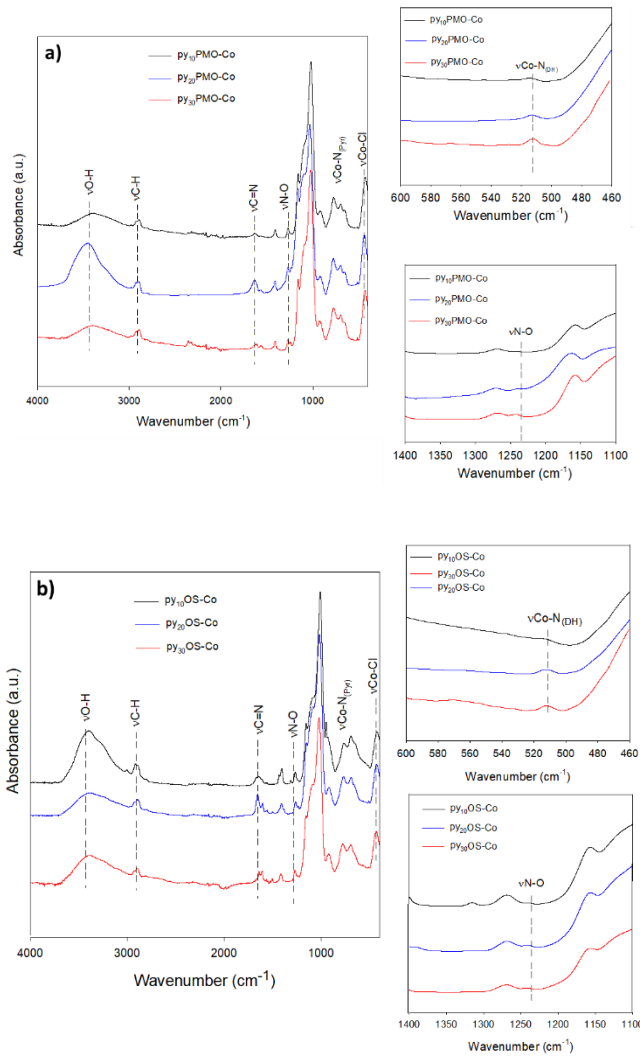

Fig 5. FT-IR spectra of py_xPMO-Co (**a**) and py_xOS-Co (**b**) catalysts.

The anchoring of the cobaloxime complex on PMO and OS materials was further confirmed by ^{13}C RMN measurements (**Fig 6**). CP/MAS RMN spectra of both supports, py_{30}PMO and py_{30}OS, showed an intense signal at ca. 5 ppm attributed to ethylene bridges in the precursor 1 [40]. In addition, signals at 19, 30, 128 and 142 ppm confirmed the presence of pyridylethyl groups at the pore channels. It is important to note that the presence of weak signals at 18 and 58 ppm on PMO supports is indicative of non-hydrolysed ethoxy groups during the co-condensation process. Unlike these signals were absent on organosilica materials where the use of NH_3 as gelling agent leads to a complete hydrolysis of the ethoxy groups. After coordination of the cobalt complex on the pyridine moieties, py_{30}PMO-Co and py_{30}OS-Co catalysts showed new signals at 150 and 13 ppm associated to the glyoximate ligands. The presence of a signal at 49 ppm on py_{30}PMO-Co was attributed to residual CH_3OH used as solvent during the immobilization process and washed.

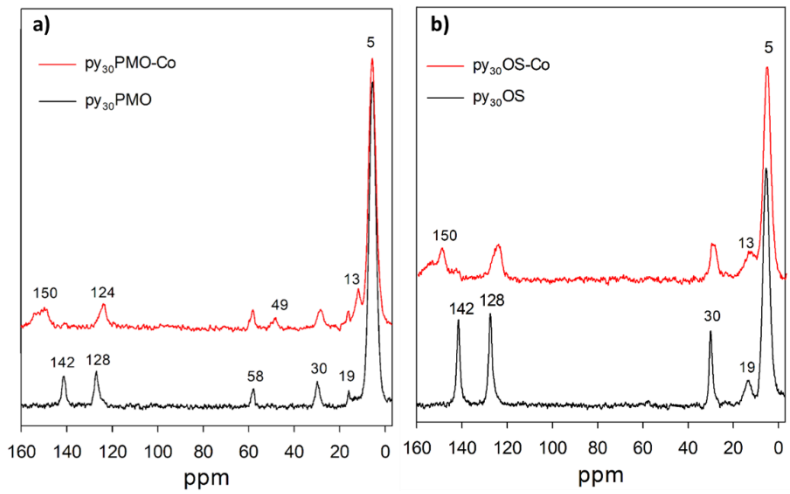

Fig 6. ^{13}C CP/MAS NMR spectra of PMO (a) and OS (b) materials: py_{30}PMO and py_{30}OS (black lines) and py_{30}PMO-Co and py_{30}OS-Co (red lines).

The local coordination and electronic environment of the Co centres in py_xPMO-Co and py_xOS-Co catalysts were explored using Co K-edge x-ray absorption spectroscopy (XAS). The x-ray absorption near edge structure (XANES) and the Fourier transform (FT) of the k^2 weighted extended x-ray absorption fine structure (EXAFS) regions are reported in **Fig 7** left and right panel, respectively. All the samples' XANES spectra approached that of the $Co(dmgH)_2pyCl$ reference, suggesting a similar average Co local structure. The XANES rising edge energy position, characterizing the effective Co oxidation state, has been identified at half height of the rising edge and is reported in the inset of the left panel. In the case of py_xPMO-Co, the XANES showed a rising edge profile shifted toward lower energy with respect to the $Co(dmgH)_2pyCl$ reference compound, which is consistent with a more reduced Co environment (**Figure 7**-left). This result corroborates the conclusions from FT-IR, which indicated a more electron donating environment within py_xPMO. The py_xOS-Co series showed stronger shifts of the rising edge towards lower energy relative to py_xPMO-Co. In particular, in the case of py_{30}OS-Co the rising edge approaches what might be expected from a +2 Co center [41]. In both cases the rising edge shifted toward lower values with increasing pyridine amount and catalyst loading.

The FTs of the EXAFS signals support the XANES results indicating that the overall Co coordination environment was maintained in all the samples. Indeed, all the FTs presented two main features in the R-space at 1.5 Å and 1.9 Å attributable to the first and second shell coordination of N and Cl atoms, respectively. Above 2 Å the signals corresponded to the extended ligand structure, similar for all samples and as well as to the $Co(dmgH)_2pyCl$ and $Co(dmgH)_2Cl_2$ references.

Interestingly, the relative intensity of the FT signals at 1.9 Å showed significant variations between samples. In particular, its intensity increase is

indicative of a higher amount of Co-Cl bonds. A comparison between ordered and disordered catalysts with similar pyridine amounts revealed the presence of unreacted $Co(dmgH)_2Cl_2$ in py_{10}OS-Co and particularly py_{30}OS-Co. This corresponds as well to an increased effective Co reduction (inset in **Figure 7**, left panel), in agreement with the Co reduction shown from $Co(dmgH)_2$pyCl to $Co(dmgH)_2Cl_2$.This strongly suggests that tethering of the cobaloxime to the pyOS materials was not as efficient as to pyPMO catalysts. Finally, from the XAS data, it appears that the Co local electronic and structural properties of py_{20}PMO-Co and py_{20}OS-Co can be directly compared. In the disordered system only the FT feature at 1.5 Å decreased in intensity with respect to the ordered counterpart, probably due to a decreased coordination number. Indeed, this is compatible with the concomitant detected Co reduction.

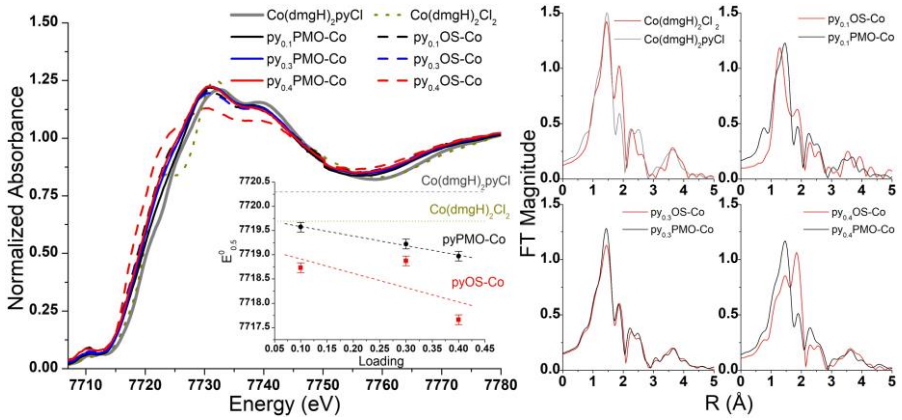

Fig 7. (left) Co K-edge XANES spectra for the py_xOS-Co and py_xPMO-Co series along with $Co(dmgH)_2$pyCl and $Co(dmgH)_2Cl_2$ references. Inset: rising edge energy at half height as a function of pyridine loading compared with the values obtained for the two references. The dotted lines are guide for the eyes; (right) Fourier transforms of the k^2 weighted EXAFS oscillations in the 3-14 $Å^{-1}$ k-range obtained with a Hanning window.

The nitrogen content of the different supports was determined by elemental analysis. Values obtained were ranged between 0.1 – 0.7 mmol g^{-1} and

0.7 – 1.5 mmol g^{-1} for py_xPMO and py_xOS-Co materials, respectively (**Table S1**). In the latter case, the presence of adsorbed ammonia, used as gelling agent, cannot be ruled out, which would explain the huge differences in N content among both series of materials. In addition, the amount of cobaloxime complex attached to the different materials was determined by ICP/MS (**Table 3**). For py_xOS-Co catalysts, the loading of Co was lower than obtained by py_xPMO catalysts even though the former exhibited a larger N content. This could be ascribed to the difficulty of coordinating cobaloxime catalyst on the pyridine groups anchored on the disordered structure of such supports. For py_xPMO catalysts, the cobalt/nitrogen ratios were 0.55, 0.40 and 0.25 py_{10}PMO, py_{20}PMO and py_{30}PMO, respectively. This means that approximately half of the pyridine groups are non-coordinated to the cobalt center.

5.3.2 Photocatalytic results

Photocatalytic hydrogen production of all catalysts was carried out under UV-filtered simulated solar light irradiation (Xe lamp, $\lambda > 400$ nm) with EY and TEOA as photosensitizer and sacrificial electron donor, respectively. Control experiments without one of the components of the system - visible light irradiation, electron donor, photosensitizer, or catalyst - showed negligible hydrogen production, therefore confirming the role of all components on the photocatalytic system.

The photocatalytic performances of all catalysts with ordered (py_xPMO-Co) and non-ordered (py_xOS-Co) structures and different loadings are shown in **Fig 8**. Although all the catalysts produced significant H_2 under visible light in an aqueous/organic solvent mixture, the series of py_xPMO-Co materials displayed the highest H_2 production yields under analogous conditions.

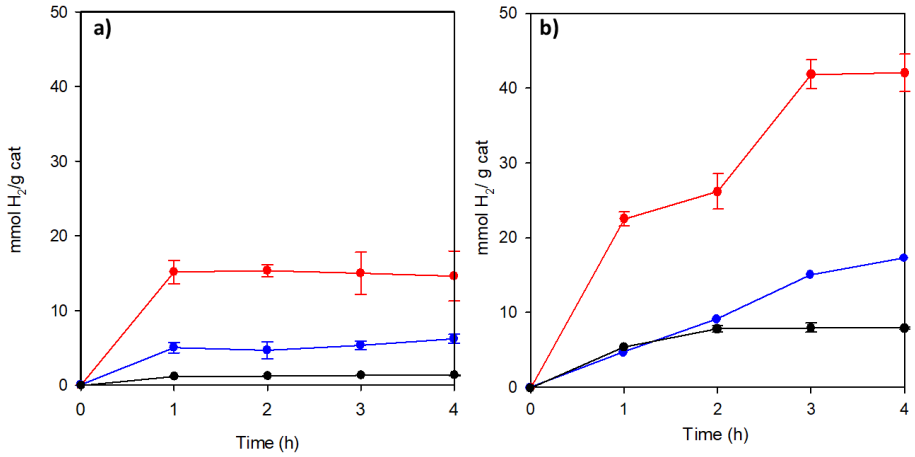

Fig 8. Photocatalytic hydrogen production with py_xOS-Co catalysts (**a**) (py_{10}OS-Co (black), py_{20}OS-Co (blue) and py_{30}OS-Co (red)) and py_xPMO-Co catalysts (**b**) (py_{10}PMO-CO (black), py_{20}PMO-Co (blue) and py_{30}PMO-Co (red) catalyst)

On the one hand, among series of non-ordered catalysts, py_{30}OS-Co with the highest cobalt loading reached at a maximal value of 14.6 mmol H_2, which corresponds to a TON of 111. For this series, the rate of hydrogen production remained linear for a shorter time (1 h), before totally ceasing the catalytic activity. These results are in concordance with the lack of structural ordering in these supports where cobaloxime units might be retain only in the pore mouth on the surface, suffering a quick deactivativation. This type of complexes is well-known to disintegrate due to the labile axial pyridine ligand decoordinates during the photocatalytic process [42].

Conversely, the series of ordered catalysts with well-ordered structures, high surface areas and regular pore sizes showed quite different performances for hydrogen production. It increases exponentially with the amount of cobalt present in the catalyst, from 8 to 18.1 mmol of hydrogen for py_{10}PMO-Co and py_{20}PMO-Co, respectively. In contrast, py_{30}PMO-Co, showing a similar cobalt content than py_{20}PMO-Co (see Table 2) evolved 42.40 mmol H_2 within 4h, which

corresponds to a TON of 244. This huge difference could be ascribed to the low Co/N ratio of this latter. Compared to py_{20}PMO-Co, it showed an 8.6% increase in Co content but a 75 % increase in N content, which resulted in a Co/N ratio of 0.25. These results support the hypothesis that previous findings on MOFs about the recoordination of the cobaloxime units to pyridine sites during the photocatalytic process. Those detached cobaloxime species to the solution would remain close to the uncoordinated pyridine ligands present on the pores of the PMOs, therefore favouring the quick restoration of the Co-pyridine bond. That means that those detached cobaloxime units from the support with higher N content will have much more chances to be recoordinated to pyridine sites, giving risen to higher photocatalytic activity [42–44].

This phenomenon would also explain the different hydrogen evolution among series of catalyst. While py_x-OS-Co catalysts totally ceased their activity after 1 h (vide supra), the hydrogen evolution for py_x-PMO-Co catalysts levelled off at longer irradiation times, around 3 - 4 h.

As shown in a previous work [45], the hydrogen production is not catalysed by soluble cobaloxime species that could be present in the reaction medium but by cobaloxime complexed to pyridine sites of the PMO. In order to reuse the catalysts, a reactivation process should be performed on the support, which includes the reattachment of cobaloxime complexes (see Experimental section). The resulting catalyst exhibited a TON of 222 after 4 h irradiation, which is comparable to that obtained by the original catalyst (TON= 244) (**Fig. S6**). These results evidenced the high stability of the support and the facile reconstitution of the catalytic center.

Furthermore, compared to similar hybrid catalysts for hydrogen evolution reaction in literature, such as a cobaloxime complex immobilized in a MOF [23] (TON of 20), in a COF [24] (TON of 20) or in a polymer [46] (TON of 170), the

catalyst py_{30}PMO-Co showed the best hydrogen performance. The highly ordered structure and regular pore size have an important role in the diffusion of the reactants and improve the stability of the cobaloxime in the reaction increasing in such a way hydrogen production.

5.4 CONCLUSIONS

In summary, co-condensation reactions of 1,2-bis(triethoxysilyl)ethane and 2-(4-pyridylethyl)triethoxysilane at different ratios, in the presence of OTAB or CTAB as surfactant, under basic conditions with NaOH or ammonia as gelling agent, proved to lead successfully to the formation of series of periodic mesoporous organosilicas or non-ordered organosilicas. These organic-inorganic hybrid materials with pendant pyridine moieties on their structure provide anchoring points to axially coordinate a molecular cobaloxime catalyst. All cobaloxime-hybrid materials (ordered and non-ordered) were evaluated as catalysts for the photocatalytic hydrogen production in presence of eosin Y and TEOA as photosensitizer and sacrificial electron donor, respectively. Under similar photocatalytic conditions, those cobaloxime-PMO systems showed the highest hydrogen production compared to those cobaloxime catalysts immobilized on non-ordered organosilicas. Our results evidence that ordered mesostructures lead to effective confinement of the molecular catalyst into pores of the support, resulting in higher longevity and activity for hydrogen evolution reaction.

5.5 REFERENCES

[1] C. Tarhan, M.A. Çil, A study on hydrogen, the clean energy of the future: Hydrogen storage methods, J. Energy Storage. 40 (2021) 102676. https://doi.org/10.1016/j.est.2021.102676.

[2] F. Martins, C. Felgueiras, M. Smitková, Fossil fuel energy consumption in European countries, Energy Procedia. 153 (2018) 107–111. https://doi.org/10.1016/j.egypro.2018.10.050.

[3] J. Zhang, W. Hu, S. Cao, L. Piao, Recent progress for hydrogen production by photocatalytic natural or simulated seawater splitting, Nano Res. 13 (2020) 2313–2322. https://doi.org/10.1007/s12274-020-2880-z.

[4] Y. Kojima, Hydrogen storage materials for hydrogen and energy carriers, Int. J. Hydrogen Energy. 44 (2019) 18179–18192. https://doi.org/10.1016/j.ijhydene.2019.05.119.

[5] D. Kim, K.K. Sakimoto, D. Hong, P. Yang, Artificial photosynthesis for sustainable fuel and chemical production, Angew. Chemie - Int. Ed. 54 (2015) 3259–3266. https://doi.org/10.1002/anie.201409116.

[6] S. Berardi, S. Drouet, L. Francàs, C. Gimbert-Suriñach, M. Guttentag, C. Richmond, T. Stoll, A. Llobet, Molecular artificial photosynthesis, Chem. Soc. Rev. 43 (2014) 7501–7519. https://doi.org/10.1039/c3cs60405e.

[7] S. Fang, Y.H. Hu, Recent progress in photocatalysts for overall water splitting, Int. J. Energy Res. 43 (2019) 1082–1098. https://doi.org/10.1002/er.4259.

[8] M. Wang, G. Wang, Z. Sun, Y. Zhang, D. Xu, Review of renewable energy-based hydrogen production processes for sustainable energy innovation, Glob. Energy Interconnect. 2 (2020) 436–443. https://doi.org/10.1016/j.gloei.2019.11.019.

[9] P.D. Cavaliere, A. Perrone, A. Silvello, Water Electrolysis for the Production of Hydrogen to Be Employed in the Ironmaking and Steelmaking Industry, Adv. Ironmak. Steelmak. Process. 11 (2021) 1816. https://doi.org/10.3390/met11111816.

[10] C. Xing, L. Yonghe, Z. Lirong, Y. Yong, C. Ge, S. Sun, Z. Jiujun, Highly active, stable oxidized platinum clusters as electrocatalysts for the hydrogen evolution reaction, Energy Environ. Sci. 10 (2017) 2450–2458. https://doi.org/10.1039/C7EE02537H.

[11] M. Wang, K. Han, S. Zhang, L. Sun, Integration of organometallic complexes with semiconductors and other nanomaterials for photocatalytic H_2 production, Coord. Chem. Rev. 287 (2015) 1–14. https://doi.org/10.1016/j.ccr.2014.12.005.

[12] A. Mazzeo, S. Santalla, C. Gaviglio, F. Doctorovich, J. Pellegrino, Recent progress in homogeneous light-driven hydrogen evolution using first-row transition metal catalysts, Inorganica Chim. Acta. 517 (2020) 119950. https://doi.org/10.1016/j.ica.2020.119950.

[13] J. Amaro-Gahete, D. Esquivel, M. V. Pavliuk, C. Jiménez-Sanchidrián, H. Tian, S. Ott, F.J. Romero-Salguero, Hydroxyl-Decorated Diiron Complex as a [FeFe]-Hydrogenase Active Site Model Complex: Light-Driven Photocatalytic Activity and Heterogenization on Ethylene-Bridged Periodic Mesoporous Organosilica, Catalysts. 12 (2022) 254. https://doi.org/10.3390/catal12030254.

[14] G.B. Bodedla, W.-Y. Wong, X. Zhu, Coupling of a new porphyrin photosensitizer and cobaloxime cocatalyst for highly efficient photocatalytic H_2 evolution, J. Mater. Chem. A. 9 (2021) 20645–20652. https://doi.org/10.1039/d1ta04517b.

[15] F. Lucarini, J. Fize, A. Morozan, M. Marazzi, M. Natali, M. Pastore, V. Artero, A. Ruggi, Insights into the mechanism of photosynthetic H_2 evolution catalyzed by a heptacoordinate cobalt complex, Sustain. Energy Fuels. 4 (2020) 589–599. https://doi.org/10.1039/c9se00434c.

[16] J. Amaro-Gahete, M. V. Pavliuk, H. Tian, D. Esquivel, F.J. Romero-Salguero, S. Ott, Catalytic systems mimicking the [FeFe]-hydrogenase active site for visible-light-driven hydrogen production, Coord. Chem. Rev. 448 (2021) 214172. https://doi.org/10.1016/j.ccr.2021.214172.

[17] J. Hawecker, J.-M. Lehn, R. Ziessel, Efficient photochemical reduction of CO_2 to CO by visible light irradiation of systems containing $Re(bipy)(CO)_3X$ or $Ru(bipy)_3^{2+}$-Co^{2+} combinations as homogeneous catalysts, J. Chem. Soc., Chem. Commun. (1983) 536–538. https://doi.org/10.1039/C39830000536.

[18] D. Dolui, S. Khandelwal, P. Majumder, A. Dutta, The odyssey of cobaloximes for catalytic H_2 production and their recent revival with enzyme-inspired design, Chem. Commun. 56 (2020) 8166–8181. https://doi.org/10.1039/d0cc03103h.

[19] S. Sowmya, V. Vijaikanth, Electrochemistry and Electrocatalytic Activity of Cobaloxime Complexes, ChemistrySelect. 7 (2022). https://doi.org/10.1002/slct.202104044.

[20] S. Donck, J. Fize, E. Gravel, E. Doris, V. Artero, Supramolecular assembly of cobaloxime on nanoring-coated carbon nanotubes: Addressing the stability of the pyridine-cobalt linkage under hydrogen evolution turnover conditions, Chem. Commun. 52 (2016) 11783–11786. https://doi.org/10.1039/c6cc06059e.

[21] B. Reuillard, J. Warnan, J.J. Leung, D.W. Wakerley, E. Reisner, A Poly(cobaloxime)/Carbon Nanotube Electrode: Freestanding Buckypaper with Polymer-Enhanced H_2-Evolution Performance, Angew. Chemie - Int. Ed. 55 (2016) 3952–3957. https://doi.org/10.1002/anie.201511378.

[22] A. Krawicz, D. Cedeno, G.F. Moore, Energetics and efficiency analysis of a cobaloxime-modified semiconductor under simulated air mass 1.5 illumination, Phys. Chem. Chem. Phys. 16 (2014) 15818–15824. https://doi.org/10.1039/C4CP00495G.

[23] S. Roy, A. Bhunia, N. Schuth, M. Haumann, S. Ott, Light-driven hydrogen evolution catalyzed by a cobaloxime catalyst incorporated in a MIL-101(Cr) metal-organic framework, Sustain. Energy Fuels. 2 (2018) 1148–1152. https://doi.org/10.1039/c8se00072g.

[24] K. Gottschling, G. Savasci, H. Vignolo-González, S. Schmidt, P. Mauker, T. Banerjee, P. Rovó, C. Ochsenfeld, B. V. Lotsch, Rational Design of Covalent Cobaloxime-Covalent Organic Framework Hybrids for Enhanced Photocatalytic Hydrogen Evolution, J. Am. Chem. Soc. 142 (2020) 12146–12156. https://doi.org/10.1021/jacs.0c02155.

[25] P. Van Der Voort, D. Esquivel, E. De Canck, F. Goethals, I. Van Driessche, F.J. Romero-Salguero, Periodic Mesoporous Organosilicas: from simple to complex bridges; a comprehensive overview of functions, morphologies and applications, Chem. Soc. Rev. 42 (2013) 3913–3955. https://doi.org/10.1039/C2CS35222B.

[26] M. Waki, N. Mizoshita, T. Tani, S. Inagaki, Periodic mesoporous organosilica derivatives bearing a high density of metal complexes on pore surfaces, Angew. Chemie - Int. Ed. 50 (2011) 11667–11671. https://doi.org/10.1002/anie.201104063.

[27] A.M. Kaczmarek, S. Abednatanzi, D. Esquivel, C. Krishnaraj, H.S. Jena, G. Wang, K. Leus, R. Van Deun, F.J. Romero-Salguero, P. Van Der Voort, Amine-containing (nano-) Periodic Mesoporous Organosilica and its application in catalysis, sorption and luminescence, Microporous Mesoporous Mater. 291 (2020) 109687. https://doi.org/10.1016/j.micromeso.2019.109687.

[28] A. Bigotto, G. Costa, G. Mestroni, G. Pellizer, A. Puxeddu, E. Reisenhofer, L. Stefani, G. Tauzher, Extension of the approach to the study of coordination chemistry of vit. B_{12} group compounds, Inorganica Chim. Acta Rev. 4 (1970) 41–49. https://doi.org/10.1016/0073-8085(70)80011-0.

[29] L. Simonelli, C. Marini, W. Olszewski, M. Ávila Pérez, N. Ramanan, G. Guilera, V. Cuartero, K. Klementiev, CLAESS: The hard X-ray absorption beamline of the ALBA CELLS synchrotron, Cogent Phys. 3 (2016). https://doi.org/10.1080/23311940.2016.1231987.

[30] B. Ravel, M. Newville, ATHENA , ARTEMIS , HEPHAESTUS : data analysis for X-ray absorption spectroscopy using IFEFFIT, J. Synchrotron Radiat. 12 (2005) 537–541. https://doi.org/10.1107/S0909049505012719.

[31] Y. Du, K. Mao, P. Kamakoti, B. Wooler, S. Cundy, Q. Li, P. Ravikovitch, D. Calabro, The effects of pyridine on the structure of B-COFs and the underlying mechanism, J. Mater. Chem. A. 1 (2013) 13171–13178. https://doi.org/10.1039/c3ta12515g.

[32] N. Yuan, Y. Liang, E.S. Erichsen, R. Anwander, Lanthanide complex-incorporated periodic mesoporous organosilica nanospheres with tunable photoluminescence, RSC Adv. 5 (2015) 83368–83376. https://doi.org/10.1039/c5ra14694a.

[33] M. Barczak, Synthesis and structure of pyridine-functionalized mesoporous SBA-15 organosilicas and their application for sorption of diclofenac, J. Solid State Chem. 258 (2018) 232–242. https://doi.org/10.1016/j.jssc.2017.10.006.

[34] M. Waki, Y. Maegawa, N. Mizoshita, T. Tani, S. Inagaki, Pyridyl Ligand-bridged Mesoporous Organosilicas for Metal Complex Formation on the Pore Surfaces, 47 (2016) 57–66.

[35] Y. Awoke, Y. Chebude, I. Díaz, Controlling Particle Morphology and Pore Size in the Synthesis of Ordered Mesoporous Materials, Molecules. 25 (2020) 1–12. https://doi.org/10.3390/molecules25214909.

[36] J. Wan, K. Qian, J. Zhang, F. Liu, Y. Wang, P. Yang, B. Liu, C. Yu, Functionalized Periodic Mesoporous Organosilicas for Enhanced and Selective Peptide Enrichment, Langmuir. 26 (2010) 7444–7450. https://doi.org/10.1021/la9041698.

[37] S. Nie, P.A. Marzilli, L.G. Marzilli, N.T. Yu, Near-infrared Fourier transform Raman spectroscopy of photolabile organocobalt B_{12} and model compounds. 3. Vibrational assessment of factors affecting the cobalt-carbon bond in models, J. Am. Chem. Soc. 112 (1990) 6084–6091. https://doi.org/10.1021/ja00172a026.

[38] K. Kanamori, T. Morikawa, K. Kawai, Raman Spectra of Cobalt (III) Complexes. II. Nitroammine Series of Cobalt (III) Complexes, Bull. Chem. Soc. Jpn. 53 (1980) 2787–2791. https://doi.org/10.1246/bcsj.53.2787.

[39] N. Yamazaki, Y. Hohokabe, Studies on Cobaloxime Compounds. Synthesis of various cobaloximes and investigation on their infrared and Far-Infrared Spectra., Bull. Chem. Soc. Japan. 44 (1871) 63–69. https://doi.org/10.1246/bcsj.44.63.

[40] J.R. Deka, H. Kao, S. Huang, W. Chang, Ethane-Bridged Periodic Mesoporous Organosilicas Functionalized with High Loadings of Carboxylic Acid Groups : Synthesis, Bifunctionalization, and Fabrication of Metal Nanoparticles, Chem. - A Eur. J. 20 (2014) 894–903. https://doi.org/10.1002/chem.201303167.

[41] O. Planas, C.J. Whiteoak, V. Martin-diaconescu, J.M. Luis, T. Parella, A. Company, X. Ribas, O. Planas, C.J. Whiteoak, V. Martin-diaconescu, I. Gamba, J.M. Luis, T. Parella, A. Company, X. Ribas, Isolation of Key Organometallic Aryl-Co (III) Intermediates Insights into Alkyne Annulation Reaction Mechanisms Isolation of Key Organometallic Aryl-Co (III) Intermediates in Co-Catalyzed C(sp^2)-H Functionalizations and New Insights into Alkyne, J. Am. Chem. Soc. 138 (2016) 14388–14397. https://doi.org/10.1021/jacs.6b08593.

[42] A. Panagiotopoulos, K. Ladomenou, D. Sun, V. Artero, A.G. Coutsolelos, Photochemical hydrogen production and cobaloximes: The influence of the cobalt axial N-ligand on the system stability, Dalt. Trans. 45 (2016) 6732–6738. https://doi.org/10.1039/c5dt04502a.

[43] M.Á. Navarro, D. Cosano, A. Bhunia, L. Simonelli, V. Martin-Diaconescu, F.J. Romero-Salguero, D. Esquivel, Cobaloxime tethered pyridine-functionalized ethylene-bridged periodic mesoporous organosilica as an efficient HER catalyst, Sustain. Energy Fuels. 6 (2022) 398–407. https://doi.org/10.1039/D1SE01437D.

[44] R.R. Haikal, X. Wang, Y.S. Hassan, M.R. Parida, B. Murali, O.F. Mohammed, P.J. Pellechia, M. Fontecave, M.H. Alkordi, Porous-Hybrid Polymers as Platforms for Heterogeneous Photochemical Catalysis, ACS Appl. Mater. Interfaces. 8 (2016) 19994–20002. https://doi.org/10.1021/acsami.6b05031.

Supplementary Information

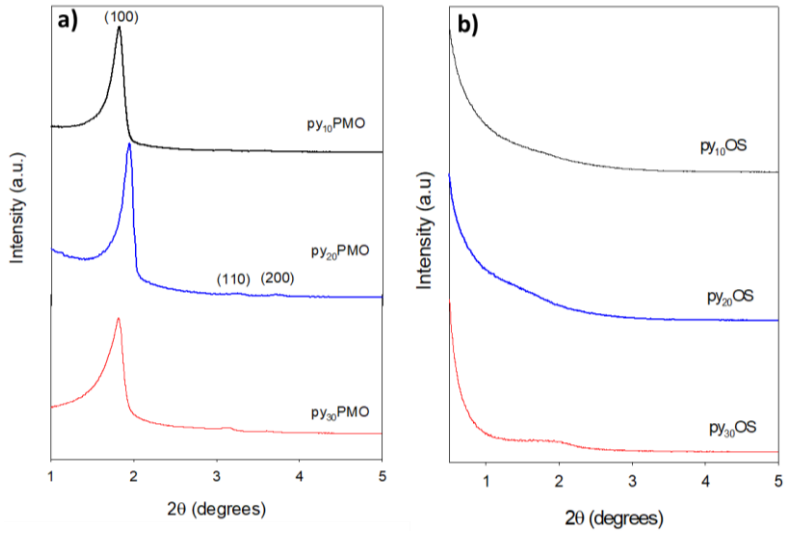

Fig S1. XRD patterns of py_xPMO (**a**) and py_xOS (**b**) materials.

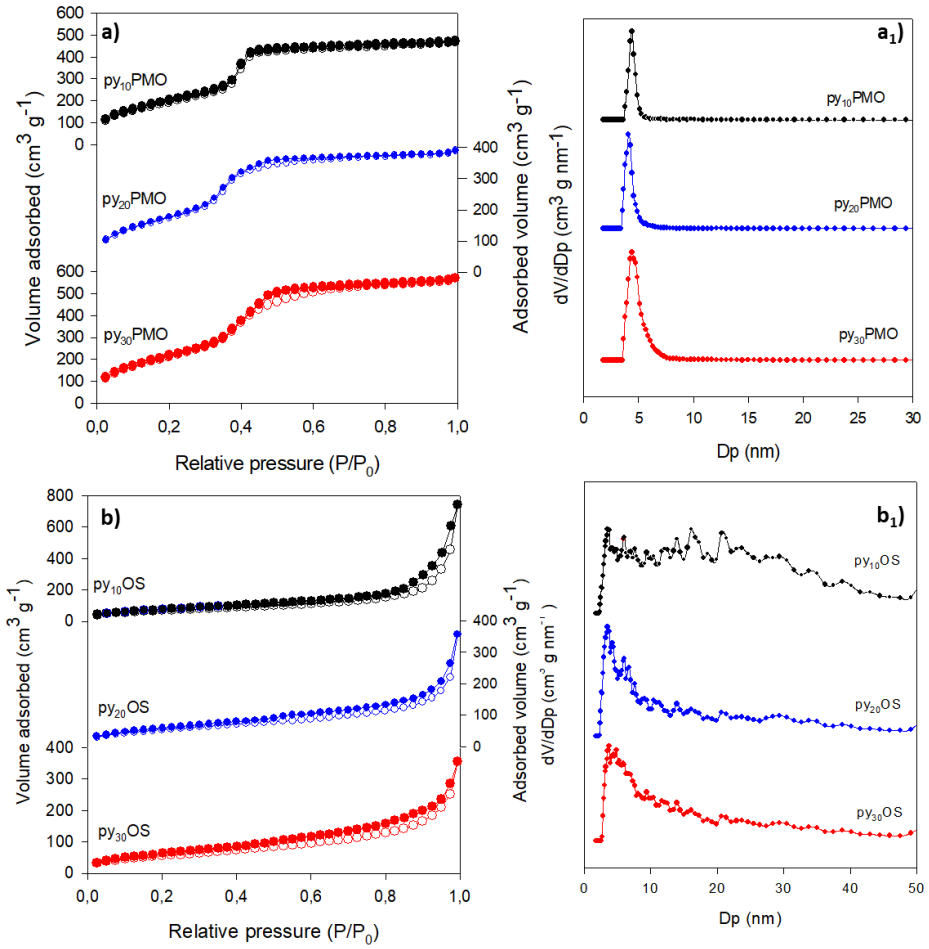

Fig S2. N_2 adsorption-desorption isotherms and DFT pore distributions of py_xPMO (a, a_1) and py_xOS (b, b_1) materials.

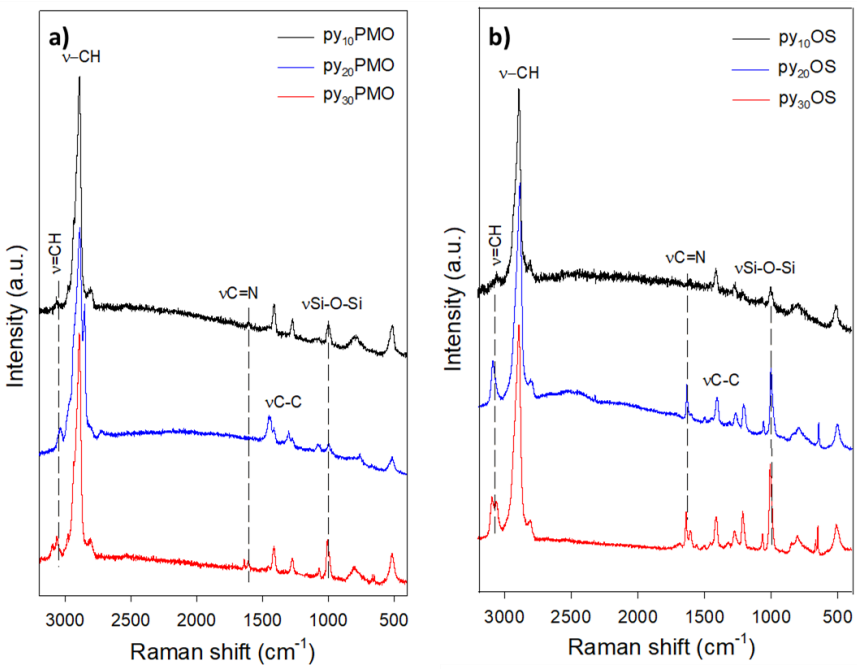

Fig S3. Raman spectra of py_xPMO (**a**) and py_xOS (**b**) supports.

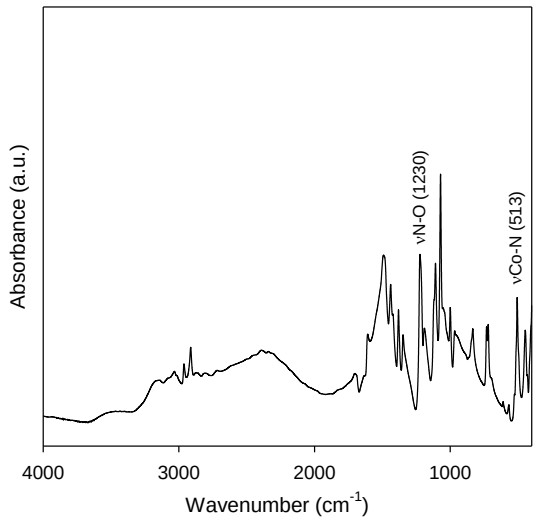

Fig S4. FT-IR spectra of dichlorocobaloxime complex.

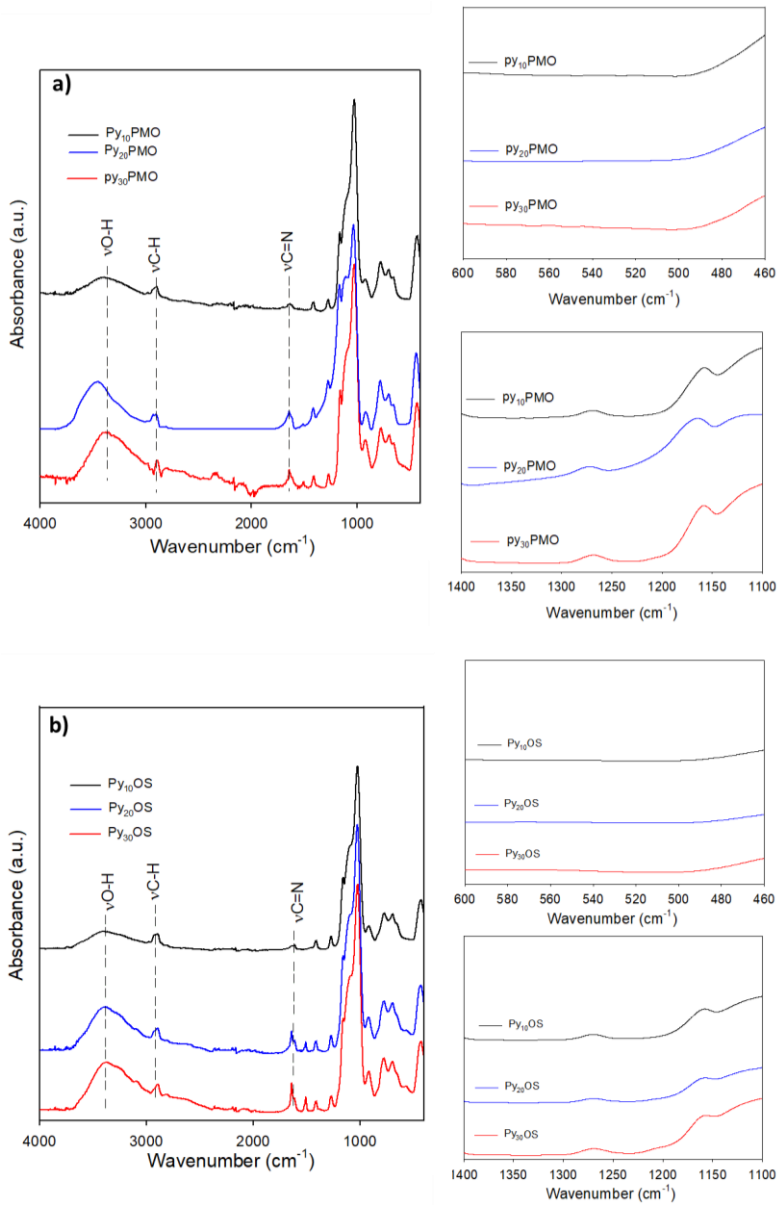

Fig S5. FT-IR spectra of py_xPMO (**a**) and py_xOS (**b**) supports.

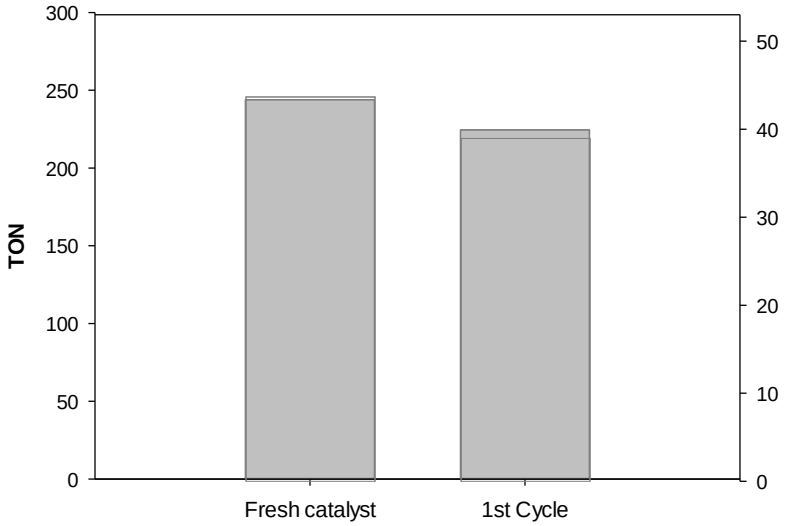

Fig S8. Catalyst recycling test of Py_{30}PMO-Co catalyst at 4h of reaction.

Table S1. Textural properties of py_xPMO and py_xOS supports.

MATERIAL	S_{BET} (m^2/g)	V_p[a] (cm^3/g)	D_p[a] (nm)	a_0[b] (nm)	Wall thickness[c] (nm)	Nitrogen content (mmol g^{-1})
py_{10}PMO	750	0.70	4.4	5.5	1.1	0.17
py_{20}PMO	683	0.57	4.1	4.7	0.6	0.57
py_{30}PMO	852	0.84	4.4	5.7	1.3	0.93
py_{10}OS	257	0.91	n.d.	n.d.	n.d.	1.02
py_{20}OS	200	0.43	n.d.	n.d.	n.d.	1.78
py_{30}OS	206	0.46	n.d.	n.d.	n.d.	2.16

[a] Calculated from DFT analysis
[b] Unit cell parameter calculated from formula, $a_0=2d_{100}/\sqrt{3}$
[c] Calculated from the difference between a_0 and D_p

CHAPTER 6.

RESULTS AND DISCUSSION

(PAPER 3)

Chapter 6. **Improved Photocatalytic H_2 Evolution by Cobaloxime-Tethered Imidazole-Functionalized Periodic Mesoporous Organosilica**

PAPER 3

Improved Photocatalytic H_2 Evolution by Cobaloxime-Tethered Imidazole-Functionalized Periodic Mesoporous Organosilica

M. Ángeles Navarro, Miguel A. Martín, José Rafael Ruiz, César Jiménez-Sanchidrián, Francisco J. Romero-Salguero* and Dolores Esquivel*.

Departamento de Química Orgánica, Instituto Químico para la Energía y el Medioambiente (IQUEMA),

Facultad de Ciencias, Universidad de Córdoba, Campus de Rabanales, 14071 Córdoba, Spain; q32nanum@uco.es (M.Á.N.); mmartinneri29@gmail.com (M.A.M.); qo1ruarj@uco.es (J.R.R.); qo1jisac@uco.es (C.J.-S.)

**Correspondence: qo2rosaf@uco.es (F.J.R.-S.); q12esmem@uco.es (D.E.); Tel.: +34-957-218638 (F.J.R.-S.); +34 957-211050 (D.E.)*

Open Access Article

Improved Photocatalytic H_2 Evolution by Cobaloxime-Tethered Imidazole-Functionalized Periodic Mesoporous Organosilica

by M. Ángeles Navarro, Miguel A. Martín, José Rafael Ruiz, César Jiménez-Sanchidrián, Francisco J. Romero-Salguero * and Dolores Esquivel *

Departamento de Química Orgánica, Instituto Químico para la Energía y el Medioambiente (IQUEMA), Facultad de Ciencias, Campus de Rabanales, Universidad de Córdoba, 14071 Córdoba, Spain

* Authors to whom correspondence should be addressed.

Hydrogen **2023**, *4*(1), 120-132; **https://doi.org/10.3390/hydrogen4010008**

Received: 5 November 2022 / Revised: 19 January 2023 / Accepted: 30 January 2023 / Published: 2 February 2023

(This article belongs to the Special Issue **Catalysts for Hydrogen Generation**)

hydrogen

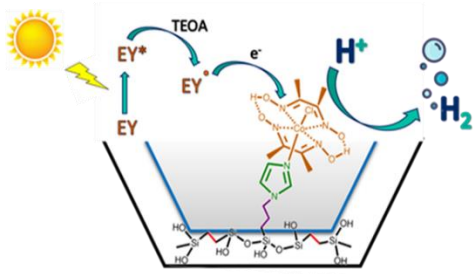

ABSTRACT

Molecular cobaloxime-based heterogeneous systems have attracted great interest during the last decades in light-driven hydrogen production. Here, we present a novel cobaloxime-tethered periodic mesoporous organosilica (PMO) hybrid (Im-EtPMO-Co) prepared through the immobilization of a molecular cobaloxime complex on the imidazole groups present in ethylene bridged PMO. The successful assembly of a molecular cobaloxime catalyst via cobalt imidazole axial ligation has been evidenced by several techniques, such as ^{13}C NMR, Raman spectroscopy, ICP-MS, and XPS. The catalytic performance of Im-EtPMO-Co catalyst was essayed on the hydrogen evolution reaction (HER) under visible light in presence of a photosensitizer (eosin Y) and an electron donor (TEOA). It showed an excellent hydrogen production of 95 mmol hydrogen at 2.5 h, which corresponded to a TON of 138. These results reflect an improved photocatalytic activity with respect to its homogenous counterpart $[Co(dmgH)_2(Im)Cl]$ as well as a previous cobaloxime-PMO system with pyridine axial ligation to the cobaloxime complex.

Keywords: cobaloxime; periodic mesoporous organosilicas; photocatalysis; hydrogen evolution reaction; primary axial coordination.

6.1 INTRODUCTION

Mimicking biological procedures has always been a good approach to tackling energy questions. In recent years, numerous efforts have been made for the development of natural photosynthesis-inspired technologies for the efficient transformation of the energy from sunlight into chemical energy [1]. Hydrogen is considered an efficient energy vector due to the high energy density of the H_2 molecule (119 kJ/g) and its ability to be stored in large quantities. Furthermore, hydrogen combustion with air only produces water as residue, so it is considered a cyclic and environmentally friendly process [2].

Aiming at designing efficient hydrogen evolution catalysts, alternative to traditional Pt-based catalysts, the first studies were focused on simulating the activity of hydrogenase enzymes (especially metalloproteins) for hydrogen production [3,4]. In fact, hydrogenases utilizing earth-abundant metals such as Fe or Ni-Fe are the most active molecular catalysts for hydrogen production [5,6]. Although numerous studies have been performed on the design of biomimetic models of [Fe]-hydrogenases for hydrogen production, their inherent instability during the catalytic process has limited their applicability. In this sense, to solve these drawbacks, recent approaches have been focused on the assembly of biomimetic di-iron catalysts on heterogenous supports, such as metal organic frameworks (MOFs) [7], silica-based mesoporous materials [8] or graphene-based materials [9] for light-induced hydrogen production. These heterogeneous matrices have provided improved stability for the anchored molecular catalyst, overcoming those issues related to its water solubility and photostability [10].

Conversely, in the past decades, cobalt compounds have provided an appealing alternative to hydrogenase mimic complexes as efficient and low-cost HER catalysts. Inspired by the structure of vitamin B_{12} and more specifically in the stable organometallic cobalt complex, 5-deoxyadenosyl-(5,6-

dimethylbenzimidazolyl)-cobinamide, present in its core [11], cobaloxime catalysts have been widely studied for electro and photocatalytic hydrogen production. Their great interest as molecular catalysts is given by their high O_2 tolerance [12,13], which allows their use under aerobic conditions, their facile synthesis, and their tunable catalytic properties only modifying the substituents on the equatorial and/or axial ligands [14,15]. Furthermore, they show high proton-reduction activity at moderately low overpotential [16] and can work in aqueous solutions [17].

Since the first example reported by Ziessel and co-workers about a cobaloxime complex for photocatalytic hydrogen production [18], numerous advances have been achieved in the design of more efficient molecular cobaloxime catalysts. Among them, one of the most interesting approaches to improve their catalytic activity is based on the heterogenization of such complexes and derivatives on solid supports. This approach is highly attractive because it improves the stability of the molecular catalysts while allowing their recyclability. Until now, most of the synthetic strategies used for that purpose have been focused on the development of materials containing surface pyridine moieties, which can act as ligands to axially coordinate a cobaloxime core. It is well documented that the catalytic properties of cobalt-diimine complexes can be improved by the presence of N donor groups in the axial position [19]. In the last decades, several studies have revealed an increase in the electrocatalytic HER efficiency with cobaloximes assembled on the surface of carbon-based materials [20] and semiconductors [21].

Recently, this methodology has been extended to other non-conductive porous supports, such as metal organic frameworks (MOFs) [22,23], covalent organic frame-works (COFs) [24], and most recently, on periodic mesoporous organosilicas (PMOs) [25] for light-driven photocatalytic hydrogen production.

Nevertheless, the major drawbacks and limitations of these molecular assemblies are the degradation of the equatorial ligand [26] and the de-coordination of the axial ligand [14] under catalytic conditions.

These findings indicate the relevance of considering enzyme-inspired outer coordination spheres (OCS) features around the cobalt core during the artificial catalyst design, therefore mimicking the protein scaffold of natural hydrogenases [27]. In this sense, initial studies reported by Wakerley and Reisner analyzed the influence of over 20 different substituted-pyridine ligands axially coordinated to a cobaloxime core for H_2 production. They found that the presence of more electron-donating pyridine ligands gave rise to an enhancement of the catalytic activity [15]. More recently, Dutta et al. [28] demonstrated that the improvement in the catalytic efficiency and long-term stability of a synthetic cobaloxime complex on electrocatalytic H_2 production was influenced by the number of basic groups on the outer coordination sphere of the cobaloxime core. Recently, these researchers extended the OCS studies to axial-imidazole-linked cobaloxime, one of the most active homogeneous cobalt complexes [29]. As previous results obtained by axial-pyridine-linked cobaloxime, the presence of peripheral basic functionalities around the same cobaloxime core enhanced the electro- and photocatalytic hydrogen production. These results show the relevance of the appropriated primary axial coordination sphere substituents to the catalytic cobalt center. It is important to note that most of the research in this field relies on the study of the electro- and photocatalytic HER performance of homogenous cobaloxime catalysts, with scarce studies on heterogenous systems.

In this context, our recently developed cobaloxime-PMO hybrid provides an approach for the design of heterogeneous cobaloxime systems [25]. In previous work, an efficient cobaloxime HER catalyst was synthesized through the coordination of a cobalt complex, $Co(dmgH_2)(dmgH)Cl_2$, on an ethylene-bridged

periodic mesoporous organosilica (PMO) containing pyridine moieties. Compared to its homogenous counterparts, this system provided increased stability of the cobalt complex into the mesopores, which was reflected in its enhanced catalytic efficiency. Until now, it was a unique example of anchoring cobaloxime HER catalysts on the surface of a PMO.

Herein, we report the synthesis of a novel cobaloxime-PMO hybrid material by axial coordination of a cobaloxime catalyst [$Co(dmgH_2)(dmgH)Cl_2$] on the imidazole ligands present on the surface of an ethylene-bridged PMO. The hybrid system was fully characterized by different techniques and evaluated as a catalyst in the photocatalytic hydrogen evolution reaction.

6.2 EXPERIMENTAL SECTION

6.2.1 Chemicals

The reagents for the synthesis of the different PMO materials, including octadecyltrimethylammonium bromide (OTAB, Sigma-Aldrich, Lyon, France), sodium hydroxide (NaOH, Sigma-Aldrich, Schnelldorf), 3-(chloropropyl)-triethoxysilane (95 %, Sigma-Aldrich, Lyon, France), 1,2-bis(triethoxysilyl)ethane (96 %, BTEE, Sigma-Aldrich, Lyon, France), and imidazole (99 %, Sigma-Aldrich, Lyon, France), were used as received without further purification. Dimethylglyoxime (99 %, Sigma-Aldrich, Lyon, France), acetone (>99.5 %, Sigma-Aldrich, Lyon, France), cobalt (II) chloride hexahydrate (Acros Organics, Geel, Belgium), methanol (>99.9 %, PanReac, Barcelona, Spain), imidazole (>99.9 %, Sigma-Aldrich, Lyon, France), and chloroform (99.9 %, Sigma-Aldrich, Lyon, France), employed for the synthesis of the cobalt complex, were used as supplied. Photocatalytic experiments were performed using acetonitrile (99.7 %, PanReac, Barcelona, Spain) and Milli-Q-water as

solvents, eosin Y (>95 %, TCI, Zwijndrecht, Belgium) as photosensitizer and triethanolamine (>99 %, TEOA, Sigma-Aldrich, Lyon, France) as a sacrificial electron donor.

6.2.2 Synthesis of the Materials

6.2.2.1 Synthesis of Cobaloxime Complexes: $Co(dmgH_2)(dmgH)Cl_2$ and $Co(dmgH)_2(Im)Cl$

$Co(dmgH_2)(dmgH)Cl_2$ complex was synthesized according to a previously reported procedure [30]. $CoCl_2 \cdot 6H_2O$ (2.1 mmol, 0.5 g) and dimethylglyoxime (4.2 mmol, 0.49 g) were dissolved in dry acetone (15 mL). The resulting solution was kept under stirring at room temperature for 30 min, after which it was filtered to eliminate any unreacted reactant. The filtrate was cooled overnight to form green crystals. These crystals were recovered by filtration and washed with cold acetone. The $Co(dmgH_2)(dmgH)Cl_2$ complex was dried under vacuum at 80 °C.

For the synthesis of the cobaloxime complex containing an axial imidazole ligand, $Co(dmgH_2)(dmgH)Cl_2$ complex (0.92 mmol, 0.33 g) was dispersed in 4 mL of chloroform and then the solution was stirred at room temperature for 10 min. Afterward, the imidazole ligand (2.28 mmol), previously dissolved in 4.5 mL of $CHCl_3$, was added dropwise to the solution. During this process, the green solution turned brown, indicating the ligand exchange had gone to completion. Subsequently, 3 mL of distilled H_2O was added to the solution, and it was stirred for 2 h. The aqueous phase was separated by decantation and the organic phase was washed with H_2O (3 × 15 mL). Finally, the product was washed with ethanol and dried under vacuum at 80 °C overnight. The final complex was named $Co(dmgH)_2(Im)Cl$ [19].

6.2.2.2 Synthesis of Chloropropyl Functionalized Ethylene-Bridged Periodic Mesoporous Organosilicas (Cl-EtPMO)

In a typical synthesis [31], the OTAB surfactant (0.85 g) was dissolved in a basic solution of NaOH (0.89 mL, 6 M) and Milli-Q water (53 mL). The solution was stirred overnight at 45 °C. Then, a mixture of organosilane precursors (2.04 mmol in total) in a molar ratio of 80% 1,2-bis(triethoxysilyl)ethane and 20 % (3-chloropropyl)triethoxysilane was added dropwise under stirring. The resulting solution was stirred at the same temperature for 24 h.

Afterward, the mixture was aged at 97 °C for 4 days under static conditions. The obtained solid was collected by filtration and thoroughly washed with water. In order to remove the surfactant, 1 g of as-synthesized material was refluxed in an ethanolic solution (50 mL of ethanol with 1 mL of HCl 37 wt%) for 12 h. This procedure was repeated twice. The final material was filtered out and dried at 100 °C under vacuum. It was named *Cl-EtPMO*.

6.2.2.3 Anchoring of Imidazole on Cl-EtPMO

The functionalization of Cl-EtPMO material by imidazole groups was carried out following the procedure reported by Zhang et al. [32]. The material Cl-EtPMO (1.97 g) was dispersed in a solution of imidazole (0.18 g) in toluene (40 mL). The reaction mixture was stirred at 120 °C for 24 h, after which the solid was recovered by filtration and washed with toluene in order to remove the excess imidazole not anchored in the PMO structure. The final material was dried at 80 °C under vacuum overnight. The functionalized material was named *Im-EtPMO*.

6.2.2.4 Immobilization of Dichlorocobaloxime on Im-EtPMO

The immobilization of dichlorocobaloxime complex on the PMO structure through imidazole groups was carried out with the following procedure: Im-EtPMO (0.5 g) was dispersed in methanol (10 mL) and then, dichlorocobaloxime complex (0.3 g) was added to the solution. The resulting mixture was stirred at 80 °C for 24 h. Afterward, the solution was filtered and washed with methanol in order to remove the excess dichlorocobaloxime complex. The final product was dried at 80 °C under vacuum. The heterogenous catalyst was named Im-*EtPMO-Co*.

6.2.3 Physicochemical Characterization

X-ray powder diffraction (XRD) patterns were collected on a Bruker D8 Discover A25 diffractometer using Cu Kα radiation. High-resolution transmission electron microscopy images were recorded on a JEOL JEM 1400 microscope. N_2 adsorption–desorption isotherms were recorded at −196 °C using an Autosorb-iQ MP/MP-XR instrument. Before measurement, all the samples were outgassed overnight at 100 °C. The surface area was calculated using the Brunauer–Emmett–Teller (BET) method and the pore size distribution was determined using the Density Functional Theory (DFT) method. The solid-state ^{13}C CP/MAS NMR spectra were recorded on a Bruker Avance III HD 400 WB spectrometer at 13 kHz. The excitation pulse and recycle time for ^{13}C CP/MAS NMR were 3.6 ms and 2 s, respectively. Chemical shifts were referenced to the tetramethylsilane (TMS) standard. Raman spectra of the samples were collected with a Renishaw Raman instrument with green laser light (532 nm). X-ray photoelectron spectroscopy (XPS) was performed on a SPECS Phoibos HAS 3500 150 MCD X-ray photoelectron spectrometer with a monochromatic Al anode (1486.7 eV). Regions were calibrated using the reference value BE (C1s) = 284.8 eV. Inductively coupled plasma mass spectrometry (ICP-MS) for the ^{59}Co isotope was

measured using a NexION 350X spectrometer. Before the measurement, the sample was digested in an UltraWave microwave system.

6.2.4 Photocatalytic Hydrogen Production Tests

Light-driven photocatalytic hydrogen production was carried out in a Restek vial (20 mL) with constant stirring under visible-light irradiation using a 300W Xe lamp (ORIEL) equipped with a Newport filter (FSQGC400, $\lambda \geq 400$ nm), at 10 cm distance. In a typical reaction, 1 mg of Im-EtPMO-Co catalyst was suspended in 11.4 mL of CH_3CN:H_2O (1:1) solution containing TEOA (10 %) and eosin Y (0.05 mM). The pH of the reaction was adjusted to 7.4 with HCl (37 wt%). Subsequently, the solution was degassed bubbling N_2 for 30 min and irradiated with a Xe lamp. Sample aliquots (50 µL) were taken at different reaction times using a gas-tight syringe and quantified by using a gas chromatograph (Shimadzu GC-2010 Plus) equipped with a barrier discharge ionization detector (BID) and a ShinCarbon ST column (2 m × 2 mm i.d.). For the homogeneous catalyst, 1 mg of the molecular catalyst, $Co(dmgH)_2(Im)Cl$, was dispersed in 1:1 CH_3CN/H_2O (11.4 mL) containing EY (0.05 mM) and TEOA (10 %), and the pH was adjusted with HCl to 7.4.

6.3 RESULTS AND DISCUSSION

6.3.1 Synthetic Strategy for Cobaloxime-Tethered Imidazole-Functionalized Ethylene-Bridged PMO Catalyst

The approach proposed for the development of a novel cobaloxime-PMO hybrid catalyst is shown in Scheme 1. As can be observed, several steps were strictly needed to achieve the functionality required on the pore channels of the PMO material due to the non-availability of a functional mono-silane precursor with imidazole groups. For that, self-assembly assisted co-condensation reaction

of a conventional bis-silane precursor, 1,2-bis(triethoxysilyl)ethane (BTEE), and chloropropyltriethoxysilane in the presence of OTAB as surfactant under basic conditions led to an ordered ethylene-bridged PMO with chloropropyl groups attached to the pore walls. Subsequently, the nucleophilic substitution of chlorine atoms by imidazole accompanied by the release of HCl gave rise to a PMO support containing imidazole groups on their pore channels. These organic groups can act as attachment points to further assemble cobaloxime catalysts on the surface of the PMO. To corroborate it, pictures depicted in Scheme 1 of the support before and after the immobilization of the cobaloxime complex clearly reflected the color change of the solid from white to light brown produced by the anchoring of the molecular cobaloxime catalyst on the imidazole groups present on the PMO channels.

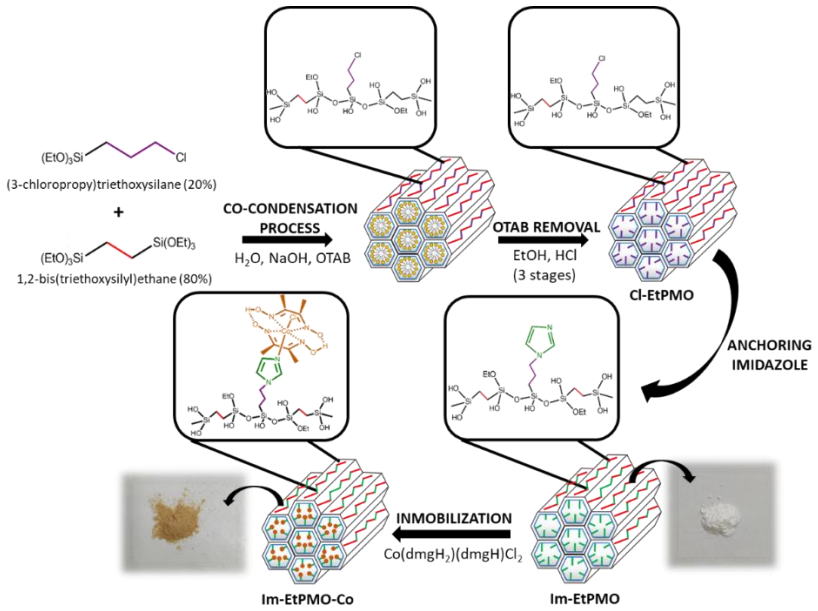

Scheme 1. Synthetic strategy of Im-EtPMO-Co catalyst.

6.3.2 Structural Characterization

The powder X-Ray diffraction (PXRD) patterns of all synthesized materials are depicted in Figure 1. The parent material (Cl-EtPMO) showed three reflection peaks in the low-angle region ($2\theta < 5°$). The first diffraction peak at 1.78° corresponded to the (100) reflection with a d-spacing of 5 nm. The two second-order peaks were attributed to the (110) and (200) reflections with d-spacing of 2.9 and 2.5 nm, respectively. These diffraction peaks are characteristics of 2D-hexagonal ordered (*p6mm*) mesostructures [33]. After functionalization by imidazole, the resulting Im-EtPMO material exhibited a similar diffraction pattern. Likewise, the subsequent anchoring of cobaloxime molecular catalyst through imidazole ligands preserved the initial ordered mesostructure.

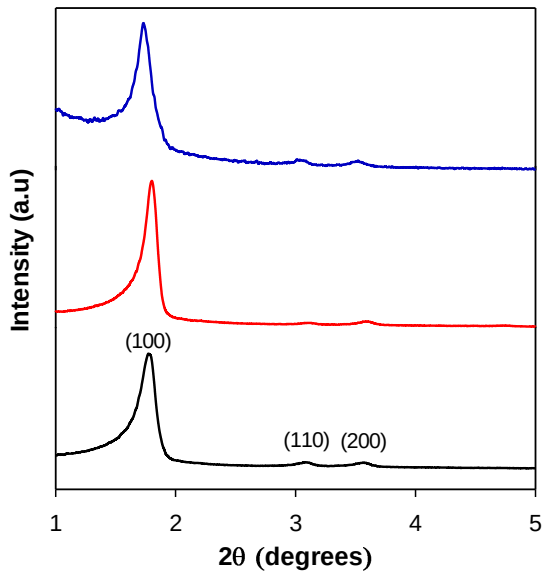

Figure 1. PXRD of Cl-EtPMO (black line), Im-EtPMO (red line), and Im-EtPMO-Co (blue line).

Transmission electron microscopy (TEM) images of Cl-EtPMO, Im-EtPMO, and Im EtPMO-Co materials are depicted in Figure 2. TEM images showed that all PMO materials had highly ordered structures with uniform and parallel channel pores, which confirmed the findings obtained by XRD.

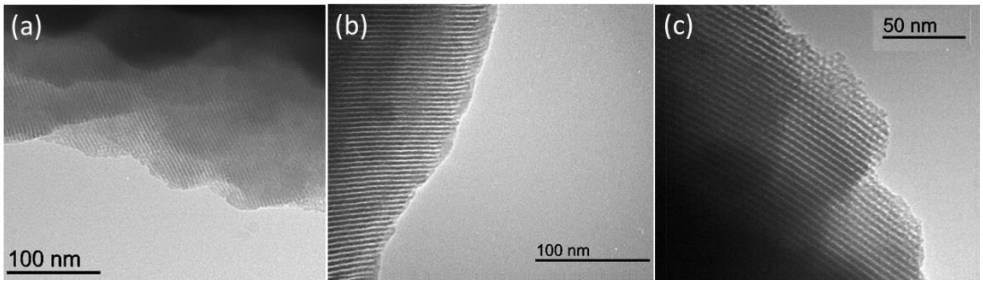

Figure 2. TEM images of Cl-EtPMO (**a**), Im-EtPMO (**b**), and Im-EtPMO-Co (**c**).

Im-EtPMO and Im-EtPMO-Co materials exhibited type-IV isotherms according to the IUPAC [34] with a condensation step at P/P_0 = 0.3–0.7, characteristic of mesoporous materials (Figure 3). Both materials showed a non-distinctive hysteresis loop, which is typical of materials with small mesopores [35]. The narrow pore size distribution and average pore size confirmed pores in the meso range. Table 1 summarizes the textural properties of the materials. Im-EtPMO showed a BET surface area, pore volume, and pore diameter of 583 m^2 g^{-1}, 0.5 cm^3 g^{-1}, and 4.2 nm, respectively. The anchoring of the molecular cobaloxime catalyst on the pendant imidazole groups gave rise to a slight decrease in surface area and pore volume.

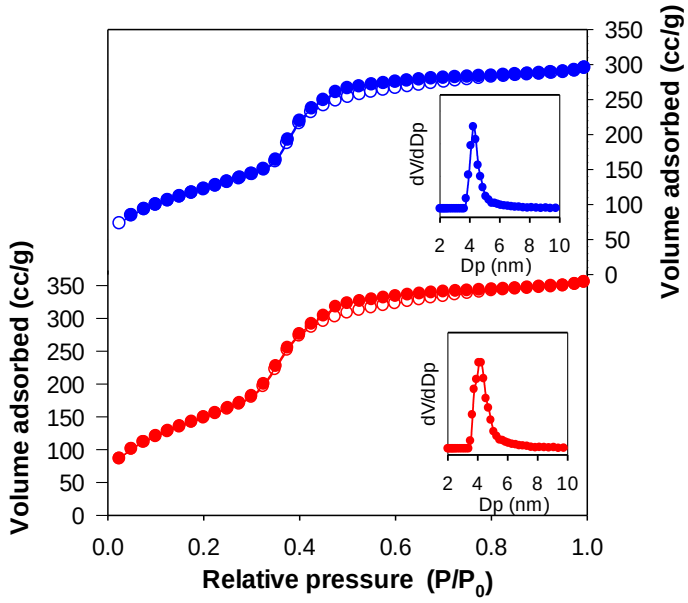

Figure 3. Nitrogen adsorption–desorption isotherms and pore size distributions (inset) of Im-EtPMO (red line) and Im-EtPMO-Co (blue line).

Table 1. Physicochemical properties of Im-EtPMO and Im-EtPMO-Co materials.

Sample	a_0 [b] (nm)	S_{BET} ($m^2\ g^{-1}$)	V_p ($cm^3\ g^{-1}$)	D_p [a] (nm)	w [b] (nm)
Im-EtPMO	5.6	583	0.52	4.2	5.6
Im-EtPMO-Co	5.7	455	0.43	4.2	5.7

[a] Unit cell parameter calculated as $a_0 = 2d_{100}/\sqrt{3}$. [b] Calculated from DFT analysis. [c] Determined from the difference between a_0—D_p.

The ^{13}C CP/MAS NMR measurements confirmed the presence of the organic bridging groups in the silica framework as well as the different organic groups anchored on the mesochannels (Figure 4). The Cl-EtPMO material showed an intense peak centered at 6 ppm associated with the Csp3 of the ethylene groups present in the pore walls [36]. Small peaks at 50, 26, and 9 ppm correspond to the three carbon atoms in the chloroalkyl chain. The additional peaks at 58 and 17

ppm, corresponding to the -OCH_2- and -CH_3 groups, respectively, derived from the incomplete hydrolysis of the ethoxy groups under synthesis conditions. After functionalization with imidazole, Im-EtPMO material showed new signals at low fields (136 and 123 ppm) attributed to the Csp^2 in the imidazole ring [37]. After immobilization of the cobaloxime complex on the surface of the PMO-containing imidazole groups, signals associated with C=N (154 ppm) and -CH_3 (13 ppm) groups from the glyoximate ligands were clearly present [38]. Additionally, an aromatic signal at 130 ppm confirmed the coordination of nitrogen to cobalt atoms. The signal at 50 ppm is assigned to residual CH_3OH employed in the washing process to remove unreacted cobaloxime complex. These results were further confirmed by Raman spectroscopy.

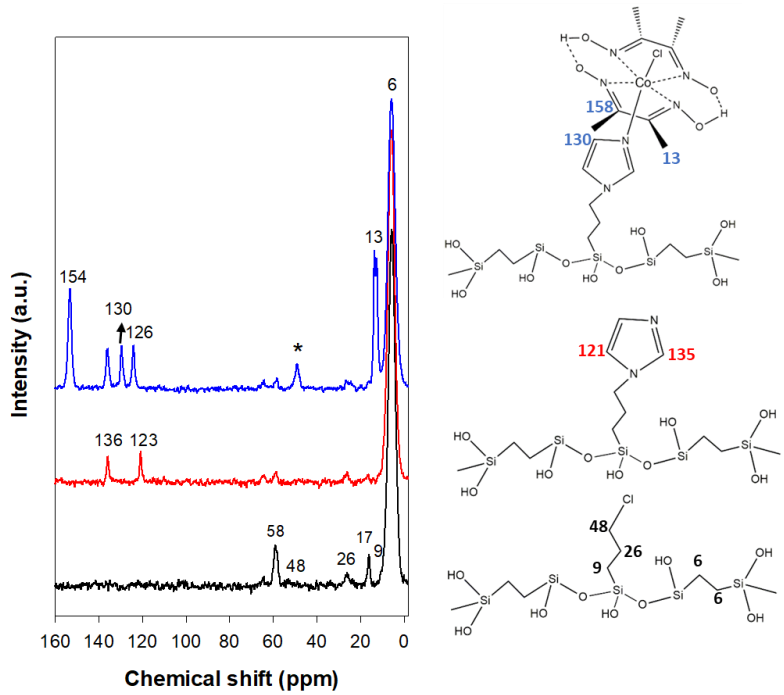

Figure 4. ^{13}C CP/MAS NMR spectra of Cl-EtPMO (black line), Im-EtPMO (red line), and Im-EtPMO-Co (blue line). Predicted chemical shifts on the right.

Raman spectra of all synthesized materials are shown in Figure 5. Cl-EtPMO showed intense signals below 3000 cm^{-1}, associated with the C-H stretching of propyl chains as well as the ethylene bridges. After substitution with imidazole, the resulting material exhibited new signals above 3000 cm^{-1} attributed to =C-H stretching vibration from the imidazole ring. Additionally, peaks in the region of 1500–1400 cm^{-1} were associated with the C=C and C=N stretching vibrations of imidazole moieties [39,40]. After the immobilization of the cobaloxime complex, new vibrations at 1620 and 1220 cm^{-1} were assigned to C=N and N-O stretching vibrations, respectively, for dimethyl-glyoxime groups of the cobaloxime [41].

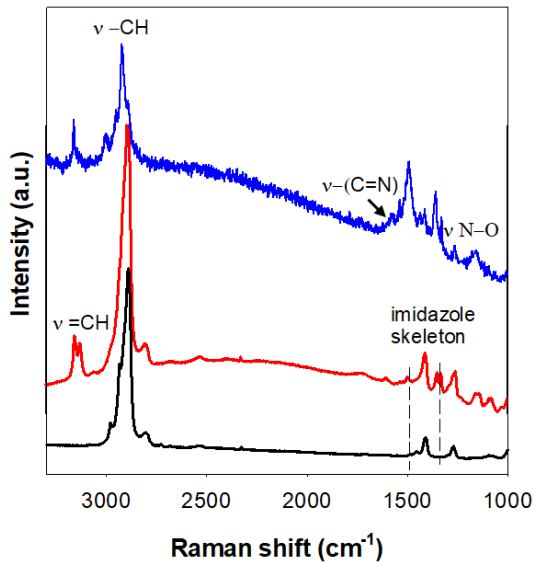

Figure 5. Raman spectra of Cl-EtPMO (black line), Im-EtPMO (red line), and Im-EtPMO-Co (blue line).

X-ray photoelectron spectroscopy (XPS) measurements provided evidence about the incorporation of cobaloxime catalyst on the surface of PMO as well as the oxidation state of the cobalt species (Figure 6). The survey spectrum

of Im-EtPMO showed peaks related to O, C, N, Cl, and Si elements. After the immobilization of the cobaloxime catalyst, an additional peak associated with the Co element was present. The N1s high-resolution spectrum of Im-EtPMO showed a broad peak around 400.8 eV, which was attributed to the nitrogen atoms present on the imidazole ring (Figure 6a) [42,43]. A similar N1s XPS spectrum was obtained for Im-EtPMO-Co, but with the maximum slightly shifted towards lower binding energy (400.3 eV). This peak would encompass the pyridinic-N coordinated to the Co centers, the N-C groups present on the imidazole groups, as well as the N=C bonds from the glyoximate ligands of the cobaloxime. Furthermore, the study of the Co 2p region (810–770 eV) clearly evidenced the presence of cobalt species in the Im-EtPMO-Co sample (Figure 6b). The high-resolution Co2p spectrum exhibited two symmetrical doublet peaks at 781 and 796 eV corresponding to the $2p_{3/2}$ and $2p_{1/2}$ levels in a 2:1 expected ratio [44]. The 15.0 eV of distance and the lack of satellite bands undoubtedly evidenced the presence of cobalt in a +3 oxidation state in the cobaloxime complex [45].

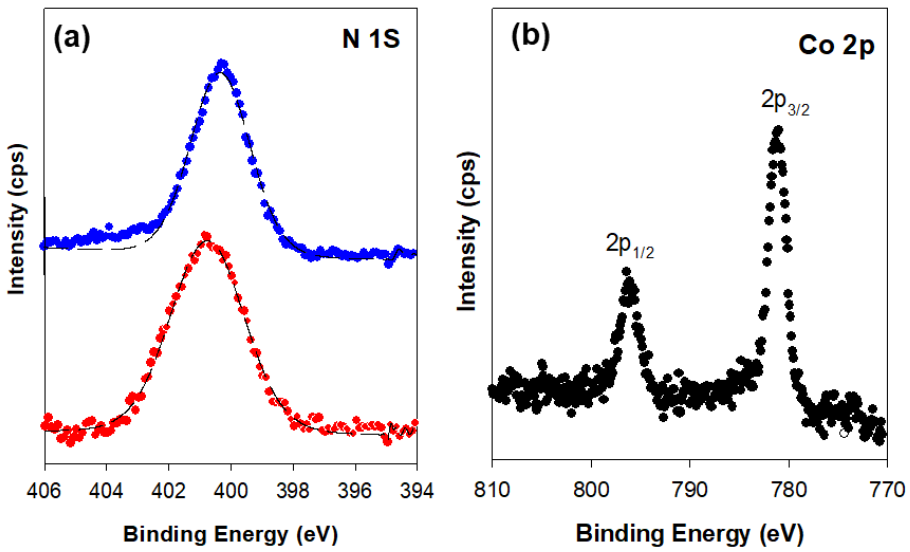

Figure 6. (a) High-resolution XPS spectra of N1s for Im-EtPMO (red line) and Im-EtPMO-Co (blue line). (b) High-resolution Co2p XPS spectrum for Im-EtPMO-Co.

The functionalization degree of Cl-EtPMO material by imidazole was analyzed by elemental analysis. The nitrogen content for Im-EtPMO was 1.38 mmol g^{-1}. After the immobilization of the cobalt complex via the cobalt-imidazole axial bond, the cobalt loading analyzed by ICP-MS was 0.70 mmol g^{-1}. According to these results, the N/Co ratio on the Im-EtPMO-Co catalyst was ca. 2.0. It means that one cobaloxime complex was coordinated per imidazole group on the PMO support. These findings revealed that all surface imidazole ligands were completely accessible and acted as attachment points to assemble the cobaloxime catalyst.

6.3.3 Photocatalytic Hydrogen Evolution Reaction

Once the successful anchoring of the cobaloxime catalyst via axial ligation of imidazole groups present on the surface of the PMO support was confirmed, 1 mg of Im-EtPMO-Co catalyst was assessed towards H_2 production in a water: acetonitrile solution under continuous visible light irradiation (>400 nm) in the presence of eosin Y and TEOA as photosensitizer and electron donor, respectively. According to the literature, as depicted in Scheme 2, the photocatalytic hydrogen evolution reaction commences with the reductive quenching of photoexcited [EY]. Subsequently, [EY^{*-}] reductant transfers an electron to the proton reduction catalyst (Im-EtPMO-Co) to produce hydrogen.
Previous similar works had shown that all components - photosensitizer, electron donor, and catalyst - were strictly necessary to carry out the hydrogen evolution reaction [25]. Figure 7a depicts the catalytic HER turnover numbers (TON) (vs [Co]) after 4 h of irradiation. As can be observed, our catalytic system demonstrated photocatalytic H_2 production with an initial rate of 68.1 mmol h^{-1} g^{-1}. The HER was leveled off after 2.5 h of irradiation, reaching a hydrogen production maximum of 95 mmol g^{-1}. This corresponded to a TON (vs [Co]) of 138. The photocatalytic activity was optimized by increasing the amount of

catalyst from 1 mg to 3.6 mg. Under similar reaction conditions, a gradual drop in hydrogen production was observed by increasing the concentration of Im-EtPMO-Co in the system. The TON decreased from 138 (1 mg catalyst) to 109 (1.5 mg), 94 (2 mg), and 54 (3.6 mg). In light-induced hydrogen production systems, an increase in the amount of solid catalyst is accompanied by a decrease in the amount of H_2 generated due to the blocking of light radiation by the catalyst particles [8,46,47].

For comparison, $Co(dmgH)_2(Im)Cl$ complex was tested as a homogenous catalyst under analogous reaction conditions. After 2.5 h, the total amount of evolved hydrogen corresponded to a TON (vs [Co]) of 40. This value was in the range of that reported by Dolui et al. [29] for the same homogenous chloro-imidazole cobaloxime complex. These results clearly reflected an increase in the photocatalytic activity of the molecular cobaloxime catalyst after its immobilization on a PMO material. Previous reports have attributed the activity enhancement undergone by immobilized cobaloxime catalysts, compared to their homogenous counterparts, to the confinement of the molecular catalysts into pores of the material [23,24]. It is well known that cobaloximes are degraded under photocatalytic conditions due to the decoordination of the N-donating ligand from the cobaloxime core. Although this fact would limit the stability of the cobaloxime species in a solution capable of being reduced, the possible re-coordination of these species to the N-donating ligands present in the pores of the material would lead to the reactivation of the cobaloxime center.

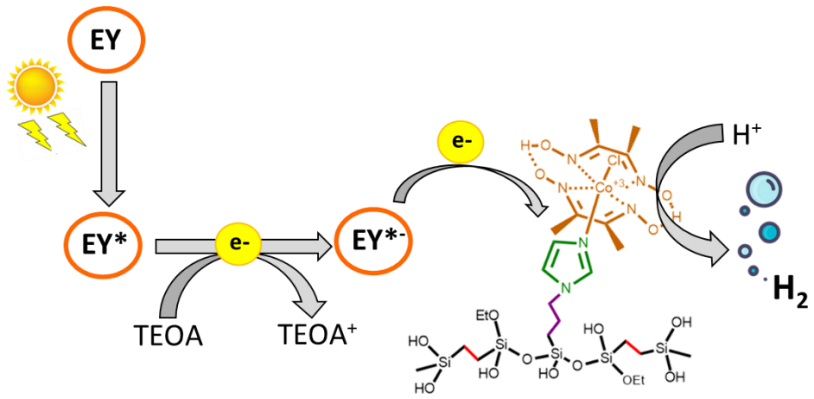

Scheme 2. Schematic representation of photocatalytic hydrogen evolution reaction with TEOA and eosin Y (EY and photoexcited EY, EY*) as electron donor and photosensitizer, respectively.

Finally, aiming at proving the role of the primary axial coordination sphere in cobaloxime complexes on HER, our proposed system, Im-EtPMO-Co, was compared with a recently reported cobaloxime-hybrid PMO, py-etPMO-Co. In this system, the cobaloxime units were assembled via a cobalt-pyridine axial bond on the porous channels of the PMO [25]. Under the same photochemical conditions, the py-etPMO-Co catalyst was less active for the photoinduced hydrogen evolution, reaching a TON (vs [Co]) of 80 (Figure 7b). This lower hydrogen production can be explained on the basis of the basicity of N-aromatic ligands coordinated with the cobaloxime catalyst. It is reported that a higher pKa of axial N-based aromatic ligands is directly correlated with a higher stability and activity of the corresponding catalyst [14]. On this basis, the higher pKa of N-alkyl imidazole ligand compared to the pyridine one resulted in a higher photocatalytic HER activity of N-methyl imidazole-linked cobaloximes in comparison to axial pyridine-linked cobaloximes.

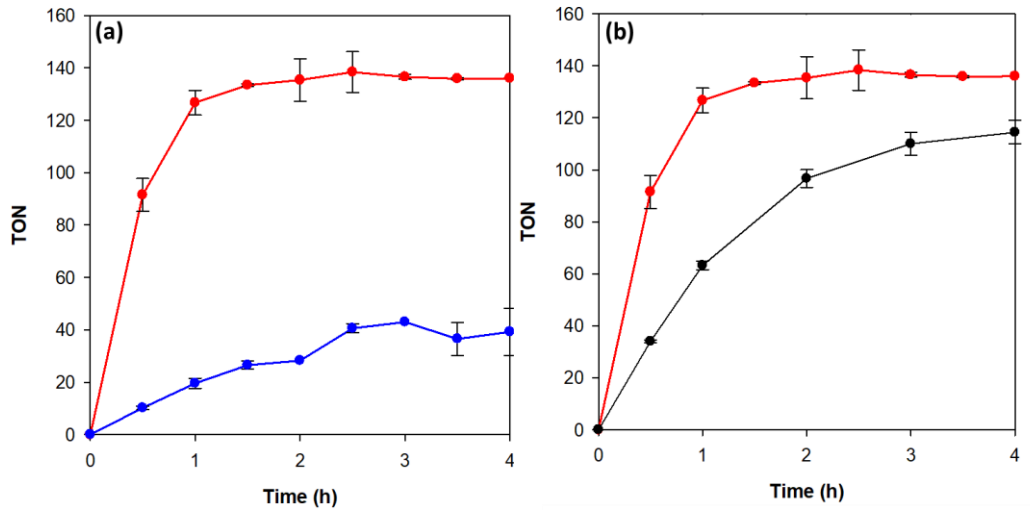

Figure 7. (**a**) Photocatalytic HER with Im-EtPMO-Co (red line) and $Co(dmgH)_2(Im)Cl$ homogeneous catalyst (blue line). (**b**) Photocatalytic HER with Im-EtPMO-Co (red line) and py-etPMO-Co (black line) as catalysts.

6.4 CONCLUSIONS

In this work, we present a novel cobaloxime-PMO hybrid synthesized by axial coordination of the cobaloxime core onto the imidazole groups present on the surface of an ethylene-bridged periodic mesoporous organosilica. The cobaloxime hydrogen evolution catalyst was evaluated in the photocatalytic hydrogen production in presence of eosin Y and TEOA, as photosensitizer and electron donor, respectively. This catalytic system reached a hydrogen production maximum of 95 mmol g^{-1}, which corresponded to a TON (vs [Co]) of 138. This value largely exceeded that obtained by its homogenous counterpart, therefore corroborating the positive confinement effect of the molecular cobaloxime catalyst in the pores of the PMO material. Likewise, the existence of an axial cobalt-imidazole ligation on this system led to an enhanced photocatalytic hydrogen production compared to a previously reported cobaloxime-PMO hybrid with cobalt-pyridine ligation.

6.5 REFERENCES

[1] D.G. Nocera, The Artificial Leaf, Acc. Chem. Res. 45 (2012) 767–776. https://doi.org/10.1021/ar2003013.

[2] C. Koroneos, A. Dompros, G. Roumbas, N. Moussiopoulos, Life cycle assessment of hydrogen fuel production processes, Int. J. Hydrogen Energy. 29 (2004) 1443–1450. https://doi.org/10.1016/j.ijhydene.2004.01.016.

[3] A. Le Goff, V. Artero, B. Jousselme, P.D. Tran, N. Guillet, R. Métayé, A. Fihri, S. Palacin, M. Fontecave, From Hydrogenases to Noble Metal–Free Catalytic Nanomaterials for H_2 Production and Uptake, Science. 326 (2009) 1384–1387. https://doi.org/10.1126/science.1179773.

[4] S. Gao, W. Fan, Y. Liu, D. Jiang, Q. Duan, Artificial water-soluble systems inspired by [FeFe]-hydrogenases for electro- and photocatalytic hydrogen production, Int. J. Hydrogen Energy. 19 (2020) 4305–4327. https://doi.org/10.1016/j.ijhydene.2019.11.206.

[5] Y. Lu, J. Koo, O_2 sensitivity and H_2 production activity of hydrogenases-A review, Biotechnol. Bioeng. 116 (2019) 3124–3135. https://doi.org/10.1002/bit.27136.

[6] M.Y. Azwar, M.A. Hussain, A.K. Abdul-wahab, Development of biohydrogen production by photobiological, fermentation and electrochemical processes: A review, Renew. Sustain. Energy Rev. 31 (2014) 158–173. https://doi.org/10.1016/j.rser.2013.11.022.

[7] S. Pullen, H. Fei, A. Orthaber, S.M. Cohen, S. Ott, Enhanced photochemical hydrogen production by a molecular diiron catalyst incorporated into a metal-organic framework, J. Am. Chem. Soc. 135 (2013) 16997–17003. https://doi.org/10.1021/ja407176p.

[8] T. Himiyama, M. Waki, D. Esquivel, A. Onoda, T. Hayashi, P. Van Der Voort, S. Inagaki, A Heterogeneous Hydrogen-Evolution Catalyst Based on a Mesoporous Organosilica with a Diiron Catalytic Center Modelling [FeFe]-Hydrogenase, ChemCatChem. 10 (2018) 4908–4913. https://doi.org/10.1002/cctc.201801257.

[9] R.-X. Li, X.-T. Ren, M.-Y. Tang, M.-X. Chen, G.-B. Huang, C.-H. Fang, T. Liu, Z.-H. Feng, Y.-B. Yin, Y.-M. Guo, S.-K. Mei, J. Yan, Fabrication of covalently linked graphene-mediated [FeFe]-hydrogenases biomimetic photocatalytic hydrogen evolution system in aqueous solution, Appl. Catal. B Environ. 224 (2018) 772–782. https://doi.org/10.1016/j.apcatb.2017.09.062.

[10] J. Amaro-Gahete, M. V. Pavliuk, H. Tian, D. Esquivel, F.J. Romero-Salguero, S. Ott, Catalytic systems mimicking the [FeFe]-hydrogenase active site for visible-light-driven hydrogen production, Coord. Chem. Rev. 448 (2021) 214172. https://doi.org/10.1016/j.ccr.2021.214172.

[11] Gerhard N. Schrauzer, Organocobalt chemistry of vitamin B_{12} model compounds (cobaloximes), Acc. Chem. Res. 1 (1968) 97–103. https://doi.org/10.1021/ar50004a001.

[12] F. Lakadamyali, M. Kato, N.M. Muresan, E. Reisner, Selective Reduction of Aqueous Protons to Hydrogen with a Synthetic Cobaloxime Catalyst in the Presence of Atmospheric Oxygen, Angew. Chemie - Int. Ed. 51 (2012) 9381–9384. https://doi.org/10.1002/anie.201204180.

[13] D.W. Wakerley, M.A. Gross, E. Reisner, Proton reduction by molecular catalysts in water under demanding atmospheres, Chem. Commun. 50 (2014) 15995–15998. https://doi.org/10.1039/c4cc06159d.

[14] J. Willkomm, N.M. Muresan, E. Reisner, Enhancing H_2 evolution performance of an immobilised cobalt catalyst by rational ligand design, Chem. Sci. 6 (2015) 2727–2736. https://doi.org/10.1039/c4sc03946g.

[15] D.W. Wakerley, E. Reisner, Development and understanding of cobaloxime activity through electrochemical molecular catalyst screening, Phys. Chem. Chem. Phys. 16 (2014) 5739–5746. https://doi.org/10.1039/C4CP00453A.

[16] V. Artero, J. Pe, M. Fontecave, Cobalt and nickel diimine-dioxime complexes as molecular electrocatalysts for hydrogen evolution with low overvoltages, PNAS. 106 (2009) 20627–20632. https://doi.org/10.1073pnas.0907775106.

[17] E.S. Andreiadis, P.A. Jacques, P.D. Tran, A. Leyris, M. Chavarot-Kerlidou, B. Jousselme, M. Matheron, J. Pécaut, S. Palacin, M. Fontecave, V. Artero, Molecular engineering of a cobalt-based electrocatalytic nanomaterial for H_2 evolution under fully aqueous conditions, Nat. Chem. 5 (2013) 48–53. https://doi.org/10.1038/nchem.1481.

[18] J. Hawecker, J.M Lehn, R. Ziessel, Efficient Homogeneous Photochemical Hydrogen Generation and Water Reduction Mediated by Cobaloxime or Macrocyclic Cobalt Complexes, Nouv. J. Chim. 7 (1983) 271–277. https://doi.org/10.1002/chin.198340125.

[19] A. Panagiotopoulos, K. Ladomenou, D. Sun, V. Artero, A.G. Coutsolelos, Photochemical hydrogen production and cobaloximes: the influence of the cobalt axial N-ligand on the system stability, Dalt. Trans. 45 (2016) 6732–6738. https://doi.org/10.1039/C5DT04502A.

[20] I.K. Sideri, G. Charalambidis, A.G. Coutsolelos, R. Arenal, N. Tagmatarchis, Pyridine vs. Imidazole Axial Ligation on Cobaloxime Grafted Graphene: Hydrogen Evolution Reaction Insights, Nanomaterials. 12 (2022) 3077. https://doi.org/10.3390/nano12173077.

[21] B.L. Wadsworth, D. Nishiori, N.P. Nguyen, E.A.R. Cruz, Electrochemistry of Polymeric Cobaloxime-Containing Assemblies in Organic and Aqueous Solvents, ECS J. Solid State Sci. Technol. 9 (2020) 061018. https://doi.org/10.1149/2162-8777/aba1ff.

[22] S. Roy, Z. Huang, A. Bhunia, A. Castner, A.K. Gupta, X. Zou, S. Ott, Electrocatalytic Hydrogen Evolution from a Cobaloxime-Based Metal-Organic Framework Thin Film, J. Am. Chem. Soc. 141 (2019) 15942–15950. https://doi.org/10.1021/jacs.9b07084.

[23] S. Roy, A. Bhunia, N. Schuth, M. Haumann, S. Ott, Light-driven hydrogen evolution catalyzed by a cobaloxime catalyst incorporated in a MIL-101(Cr) metal-organic framework, Sustain. Energy Fuels. 2 (2018) 1148–1152. https://doi.org/10.1039/c8se00072g.

[24] K. Gottschling, G. Savasci, H. Vignolo-González, S. Schmidt, P. Mauker, T. Banerjee, P. Rovó, C. Ochsenfeld, B. V. Lotsch, Rational Design of Covalent Cobaloxime-Covalent Organic Framework Hybrids for Enhanced Photocatalytic Hydrogen Evolution, J. Am. Chem. Soc. 142 (2020) 12146–12156. https://doi.org/10.1021/jacs.0c02155.

[25] M.Á. Navarro, D. Cosano, A. Bhunia, L. Simonelli, V. Martin-Diaconescu, F.J. Romero-Salguero, D. Esquivel, Cobaloxime tethered pyridine-functionalized ethylene-bridged periodic mesoporous organosilica as an efficient HER catalyst, Sustain. Energy Fuels. 6 (2022) 398–407. https://doi.org/10.1039/D1SE01437D.

[26] T.M. McCormick, Z. Han, D.J. Weinberg, W.W. Brennessel, P.L. Holland, R. Eisenberg, Impact of Ligand Exchange in Hydrogen Production from Cobaloxime-Containing Photocatalytic Systems, Inorg. Chem. 50 (2011) 10660–10666. https://doi.org/10.1021/ic2010166.

[27] D. Dolui, S. Khandelwal, P. Majumder, A. Dutta, The odyssey of cobaloximes for catalytic H_2 production and their recent revival with enzyme-inspired design, Chem. Commun. 56 (2020) 8166–8181. https://doi.org/10.1039/D0CC03103H.

[28] D. Dolui, S. Khandelwal, A. Shaik, D. Gaat, V. Thiruvenkatam, A. Dutta, Enzyme-Inspired Synthetic Proton Relays Generate Fast and Acid- Stable Cobalt-Based H_2 Production Electrocatalysts, ACS Catal. 9 (2019) 10115–10125. https://doi.org/10.1021/acscatal.9b02953.

[29] D. Dolui, S. Das, J. Bharti, S. Kumar, P. Kumar, A. Dutta, Bio-inspired Cobalt Catalyst Enables Natural-Sunlight-Driven Hydrogen Production from Aerobic Neutral Aqueous Solution, Cell Reports Phys. Sci. 1 (2020) 100007. https://doi.org/10.1016/j.xcrp.2019.100007.

[30] W.C. Trogler, R.C. Stewart, Cis and Trans Effects on the Proton Magnetic Resonance Spectra of Cobaloximes, Inorg. Chem. 13 (1974) 1564–1570. https://doi.org/10.1021/ic50137a005.

[31] M. Waki, N. Mizoshita, T. Tani, S. Inagaki, Periodic mesoporous organosilica derivatives bearing a high density of metal complexes on pore surfaces, Angew. Chemie - Int. Ed. 50 (2011) 11667–11671. https://doi.org/10.1002/anie.201104063.

[32] P. Zhang, Y. Sun, Q. Zhang, Y. Guo, D. Song, Upgrading of pyrolysis biofuel via esterification of acetic acid with benzyl alcohol catalyzed by BrØnsted acidic ionic liquid functionalized ethyl-bridged organosilica hollow nanospheres, Fuel. 228 (2018) 175–186. https://doi.org/10.1016/j.fuel.2018.04.107.

[33] Y. Xia, R. Mokaya, To stir or not to stir: formation of hierarchical superstructures of molecularly ordered ethylene-bridged periodic mesoporous organosilicas, J. Mater. Chem. 16 (2006) 395–400. https://doi.org/10.1039/B511339C.

[34] K.S.W. Sing, Reporting physisorption data for gas/solid systems with Special Reference to the Determination of S, Pure Appl. Chem. 54 (1982) 2201–2218.

[35] W. Liu, A.M. Kaczmarek, K. Folens, G. Du Laing, P. Van Der Voort, R. Van Deun, Rational design of lanthanide nano periodic mesoporous organosilicas (Ln-nano-PMOs) for near-infrared emission, Dalt. Trans. 50 (2021) 2774–2781. https://doi.org/10.1039/D1DT00032B.

[36] M.Á. Navarro, J. Amaro-Gahete, J.R. Ruiz, C. Jiménez-Sanchidrián, F.J. Romero-Salguero, D. Esquivel, Copper-complexed dipyridyl-pyridazine functionalized periodic mesoporous organosilica as a heterogeneous catalyst for styrene epoxidation, Dalt. Trans. 51 (2022) 4884–4897. https://doi.org/10.1039/D2DT00018K.

[37] S. Li, L. Zhou, Y. Su, B. Han, F. Deng, ^{13}C and ^{15}N spectral editing inside histidine imidazole ring through solid-state NMR spectroscopy, Solid State Nucl. Magn. Reson. 54 (2013) 13–17. https://doi.org/10.1016/j.ssnmr.2013.05.002.

[38] R.. Bisergaeva, Y.. Sirieva, Synthesis of some cobaloxime derivatives, IOP Conf. Ser. Earth Environ. Sci. 421 (2020) 072007. https://doi.org/10.1088/1755-1315/421/7/072007.

[39] L.M. Markham, L.C. Mayne, B.S. Hudson, M.Z. Zgierski, Resonance Raman studies of imidazole, imidazolium, and their derivatives: The effect of deuterium substitution, J. Phys. Chem. 97 (1993) 10319–10325. https://doi.org/10.1021/j100142a010.

[40] Bottari, Rossi, Mele, Damin, Bordiga, Musso, Gessini, Masciovecchio, Synchrotron-based UV resonance Raman scattering for investigating ionic liquid-water solutions, Condens. Matter Phys. 22 (2019) 43301. https://doi.org/10.5488/CMP.22.43301.

[41] S. Salama, T.G. Spiro, Resonance Raman Spectra of Cobalt(II)-Imidazole Complexes: Analogues of the Binding Site of Cobalt-Substituted Zinc Proteins, J. Am. Chem. Soc. 100 (1978) 1105–1111. https://doi.org/10.1021/ja00472a014.

[42] G. Xue, Q. Dai, S. Jiang, Chemical reactions of imidazole with metallic silver studied by the use of SERS and XPS techniques, J. Am. Chem. Soc. 110 (1988) 2393–2395. https://doi.org/10.1021/ja00216a009.

[43] B. Grzyb, S. Gryglewicz, A. Śliwak, N. Díez, J. Machnikowski, G. Gryglewicz, Guanidine, amitrole and imidazole as nitrogen dopants for the synthesis of N-graphenes, RSC Adv. 6 (2016) 15782–15787. https://doi.org/10.1039/C5RA24624E.

[44] T.J. Chuang, C.R. Brundle, D.W. Rice, Interpretation of the x-ray photoemission spectra of cobalt oxides and cobalt oxide surfaces, Surf. Sci. 59 (1976) 413–429. https://doi.org/10.1016/0039-6028(76)90026-1.

[45] D.G. Brown, U. Weser, XPS Spectra of Spin-Triplet Cobalt(III) Complexes, Zeitschrift Für Naturforsch. B. 34 (1979) 1468–1470. https://doi.org/10.1515/znb-1979-1027.

[46] A. Kumar, G. Pandey, A Review on the Factors Affecting the Photocatalytic Degradation of Hazardous Materials, Mater. Sci. Eng. Int. J. 1 (2017) 106–114. https://doi.org/10.15406/mseij.2017.01.00018.

[47] M. Angeles Navarro, S. Sain, M. Wünschek, C.M. Pichler, F.J. Romero-Salguero, D. Esquivel, S. Roy, Solar driven CO_2 reduction with a molecularly engineered periodic mesoporous organosilica containing cobalt phthalocyanine, Nanoscale. (2023). https://doi.org/10.1039/D2NR06026D.

CHAPTER 7.

RESULTS AND DISCUSSION

(PAPER 4)

Chapter 7. **Solar driven CO_2 reduction with a molecularly engineered periodic mesoporous organosilica containing cobalt phthalocyanine**

PAPER 4

Solar driven CO_2 reduction with a molecularly engineered periodic mesoporous organosilica containing cobalt phthalocyanine

M. Ángeles Navarro[a,b], Sunanda Sain[b], Maximilian Wünschek[c], Christian M. Pichler[c,d] Francisco J. Romero-Salguero[a], Dolores Esquivel[*a], Souvik Roy[*b]

[a]*Departamento de Química Orgánica, Instituto Químico para la Energía y el Medioambiente (IQUEMA), Facultad de Ciencias, Universidad de Córdoba, Campus de Rabanales, 14071 Córdoba, Spain. Email: q12esmem@uco.es*

[b]*School of Chemistry, The University of Lincoln, Green Lane, Lincoln LN6 7TS, UK. Email: sroy@lincoln.ac.uk*

[c]*Institute of applied Physics, TU Vienna, Wiedner Hauptstraße 8-10, 1040 Vienna, Austria*

[d]*Centre of electrochemical and surface technology, Viktor Kaplan Straße 2, 2700 Wiener Neustadt, Austria*

Corresponding authors: Email address; q12esmem@uco.es (D.E.): sroy@lincoln.ac.uk (SR)

Paper

Solar driven CO_2 reduction with a molecularly engineered periodic mesoporous organosilica containing cobalt phthalocyanine

M. Angeles Navarro, Sunanda Sain, Maximilian Wünschek, Christian M. Pichler, Francisco J. Romero-Salguero, Dolores Esquivel and Souvik Roy

Efficient CO_2 photoreduction to CO with >70% product selectivity over a periodic mesoporous organosilica-based heterogeneous catalyst containing molecular cobalt phthalocyanine units.

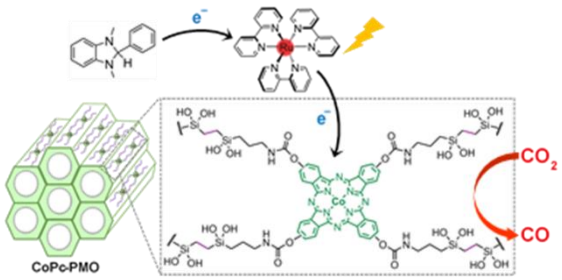

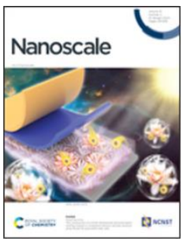

From the themed collection: Nanoscale 2023 Emerging Investigators

The article was first published on 11 Jan 2023
Nanoscale, 2023, Advance Article
https://doi.org/10.1039/D2NR06026D

ABSTRACT

A molecular cobalt phthalocyanine (CoPc) catalyst has been integrated in an ethylene-bridged periodic mesoporous organosilica (PMO) to fabricate a hybrid material, CoPc-PMO, that catalyses CO_2 reduction to CO in a photocatalytic system using $[Ru(bpy)_3]^{2+}$ (bpy = 2,2′-bipyridine) as a photosensitizer and 1,3-dimethyl-2-phenyl-2,3-dihydro-1Hbenzo[d]imidazole (BIH) as an electron donor. CoPc-PMO displays a Co-based turnover number (TON_{CO}) of >6000 for CO evolution with >70 % CO-selectivity after 4 h irradiation with UV-filtered simulated solar light, and a quantum yield of 1.95 % at 467 nm towards CO. This system demonstrates a benchmark TON_{CO} for immobilised CoPc-based catalysts towards visible light-driven CO_2 reduction.

7.1 INTRODUCTION

Climate change induced by the increasing atmospheric CO_2 levels, combined with growing global energy demand, have spurred widespread interest in developing CO_2 mitigation technology that will allow CO_2 upcycling into value-added products. To that goal, solar-driven CO_2 conversion into carbon-based energy carriers and feedstocks represents a promising strategy towards CO_2 utilisation and recycling [1]. Since the pioneering work reported by Lehn and co-workers [2] on photochemical reduction of CO_2 using Re^I complexes as photosensitizer and catalytic unit, a wide range of molecular catalysts based on transition metal complexes have been developed to mediate light-driven CO_2 conversion to C_1 feedstocks, CO and formic acid [3]. While molecular catalysts offer distinct advantages including tuneability, high product selectivity, and low overpotential, they are typically used in solution as homogeneous catalysts, which prevents catalyst recycling and often leads to decomposition via diffusional pathways [4]. Heterogenization of molecular catalysts on solid supports presents a promising strategy to circumvent these problems and combine the benefits of homogeneous and heterogeneous systems [5,6].

Cobalt phthalocyanine (CoPc) has been studied for electrocatalytic CO_2 reduction since the 1970s [7,8], and has recently attracted renewed attention due to its excellent catalytic performance upon heterogenisation on electrodes [9–11], reticular materials [12], and semiconductors [13,14]. Among them, integration of CoPc into high-surface area scaffolds with ordered micro- or meso-porosity is particularly interesting because such architecture offer high loading of accessible catalyst units. Metal organic frameworks (MOFs) and covalent organic frameworks (COFs) have been employed as scaffolds to immobilise metal phthalocyanines into their skeleton. However these systems have been targeted towards conductive frameworks for application in CO_2 electroreduction reaction (eCO2R) [15–17]. There are relatively few reports on photocatalytic CO_2

reduction using heterogenised CoPc in colloidal suspension in the presence of a separate light absorber and electron donor [13,18]. A porous support is key in such photocatalyst design to allow diffusion of different components (sensitiser, donor, and substrate) within the pores and reaction with the immobilised CoPc units.

In this context, periodic mesoporous organosilicas (PMOs) present a promising family of porous materials with well-ordered structures that have attracted great interest as a scaffold for mounting molecular catalysts [19]. These hybrid materials, synthesized from organo-bridged alkoxysilane precursors in presence of a structure-directing agent, possess ordered mesostructures with high surfaces areas, tailored hydrophocity/hydrophicity and tuneable pore sizes, making them a versatile platform for introducing molecular metal complexes for CO_2 reduction. However, their insulating character has limited their application exclusively to photocatalytic applications. Until now, the few examples of PMOs reported in literature as heterogenous catalysts for photochemical CO_2 reduction are based on anchored metal bipyridine complexes on the mesochannels or into pore walls of these materials [20–24]. First studies developed PMOs with chromophores in the framework, such as biphenyl and acridone groups [21], and Re-bipyridine complexes anchored in their mesochannels. The PMO support was used as light-harvesting antenna to enhance the photocatalytic CO_2 reduction of the ReI complex. More recently, bipyridine-bridged PMOs that allow immobilisation of metal complexes have been developed. The first pioneering study on bipyridine-PMOs for CO_2 photoreduction was reported by Inagaki et al. [22], who successfully integrated molecular Ru- and Re-bipyridine complexes as photosensitizer and catalytic units in the same framework. Following a similar approach, a precious-metal-free, Mn carbonyl bipyridine-PMO catalyst was synthesised through the immobilisation of Mn-complexes on the appended bipyridine ligands on PMO [23]. The Mn-bpy-PMO material displayed

photocatalytic CO_2 reduction activity in the presence of $Ru(bpy)_3^{2+}$ sensitiser, albeit with poor product selectivity. Both CO and formate were produced from CO_2 with Mn-based turnover numbers of 168 and 292, respectively.

Herein, we aim to integrate cobalt-phthalocyanine molecular catalysts into the pore walls of a periodic mesoporous organosilica for photocatalytic reduction of CO_2 to CO. For this, we firstly prepared a novel cobalt-phthalocyanine bridged precursor bearing four alkoxysilane groups tethered from cobalt-phthalocyanine skeleton. Then, this precursor was successfully incorporated into the ordered mesostructure of an ethylene-bridged periodic mesoporous organosilica using a one-pot synthesis via co-condensation method in the presence of octadecyltrimethylammonium bromide (OTAB) as structure-directing agent.

7.2 EXPERIMENTAL SECTION

7.2.1 Synthesis of cobalt phthalocyanine bridged periodic mesoporous organosilica material (CoPc-PMO).

CoPc-PMO material was prepared via self-assembly assisted co-condensation of the cobalt phthalocyanine bridged alkoxysilane precursor, CoPc(NCO), and conventional bis-silane precursor, BTEE (1,2-bis(triethoxysilyl)ethane) (Fig. 1) (see SI for experimental details, Scheme S1). In a general synthesis [25], octadecyltrimethylammonium bromide (OTAB) (0.85 g, 2.1 mmol) was dissolved in a basic solution of milli-Q water (53 mL) and NaOH (6M, 0.89 mL). After stirring this solution overnight at 40 °C, the mixture of organosilanes (2.04 mmol) (3 mol % CoPc(NCO) in 5 mL of ethanol and 97 % mol BTEE) was added dropwise to the reaction mixture under vigorous stirring. The resulting mixture was stirred at room temperature for 24 h and was further aged at 97 °C for 4 days under static conditions. A greenish blue powder was collected by filtration and thoroughly washed with distilled water. The

as-synthesized material (1 g) was refluxed in a solution containing 50 mL EtOH and 1 mL HCl solution (32 % wt) for 12 h to remove the surfactants from the pores. After repeating this extraction process twice, the residual solid was filtered, washed with EtOH and dried under vacuum at 80 °C to give CoPc-PMO (0.44 g).

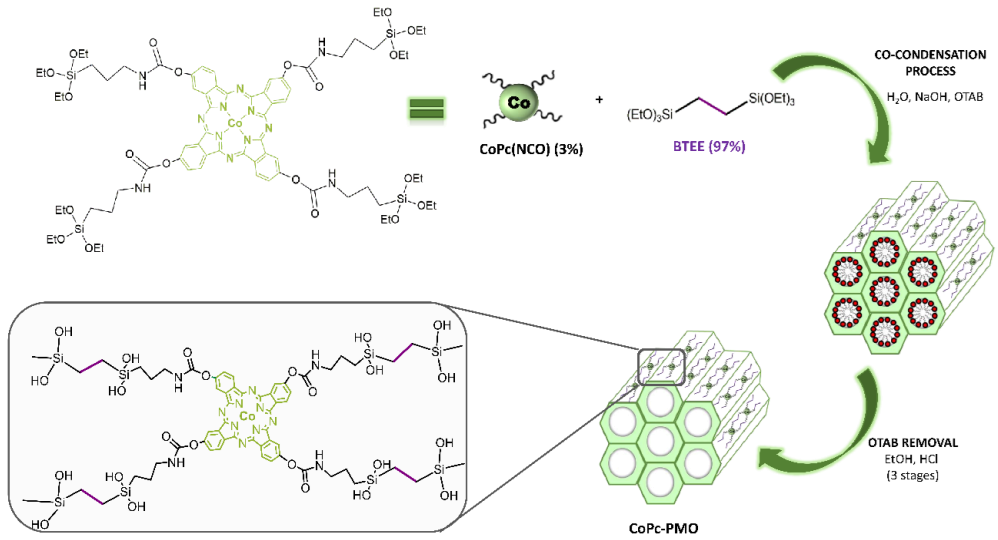

Fig. 1 Schematic illustration of the synthesis of CoPc-PMO using a molecular CoPc building block containing four alkoxysilane anchors.

7.2.2 Photocatalytic CO_2 reduction experiments

Photocatalytic experiments were carried out in a borosilicate vial (total volume 8 mL) with constant stirring under visible light irradiation using a solar light simulator (SciSun-LP-150) equipped with AM 1.5G filter and an UV cut-off filter (>400 nm). Typically, CoPc-PMO catalyst (1–3 mg) was suspended into 4:1 acetonitrile/triethanolamine mixture (4 mL) containing $Ru(bpy)_3(PF_6)_2$ (0.5 mM) and BIH (20 mM). When BIH was not present, TEOA served as the electron donor. The solution was sonicated in an ultrasonic bath for 15 min, and purged with CO_2 for 15 min. The head space above the reaction solution was sampled with a gas-tight syringe at different time intervals for product analysis using an SRI gas chromatograph.

Control experiments were performed under identical conditions without one of the components: visible light, sacrificial donor (BIH and TEOA), photosensitizer, catalyst, and CO_2. Turnover number for CO (TON_{CO}) was determined using the following equation, $TON_{CO} = n_{CO}/n_{CoPc}$ (n_{CO} = moles of CO produced per mg catalyst, n_{CoPc} = moles of CoPc present per mg catalyst). CO selectivity was calculated from the following equation, % CO = $[n_{CO}/(n_{CO}+n_{H2})]$ ×100 %.

7.2.3 Recycling tests

For the recycling experiments, the photocatalytic reaction mixture was centrifuged after 1 h irradiation, and the catalyst was washed three times with acetonitrile to remove adsorbed TEOA and $Ru(bpy)_3(PF_6)_2$. The catalyst was redispersed in fresh MeCN/TEOA solution containing $Ru(bpy)_3(PF_6)_2$ (0.5 mM) and BIH (20 mM) and irradiated under identical conditions.

7.2.4 In situ ICP analysis

Measurements were performed using an Agilent 7900 ICP-MS. The ICP-MS uses a collision cell with 5 mL/min flow of helium as cell gas. External calibration was performed with multielement standard solutions provided by Agilent and Inorganic Ventures. Downstream of the electrochemical cell the analyte was mixed with an internal standard solution containing gallium having a similar mass as cobalt. The in-house built electrochemical flow cell was made from PTFE with an opening for introducing a blue LED (465 nm, 3500 mcd light intensity). 250 µl of a CoPc-PMO suspension in acetone (concentration 20 mg mL^{-1}) was deposited on carbon paper on an area of approx. 3 mm^2, which was corresponding to irradiation area of the blue LED. As electrolyte 10 % TEOA, 90 % H_2O and 320 mg L^{-1} $Ru(bpy)_3Cl_2$, purged with CO_2 was used and pumped with

a flow of 2.4 mg s^{-1} through the measurement cell. Flow measurements were conducted for a duration of 1 h with alternating light on-off cycles of 2 min.

7.3 RESULTS AND DISCUSSION

7.3.1 Synthesis and Characterisation

The novel PMO material with cobalt phthalocyanine (CoPc) moieties integrated on the pore walls of the silica framework was synthesised by co-condensation of CoPc-bridged alkoxysilane precursor (CoPc(NCO)) and a large excess of a conventional bis-silane precursor, 1,2-bis(triethoxysilyl)ethane (BTEE) (97 %), in the presence of a cationic surfactant (Fig. 1). The surfactant was removed from the as-synthesized CoPc-PMO by solvent extraction using a mixture of aqueous HCl and ethanol to produce a pale greenish blue solid. The cobalt loading in the CoPc-PMO material was determined by ICP-MS after acid-digestion of the sample. Two materials were synthesised with Co loading of 4.6 and 2.7 µmol g^{-1}. All physical characterisation discussed below and the photocatalysis experiments were carried out using CoPc-PMO with 4.6 µmol Co g^{-1}, unless noted otherwise.

Powder X-ray diffraction (PXRD) pattern of CoPc-PMO catalyst is depicted in Fig. 2a, which displayed an intense diffraction peak at $2\theta = 1.8$ ° with a d-spacing of 49.5 Å and two broad peaks at higher incidence angles. These peaks can be indexed as (100), (110) and (200) reflections, indicative of materials with 2D-hexagonal (*p6mm*) mesostructures [26]. These findings were further confirmed by transmission electron microscopy of CoPc-PMO which showed a highly ordered structure with parallel channel pores of uniform diameter (Fig.2b).

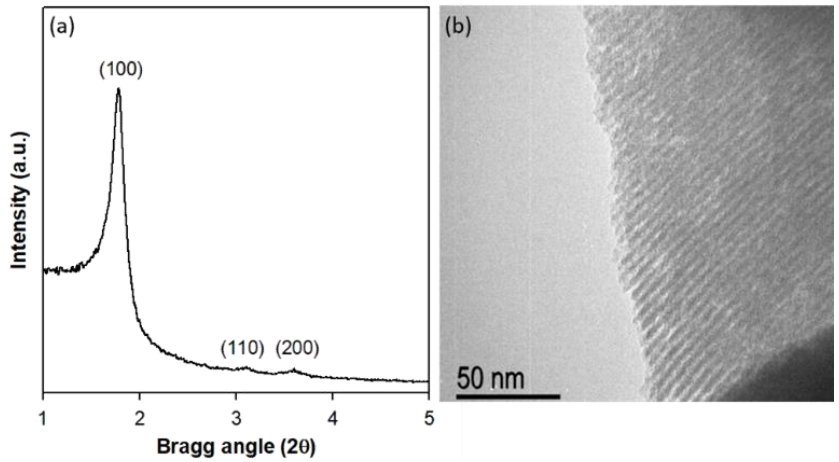

Fig. 2 Powder X-ray diffraction pattern (a) and TEM image (b) of CoPc-PMO catalyst.

Nitrogen adsorption-desorption isotherm of CoPc-PMO displayed a type-IV isotherm with a capillary step at P/P_0 = 0.4 - 0.8 (Fig. S1). The isotherm pattern is consistent with the mesoporous structure of CoPc-PMO with relatively broad pore size distributions ranging from 2 - 10 nm (Fig. S1 inset). Similar results were obtained for PMOs containing heterocyclic rings of tris[3-(trimethoxysilyl)propyl]isocyanurate in the pore walls [27,28]. The BET specific surface area of CoPc-PMO was 949 $m^2\ g^{-1}$ with BJH average pore diameter around 3.4 nm and total pore volume of 1.1 cm^3g^{-1}.

IR analyses was used to confirm the formation of CoPc(NCO) from hydroxylated CoPc-precursor [$CoPc(OH)_4$] as well as to demonstrate the successful incorporation of the CoPc building blocks into the pore walls of PMO. ATR-FTIR monitoring of the reaction between $CoPc(OH)_4$ and 3-(triethoxysilyl)propyl isocyanate showed disappearance of the -N=C=O stretching band at 2265 cm^{-1} and concurrent appearance of a new stretching vibration at 1710 cm^{-1}, consistent with formation of the carbamate linkage (Fig. S2) [29,30].

Additionally, the FT-IR spectrum of CoPc-NCO precursor (Fig. 3a) displayed the characteristic vibrational bands of the phthalocyanine skeleton at 1605, 1549, 1390 and 1093 cm^{-1} and the Co-N bond at 910 and 804 cm^{-1} [31,32]. Retention of the CoPc fingerprint IR bands in the FT-IR spectrum of CoPc-PMO confirmed the immobilisation of CoPc. Additional vibrations at ~2900 cm^{-1} in CoPc-PMO can be assigned to the C-H stretching of propyl chains of the silane precursor and the ethylene bridges [33]. The presence of molecular CoPc units in the material was further confirmed by UV-vis spectroscopy. The transmission UV-vis spectrum of $CoPc(OH)_4$ in DMF consisted of the characteristic B-band (or Soret band) at 280 nm, associated to the metal to ligand charge transfer (S0→S2), and the Q band at 674 nm, associated with the transitions from the highest occupied molecular orbital (HOMO) to the lowest unoccupied molecular orbital (LUMO) S0→S1) (Fig. 3b) [34]. Once this cobalt phthalocyanine compound was incorporated in the PMO through the corresponding CoPc(NCO) silane precursor, the resulting PMO material preserved both adsorption bands. Interestingly, a small red-shift of the Q-band maximum to ~ 695 nm was observed alongside an additional shoulder peak at ~ 640 nm, indicative of a face-to-face aggregation. The spectrum also showed peak broadening in CoPc-PMO, which have been reported in aggregated phthalocyanines and cofacially-aligned phthalocyanine aggregates on covalent organic frameworks and PMOs [35,36].

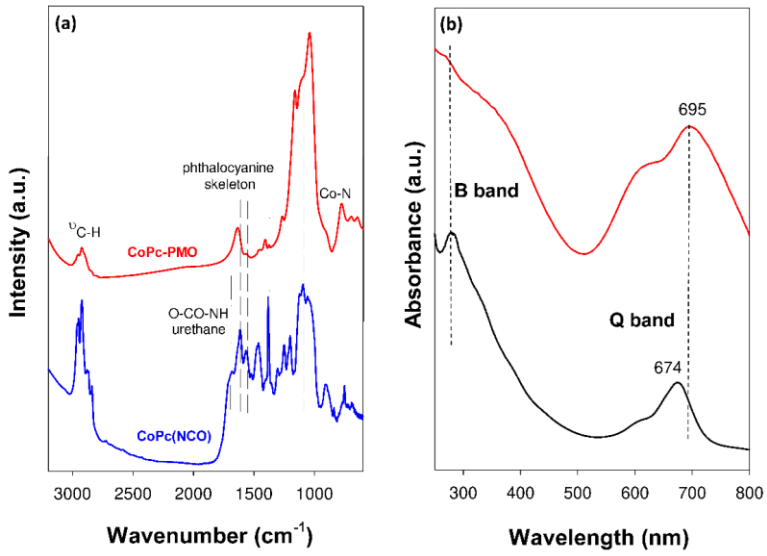

Fig. 3 (a) FT-IR spectra of CoPc(NCO) and CoPc-PMO catalyst. (b) UV-vis spectrum of $CoPc(OH)_4$ in solution (CH_3OH) (black line) and UV-vis DRS of CoPc-PMO (red line).

X-ray photoelectron spectroscopy (XPS) measurements were performed to confirm the incorporation of the phthalocyanine moieties on the material as well as the oxidation state of cobalt species on the samples. The survey spectra of $CoPc(OH)_4$ and CoPc-PMO showed the peaks of Si, C, N, O and Co (Fig. 4a). The high resolution C1s spectrum of $CoPc(OH)_4$ was fitted with four components at 284.7, 285.6, 286.5 and 288.4 eV, assigned to the carbon atoms of the aromatic rings (Car), carbon linked to hydroxyl groups (C-O), pyrrole carbons linked to nitrogen (C=N) and π-π* excitations, respectively [37]. These characteristic peaks from phthalocyanine skeleton were also observed on the C1s XPS spectrum of CoPc-PMO along with two new contributions at 285.2 and 287.5 eV for C-N and C=O bonds from urethane groups (Fig. 4b).

In the N1s region (Fig. 4c), the existence of two peaks at 398.8 and 400.2 eV for $CoPc(OH)_4$ are associated to the two types of characteristic nitrogen atoms for phthalocyanines: the central N atoms coordinated to the Co^{+2} and the aza

nitrogen atoms on the macrocycle, respectively [38]. For CoPc-PMO catalyst, these contributions were accompanied by two additional peaks for -NHCO- and C-N^+ with binding energies at 400.9 and 402.8 eV, respectively. The latter peak indicates the existence of quaternary nitrogen, which could be attributed to the remaining OTAB surfactants in pores after extraction processes [39]. The Co2p spectrum for $CoPc(OH)_4$ showed two intense peaks at 780.9 and 796.4 eV associated to electron transitions of $Co2p_{3/2}$ and $Co2p_{1/2}$, respectively, along with their shake-up satellite bands at 786.5 and 803.1 eV (Fig. 4d). These observations are consistent with the Co^{II} oxidation state. These typical characteristic peaks were also observed for CoPc-PMO sample supporting the integration of molecular CoPc units in the PMO.

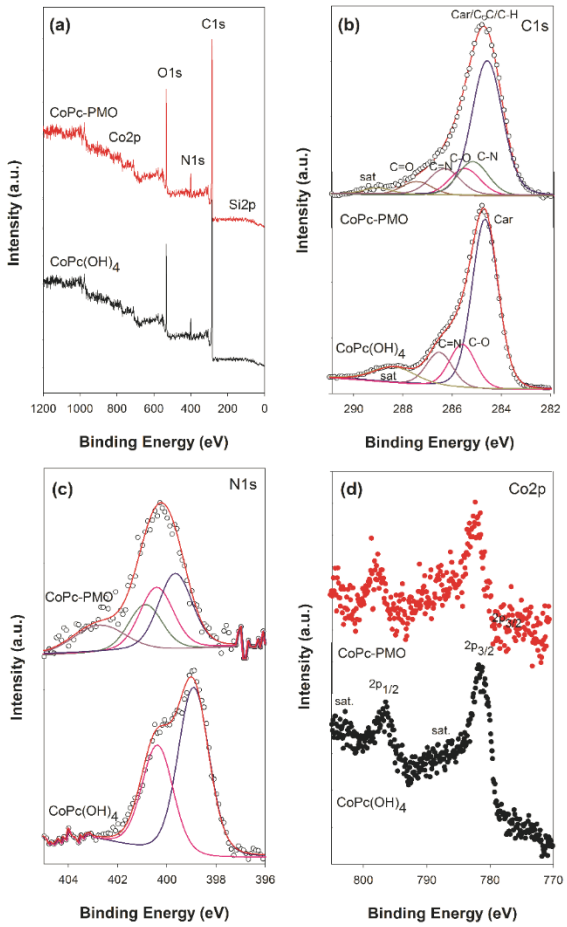

Fig. 4 (a) Survey spectra, (b) C1s, (c) N1s and (d) Co2p high-resolution XPS spectra of $CoPc(OH)_4$ and CoPc-PMO.

7.3.2 Photocatalysis studies

In a typical experiment 1 mg of CoPc-PMO was dispersed in a CH_3CN:TEOA (4:1) mixture containing $Ru(bpy)_3(PF_6)_2$ (0.5 mM), purged with CO_2 to saturate the colloidal suspension, and irradiated under non-filtered simulated solar light (100 mW cm^{-2}, AM 1.5G). Evolution of the gaseous products was monitored by analysing the headspace gas by gas chromatography. The photocatalytic reaction produced syngas with 34.1 % CO after 2 h irradiation

(entry 1, Table 1). The amount of CO evolved after 2 h was 0.58 ± 0.08 μmol per mg of catalyst, corresponding to a turnover number (TON_{CO}) of 126 ± 18 based on the initial CoPc loading. The syngas ratio dropped to ~ 25 % CO after 24 h, which was presumably caused by photodegradation of catalyst (CoPc-PMO) and/or photosensitiser $[Ru(bpy)_3]^{2+}$. The photocatalytic reaction was optimised by increasing the amount of CoPc-PMO from 1 mg to 3 mg, which showed that higher CoPc-PMO concentration in photoreactor is detrimental to the catalysis, with the TON_{CO} dropping from 126 (1 mg catalyst), to 70 (2 mg catalyst) and 60 (3 mg catalyst), albeit with slight gain in CO selectivity from 34 % (1 mg catalyst) to 43 % (3 mg catalyst) (Fig. S3). While increasing the amount of catalyst increases the number of active sites, high loading on solid catalyst can make the suspension turbid and block the light penetration [40].

The CO-selectivity of the CoPc-PMO/$Ru(bpy)_3^{2+}$ combination was relatively low (30 - 40 %) in comparison to electrocatalytic CO_2R by CoPc, which is well known for its high CO selectivity. This could be attributed to UV-light mediated photodegradation of $Ru(bpy)_3^{2+}$ [41], which is greatly enhanced by the presence of CO_2 to yield chemical species that are active towards H_2 production [42,43]. Control experiment in the absence of CoPc-PMO supports this hypothesis since a comparable amount of H_2 (1.12 μmol and 0.75 μmol H_2 in the presence and absence of CoPc-PMO, respectively, under identical conditions) and negligible CO are produced (entry 5, Table 1). To minimise photodegradation of the sensitiser, an UV cut-off filter (λ>400 nm) was employed and the photocatalysis was performed under visible light irradiation. A similar amount of CO was generated after 2 h, while the H_2 evolution was significantly suppressed leading to an improved CO selectivity of 48.1% and a TON_{CO} of 111 (entry 6, Table 1). As shown in Fig. 5a, CO evolution started to plateau around 4-6 h and a total of 1.10 ± 0.02 μmol CO was produced per mg of CoPc-PMO after 6 h, corresponding to a TON_{CO} of 233 ± 6. However, H_2 evolution continued at a

nearly constant rate during 6 h irradiation. Interestingly, under non-filtered irradiation, the CO evolution activity levelled off at ~2 h, further supporting photodegradation of the sensitiser and/or catalyst in UV light (Fig. 5a and Fig. S3).

Table 1. Photocatalytic reduction of CO_2 by CoPc-PMO upon UV-visible light irradiation for two hours[a]

Entry	**PS**	**Catalyst**	**e^- donor**	**λ range (nm)**	**CO (μmol mg^{-1})**	**H_2 (μmol mg^{-1})**	**TON_{CO}**
1	$Ru(bpy)_3^{2+}$	CoPc-PMO	TEOA	>300	0.58	1.12	126
2	$Ru(bpy)_3^{2+}$	CoPc-PMO	TEOA	dark	0	0	-
3	$Ru(bpy)_3^{2+}$	CoPc-PMO	-	>300	0	0	-
4	-	CoPc-PMO	TEOA	>300	0	0	-
5	$Ru(bpy)_3^{2+}$	-	TEOA	>300	0	0.75[d]	-
6	$Ru(bpy)_3^{2+}$	CoPc-PMO	TEOA	>400	0.51	0.55	111
7[b]	$Ru(bpy)_3^{2+}$	CoPc-PMO	BIH	>400	6.35	3.20	1377
8[c]	$Ru(bpy)_3^{2+}$	CoPc-PMO	BIH	>400	5.32	1.48	1972
9	$Ru(bpy)_3^{2+}$	-	BIH	>400	0.10[d]	0.92[d]	-
10	eosin Y	CoPc-PMO	TEOA	>400	0	0	-
11	4CzIPN	CoPc-PMO	TEOA	>400	0	0	-

[a]condition: 1 mg CoPc-PMO (4.6 μmol Co g^{-1}), 4 mL MeCN/TEOA (4:1), 0.5 mM $Ru(bpy)_3^{2+}$, 2 h irradiation under UV-visible light; [b][BIH] = 10 mM; [c]CoPc-PMO with a Co loading of 2.7 μmol g^{-1}; [d]total H_2/CO in the headspace after 2 h

The TON_{CO} values obtained for CoPc-PMO are comparable to those reported for other supported CoPc-based materials tested under similar photocatalytic conditions [14]. In control experiments without $Ru(bpy)_3^{2+}$, TEOA, CO_2, and light (Table 1), CO was not detected by GC, confirming CO_2 as the source of CO. Substituting $Ru(bpy)_3^{2+}$ with two other molecular organic

sensitisers, eosin Y and 4CzIPN, led to zero photocatalytic activity (entry 10 and 11, Table 1). This indicates that CoPc-PMO is not a stand-alone photocatalyst for CO_2R and it is only active when Ru-sensitiser is used. The photoexcited states of the alternative organic sensitisers might not be sufficiently reducing to mediate the CO_2 reduction catalysis. Photostability of CoPc-PMO was probed using in situ ICP MS analysis under continuous flow. CoPc-PMO was deposited on carbon paper and mounted in an in situ flow cell while the photocatalysis solution (CO_2 saturated aqueous solution containing 0.5 mM $Ru(bpy)_3Cl_2$ and 10 % TEOA) was constantly passed through the cell and fed into the ICP-MS at a flow rate of 2.4 mg s^{-1}. Carbon paper is a suitable support that prevents physical detachment of the catalyst powder and ensures that the Co detected is derived only from chemical leaching and/or photocorrosion. A blue LED was mounted in the flow cell to directly irradiate the catalyst coated carbon paper, and by alternating on/off cycles of 2 minutes, it can be determined if light irradiation has any influence on the Co leaching from the material. As shown in Figure 5e, the Co signal of the ICP-MS is low and close to the baseline, indicating that the loss of Co through leaching is minimal. More importantly, the presence of light has no influence on the degree of Co leaching. If significant photo-induced Co leaching would be occurring, it would be expected that the Co counts in the ICP-MS would rise during the "light on" phases. However, the Co signal remained steady throughout the light on/off cycles, demonstrating good photostability of CoPc-PMO material.

The Co loss observed during longer measurement times can be attributed to the accumulation of the very low baseline Co leaching observed in the 1 h experiment.

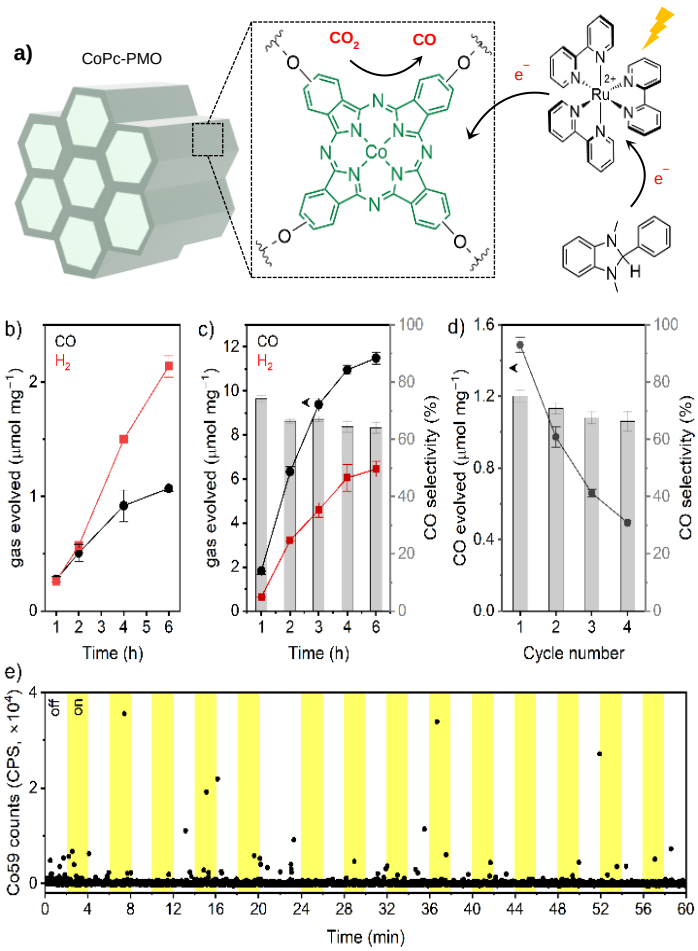

Fig. 5 (a) Proposed photocatalytic reaction scheme for CO_2 reduction (b) Time course for photocatalytic CO and H_2 evolution by CoPc-PMO in the presence of $Ru(bpy)_3^{2+}$ as sensitiser and TEOA as donor. Condition: CO_2-saturated 4:1 MeCN/TEOA, ~ 1 mg CoPc-PMO (Co loading 4.6 μmol mg^{-1}), 0.5 mM $[Ru(bpy)_3]^{2+}$, and visible light irradiation (100 mW cm^{-2}, AM 1.5G, λ > 400 nm. (c) CO and H_2 evolution trace when BIH (10 mM) was used as the donor. The CO selectivity is shown as a bar plot. Reaction conditions are same as (b). (d) CO evolved during four 1-hour recycling runs with CoPc-PMO (≈ 4 mg) is plotted as black trace and the grey bar plot shows the CO selectivity (%). (e) Cobalt ICP-MS signal in solution during chopped irradiation of CoPc-PMO under continuous flow of CO_2 saturated photocatalysis solution. Condition: 5 mg

CoPc-PMO deposited on carbon paper, 0.5 mM $[Ru(bpy)_3]^{2+}$ solution in aqueous 10 % TEOA, blue LED, 2 min light/dark cycle.

After the promising results with TEOA as the sacrificial donor, we investigated whether the photocatalytic activity of CoPc-PMO could be further improved by using BIH (1,3-dimethyl-2-phenyl-2,3-dihydro-1H-benzo[d]-imidazole) as a donor to supplement TEOA. Photocatalysis was performed in CO_2 saturated acetonitrile/TEOA mixture (4:1 v/v) in the presence of $[Ru(bpy)_3]^{2+}$ (0.5 mM) and BIH (10 mM) under visible light irradiation. As shown in Fig. 5c, addition of BIH led to much improved catalytic performance with evolution of 6.35 ± 0.22 μmol CO mg^{-1} after 2 h irradiation at (66.5 ± 0.7) % CO-selectivity (entry 7, Table 1). The total amount of CO produced after 6 h was 11.5 ± 0.3 μmol CO mg^{-1} (average rate ~1.9 μmol CO mg^{-1} h^{-1}), corresponding to a Co-based TON_{CO} of 2478 ± 41, which is an order of magnitude higher than analogous CoPc-based photocatalysts reported in literature. For comparison, photocatalysts with CoPc-based catalysts supported on C_3N_4 (carbon nitride) and TiO_2 have shown Co-based TON_{CO} of 10 - 100 with the CO evolution rates ranging from 0.01 to 0.25 μmol CO mg^{-1} h^{-1}, under similar reaction conditions [14,32]. The CO-selectivity of CoPc-PMO system dropped slightly after the first hour, but it remained approximately constant afterwards at ~ 65 % (Fig. 5c). Control experiment without CoPc-PMO showed generation of trace amount of CO (entry 9, Table 1).

Interestingly, lowering the CoPc loading in the material from 4.6 μmol g^{-1} to 2.7 μmol g^{-1} led to a superior activity towards CO evolution with a formation of 16.32 ± 1.36 μmol CO mg^{-1} at 72 % CO selectivity after 4 h visible light irradiation (Fig. S4, entry 8, Table 1). This corresponds to an average TOF_{CO} (turnover frequency) of 1511 ± 123 h^{-1} over the course of 4 h. After overnight irradiation (15 h), the CO evolution ceased and a TON_{CO} of 6836 ± 112 was

obtained, which represents the total CoPc turnovers for the system before complete catalyst deactivation. Notably, an excellent CO selectivity of ~ 84 % was observed during the first hour of photocatalysis (CO yield 1.74 ± 0.07 μmol h^{-1} mg^{-1}), which gradually decreased as H_2 evolution rate was enhanced from Ru-sensitiser-derived by-products. The quantum yield (QY) for CO evolution by CoPc-PMO was determined to be (1.95 ± 0.08) % at 467 nm irradiation (blue LED), by the ferrioxalate actinometer method (Fig. S5 and S6).

Heterogenous nature of the CoPc-PMO catalyst was studied by four 1 h recycling experiments which showed a steady loss of CO evolution activity after each run (Fig. 5d). However, the CO-selectivity was maintained at ~ 65 % throughout all four cycles, suggesting that the lower CO evolution is caused by loss active catalytic centres by Co^{2+} leaching (Fig. 5d). The degradation products in solution promotes H_2 evolution and therefore, upon recycling the solid catalyst the CO selectivity remained unchanged. The loss of Co^{2+} was confirmed by ICP analysis which showed a Co loading of 0.0021 mmol g^{-1} after four recycling runs, corresponding to a loss of 53 % Co. Recycling experiments performed without BIH displayed similar trend albeit with a lower yield and selectivity towards CO (Fig. S7). Post catalysis characterisation of CoPc-PMO by PXRD and TEM showed retention of its inherent hexagonal mesostructure (Fig S8). FT-IR spectrum of CoPc-PMO after four catalytic cycles showed vibration bands characteristic of phthalocyanine rings (Fig. S9). However, UV-vis spectrum of the material after photocatalysis was dominated by adsorbed $Ru(bpy)_3^{2+}$ species which masked the potential peaks for CoPc (Fig S10).

From a mechanistic perspective, the reaction is initiated by photoexcitation of $Ru(bpy)_3^{2+}$ to the triplet state which is reductively quenched by BIH to generate $[Ru(bpy)_2(bpy^{\bullet -})]^+$ [44]. The oxidised BIH is deprotonated by TEOA, yielding strongly reducing BI• species that reduces $Ru(bpy)_3^{2+}$ to generate

a second $[Ru(bpy)_2(bpy^{\bullet -})]^+$ species. Two equivalents of reduced sensitisers subsequently reduce CoPc-PMO to ($CoPc^{2-}$)-PMO that can mediate CO_2 to CO conversion [45].

7.4 CONCLUSIONS

In summary, we have reported highly efficient and selective photocatalytic CO_2 reduction by a robust Co-phthalocyanine-PMO catalyst. Under visible light irradiation and in the presence of $Ru(bpy)_3^{2+}$ sensitiser and BIH donor, CoPc-PMO material shows a Co-based TON_{CO} of ~ 6800 for CO evolution and an average TOF_{CO} of ~1500 h^{-1} over the course of 4 h; these are among the highest values reported for supported non-precious metal-based molecular catalysts and compares favourably to previously reported PMO-based material containing molecular Mn-catalyst. Furthermore, this work provides a rare example of directly integrating a CO_2 reduction catalyst into PMO by a co-condensation method and provides a versatile platform for heterogenisation of molecular catalysts on inorganic porous matrices

7.5 REFERENCES

[1] K. Li, B. Peng, T. Peng, Recent Advances in Heterogeneous Photocatalytic CO_2 Conversion to Solar Fuels, ACS Catal. 6 (2016) 7485–7527. https://doi.org/10.1021/acscatal.6b02089.

[2] J. Hawecker, J.-M. Lehn, R. Ziessel, Efficient photochemical reduction of CO_2 to CO by visible light irradiation of systems containing $Re(bipy)(CO)_3X$ or $Ru(bipy)_3^{2+}$–Co^{2+} combinations as homogeneous catalysts, J. Chem. Soc., Chem. Commun. (1983) 536–538. https://doi.org/10.1039/C39830000536.

[3] E.E. Benson, C.P. Kubiak, A.J. Sathrum, J.M. Smieja, Electrocatalytic and homogeneous approaches to conversion of CO_2 to liquid fuels, Chem. Soc. Rev. 38 (2009) 89–99. https://doi.org/10.1039/B804323J.

[4] C.D. Windle, E. Reisner, Heterogenised Molecular Catalysts for the Reduction of CO_2 to Fuels, Chimia (Aarau). 69 (2015) 435. https://doi.org/10.2533/chimia.2015.435.

[5] A. Perazio, G. Lowe, R. Gobetto, J. Bonin, M. Robert, Light-driven catalytic conversion of CO_2 with heterogenized molecular catalysts based on fourth period transition metals, Coord. Chem. Rev. 443 (2021) 214018. https://doi.org/10.1016/j.ccr.2021.214018.

[6] X. Liu, S. Inagaki, J. Gong, Heterogeneous Molecular Systems for Photocatalytic CO_2 Reduction with Water Oxidation, Angew. Chemie Int. Ed. 55 (2016) 14924–14950. https://doi.org/10.1002/anie.201600395.

[7] C.M. Lieber, N.S. Lewis, Catalytic reduction of carbon dioxide at carbon electrodes modified with cobalt phthalocyanine, J. Am. Chem. Soc. 106 (1984) 5033–5034. https://doi.org/10.1021/ja00329a082.

[8] S. Meshitsuka, M. Ichikawa, K. Tamaru, Electrocatalysis by metal phthalocyanines in the reduction of carbon dioxide, J. Chem. Soc. Chem. Commun. (1974) 158. https://doi.org/10.1039/c39740000158.

[9] N. Han, Y. Wang, L. Ma, J. Wen, J. Li, H. Zheng, K. Nie, X. Wang, F. Zhao, Y. Li, J. Fan, J. Zhong, T. Wu, D.J. Miller, J. Lu, S.-T. Lee, Y. Li, Supported Cobalt Polyphthalocyanine for High-Performance Electrocatalytic CO_2 Reduction, Chem. 3 (2017) 652–664. https://doi.org/10.1016/j.chempr.2017.08.002.

[10] M. Wang, K. Torbensen, D. Salvatore, S. Ren, D. Joulié, F. Dumoulin, D. Mendoza, B. Lassalle-Kaiser, U. Işci, C.P. Berlinguette, M. Robert, CO_2 electrochemical catalytic reduction with a highly active cobalt phthalocyanine, Nat. Commun. 10 (2019) 3602. https://doi.org/10.1038/s41467-019-11542-w.

[11] S. Ren, D. Joulié, D. Salvatore, K. Torbensen, M. Wang, M. Robert, C.P. Berlinguette, Molecular electrocatalysts can mediate fast, selective CO_2 reduction in a flow cell, Science. 365 (2019) 367–369. https://doi.org/10.1126/science.aax4608.

[12] N. Huang, K.H. Lee, Y. Yue, X. Xu, S. Irle, Q. Jiang, D. Jiang, A Stable and Conductive Metallophthalocyanine Framework for Electrocatalytic Carbon Dioxide Reduction in Water, Angew. Chemie Int. Ed. 59 (2020) 16587–16593. https://doi.org/10.1002/anie.202005274.

[13] S. Roy, E. Reisner, Visible-Light-Driven CO_2 Reduction by Mesoporous Carbon Nitride Modified with Polymeric Cobalt Phthalocyanine, Angew. Chemie Int. Ed. 58 (2019) 12180–12184. https://doi.org/10.1002/anie.201907082.

[14] H. Li, W. Xu, J. Qian, T.-T. Li, Construction of a polymeric cobalt phthalocyanine@mesoporous graphitic carbon nitride composite for efficient photocatalytic CO_2 reduction, Chem. Commun. 57 (2021) 6987–6990. https://doi.org/10.1039/D1CC02468J.

[15] J. Yi, D. Si, R. Xie, Q. Yin, M. Zhang, Q. Wu, G. Chai, Y. Huang, R. Cao, Conductive Two-Dimensional Phthalocyanine-based Metal–Organic Framework Nanosheets for Efficient Electroreduction of CO_2, Angew. Chemie Int. Ed. 60 (2021) 17108–17114. https://doi.org/10.1002/anie.202104564.

[16] M. Lu, M. Zhang, C. Liu, J. Liu, L. Shang, M. Wang, J. Chang, S. Li, Y. Lan, Stable Dioxin-Linked Metallophthalocyanine Covalent Organic Frameworks (COFs) as Photo-Coupled Electrocatalysts for CO_2 Reduction, Angew. Chemie Int. Ed. 60 (2021) 4864–4871. https://doi.org/10.1002/anie.202011722.

[17] B. Han, X. Ding, B. Yu, H. Wu, W. Zhou, W. Liu, C. Wei, B. Chen, D. Qi, H. Wang, K. Wang, Y. Chen, B. Chen, J. Jiang, Two-Dimensional Covalent Organic Frameworks with Cobalt(II)-Phthalocyanine Sites for Efficient Electrocatalytic Carbon Dioxide Reduction, J. Am. Chem. Soc. 143 (2021) 7104–7113. https://doi.org/10.1021/jacs.1c02145.

[18] T. Dhanasekaran, J. Grodkowski, P. Neta, P. Hambright, E. Fujita, p -Terphenyl-Sensitized Photoreduction of CO_2 with Cobalt and Iron Porphyrins. Interaction between CO and Reduced Metalloporphyrins, J. Phys. Chem. A. 103 (1999) 7742–7748. https://doi.org/10.1021/jp991423u.

[19] P. Van Der Voort, D. Esquivel, E. De Canck, F. Goethals, I. Van Driessche, F.J. Romero-Salguero, Periodic Mesoporous Organosilicas: from simple to complex bridges; a comprehensive overview of functions, morphologies and applications, Chem. Soc. Rev. 42 (2013) 3913–3955. https://doi.org/10.1039/C2CS35222B.

[20] H. Takeda, M. Ohashi, T. Tani, O. Ishitani, S. Inagaki, Enhanced Photocatalysis of Rhenium(I) Complex by Light-Harvesting Periodic Mesoporous Organosilica, Inorg. Chem. 49 (2010) 4554–4559. https://doi.org/10.1021/ic1000914.

[21] Y. Ueda, H. Takeda, T. Yui, K. Koike, Y. Goto, S. Inagaki, O. Ishitani, A Visible-Light Harvesting System for CO_2 Reduction Using a Ru^{II}-Re^{I} Photocatalyst Adsorbed in Mesoporous Organosilica, ChemSusChem. 8 (2015) 439–442. https://doi.org/10.1002/cssc.201403194.

[22] Y. Kuramochi, M. Sekine, K. Kitamura, Y. Maegawa, Y. Goto, S. Shirai, S. Inagaki, H. Ishida, Photocatalytic CO_2 Reduction by Periodic Mesoporous Organosilica (PMO) Containing Two Different Ruthenium Complexes as Photosensitizing and Catalytic Sites, Chem. – A Eur. J. 23 (2017) 10301–10309. https://doi.org/10.1002/chem.201701466.

[23] X. Wang, I. Thiel, A. Fedorov, C. Copéret, V. Mougel, M. Fontecave, Site-isolated manganese carbonyl on bipyridine-functionalities of periodic mesoporous organosilicas: efficient CO_2 photoreduction and detection of key reaction intermediates, Chem. Sci. 8 (2017) 8204–8213. https://doi.org/10.1039/C7SC03512H.

[24] M. Waki, K. Yamanaka, S. Shirai, Y. Maegawa, Y. Goto, Y. Yamada, S. Inagaki, $Re(bpy)(CO)_3Cl$ Immobilized on Bipyridine-Periodic Mesoporous Organosilica for Photocatalytic CO_2 Reduction, Chem. – A Eur. J. 24 (2018) 3846–3853. https://doi.org/10.1002/chem.201705792.

[25] M. Waki, N. Mizoshita, T. Tani, S. Inagaki, Periodic mesoporous organosilica derivatives bearing a high density of metal complexes on pore surfaces, Angew. Chemie-International Ed. 50 (2011) 11667–11671. https://doi.org/10.1002/anie.201104063.

[26] M.Á. Navarro, D. Cosano, A. Bhunia, L. Simonelli, V. Martin-Diaconescu, F.J. Romero-Salguero, D. Esquivel, Cobaloxime tethered pyridine-functionalized ethylene-bridged periodic mesoporous organosilica as an efficient HER catalyst, Sustain. Energy Fuels. 6 (2022) 398–407. https://doi.org/10.1039/D1SE01437D.

[27] M.G. Dekamin, E. Arefi, A. Yaghoubi, Isocyanurate-based periodic mesoporous organosilica (PMO-ICS): a highly efficient and recoverable nanocatalyst for the one-pot synthesis of substituted imidazoles and benzimidazoles, RSC Adv. 6 (2016) 86982–86988. https://doi.org/10.1039/C6RA14550G.

[28] A. Yaghoubi, M.G. Dekamin, E. Arefi, B. Karimi, Propylsulfonic acid-anchored isocyanurate-based periodic mesoporous organosilica (PMO-ICS-Pr-SO_3H): A new and highly efficient recoverable nanoporous catalyst for the one-pot synthesis of bis(indolyl)methane derivatives, J. Colloid Interface Sci. 505 (2017) 956–963. https://doi.org/10.1016/j.jcis.2017.06.055.

[29] A. Corma, D. Das, H. García, A. Leyva, A periodic mesoporous organosilica containing a carbapalladacycle complex as heterogeneous catalyst for Suzuki cross-coupling, J. Catal. 229 (2005) 322–331. https://doi.org/10.1016/j.jcat.2004.11.006.

[30] J. Amaro-Gahete, D. Esquivel, M. V. Pavliuk, C. Jiménez-Sanchidrián, H. Tian, S. Ott, F.J. Romero-Salguero, Hydroxyl-Decorated Diiron Complex as a [FeFe]-Hydrogenase Active Site Model Complex: Light-Driven Photocatalytic Activity and Heterogenization on Ethylene-Bridged Periodic Mesoporous Organosilica, Catalysts. 12 (2022) 254. https://doi.org/10.3390/catal12030254.

[31] D. Verma, R. Dash, K.S. Katti, D.L. Schulz, A.N. Caruso, Role of coordinated metal ions on the orientation of phthalocyanine based coatings, Spectrochim. Acta Part A Mol. Biomol. Spectrosc. 70 (2008) 1180–1186. https://doi.org/10.1016/j.saa.2007.10.050.

[32] G. Liu, Y. Wang, Y. Zhou, J. Cao, M. Yuan, H. Lv, Phosphorous doped g-C_3N_4 supported cobalt phthalocyanine: An efficient photocatalyst for reduction of CO_2 under visible-light irradiation, J. Colloid Interface Sci. 594 (2021) 658–668. https://doi.org/10.1016/j.jcis.2021.02.005.

[33] M.Á. Navarro, J. Amaro-Gahete, J.R. Ruiz, C. Jiménez-Sanchidrián, F.J. Romero-Salguero, D. Esquivel, Copper-complexed dipyridyl-pyridazine functionalized periodic mesoporous organosilica as a heterogeneous catalyst for styrene epoxidation, Dalt. Trans. 51 (2022) 4884–4897. https://doi.org/10.1039/D2DT00018K.

[34] C.G. Claessens, U. Hahn, T. Torres, Phthalocyanines: From outstanding electronic properties to emerging applications, Chem. Rec. 8 (2008) 75–97. https://doi.org/10.1002/tcr.20139.

[35] E.L. Spitler, W.R. Dichtel, Lewis acid-catalysed formation of two-dimensional phthalocyanine covalent organic frameworks, Nat. Chem. 2 (2010) 672–677. https://doi.org/10.1038/nchem.695.

[36] F. Auras, Y. Li, F. Löbermann, M. Döblinger, J. Schuster, L.M. Peter, D. Trauner, T. Bein, A Zinc Phthalocyanine Based Periodic Mesoporous Organosilica Exhibiting Charge Transfer to Fullerenes, Chem. - A Eur. J. 20 (2014) 14971–14975. https://doi.org/10.1002/chem.201404169.

[37] V. V. Maslyuk, V.Y. Aristov, O. V. Molodtsova, D. V. Vyalikh, V.M. Zhilin, Y.A. Ossipyan, T. Bredow, I. Mertig, M. Knupfer, The electronic structure of cobalt phthalocyanine, Appl. Phys. A. 94 (2009) 485–489. https://doi.org/10.1007/s00339-008-4922-3.

[38] K. Müller, M. Richter, D. Friedrich, I. Paloumpa, U.I. Kramm, D. Schmeißer, Spectroscopic characterization of Cobalt-Phthalocyanine electrocatalysts for fuel cell applications, Solid State Ionics. 216 (2012) 78–82. https://doi.org/10.1016/j.ssi.2011.12.013.

[39] X. Li, Y. Tang, L. Liu, Y. Zhang, R. Sheng, Y. NuLi, Ti_3C_2 MXene with pillared structure for hybrid magnesium-lithium batteries cathode material with long cycle life and high rate capability, J. Colloid Interface Sci. 608 (2022) 2455–2462. https://doi.org/10.1016/j.jcis.2021.10.175.

[40] A. Kumar, A Review on the Factors Affecting the Photocatalytic Degradation of Hazardous Materials, Mater. Sci. Eng. Int. J. 1 (2017). https://doi.org/10.15406/mseij.2017.01.00018.

[41] A. Call, M. Cibian, K. Yamamoto, T. Nakazono, K. Yamauchi, K. Sakai, Highly Efficient and Selective Photocatalytic CO_2 Reduction to CO in Water by a Cobalt Porphyrin Molecular Catalyst, ACS Catal. 9 (2019) 4867–4874. https://doi.org/10.1021/acscatal.8b04975.

[42] J. Hawecker, JM.Lehn, R. Ziessel, Efficient homogeneous photochemical hydrogen generation and water reduction mediated by cobaloxime or macrocyclic cobalt complexes, Nouv. J. Chim. 7 (1983) 271–277. https://doi.org/10.1002/CHIN.198340125.

[43] J.L. Grant, K. Goswami, L.O. Spreer, J.W. Otvos, M. Calvin, Photochemical reduction of carbon dioxide to carbon monoxide in water using a nickel (II) tetra-azamacrocycle complex as catalyst, J. Chem. Soc. Dalt. Trans. (1987) 2105–2109. https://doi.org/10.1039/dt9870002105.

[44] D. Hong, Y. Tsukakoshi, H. Kotani, T. Ishizuka, T. Kojima, Visible-Light-Driven Photocatalytic CO_2 Reduction by a Ni (II) Complex Bearing a Bioinspired Tetradentate Ligand for Selective CO Production, J. Am. Chem. Soc. 139 (2017) 6538–6541. https://doi.org/10.1021/jacs.7b01956.

[45] M. Zhu, R. Ye, K. Jin, N. Lazouski, K. Manthiram, Elucidating the Reactivity and Mechanism of CO_2 Electroreduction at Highly Dispersed Cobalt Phthalocyanine, ACS Energy Lett. 3 (2018) 1381–1386. https://doi.org/10.1021/acsenergylett.8b00519.

Supplementary Information

Solar driven CO_2 reduction with a molecularly engineered periodic mesoporous organosilica containing cobalt phthalocyanine

M. Angeles Navarro[a,b], Sunanda Sain[b], Maximilian Wünschek[c], Christian M. Pichler[c,d], Francisco J. Romero-Salguero[a], Dolores Esquivel*[a], Souvik Roy*[b]

[a] Departamento de Química Orgánica, Instituto Químico para la Energía y el Medioambiente (IQUEMA), Facultad de Ciencias, Universidad de Córdoba, Campus de Rabanales, 14071 Córdoba, Spain. Email: q12esmem@uco.es

[b] School of Chemistry, University of Lincoln, Green Lane, Lincoln, LN6 7TS, UK. Email: sroy@lincoln.ac.uk

[c] Institute of Applied Physics, TU Vienna, Wiedner Hauptstraße 8-10, 1040 Vienna, Austria

[d] Centre of electrochemical and surface technology, Viktor Kaplan Straße 2, 2700 Wiener Neustadt, Austria

General Methods and Instrumentation

All chemicals were purchased from commercial suppliers (Fluorochem, Merck and PanReac) and used without further purification. X-ray powder diffraction (XRD) patters were collected in a Bruker D8 Discover A25 diffractometer using Cu Kα radiation (40 kV and 30 mA) from 0.5 to 5.0 (2θ). Transmission electron microscopy images were obtained using a JEOL JEM 1400 microscope, operating at 300 kV. For TEM measurements, isopropanol solutions of the samples were drop-casted on carbon-coated microgrids (Holey Carbon Film 200) and then dried. N_2 adsorption-desorption isotherms were obtained at – 196 °C using Micromeritics ASAP 2020 V4.04J instrument. Prior to measurement, the sample was outgassed overnight at 100 °C. Surface area and pore size distribution were calculated using the Brunauer-Emmett-Teller (BET) and Barrett-Joyner-Halenda (BJH) methods, respectively. ATR- and FT-IR measurements were carried out on a Perkin-Elmer 2000 FTIR spectrometer. UV-Vis spectra were recorded on a UV-visible diffuse reflectance spectrophotometer Varian Carey IE UV-vis equipped with a 60 mm integration sphere. X-ray photoelectron spectroscopy (XPS) was performed on a SPECS Phoibos HAS 3500 150 MCD X-ray photoelectron spectrometer with a monochromatic Al anode (1486.7 eV). Accurate binding energies were determined with respect to the position of C 1s peak at 284.4 eV. The charge neutralization function was employed during the measurement to compensate for accumulated charge in solid samples by X-ray irradiation. Inductively coupled plasma mass spectrometry (ICP-MS) for the isotope ^{59}Co was performed using a NexION 350X spectrometer. Prior to the measurement, the sample was digested in an UltraWave microwave system. Photocatalysis experiments were performed using a SciSun-LP-150 solar simulator from ScienceTech, equipped with an air mass 1.5 global filter (AM 1.5G) and a UV-filter (> 400 nm) unless mentioned otherwise. The quantification of H_2 and CO was conducted using an SRI gas

chromatograph (multiple gas analyser #1) equipped with a thermal conductivity detector (TCD) and a flame ionisation detector (FID) with a built-in methaniser attachment. A silica gel column (6 ft) column was used to block CO_2 and H_2O, and molecular sieve 13X (6 ft) main column was used to separate H_2 and CO. N_2 was used as the carrier gas at 23 psi pressure. The GC was calibrated regularly using a known standard for H_2, CO and CH_4 (2000 ppm H_2 / 2000 ppm CO / 2000 ppm CH_4 in balance gas N_2). A representative gas chromatogram obtained during photocatalysis is shown in Fig. S11.

Synthetic procedures

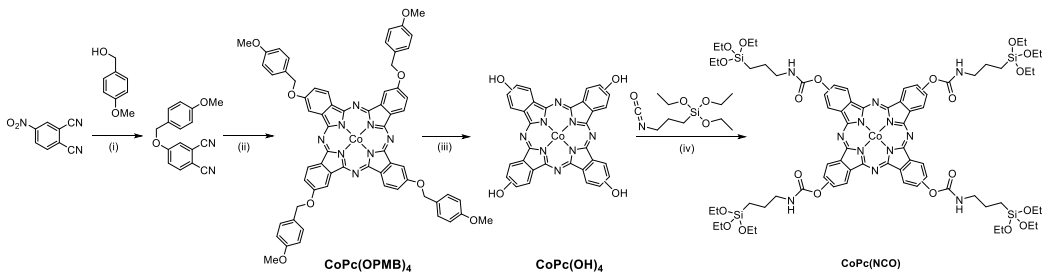

Scheme S1. Synthesis of CoPc(NCO) complex : (i) K_2CO_3, DMSO, 50 °C, 16 h; (ii) $Co(OAc)_2$, DBU, 1-pentanol, 160 °C, 16 h, N_2; (iii) TFA, CH_2Cl_2, r.t., 3h; (iv) acetone, r.t., 3 days, N_2.

Synthesis of cobalt phthalocyanine bridged alkoxysilane precursor (CoPc (NCO)).

The synthesis of CoPc(NCO) is shown in Scheme S1. 4-((4-Methoxybenzyl)oxy)phthalonitrile was synthesised from 4-nitrophthalonitrile following published procedure [1].

CoPc(OPMB)$_4$: 4-((4-Methoxybenzyl)oxy)phthalonitrile (1.30 g, 5 mmol) was suspended in 1-pentanol (30 mL) in a three-necked round bottom flask, purged with N_2 for 30 min and stirred for 10 min. $Co(OAc)_2.4H_2O$ (2 mmol) and 1,8-diazabicyclo[5.4.0]undec-7-ene (DBU, 2 mmol) was added to the reaction flask under N_2 and the reaction mixture was heated at 160 °C for 16 h. After cooling to room temperature, CH_3OH (20 mL) was added to the reaction mixture and the precipitated solid was collected by filtration. The solid was extracted with CH_2Cl_2 and concentrated under reduced pressure to give a dark blue solid. The solid was dissolved in 15-20 mL CH_2Cl_2 and poured over ~ 50 mL ether. The dark solid was collected by filtration and washed sequentially with water, 0.1 M HCl, water, methanol, and acetone/methanol mixture (1:1) to give CoPc(OPMB)$_4$ as a dark blue solid. Yield: 0.6 g (43%). ESI-MS (+): m/z calculated for $C_{64}H_{48}CoN_8O_8^+$ 1115.2327, found 1115.2930. UV-vis, λ_{max} (nm) (ε, M^{-1} cm^{-1}) (DMF): 330 (5.5×10^4), 672 (7.8×10^4). ATR-IR (cm^{-1}): 1609, 1530, 1458, 1407, 1376, 1340, 1237, 1173, 1096, 1029 (br), 811, 750.

CoPc(OH)$_4$: CoPc(OPMB)$_4$ (550 mg, 0.5 mmol) was dissolved in CH_2Cl_2 (20 mL) followed by addition of trifluoroacetic acid (TFA, 6 mL) under stirring. After 3 h, the solvent was removed under reduced pressure and the residue was washed thoroughly with water and ether till washings were colourless. The crude solid was dissolved in CH_3OH (50 mL), filtered, and concentrated under reduced pressure to 5 - 10 mL. The dark blue solution was poured over ether to yield a dark blue solid. The product **CoPc(OH)$_4$** was collected by filtration and washed with ether. Yield: 0.15 g (47 %). ESI-MS (+): m/z calculated for $C_{32}H_{16}CoN_8O_4^+$ 635.0626, found 635.0655. UV-vis, λ_{max} (nm) (ε, M^{-1} cm^{-1}) (DMF): 680 (6.7×10^4). ATR-IR (cm^{-1}): 3177 (br), 1590, 1480, 1394, 1299, 1250, 1186, 1068 (br), 870 (w), 830, 751.

CoPc(NCO): CoPc(OH)$_4$ (100 mg, 0.157 mmol) was dissolved in 20 mL of anhydrous acetone under N_2 atmosphere. The green dark solution was stirred at

room temperature during 30 min. Afterwards, 3-(triethoxysilyl)propyl isocyanate (0.165 mL, 0.628 mmol) was slowly added dropwise to the solution under N_2 atmosphere, and it was kept under stirring at room temperature for 3 days. The reaction was monitored through the disappearance of the isocyanate vibration band ($\nu_{N=C=O}$ 2265 cm^{-1}) together with the appearance of the urethane band ($\nu_{C=O\ urethane}$ 1710 cm^{-1}) by ATR-FTIR spectroscopy (Fig. S2).

BIH Synthesis.[2] To a solution of 2-phenylbenzimidazole (4 g, 20 mmol) and NaOH (1 g, 25 mmol) in absolute MeOH (120 mL), methyl iodide (17.6 mL, 282.7 mmol) was added slowly. The mixture was heated overnight (16 h) at 110 °C in a pressure tube. After cooling the reaction mixture, the solvent was removed under reduced pressure and the crude product was washed with a small amount of acetone. Recrystallisation from absolute ethanol yielded pale yellow crystals of 1,3-dimethyl-2-phenylbenzo[d]imidazolium iodide (3.5 g). ^{1}H NMR (methanol-d_4): δ = 8.01 (m, 2H), 7.77-7.87 (m, 7H), 3.97 (s, 6H).

The methylated phenylbenzimidazol salt (2.1 g, 6 mmol) was dissolved in 60 mL dry MeOH and $NaBH_4$ (1.2 g) was added slowly in small portions over 15 min. The reaction mixture was stirred for 1 h under N_2 to form a white suspension. After removal of the solvent, the residue was extracted with CH_2Cl_2 and washed with water. The organic layer was dried over anhydrous $MgSO_4$ and concentrated under vacuum to give a white solid. The crude product was recrystallized from absolute ethanol to give white crystal (0.75 g). ^{1}H NMR ($CDCl_3$): δ 2.58 (s, 6H), 4.98 (s, 1H), 6.52 (m, 2H), 6.77 (m, 2H), 7.44 (m, 3H), 7.60 (m, 2H).

Quantum yield determination.

The quantum yield for the photocatalytic CO_2 reduction was determined using the following equation:

$$\boldsymbol{\phi}(\%) = \frac{\boldsymbol{CO\ evolution\ rate\ (mol\ s^{-1})}}{\boldsymbol{photon\ flux\ rate\ (Einstein\ s^{-1})}} \times \mathbf{100}\%$$

CO evolution rate was determined using gas chromatograph and the incident photon flux was measured using potassium ferrioxalate as a standard chemical actinometer.

For actinometry, 4 mL (V_1) of an aqueous solution containing the iron actinometer (6.5 mM) in H_2SO_4 (0.15 M) was irradiated with blue LED (LEDXON blue LED 467 nm). During photoreduction, aliquots of 0.25 ml (V_2) were collected at 30 s intervals (0-150 s) and 2 mL of a buffered solution of phenanthroline (2 mg ml^{-1} in 1 M NaOAc buffer) was added. The mixture was diluted to 25 mL (V_3) with deionised water H_2O. The absorbance of the solutions at 510 nm were recorded. The rate of Fe^{2+} production ($\Delta n(Fe^{2+})/\Delta t$) from photoreaction was determined from the slope of absorbance (510 nm) versus time (s), using the following equation:

$\frac{\Delta n(Fe^{2+})}{\Delta t} = \frac{V_1 \times V_3}{1000 \times V_2 \times \varepsilon_{510\ nm}} \times \frac{\Delta A}{\Delta t}$ where ($\Delta A/\Delta t$) represent the slope of A_{510nm} vs. t plot (Fig. S5) and $\varepsilon_{510\ nm}$ the extinction coefficient for Fe^{2+}-phenanthroline complex at 510 nm (11100 M^{-1} cm^{-1}).

The incident photon flux per second is calculated using the following equation:

$I_{467\ nm} = \frac{\Delta n(Fe^{2+})}{\emptyset_{467\ nm} \times \Delta t}$ where, $\varphi_{467\ nm}$ is the reported quantum yield of ferrioxalate actinometer at 467 nm (0.93).

Using this method, the final value for the rate of photon flux of the incident light from the blue LED ($I_{467\ nm}$) was determined to be (1.27×10^{-7}) Einstein s^{-1}.

To determine the quantum yield, a colloidal suspension of MeCN/TEOA (4:1 v/v) (4.0 mL) containing CoPc-PMO (2 mg, 2.7 µmol Co mg^{-1}), $[Ru(bpy)_3]Cl_2$ (0.50 mM) and BIH (10 mM) was irradiated with LEDXON blue LED (λ = 467 nm) under identical condition. The CO evolution was monitored using a gas

chromatograph from SRI GC and the time course for CO formation over 1.5 h is shown in Fig. S6.

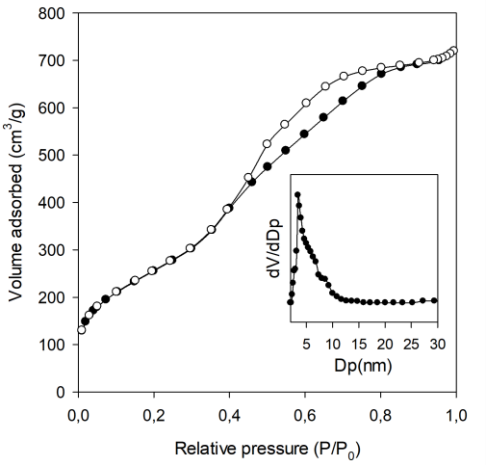

Fig. S1 N_2 adsorption-desorption isotherm and pore size distribution (inset) of CoPc-PMO.

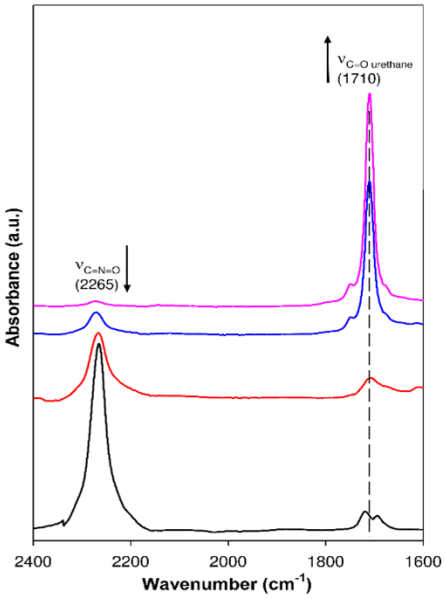

Fig. S2 ATR-FTIR spectrum of 3-(triethoxysilyl)propyl isocyanate (black line) and ATR-FTIR monitoring of the reaction of 3-(triethoxysilyl)propyl isocyanate and $CoPc(OH)_4$ after 12 h (red line), 24 h (blue line) and 72 h (pink line).

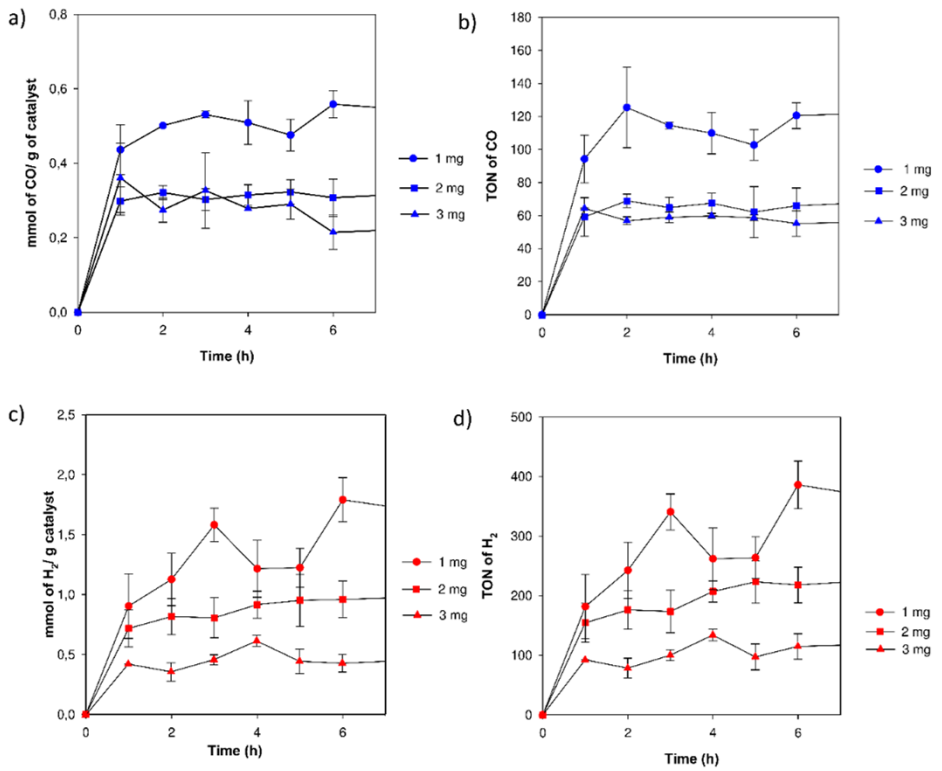

Fig. S3 Photocatalytic CO_2 reduction with different amount of CoPc-PMO catalyst (1-3 mg) under unfiltered UV-visible irradiation: (a-b) CO evolution trace and corresponding TONs, and (c-d) H_2 evolution trace and corresponding TONs. Condition: 1-3 mg CoPc-PMO, 4 ml MeCN/TEOA (4:1), $Ru(bpy)_3^{2+}$ (0.5 mM), UV-visible light irradiation (100 mW cm^{-2}, AM 1.5G, λ>300 nm), and CO_2 saturated condition.

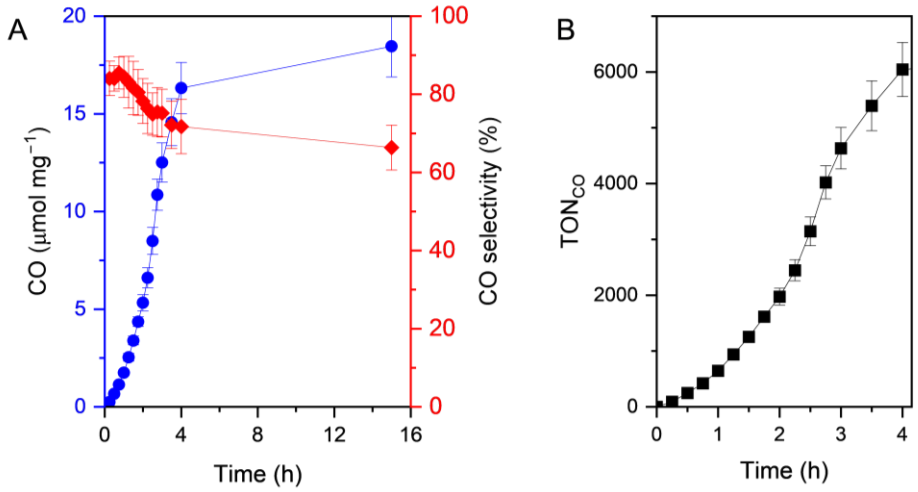

Fig. S4. Photocatalytic CO_2 reduction using CoPc-PMO with 2.7 μmol Co loading per gram. (A) Time course for CO evolution and CO selectivity during 16 h reaction, and (B) corresponding Co-based turnover number for CO evolution (TONCO) during the first four hours of irradiation. Condition: 1 mg CoPc-PMO, 4 mL 4:1 MeCN/TEOA (v/v), $[Ru(bpy)_3]^{2+}$ (0.50 mM), BIH (10 mM), visible light irradiation (100 mW cm^{-2}, AM 1.5G, $\lambda > 400$ nm), and CO_2 saturated condition.

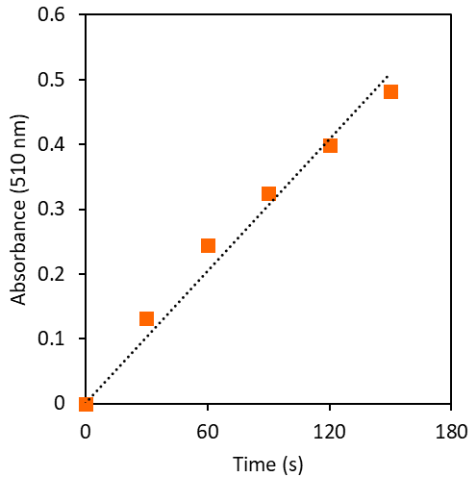

Fig. S5 Time course of absorbance at 510 nm for Fe^{2+}-phenanthroline complex obtained after photoreduction of the chemical actinometer (ferrioxalate) under blue LED irradiation (467 nm). The slope of the linear fit is 3.3×10^{-3} s^{-1}.

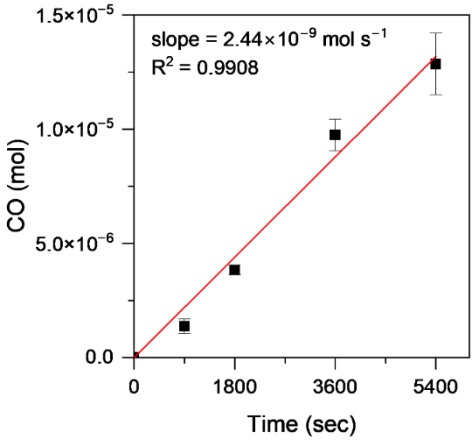

Fig. S6 Time course of CO production for the quantum yield determination in the photocatalytic reaction by irradiation (467 nm) of a MeCN/TEOA (4.0 mL, 4:1 v/v) containing CoPc-PMO (2 mg), $[Ru(bpy)_3]^{2+}$ (0.50 mM) and BIH (10 mM) under CO_2 atmosphere.

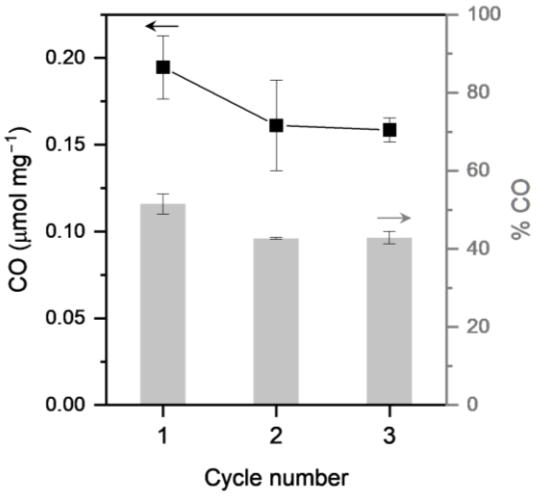

Fig. S7 Recycling experiment with CoPc-PMO in the absence of BIH donor. CO evolved (black trace) and % CO selectivity (grey bar) during three 1-h recycling run is shown. Condition: CO_2-saturated 4:1 MeCN/TEOA, ~ 2 mg PMO-CoPc, 0.5 mM $[Ru(bpy)_3]^{2+}$, and visible light irradiation (100 mW cm^{-2}, AM 1.5G, $\lambda > 400$ nm).

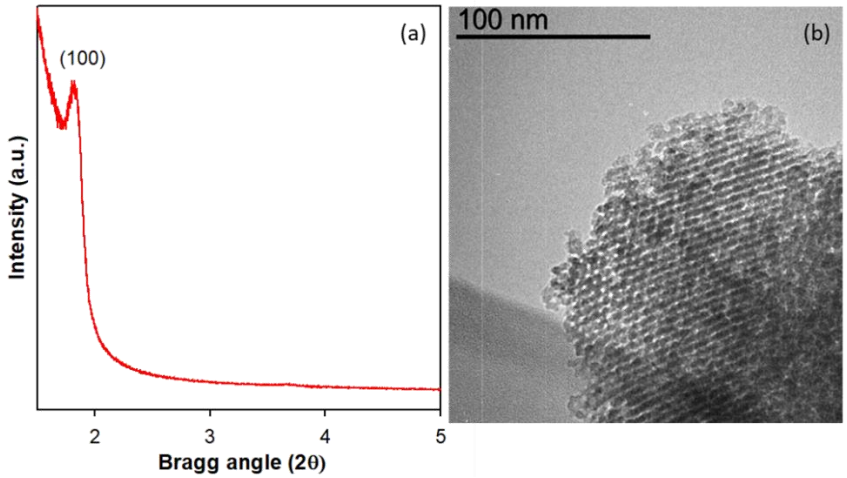

Fig. S8 Powder X-ray diffraction pattern (a) and TEM image (b) of CoPc-PMO catalyst after four catalytic cycles.

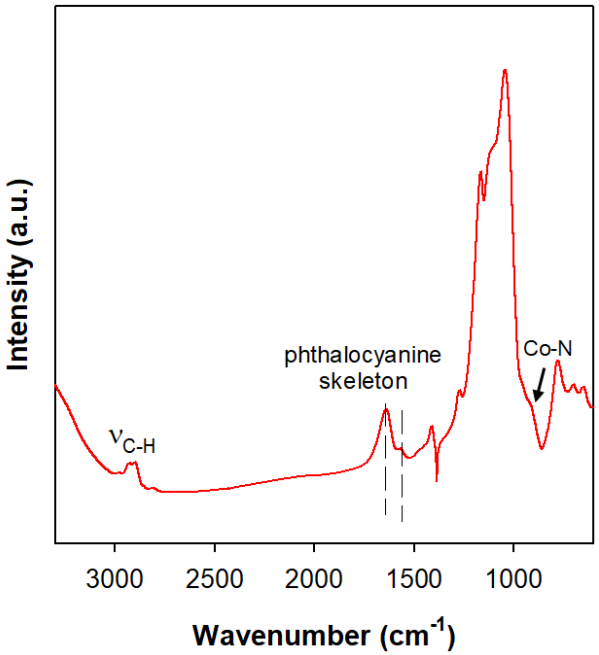

Fig. S9 FT-IR of CoPc-PMO after 4 cycles of reaction.

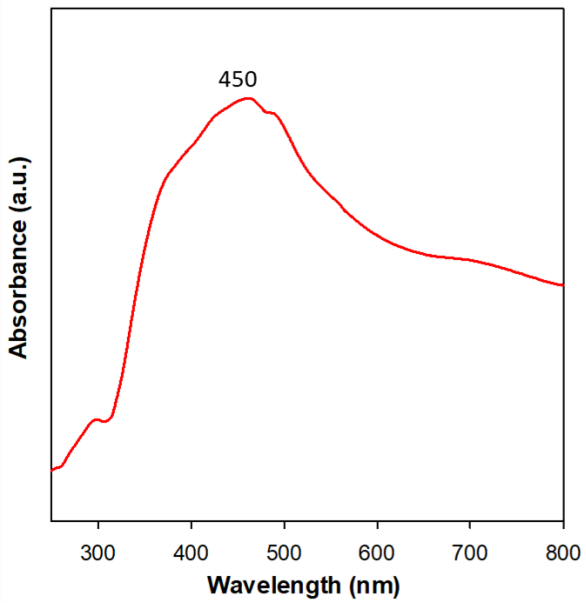

Fig. S10 UV-vis DRS of CoPc-PMO after 4 cycles of reaction.

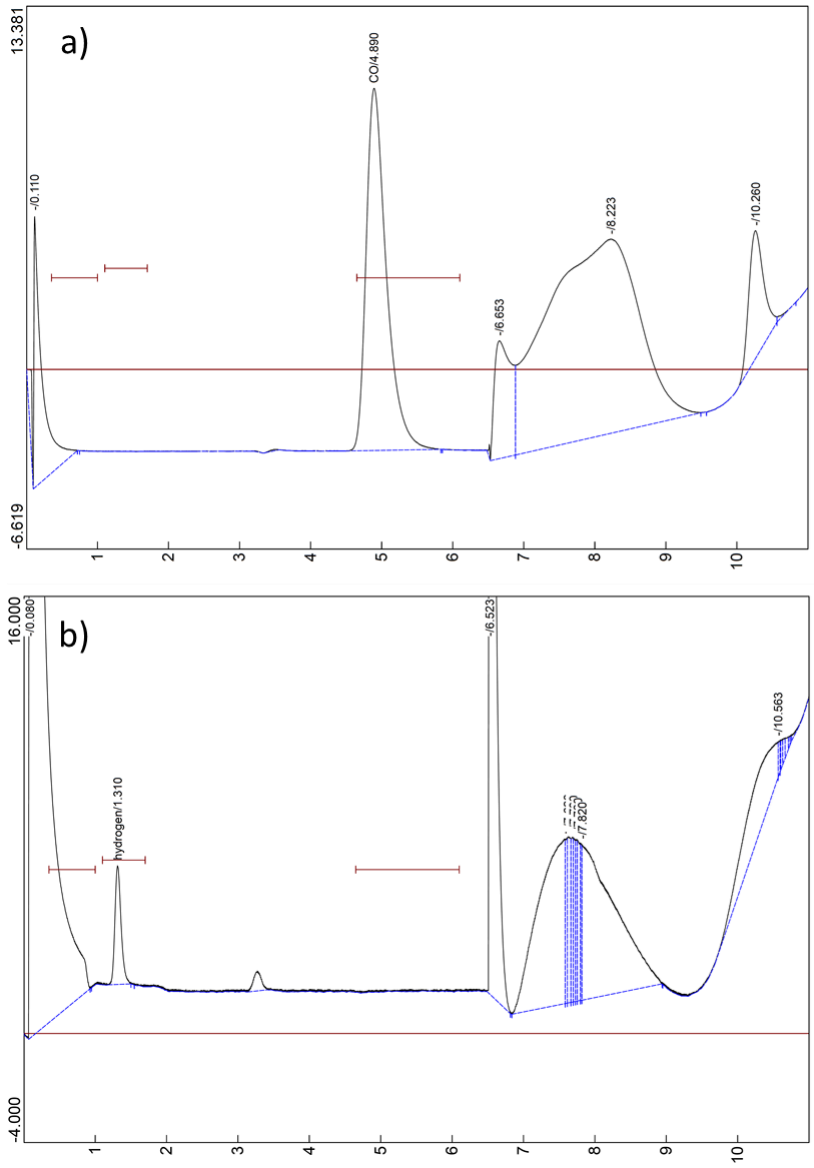

Fig. S11 Representative gas chromatogram of the headspace gas during photocatalysis with CoPc-PMO in the presence of $Ru(bpy)_3^{2+}$ (0.5 mM) and BIH (10 mM) in MeCN/TEOA. The chromatograms from FID detector (a) and TCD detector (b) are shown. GC program with 11.1 min runtime: (1) column oven temperature held at 40 °C for 6.5 min, (2) column oven heated at a ramping rate of 50 °C min^{-1} till 220 °C (3.6 min), and (3) column oven held at 220 °C for 1 min.

References

[1] N.W. Polaske, H.-C. Lin, A. Tang, M. Mayukh, L.E. Oquendo, J.T. Green, E.L. Ratcliff, N.R. Armstrong, S.S. Saavedra, D. V. McGrath, Phosphonic Acid Functionalized Asymmetric Phthalocyanines: Synthesis, Modification of Indium Tin Oxide, and Charge Transfer, Langmuir. 27 (2011) 14900–14909. https://doi.org/10.1021/la203126c.

[2] A. Rosas-Hernández, C. Steinlechner, H. Junge, M. Beller, Earth-abundant photocatalytic systems for the visible-light-driven reduction of CO_2 to CO, Green Chem. 19 (2017) 2356–2360. https://doi.org/10.1039/C6GC03527B.

CAPÍTULO 8. CONCLUSIONES/ CONCLUSIONS

CONCLUSIONES

Las investigaciones que se han llevado a cabo durante esta Tesis Doctoral permiten extraer las siguientes conclusiones generales:

- La incorporación de diferentes complejos metálicos en las paredes de la estructura porosa de organosílices ha podido realizarse siguiendo diferentes estrategias. En particular, las utilizadas en esta Tesis han implicado el uso de precursores ya dotados del complejo o de precursores que, previa funcionalización o no, han permitido la formación de compuestos de coordinación.

- La modificación superficial mediante una reacción de Diels-Alder de grupos vinilo ya incorporados mediante co-condensación en una organosílice mesoporosa periódica y posterior formación de un complejo de cobre ha dado lugar a un catalizador activo en la reacción de oxidación de estireno a óxido de estireno.

- Unidades heterocíclicas en la pared de organosílices, tales como piridina e imidazol, introducidas mediante co-condensación y, en caso necesario, funcionalización, han sido utilizadas como ligandos para el anclaje de cobaloximas. Estos materiales son activos como catalizadores heterogéneos en procesos de fotosíntesis artificial, específicamente en la reacción de producción de hidrógeno, habiéndose observado la ventaja catalítica que supone el ordenamiento de la estructura porosa.

- Un precursor silánico conteniendo una unidad de ftalocianina de cobalto ha sido sintetizado e incorporado mediante co-condensación en la estructura de una organosílice mesoporosa periódica, obteniéndose así un excelente catalizador heterogéneo para la reacción de fotorreducción de CO_2 a CO.

CONCLUSIONS

The investigations carried out during this Doctoral Thesis lead the following general conclusions:

- The incorporation of different metal complexes into the walls of organosilica porous structures has been achieved using various strategies. In particular, the ones employed in this thesis have involved the use of precursors already equipped with the complex or precursors that, through functionalization or not, have allowed the formation of coordination compounds.

- The superficial modification through Diels-Alder reaction with the vinyl groups already incorporated by means of co-condensation process in a periodic mesoporous organosilica and the posterior formation of a copper complex have been leaded to an active catalyst in the oxidation reaction from styrene to oxide styrene.

- Heterocyclic units in the wall of organosilica, such as pyridine and imidazole, introduced through co-condensation and, if necessary, functionalization, have been used as ligands for the anchoring of cobaloximes. These materials are active as heterogeneous catalysts in artificial photosynthesis processes, specifically in the hydrogen production reaction, with the catalytic advantage of the ordered porous structure being observed.

- A silane precursor containing a cobalt phthalocyanine unit has been synthesized and incorporated through co-condensation into the structure of a periodic mesoporous organosilica, resulting in an excellent heterogeneous catalyst for the photocatalytic reduction of CO_2 to CO.

ÍNDICIOS DE CALIDAD

Clave	Artículo
Título	Copper-complexed dipyridyl-pyridazine functionalized periodic mesoporous organosilica as a heterogeneous catalyst for styrene epoxidation
Autores	Navarro Mª Ángeles, Juan Amaro-Gahete, José R. Ruíz, César Jiménez-Sanchidrián, Francisco J. Romero-Salguero, Dolores Esquivel
Nombre de la revista	Dalton Transactions
Año, volumen y página	2022, 51, 4884-4897
Editorial	Royal Society of Chemistry
Revista incluida en el Journal Citation Reports (JCR)	Si
Índice de impacto (2021)	4.569
Categorías	CHEMISTRY, INORGANIC & NUCLEAR
Lugar que ocupa la revista en las categorías (2021)	7/46
Cuartil	Q1

Clave	Artículo
Título	Cobaloxime tethered pyridine-functionalized ethylene-bridged periodic mesoporous organosilica as an efficient HER catalyst
Autores	M. Ángeles Navarro, Daniel Cosano, Asamanjoy Bhunia, Laura Simonelli, Vlad Martin-Diaconescu, Francisco J. Romero-Salguero, Dolores Esquivel
Nombre de la revista	Sustainable Energy & Fuels
Año, volumen y página	2022, 6, 398
Editorial	Royal Society of Chemistry
Revista incluida en el Journal Citation Reports (JCR)	Si
Índice de impacto (2021)	6.813
Categorías	ENERGY & FUELS
Lugar que ocupa la revista en las categorías (2021)	40/119
Cuartil	Q2

Clave	Artículo
Título	Solar driven CO_2 reduction with a molecularly engineered periodic mesoporous organosilica containing cobalt phthalocyanine
Autores	M. Angeles Navarro, Sunanda Sain, Maximilian Wünschek, Christian M. Pichler, Francisco J. Romero-Salguero, Dolores Esquivel, Souvik Roy
Nombre de la revista	Nanoscale
Año, volumen y página	2023, 15, 2114-2121
Editorial	Royal Society of Chemistry
Revista incluida en el Journal Citation Reports (JCR)	Si
Índice de impacto (2021)	8.307
Categorías	CHEMISTRY, MULTIDISCIPLINARY
Lugar que ocupa la revista en las categorías (2021)	37/179
Cuartil	Q1

OTRAS APORTACIONES CIENTÍFICAS

PUBLICACIONES QUE NO FORMAN PARTE DE LA MEMORIA DE LA TESIS DOCTORAL

1. A Pd(II) Magnetically Retrievable Catalyst for Hiyama Reaction: Functionalization of Magnetic Mesoporous Silica via Click Reaction

Samira Mousavi, Yagoub Mansoori, Ayat Nuri, Dolores Esquivel, Mª Ángeles Navarro

*Catalysis Letters, Volume **152**, January 2022, Pag 3465–3478.*

2. 2-Pyridyl-benzimidazole-Pd(II)/Pd(0) Supported on Magnetic Mesoporous Silica: Aerobic Oxidation of Benzyl Alcohols/ Benzaldehydes and Reduction of Nitroarenes

Mohammad Sajedi, Yagoub Mansoori, Ayat Nuri, Somayeh Fekri, Dolores Esquivel and Mª Angeles Navarro

*Catalysis Surveys from Asia, Volume **26**, May 2022, Pag 193-210.*

3. Efficient Hydrodehalogenation of Aryl Halides Catalyzed by Bis(NHC)-Pd(II) Complex Supported on Magnetic Mesoporous Silica

Somayeh Fekri, Yagoub Mansoori, Dolores Esquivel, M. Ángeles Navarro

*Catalysis Letters, Volume **153**, March 2023.*

4. A New Bis-(NHC)-P(II) Complex Supported on Magnetic Mesoporous Silica: An Efficient Pd(II) Catalyst for the Selective Buchwald-Hartwig Monoarylation of Ammonia

Somayeh Fekri, Yagoub Mansoori, Dolores Esquivel, M. Ángeles Navarro

*ChemistrySelect, Volume **8**, April 2023, Pag e202204378.*

5. Bis(Oxime Palladacycle) Supported on Magnetized SBA-15 as an Efficient and Retriveble Catalyst for the Mizoroki–Heck Reaction

Fatemeh Ghahramani, Yagoub Mansoori, Abolfazl Bezaatpour, Dolores Esquivel, M. Ángeles Navarro

Catalysis Surveys from Asia, Volume **27**, April *2023.*

COMUNICACIONES A CONGRESOS

1. Organosílicas mesoporosas periódicas como catalizadores heterogéneos en reacciones de oxidación (Póster)

Mª Ángeles Navarro, Juan Amaro-Gahete, Francisco J. Romero-Salguero, Mª Dolores Esquivel. Encuentro sobre Nanociencia y Nanotecnología (NANOUCO VII). Córdoba (España), 2019.

2. Funcionalización de organosílicas periódicas mesoporosas y su aplicación en la reacción de oxidación de estireno

Juan Amaro-Gahete, Mª Ángeles Navarro, Daniel Cosano Hidalgo, José Rafael Ruíz Arrebola, César Jiménez Sanchidrían, Francisco J. Romero-Salguero, Mª Dolores Esquivel. Catálisis para el futuro: Avances en Estructuras, Procesos y Aplicaciones (SECAT19), Córdoba (España), 2019

3. Síntesis de organosílices periódicas mesoporosas con centros metálicos tipo cobaloxima para la obtención de hidrógeno

Mª Ángeles Navarro, Daniel Cosano, Mª Dolores Esquivel, Juan Amaro-Gahete, Raúl Rojas, José Rafael Ruiz, César Jiménez-Sanchidrián, Francisco J. Romero-Salguero. IV Encuentro de Jóvenes Investigadores de la SECAT, País Vasco (España), 2020.

4. Adsorción de nonilfenol empleando desoxicolato intercalado en hidróxidos dobles laminares (Póster)

Daniel Cosano, Mª Dolores Esquivel, Mª Ángeles Navarro, Raúl Rojas, Juan Amaro-Gahete, César Jiménez-Sanchidrián, Francisco J. Romero-Salguero, José Rafael Ruiz-Arrebola. IV Encuentro de Jóvenes Investigadores de la SECAT, País Vasco (España), 2020.

5. Síntesis de materiales híbridos orgánico-inorgánicos para la producción de hidrógeno mediante la descomposición de ácido fórmico

Raúl Rojas, Daniel Cosano, Mª Dolores Esquivel, Mª Ángeles Navarro, Juan Amaro-Gahete, José Rafael Ruiz-Arrebola, Francisco J. Romero-Salguero, César Jiménez-Sanchidrián. IV Encuentro de Jóvenes Investigadores de la SECAT, País Vasco (España), 2020.

6. Síntesis de Organosílices Mesoporososas Periódicas con centros biomiméticos de cobalto para la obtención de hidrógeno

Mª Ángeles Navarro, Mª Dolores Esquivel, Francisco J. Romero-Salguero. IX Congreso Científico de Investigadores en Formación de la Universidad de Córdoba. Nuevos desafíos, nuevas oportunidades. Córdoba (España), 2021.

7. Pt/Ru@PMO: Un eficiente sistema para la producción fotocatalítica de hidrógeno

Raúl Rojas, Mª Ángeles Navarro, Mª Dolores Esquivel, José Rafael Ruiz-Arrebola, César Jiménez-Sanchidrián, Francisco J. Romero-Salguero. Reunión Bienal de la Sociedad Española de Catálisis (2021) (SECAT 21). Alicante (España), 2021.

8. Síntesis de organosílices periódicas mesoporosas con centro de tipo cobaloxima para la producción de hidrógeno (Póster)

Mª Ángeles Navarro, Daniel Cosano, Raúl Rojas, Mª Dolores Esquivel, Francisco J. Romero-Salguero. Reunión Bienal de la Sociedad Española de Catálisis (2021) (SECAT 21). Alicante (España), 2021.

9. Cobaloxime-based periodic mesoporous organosilicas for photocatalytic hydrogen production.

Mª Ángeles Navarro, Daniel Cosano, Mª Dolores Esquivel, Francisco J. Romero-Salguero. Third energy, efficiency and environmental sustainability conference (CEES 2021). Universidad de la Serena. Santiago de Chile (Chile), 2021.

10. Síntesis De Organosílices Mesoporosas Periódicas Para Su Uso Como Catalizadores Heterogéneos En La Reacción De Epoxidación De Óxido De Estireno (Póster).

Mª Ángeles Navarro, Mª Dolores Esquivel, Francisco J. Romero-Salguero. X Congreso Científico de Investigadores en Formación: El arte de investigar. Córdoba (España), 2022.

11. Cobaloxime tethered on periodic mesoporous organosilicas for photocatalytic hydrogen production (Póster).

Mª Ángeles Navarro, Daniel Cosano, Mª Dolores Esquivel, Francisco J. Romero-Salguero, José Rafael Ruiz-Arrebola, César Jiménez-Sanchidrián. XXXVIII Reunión Bienal de la Real Sociedad Española de Química (RSEQ), Granada (España), 2022.

12. Organosílices periódicas mesoporosas como soportes de un complejo tipo cobaloxima para la producción fotocatalítica de hidrógeno.

Mª Ángeles Navarro, Daniel Cosano, Mª Dolores Esquivel, José Rafael Ruiz-Arrebola, Francisco J. Romero-Salguero, César Jiménez-Sanchidrián. V Encuentro Jóvenes Investigadores (SECAT 2022), Alicante (España), 2022.

13. Síntesis de un nuevo material PMO funcionalizado con complejos de cobaloxima para su uso en producción de hidrógeno.

MªÁngeles Navarro*, Dolores Esquivel y Francisco J. Romero-Salguero. XI Congreso Científico de Personal Investigador en Formación (PIF). Córdoba (España), 2023

PUBLICACIONES CIENTÍFICAS

ACKNOWLEDGEMENTS

All articles present in this Doctoral Thesis are reproduced with permission from the Royal Society of Chemistry

Dalton Transactions

ROYAL SOCIETY OF CHEMISTRY

PAPER

View Article Online
View Journal | View Issue

Cite this: *Dalton Trans.*, 2022, **51**, 4884

Copper-complexed dipyridyl-pyridazine functionalized periodic mesoporous organosilica as a heterogeneous catalyst for styrene epoxidation

M. Ángeles Navarro, Juan Amaro-Gahete, José R. Ruiz, César Jiménez-Sanchidrián, Francisco J. Romero-Salguero * and Dolores Esquivel *

A new heterogeneous catalyst has been synthesized by immobilization of a copper complex on dipyridyl-pyridazine functionalized periodic mesoporous organosilica (dppz-vPMO). This ordered support was first prepared by a co-condensation reaction between vinyltriethoxysilane and 1,2-bis(trimethoxysilyl)ethane and further post-functionalized through a hetero Diels–Alder reaction with 3,6-di-2-pyridyl-1,2,4,5-tetrazine. Techniques such as XRD, N_2 isotherms, TEM, ^{13}C NMR, XPS and DRIFT, among others, were employed to characterize the surface functionalized materials. These results have proven the ordered mesostructure of the materials as well as the presence of novel nitrogen-chelating heterocyclic compounds on the pore surface after the post-modification process. Additionally, the successful anchoring of a copper complex on the dipyridyl-pyridazine (dppz) ligands has been confirmed. The resulting material was evaluated as a heterogeneous catalyst in the epoxidation of styrene using *tert*-butylhydroperoxide (TBHP) as an oxidant. Under the optimized reaction conditions, Cu@dppz-vPMO showed a high styrene conversion (86.0%) and a remarkable selectivity to styrene oxide (41.9%). Indeed, this catalyst provided excellent catalytic results in terms of stability, reaction rate, conversion and selectivity compared to other bipyridine-like copper catalysts.

Received 3rd January 2022,
Accepted 23rd February 2022

DOI: 10.1039/d2dt00018k

rsc.li/dalton

1. Introduction

Epoxidation of olefins is one of the most relevant reactions in organic synthesis since the resultant epoxide products are important and versatile intermediates for the synthesis of a wide variety of fine chemicals, pharmaceuticals, agrochemicals, and perfumes, among others.[1–4] While traditional methods for the synthesis of epoxides are characterized using stoichiometric amounts of harmful oxidants (peracids) and generate enormous waste,[5–7] the recent synthetic methodologies in this field are focused to overcome them. Thus, the use of safer oxidizing agents, such as *tert*-butyl hydroperoxide (TBHP), molecular oxygen or hydrogen peroxide in styrene epoxidation provides an economical and environment friendly alternative. However, their characteristic low reactivity and selectivity in this type of reaction when they are used alone have led to the use of such oxidants in combination with transition-metal catalysts.[3,8] Over the last few decades, a wide variety of ions, oxides and complexes of transition metals have been explored through homogeneous catalytic processes. Although these systems lead to high yields in the epoxidation reactions, their immobilization on solid supports has gained much more attention from an environmental and economic perspective due to their potential applications in industry.[9–14] Nowadays, the development of efficient heterogenized catalytic systems for the epoxidation of olefins remains a challenge.[4,15–17] Different types of porous materials, such as zeolites,[18] polymers,[19] mesoporous silicas,[14] activated carbons[20] or MOFs,[21] have been employed as supports of transition metal complexes for liquid phase epoxidation of olefins.

Studies on epoxidation reactions catalysed by heterogenized Schiff-bases and other Cu(II)-complex-based catalysts have received a great deal of attention during recent years. Depending on the support, different synthetic approaches have been adopted to integrate them on their framework for the oxidation of olefins. Thus, Spodine *et al.*[22] were the first who reported the synthesis of a MOF with Cu(II) centers coordinated to bipy (2,2′-bipyridine) and H_4btec (1,2,4,5-benzenetetracarboxylic acid) ligands as a heterogeneous catalyst for oxi-

Departamento de Química Orgánica, Instituto Universitario de Nanoquímica (IUNAN), Facultad de Ciencias, Universidad de Córdoba, 14071 Córdoba, Spain. E-mail: qo2rosaf@uco.es, q12esmem@uco.es

Sustainable Energy & Fuels

ROYAL SOCIETY OF CHEMISTRY

PAPER

Cite this: *Sustainable Energy Fuels*, 2022, **6**, 398

Cobaloxime tethered pyridine-functionalized ethylene-bridged periodic mesoporous organosilica as an efficient HER catalyst†

M. Ángeles Navarro, [a] Daniel Cosano, [a] Asamanjoy Bhunia, [b] Laura Simonelli, [c] Vlad Martin-Diaconescu,[c] Francisco J. Romero-Salguero *[a] and Dolores Esquivel *[a]

An efficient cobaloxime hydrogen production catalyst has been synthesized through the coordination of a cobalt complex ($Co(dmgH_2)(dmgH)Cl_2$) on an ethylene-bridged periodic mesoporous organosilica (PMO) containing pyridine moieties. The effective assembly of cobaloxime units through cobalt–pyridine axial bonds on the porous channels of the PMO was clearly evidenced by different techniques, including ^{13}C NMR, Raman, IR and XPS. The catalyst was investigated for the hydrogen evolution reaction in a visible-light activated system in the presence of a photosensitizer (eosin Y) and a sacrificial electron donor (TEOA). It showed a good photocatalytic performance in the HER with a TON of 119 at 6 h, largely exceeding the catalytic activity of the homogeneous counterpart, $Co(dmgH)_2pyCl$, under the conditions studied. The process was proven to be photocatalytic and heterogeneous. The studied system has the cobaloxime catalyst with the highest turnover reported to date for a heterogeneous catalyst under photocatalytic conditions. After reactivation treatment with the $Co(dmgH_2)(dmgH)Cl_2$ complex, the catalytic system was able to maintain its activity after two recycling experiments.

Received 13th September 2021
Accepted 21st November 2021

DOI: 10.1039/d1se01437d

rsc.li/sustainable-energy

Introduction

In response to the dramatic increase of atmospheric levels of CO_2 due to the worldwide strong dependence on fossil fuels to obtain energy, scientists have been working on the development and implementation of sustainable carbon-free energy sources.[1]

Among them, solar energy is by far the most feasible and promising alternative to carbon fuels. Theoretically, the incident solar energy on the earth every hour is more than enough to satisfy all energy demanded by humans for the entire year.[2,3] Although electricity generation from the sun using photovoltaic cells currently contributes more than 3.5% of the world's electricity,[4] there exists barriers to the complete implementation of solar energy. The daily and seasonal fluctuations of solar flux along with the absence of methods for storing and dispatching on demand have not allowed its development as a major primary energy source.

Alternatively, an interesting approach inspired by natural photosynthesis is solar driven water-splitting, able to store energy in chemical bonds (H_2 and O_2).[5,6] As a result of the well-known complications in driving both half-reactions,[7] most of the studies have been focused on the reductive side of water splitting to obtain hydrogen as an energy vector. However, a hydrogen economy requires the design of cost-effective and efficient catalysts for hydrogen production through an economically viable process. In this context, molecular catalysts based on earth-abundant element (Co, Ni and Fe) complexes play an important role in water splitting.[8] Particularly, cobalt-based compounds have emerged as efficient molecular systems for both water oxidation[9,10] and hydrogen evolution reactions[11,12] in the last decade. Specifically, cobaloxime (cobalt bis-glyoximato complexes) compounds are among the most widely studied for electro- and photocatalytic hydrogen production due to their facile synthesis and tunable catalytic properties. These systems show high activity for proton reduction in aqueous solution at low overpotential.[13–17]

Since the pioneering studies by Ziessel and co-workers in this field,[18] numerous breakthroughs have been made in the design of efficient cobaloxime-based molecular systems for the electro- and photocatalytic hydrogen evolution reaction (HER).[19,20] One of the most versatile approaches to improve the electrocatalytic HER activity of cobaloximes is their immobilization on electroactive surfaces containing pyridine ligands. It is well documented by experimental[21–24] and computational[25–27]

[a]*Departamento de Química Orgánica, Instituto Universitario de Nanoquímica (IUNAN), Facultad de Ciencias, Universidad de Córdoba, 14071 Córdoba, Spain. E-mail: qo2rosaf@uco.es; q12esmem@uco.es*

[b]*Department of Chemistry, Inorganic Chemistry Section, Jadavpur University, Kolkata 700032, India*

[c]*ALBA Synchrotron Light Facility, Carrer de la Llum 2-26, 08290 Cerdanyola del Vallès, Spain*

† Electronic supplementary information (ESI) available. See DOI: 10.1039/d1se01437d

hydrogen

MDPI

Article

Improved Photocatalytic H_2 Evolution by Cobaloxime-Tethered Imidazole-Functionalized Periodic Mesoporous Organosilica

M. Ángeles Navarro, Miguel A. Martín, José Rafael Ruiz, César Jiménez-Sanchidrián, Francisco J. Romero-Salguero * and Dolores Esquivel *

Departamento de Química Orgánica, Instituto Químico para la Energía y el Medioambiente (IQUEMA), Facultad de Ciencias, Campus de Rabanales, Universidad de Córdoba, 14071 Córdoba, Spain

* Correspondence: qo2rosaf@uco.es (F.J.R.-S.); q12esmem@uco.es (D.E.); Tel.: +34-957-218638 (F.J.R.-S.); +34-957-211050 (D.E.)

Abstract: Molecular cobaloxime-based heterogeneous systems have attracted great interest during the last decades in light-driven hydrogen production. Here, we present a novel cobaloxime-tethered periodic mesoporous organosilica (PMO) hybrid (Im-EtPMO-Co) prepared through the immobilization of a molecular cobaloxime complex on the imidazole groups present in ethylene-bridged PMO. The successful assembly of a molecular cobaloxime catalyst via cobalt-imidazole axial ligation has been evidenced by several techniques, such as ^{13}C NMR, Raman spectroscopy, ICP-MS, and XPS. The catalytic performance of Im-EtPMO-Co catalyst was essayed on the hydrogen evolution reaction (HER) under visible light in presence of a photosensitizer (Eosin Y) and an electron donor (TEOA). It showed an excellent hydrogen production of 95 mmol hydrogen at 2.5 h, which corresponded to a TON of 138. These results reflect an improved photocatalytic activity with respect to its homogenous counterpart [*Co(dmgH)$_2$(Im)Cl*] as well as a previous cobaloxime-PMO system with pyridine axial ligation to the cobaloxime complex.

Keywords: cobaloxime; periodic mesoporous organosilicas; photocatalysis; hydrogen evolution reaction; primary axial coordination

Citation: Navarro, M.Á.; Martín, M.A.; Ruiz, J.R.; Jiménez-Sanchidrián, C.; Romero-Salguero, F.J.; Esquivel, D. Improved Photocatalytic H_2 Evolution by Cobaloxime-Tethered Imidazole-Functionalized Periodic Mesoporous Organosilica. *Hydrogen* **2023**, *4*, 120–132. https://doi.org/10.3390/hydrogen4010008

Academic Editor: Shreya Mukherjee

Received: 5 November 2022
Revised: 19 January 2023
Accepted: 30 January 2023
Published: 2 February 2023

1. Introduction

Mimicking biological procedures has always been a good approach to tackling energy questions. In recent years, numerous efforts have been made for the development of natural photosynthesis-inspired technologies for the efficient transformation of the energy from sunlight into chemical energy [1]. Hydrogen is considered an efficient energy vector due to the high energy density of the H_2 molecule (119 kJ/g) and its ability to be stored in large quantities. Furthermore, hydrogen combustion with air only produces water as residue, so it is considered a cyclic and environmentally friendly process [2].

Aiming at designing efficient hydrogen evolution catalysts, alternative to traditional Pt-based catalysts, the first studies were focused on simulating the activity of hydrogenase enzymes (especially metalloproteins) for hydrogen production [3,4]. In fact, hydrogenases utilizing earth-abundant metals such as Fe or Ni-Fe are the most active molecular catalysts for hydrogen production [5,6]. Although numerous studies have been performed on the design of biomimetic models of [Fe]-hydrogenases for hydrogen production, their inherent instability during the catalytic process has limited their applicability. In this sense, to solve these drawbacks, recent approaches have been focused on the assembly of biomimetic diiron catalysts on heterogenous supports, such as metal organic frameworks (MOFs) [7], silica-based mesoporous materials [8] or graphene-based materials [9] for light-induced hydrogen production. These heterogeneous matrices have provided improved stability for the anchored molecular catalyst, overcoming those issues related to its water solubility and photostability [10].

Nanoscale

PAPER

View Article Online
View Journal

Cite this: DOI: 10.1039/d2nr06026d

Solar driven CO_2 reduction with a molecularly engineered periodic mesoporous organosilica containing cobalt phthalocyanine†

M. Angeles Navarro,[a,b] Sunanda Sain, [b] Maximilian Wünschek, [c] Christian M. Pichler,[c,d] Francisco J. Romero-Salguero, [a] Dolores Esquivel *[a] and Souvik Roy *[b]

Received 29th October 2022,
Accepted 10th January 2023

DOI: 10.1039/d2nr06026d

rsc.li/nanoscale

A molecular cobalt phthalocyanine (CoPc) catalyst has been integrated in an ethylene-bridged periodic mesoporous organosilica (PMO) to fabricate a hybrid material, CoPc-PMO, that catalyses CO_2 reduction to CO in a photocatalytic system using $[Ru(bpy)_3]^{2+}$ (bpy = 2,2′-bipyridine) as a photosensitizer and 1,3-dimethyl-2-phenyl-2,3-dihydro-1*H*-benzo[*d*]imidazole (BIH) as an electron donor. CoPc-PMO displays a Co-based turnover number (TON_{CO}) of >6000 for CO evolution with >70% CO-selectivity after 4 h irradiation with UV-filtered simulated solar light, and a quantum yield of 1.95% at 467 nm towards CO. This system demonstrates a benchmark TON_{CO} for immobilised CoPc-based catalysts towards visible light-driven CO_2 reduction.

[a]Departamento de Química Orgánica, Instituto Químico para la Energía y el Medioambiente (IQUEMA), Facultad de Ciencias, Universidad de Córdoba, Campus de Rabanales, 14071 Córdoba, Spain. E-mail: q12esmem@uco.es
[b]School of Chemistry, The University of Lincoln, Green Lane, Lincoln LN6 7TS, UK. E-mail: sroy@lincoln.ac.uk
[c]Institute of applied Physics, TU Vienna, Wiedner Hauptstraße 8-10, 1040 Vienna, Austria
[d]Centre of electrochemical and surface technology, Viktor Kaplan Straße 2, 2700 Wiener Neustadt, Austria

†Electronic supplementary information (ESI) available. See DOI: https://doi.org/10.1039/d2nr06026d

Souvik Roy

Dr Souvik Roy is Senior Lecturer in the School of Chemistry at the University of Lincoln. He completed PhD in Chemistry from Arizona State University, followed by postdoctoral work at CEA Grenoble, Uppsala University, and finally, at University of Cambridge, where he was awarded a Marie-Curie Individual Fellowship. Since 2020, he started his independent research career at University of Lincoln, where his group works at the interface of molecular and materials chemistry, focusing on developing new concepts and technologies for production of fuels and chemicals using surplus renewable electricity and solar energy.

Introduction

Climate change induced by the increasing atmospheric CO_2 levels, combined with growing global energy demand, have spurred widespread interest in developing CO_2 mitigation technology that will allow CO_2 upcycling into value-added products. To that goal, solar-driven CO_2 conversion into carbon-based energy carriers and feedstocks represents a promising strategy towards CO_2 utilisation and recycling.[1] Since the pioneering work reported by Lehn and co-workers[2] on photochemical reduction of CO_2 using Re^I complexes as photosensitizer and catalytic unit, a wide range of molecular catalysts based on transition metal complexes have been developed to mediate light-driven CO_2 conversion to C_1 feedstocks, CO and formic acid.[3] While molecular catalysts offer distinct advantages including tuneability, high product selectivity, and low overpotential, they are typically used in solution as homogeneous catalysts, which prevents catalyst recycling and often leads to decomposition *via* diffusional pathways.[4] Heterogenization of molecular catalysts on solid supports presents a promising strategy to circumvent these problems and combine the benefits of homogeneous and heterogeneous systems.[5,6]

Cobalt phthalocyanine (CoPc) has been studied for electrocatalytic CO_2 reduction since the 1970s,[7,8] and has recently attracted renewed attention due to its excellent catalytic performance upon heterogenisation on electrodes,[9–11] reticular materials,[12] and semiconductors.[13,14] Among them, integration of CoPc into high-surface area scaffolds with ordered micro- or meso-porosity is particularly interesting because

ANEXO

TÉCNICAS DE CARACTERIZACIÓN

En el siguiente apartado se muestran las técnicas más utilizadas en el campo de la caracterización de los materiales periódicos mesoporosos ordenados (PMOs).

1) Difracción de rayos X (DRX)

La técnica de difracción de rayos X se basa en la interacción, con un determinado ángulo (θ), de la radiación X con la estructura cristalina de una muestra plana. La estructura cristalina de un sólido consiste en la repetición regular de los átomos que forman el sólido en las tres direcciones del espacio. Cuando la radiación incide sobre la muestra pueden ocurrir dos procesos. Uno consiste en que los fotones de la radiación incidente al chocar con los átomos de la muestra sufran una serie de choques inelásticos (dispersión). El otro, que algunos fotones del haz incidente sobre la muestra se desvíen, pero sin pérdida de energía (choque elástico), produciendo una radiación dispersada con la misma longitud de onda (λ) que la radiación incidente. Si existe una disposición ordenada de los átomos y se cumplen las condiciones dadas por la Ley de Bragg (**ec.1**), esta radiación da lugar al fenómeno de difracción de rayos X.

$$n\lambda = 2 * d_{hkl} * sen\theta \quad \textbf{(ec.1)}$$

Esta ecuación nos da la relación que existe entre la longitud de onda (λ), el ángulo de la radiación incidente (θ) y el espaciado entre dos planos de átomos (d_{hkl}).

Debido a que los materiales mesoporosos no tienen una disposición periódica de los átomos se puede determinar que son sólidos amorfos, pero teniendo en cuenta la disposición regular de los poros en la estructura puede dar

lugar a reflexiones a bajos ángulos de incidencia dando lugar a señales características. Poniendo como ejemplo los materiales M41s, estos poseen una simetría hexagonal (*p6mm*) (Figura 1a) con unos determinados difractogramas característicos (Figura 1b) y cuentan con un ordenamiento bidimensional de los canales de los poros, ya que sólo hay reflexiones hk0. Debido al ordenamiento hexagonal que poseen estos materiales, se puede determinar la distancia interplanar en la dirección cristalográfica (100), a través de la ley de Bragg, y el valor de celda unidad (a_0) mediante las ecuaciones 1 y 2.

$$a_0 = \frac{2*d_{100}}{\sqrt{3}} \textbf{ (ec. 1)} \qquad a_0 = Dp + e \textbf{ (ec. 2)}$$

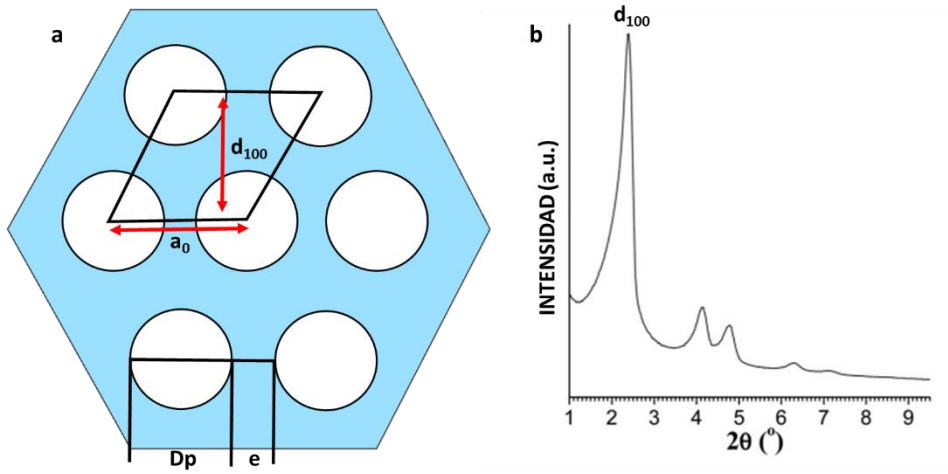

Figura 1. (**a**) Ordenamiento hexagonal del material M41s. (**b**) Difractograma de rayos X del material M41s con simetría *p6mm*.

Metodología experimental

Todos los difractogramas de rayos X han sido obtenidos en un difractómetro Bruker D8 A25. La radiación utilizada ha sido la línea Kα del Cu (λ= 1.54 Å). Los difractogramas han sido registrados mediante un barrido entre

0.5º y 5º (grados expresados en valores de 2θ). El sólido en forma de polvo es depositado en un portamuestras de manera que la muestra quede lo más plana posible y con la mayor superficie expuesta.

2) Microscopía electrónica de transmisión (TEM)

El microscopio electrónico de transmisión (TEM) se basa en los fenómenos físico-químicos que se producen cuando un haz de electrones acelerados choca con la muestra finamente preparada. Cuando los electrones son dispersados por la muestra, en función del grosor y de los átomos que forman la muestra, parte de estos electrones son dispersados selectivamente, es decir, hay relación entre los electrones que atraviesan la muestra y los electrones que son totalmente desviados. Todos estos electrones son conducidos por una serie de lentes que forman la imagen final a través de un CCD (dispositivo de carga acoplada), que captura la luz y la convierte en carga eléctrica para proporcionar datos de pixeles digitales que forman la imagen. La imagen que se obtiene con diferentes tonalidades de gris se corresponde con el grado de dispersión de los electrones incidentes.

La imagen TEM obtenida de la muestra en cuestión da información sobre la estructura de la muestra, tanto si la muestra es cristalina como amorfa.

Metodología experimental

La microscopia electrónica de transmisión ha sido realizada con un microscopio JEOL JEM 1400. La muestra se dispersa en 2-propanol y, a continuación, un par de gotas de la suspensión se añaden sobre una rejilla (Holey Carbon Film 200 rejilla de Cu). La rejilla se seca a temperatura ambiente durante al menos 24 horas antes de la medida para que la muestra se deposite.

3) Isotermas de adsorción-desorción de nitrógeno.

La adsorción es un fenómeno superficial entre una especie adsorbida (adsorbato) y una especie que adsorbe (adsorbente) debido a las fuerzas de interacción entre ambos. La fisisorción de gases es una técnica muy utilizada en la caracterización de sólidos ya que nos proporciona información sobre las características texturales de los materiales. Al ponerse en contacto el gas (normalmente nitrógeno) con la superficie del sólido se produce un equilibrio entre las moléculas del adsorbente y el adsorbato que depende de la presión del gas y de la temperatura. La relación entre las moléculas adsorbidas y la presión a una temperatura determinada se recoge en una isoterma de adsorción. Las isotermas obtenidas informan del volumen de gas adsorbido a una determinada presión. De este modo, se puede calcular el área superficial, el tamaño y distribución de poro (Figura 2). Las isotermas comprenden tanto la adsorción, proceso por el cual entran en contacto el nitrógeno gas y un sólido, como la desorción, proceso contrario.

Con independencia de su composición química, los sólidos se pueden clasificar según su superficie específica, espesor de pared, volumen de poro, diámetro de poro o distribución del tamaño de poro (función de distribución).

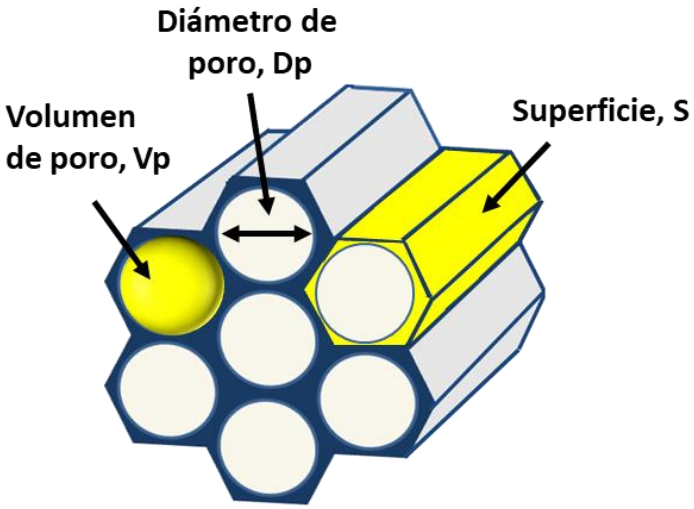

Figura 2. Caracterización textural de una sílice porosa.

Una isoterma de adsorción-desorción muestra la cantidad de gas adsorbido (moles por gramo de adsorbente) como una función de la presión relativa P/P_0 en el intervalo $0 < P/P_0 < 1$ (P= presión de vapor de equilibrio del adsorbato, P_0= presión de vapor del adsorbato líquido puro), a una temperatura dada.

Los sólidos se pueden clasificar en función del tipo de isoterma que presenten. De este modo, según la IUPAC, las isotermas de adsorción se pueden clasificar en seis grupos [1] y las histéresis en cuatro tipos (Figura 3).

Los sólidos mesoporosos, que poseen diámetros de poro entre 2 y 50 nm, muestran típicamente isotermas de tipo IV, en las que la condensación capilar da lugar a un ciclo de histéresis con una pendiente elevada a altas presiones relativas, ya que los procesos de adsorción y desorción no siguen el mismo camino, debido a que la evaporación del gas condensado en los mesoporos no se da tan fácilmente como la condensación. Por otro lado, los materiales mesoporosos también se pueden clasificar según el tipo de histéresis, exhibiendo en la mayoría de los casos histéresis de tipo I, caracterizadas por un ciclo estrecho con sus ramas de

adsorción y desorción paralelas entre sí, que se asocian a adsorbentes que tienen distribuciones de tamaño de poros muy estrechas [1].

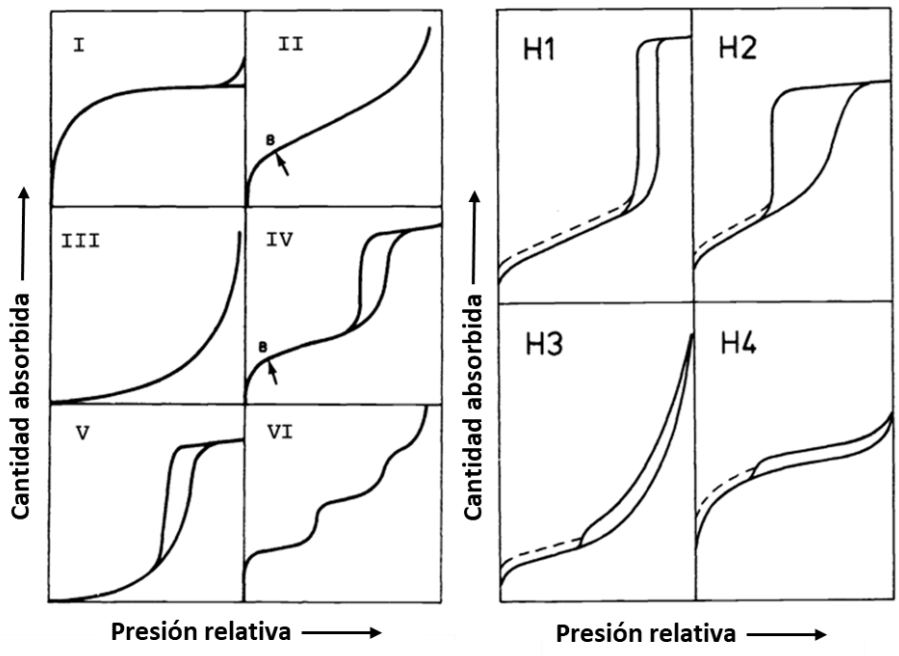

Figura 3. Tipos de isotermas de fisisorción e histéresis de acuerdo con la clasificación de la IUPAC [1].

Metodología experimental

Las propiedades texturales de los catalizadores sintetizados se han obtenido a partir de las isotermas de adsorción-desorción de nitrógeno determinadas con un equipo Autosorb-iQ MP/MP-XR a la temperatura del nitrógeno líquido (-196 ºC). Antes de la medida, la muestra es desgasificada durante toda la noche a 120 ºC.

La superficie específica ha sido obtenida mediante el método BET, la distribución de tamaño de poro, el volumen y diámetro de poro han sido obtenidos mediante el método DFT.

4) Espectroscopía Raman

La espectroscopía Raman es una técnica fotónica que proporciona información química y estructural de cualquier material o compuesto orgánico o inorgánico permitiendo su identificación. Se basa en hacer incidir un haz de luz monocromático de una determinada frecuencia sobre una muestra y examinar la luz dispersada por ella. La mayor parte de la luz dispersada tiene la misma frecuencia que la luz incidente (**dispersión Rayleigh**) y no aporta ninguna información sobre la muestra. Sin embargo, una pequeña fracción presenta un cambio frecuencial, que resulta de la interacción con la materia (**dispersión Raman**) y es la que nos proporciona información sobre la composición de la muestra.

Las variaciones de frecuencia que se observan en la dispersión Raman son equivalentes a variaciones de energía, ya que los iones y átomos que forman las muestras están sometidos a constantes movimientos vibracionales y rotacionales. A cada uno de estos movimientos rotacionales y vibracionales le corresponderá un valor determinado de energía molecular. El espectro Raman muestra la intensidad óptica dispersada en función del número de onda normalizado al que se produce. El número de onda normalizado es una magnitud proporcional a la frecuencia e inversamente proporcional a la longitud de onda (**ec. 1**).

$$\upsilon = \nu/c = 1/\lambda \ [cm^{-1}] \quad (\textbf{ec. 1})$$

Una gran ventaja que posee esta técnica frente a otras es que puede ser utilizada directamente sobre la muestra y no conlleva ninguna alteración de la superficie del material, es decir, es una técnica no-destructiva.

Metodología experimental

Los espectros Raman han sido obtenidos en un equipo Renishaw inVia usando un láser verde (532 nm). La muestra es depositada en un portamuestras lo más plana posible.

5) Espectroscopía Infrarroja (IR)

Esta técnica consiste en analizar la radiación infrarroja que se absorbe en un sólido cuando es atravesada por ella. Así, el espectro infrarrojo muestra la radiación transmitida frente a la frecuencia de la radiación incidente. Un requisito para que las moléculas absorban radiación IR es que la radiación promueva un cambio en el momento dipolar de la molécula. Cuanto mayor sea ese cambio, más intensa será la señal. El espectro vibracional obtenido para cada molécula se considera una propiedad física única y característica de esa molécula.

Una de las grandes ventajas que posee la espectroscopía IR es su gran versatilidad, ya que puede ser utilizada en cualquier muestra con independencia del estado en el que se encuentre: líquido, sólido, polvo, gas, fibras, etc. Además, el espectro IR se puede utilizar como “huella dactilar” en la identificación de muestras desconocidas comparándolas con espectros de referencia.

Metodología experimental

Los espectros de IR se han realizado en un espectrómetro Bruker Alpha II, en un intervalo de 400 a 4000 cm^{-1}, con una resolución de 8 cm^{-1} y un total de 24 barridos. Para los espectros de IR con transformada de Fourier (IR-TF), se han preparado pastillas conteniendo un 5 % en peso de la muestra y 95 % de KBr.

Los espectros de IR de reflectancia difusa (DRIFT) se han realizado con una cámara ambiental de Harrick conectada a un controlador de temperatura. Las muestras se han calentado a 200 ºC en atmósfera de argón durante 20 min antes de realizarse la medida, manteniéndose esas condiciones durante la misma. Los espectros de IR de reflectancia total atenuada (ATR) se han realizado utilizando una punta de diamante de un solo rebote.

6) Resonancia Magnética Nuclear de ^{13}C.

La espectroscopía de resonancia magnética nuclear (RMN) posibilita el estudio de la estructura molecular de un compuesto a través de la interacción de la radiación electromagnética con los núcleos de ciertos átomos inmersos en un campo magnético estático externo. Esta técnica puede utilizarse sólo para estudiar núcleos atómicos con un número impar de protones o neutrones, como en el caso del ^{13}C, ^{1}H, ^{29}Si, y ^{31}P, entre otros.

El núcleo se caracteriza por su masa, carga eléctrica, su interacción con los campos magnéticos externos y por su espín. La resonancia magnética nuclear se centra en el estudio del campo magnético y del espín. De este modo, el momento magnético (μ) deriva de su espín nuclear, I. El espín nuclear es una propiedad intrínseca de la partícula en sí misma, pero puede ser considerado como una forma de momento angular.

$$\mu = \gamma I \quad \text{dónde } \gamma \text{ es la constante giromagnética}$$

En ausencia de un campo magnético, los espines nucleares se orientan al azar, pero cuando está presente los núcleos con espines positivos se orientan en la misma dirección del campo en un estado de mínima energía (espín α) y los núcleos con espines negativos se orientan en la dirección contraria al campo en un estado de mayor energía (espín β).

Al irradiar la muestra con un pulso intenso de radiación, los núcleos con espín α son promovidos al estado de espín β. Cuando los núcleos vuelven a su estado original, emiten señales cuya frecuencia es dependiente de la diferencia de energía entre ambos estados de espín. Estas señales son recogidas por el espectrómetro de RMN que las registra como una gráfica de intensidad frente a frecuencias. El espectro contiene una serie de picos de diferentes intensidades en función de una magnitud conocida como desplazamiento químico.

El espectro de RMN proporciona mucha información sobre las moléculas presentes en la muestra, ya que cada grupo funcional se puede identificar a partir de los valores de desplazamiento químico (Figura 4).

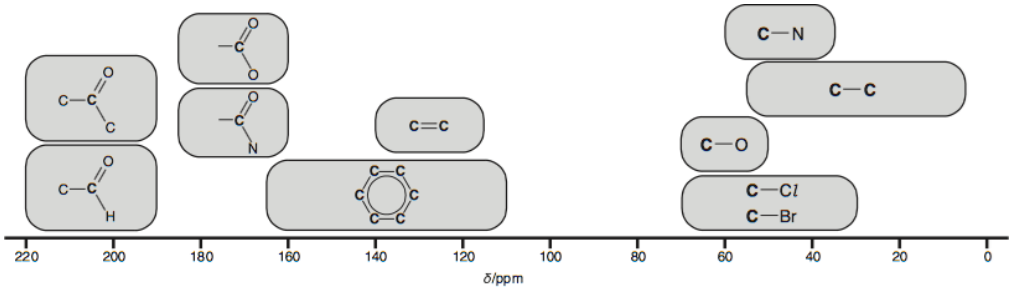

Figura 4. Desplazamiento químico típicos para diferentes tipos de átomos de carbono [2].

Metodología experimental

Los espectros de RMN del ^{13}C fueron adquiridos en un espectrómetro Bruker Avance III HD 400 WB a 13 kHz. Se acumularon 1500 barridos para cada espectro. La duración del pulso de excitación y el tiempo de reciclaje fueron de 3.6 y 2 s, respectivamente. Todos los espectros realizados han sido referenciados usando como estándar tetrametilsilano (TMS).

7) Espectroscopía fotoelectrónica de rayos X (XPS)

La espectroscopía fotoelectrónica de rayos X, XPS o ESCA (Espectroscopía Electrónica para Análisis Químico), es una técnica que implica la excitación mediante un haz de rayos X de los niveles más internos de los átomos, provocando la emisión de fotoelectrones que proporcionan información sobre la energía de cada nivel y la naturaleza de cada átomo.

Dado que la energía del haz incidente es $h\nu$, si el fotoelectrón sale con una energía cinética E_C, la diferencia entre ambas energías nos proporcionará la energía de ligadura (E_L), que es característica de cada átomo. En realidad, con esta técnica se mide la velocidad de los electrones que se emiten.

$$E_L = h\nu - E_C$$

Esta técnica es actualmente la más utilizada para la caracterización de superficies. Proporciona información cualitativa y cuantitativa de todos los elementos (excepto H y He). Además, puede ser utilizada en una gran variedad de muestras.

Metodología experimental

Los espectros de XPS fueron registrados en un espectrómetro SPECS Phoibos HAS 3500 150 MCD con un haz monocromático de Al K_α (1486.7 eV). Las energías de enlace han sido determinadas respecto a la posición del Si2p (103.4 eV). Los espectros completos han sido recopilados con una energía de paso de 60 eV, mientras que los de cada elemento han sido recogidos a 40 eV con una resolución de 0.1 eV.

8) Espectroscopía de estructura fina de la absorción de rayos X (X-Ray Absorption Fine Structure, XAFS)

Es una técnica que analiza las estructuras moleculares a nivel local, proporcionando información sobre la geometría y la estructura electrónica alrededor de un átomo absorbente. El proceso de absorción de rayos X provoca transiciones electrónicas desde los estados más internos hasta los estados de valencia. El espectro de absorción de rayos X está dividido en dos regiones. Una región en la que las interacciones se producen entre los átomos cercanos al borde de absorción (XANES, X-Ray Absorption Near Edge structure), que proporciona información sobre la coordinación química (coordinación tetraédrica, ortogonal…) y el estado de oxidación del átomo. La otra zona, posterior al borde de absorción (EXAFS, Extended X-Ray Absorption Fine Structure), es usada para determinar distancias, números de coordinación y especies vecinas presentes cerca del átomo absorbente [3] (Figura 5).

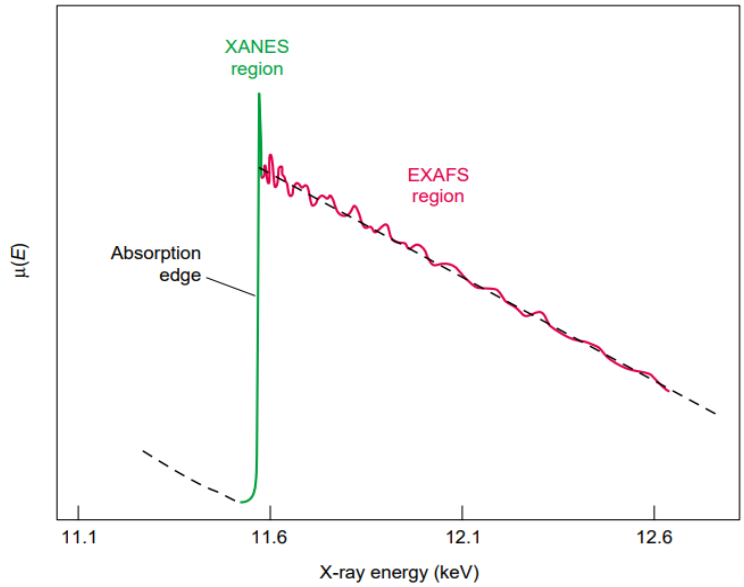

Figura 5. Espectro de XAFS de una lámina de plata [4].

En la muestra, los rayos X interaccionan con la materia y producen dos fenómenos: Fluorescencia (interacción de la radiación con la materia que produce rayos X en todas las direcciones menos en las direcciones incidentes) y Transmisión (disminución de los rayos X cuando inciden sobre la muestra).

La absorbancia se puede obtener a través de las ecuaciones:

$A = \mu(E)x = ln(I_0/I_1)$ donde x es el grosor de la muestra, I_0 es la intensidad inicial, I_1 intensidad transmitida y $\mu(E)$ es el coeficiente de atenuación.

$A = \mu(E)x = (I_f/I_0)$ donde I_f es la intensidad del haz fluorescente.

Para un átomo aislado, el coeficiente de atenuación $\mu(E)$ en el borde de absorción se corresponde con la energía de enlace del electrón interno. Si hay un átomo cerca, el fotoelectrón que se emite se dispersa en él y vuelve al átomo emisor del fotoelectrón. La onda del fotoelectrón que vuelve se interpone consigo misma. El coeficiente de atenuación depende de los estados a los que accede el fotoelectrón en el átomo absorbente que se alteran por la interferencia. La anchura

de la onda del fotoelectrón retrodispersado varía con la energía, provocando que el coeficiente $\mu(E)$ oscile dando lugar a la estructura fina o EXAFS.

EXAFS es un efecto de interferencia y depende de la naturaleza ondulatoria del fotoelectrón. Por ello, la función de EXAFS se representa en términos de número de onda del fotoelectrón, k (**ec.1**), en lugar de la energía del rayo X.

$$k = \sqrt{\frac{2m(E-E_0)}{h^2}} \quad \textbf{(ec.1)}$$

Para poder extraer información del espectro de EXAFS se utiliza la "ecuación de EXAFS" [5]. Conociendo una serie de parámetros se puede determinar Rj (la distancia a los átomos vecinos) y Nj (el número de coordinación de los átomos vecinos).

Metodología experimental

Los espectros de absorción de rayos X se registraron en la línea de luz CLAESS en el sincrotrón ALBA. La radiación de sincrotrón fue monocromada por medio de un monocromador de doble cristal Si(111), rechazando los armónicos más altos y eligiendo los ángulos y recubrimientos adecuados para los espejos de colimación y enfoque. Los datos de absorción se adquirieron en modo de transmisión. Las muestras en polvo se mezclaron uniformemente en una matriz de nitruro de boro y se prensaron en gránulos para garantizar un salto de absorción cercano a 1. Se midieron varios escaneos para garantizar la reproducibilidad y una buena relación señal/ruido. Los datos se trataron con el paquete Demeter y la energía se calibró al primer punto de inflexión de la lámina de Co, al que se dio un valor de 7709 eV.

Referencias

[1] K.S.W. Sing, Reporting physisorption data for gas / solid systems with Special Reference to the Determination of S, Pure Appl. Chem. 54 (1982) 2201-2218.

[2] No Title, (n.d.). https://revise.im/chemistry/rpa/nmr.

[3] M. Newville, Fundamentals of XAFS, Rev. Mineral. Geochemistry. 78 (2014) 33-74. https://doi.org/10.2138/rmg.2014.78.2.

[4] Conradson S. D., XAFS A Technique to Probe Local Structure, Los Alamos Sci. 26 (2000) 422-435.

[5] D.E. Sayers, E.A. Stern, F.W. Lytle, New technique for investigating noncrystalline structures: Fourier analysis of the extended x-ray-absorption fine structure, Phys. Rev. Lett. 27 (1971) 1204-1207. https://doi.org/10.1103/PhysRevLett.27.1204.